The Dissertation Committee for Alisha Marie Bohnsack Certifies that this is the approved version of the following dissertation:

Novel Multifunctional Porous Coordination Polymers from *Pre*-Synthetically Modified Organophosphorous Ligands

Committee:

Simon M. Humphrey, Supervisor

Bradley J. Holliday

Michael J. Rose

Michael J. Krische

Alexander A. Demkov

Novel Multifunctional Porous Coordination Polymers from *Pre*-synthetically Modified Organophosphorus Ligands

by

Alisha Marie Bohnsack, B.S.

Dissertation

Presented to the Faculty of the Graduate School of

The University of Texas at Austin

in Partial Fulfillment

of the Requirements

for the Degree of

Doctor of Philosophy

The University of Texas at Austin

May 2015

Dedication

To my Grandpa, who encouraged my love of science from the moment I started walking.

To my Papa, whose love of teaching and the English language have been both an inspiration and a wonderful source of conversation and humor.

To my Dad, who taught me to always be the very best I could be, and to never give up on my dreams.

Acknowledgements

Looking back on the past five years, it's hard to imagine how many people have helped make this dream become a reality. I would like to thank my research advisor, Dr. Simon Humphrey, for being an endless source of knowledge, direction, and encouragement. Not only have I learned an incredible amount about inorganic chemistry, laboratory techniques, and scientific writing, but also (and inevitably) a great deal of British sarcasm and humour.

I would like to thank all of my fellow group members – without you, this journey would not have been nearly as encouraging, supportive, and fun. Thank you for letting me play what Stephany would deem as "angry music" in the lab on busy afternoons, and for graciously tolerating my loud conversations with the chemistry in my hood. To Ilich, for your constant support and fantastic sense of humor during my first two years. To Stephany, for the (essential) Whole Foods lunches, head scratches, hair braids, and wonderful conversations. To Nolan, for sharing stories about our homeland, an epic sticky note battle, and a limitless hidden supply of chocolate. To An and Sam, for sharing an office with me during such an intense semester, yet always making me laugh, donating single French fries, and surprising me with doodles. Our board will forever be the best board.

There are many people within the chemistry department who have also been incredibly supportive throughout this experience. Thank you to all of the inorganic professors who have helped me with class material, research questions, and general words of advice and encouragement throughout the years. Thank you to Betsy Hamblen for all of the guidance, bright smiles, and amazing chocolate during our office visits.

Thank you to Steve Moore for the endless conversations about anything (and everything) related to running. Thank you to Drs. Cynthia LaBrake and Kate Biberdorf for providing sincere and invaluable career advice over the past several years. Thank you to (the newly Drs.) Scott Robotham and Nelly Membreno for being two of the best running buddies I could have asked for, and thank you to all of the graduate students I've missed for the day-to-day help, advice, stories, and laughter.

I would also like to thank someone who is very dear to me, and who has gone above and beyond during this last semester to help with anything he possibly could. To Dan, thank you so much for the love and support you've given me throughout the end of this journey. Your words of encouragement and inspiration toward achieving my goals, along with every act of kindness and selflessness, have been absolutely incredible. You are one of the most caring, bright, and thoughtful people I've ever had the pleasure of knowing, and I have no doubt that you will accomplish many amazing things in your lifetime. Thank you for being there for me, for making me laugh, and for inspiring me to continually aim to be better.

Lastly, I would like to thank my friends and family who have always been unconditionally supportive, no matter how long we may go without seeing each other. Thank you all for the phone calls, cards, words of encouragement, and bear hugs when we finally meet again. I'm now happy to be able to answer that never-ending question… "Yes, I'm finally getting out of school."

Novel Multifunctional Porous Coordination Polymers from *Pre*-synthetically Modified Organophosphorus Ligands

Alisha Marie Bohnsack, Ph.D.

The University of Texas at Austin, 2015

Supervisor: Simon M. Humphrey

Phosphine-based Porous Coordination Polymers (PCPs) have shown promising results as gas storage, gas separations, and molecular sensing materials due the versatility of the P(III)/P(V) chemistry, coupled with the inherent 3-dimensionality of the ligands. A variety of *pre*-synthetically modified organophosphine linkers have been reacted with alkali earth metals, early transition metals, and lanthanides to produce a series of Phosphine Coordination Materials (PCMs) with a wide array of topologies and pore functionalities. A *p*-carboxylated triphenylphosphine oxide linker, tctpoH_3, has been reacted with Mg(II) to form the thermally robust PCM-11, which possesses superior room-temperature CO_2 adsorption capacity at 12 bar.

A new tetrahedral phosphonium salt, tctp$^+H_3$, has been synthesized by the Pd(II)-catalyzed reaction of *p*-carboxylated triphenylphosphine with 4-iodobenzoic acid to produce a zwitterionic monophosphine precursor. Upon examination of its crystal structure, it was found that tctp$^+H_3$ possesses a high degree of hydrogen-bonding between neighboring carboxylic acid groups, which causes it to polymerize into a porous, metal-free, ionically-bonded coordination polymer, iPCM-1. This phosphonium linker has been reacted with a series of Ln(III) precursors to form an isostructural set of PCMs that exhibit characteristic lanthanide luminescence properties.

Several PCPs have been developed from a new *bis*(phosphine)MCl_2 (M = Pd, Pt) complex upon reaction with early transition metals. Zn(II)-based PCM-18 exhibits unusual and fully reversible H_2 adsorption at 150 °C, as well as *post*-synthetic reactivity inside the pores of the material. Co(II)-based PCM-24 also displays similar high-temperature H_2 sorption behavior, along with a reversible pink to blue color change upon activation, indicative of a symmetry transformation from O_h to T_d about the metal node.

Table of Contents

List of Tables

List of Figures

List of Schemes

Chapter 1: Introduction

THE DEVELOPMENT OF PCPS

Porous coordination polymers (PCPs) are a class of crystalline, porous materials that contain organic *linkers* and metal *nodes* connected by strong coordination bonds that form 1-, 2-, or 3-dimensional arrays. These materials are also widely known as Metal-Organic Frameworks (MOFs); however, this term refers specifically to 3-dimensional polymers, and as such, not all PCPs are classified as MOFs.[1] The first "coordination polymer" was described in the early 1960s,[2] and the number of reported PCP materials has skyrocketed over the past two decades (Figure 1.1).

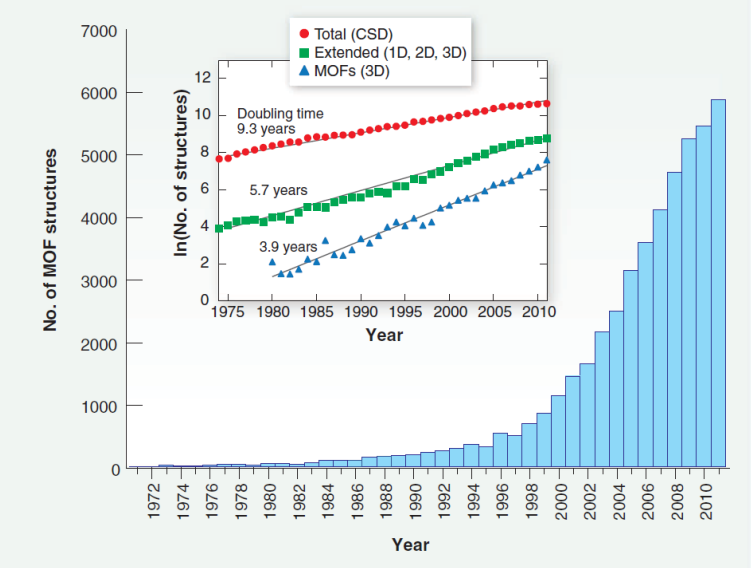

Figure 1.1: Porous coordination polymers (1D, 2D, and 3D) reported in the Cambridge Structural Database (CSD) from 1971 to 2011. The trend shows a striking increase during this period for all structure types. In particular, the doubling time for the number of 3D MOFs (inset) is the highest among all reported metal-organic structures.[1]

In the early 1990s, just before PCPs began emerging as a popular research topic, the field of porous materials was dominated by zeolites, silicas, aluminophosphates, and activated carbons.[1,2] Zeolites are 3-dimensional aluminosilicates of the general formula $M^{n+}_{x/n}[(AlO_2)_x(SiO_2)_y]^{x-}\cdot wH_2O$ (M = alkaline or alkali earth metals).[3,4] Their channels exhibit permanent porosity upon dehydration, and their sieving effects have been utilized for gas storage and heterogeneous catalysis. Aluminophosphates possess similar physical traits to zeolites but can also possess ordered crystalline structures.[5] Additionally, activated carbons have been used as gas storage materials because they exhibit both high porosities and high surface areas, but unlike PCPs and some aluminophosphates, they do not contain ordered, crystalline structures.[6,7]

At this time, research began to focus on the design of functionalized PCPs with specific applications in mind. Robson and coworkers developed a material containing 4,4',4",4"'-tetracyanotetraphenylmethane linkers and Cu(II) nodes that was capable of undergoing anion exchange in 1990.[8] Yaghi *et al*. were the first to coin the term "metal-organic framework" when describing a 3-dimensional material, $Cu(4,4'\text{-bpy})_{1.5}\cdot NO_3(H_2O)_{1.5}$, in 1995.[9] Three years later, they were also the first to report the use of gas sorption to determine the permanent porosity of $Zn(BDC)\cdot(DMF)(H_2O)$, which possessed a Langmuir surface area of 310 $m^2\,g^{-1}$.[10] In 1997, Kitagawa and coworkers were the first to report gas sorption measurements obtained at room temperature.[11] A series of Co(II)-, Ni(II)-, and Zn(II)-based PCPs composed of 4,4'-bipyridine linkers exhibited reversible CH_4 sorption, as well as moderate uptake of N_2, and O_2, at pressures up to 36 atm at 298 K.

While there are many examples of historical firsts throughout the literature, it is important to mention that the overall synthetic approach to new PCPs has adapted significantly over the past two decades. Initial methods entailed mixing simple ditopic or

tritopic linkers with metal salts and observing which synthetic conditions produced viable materials. However, the necessity to gain more structural control over the desired materials led to a process known as reticular synthesis.[12,13] This specialized type of "crystal engineering" involves the rational assembly of predesigned, rigid molecular building blocks into a specific, ordered network based on their bond lengths and bond angles. These building blocks are referred to as secondary building units (SBUs) and are used to describe both organic linkers and metal nodes (Figure 1.2).[14-16] SBUs can be selected for a preferred PCP topology by ensuring that the resulting bond angles and pore shapes are compatible.

In addition to traditional solvothermal routes, which involve the reaction of organic and inorganic species in closed vessels under autogenous pressure above the boiling point of the solvent,[17] the development of new PCPs has also been achieved by recent utilization of microwave-assisted, electrochemical, mechanochemical, and sonochemical syntheses.[18]

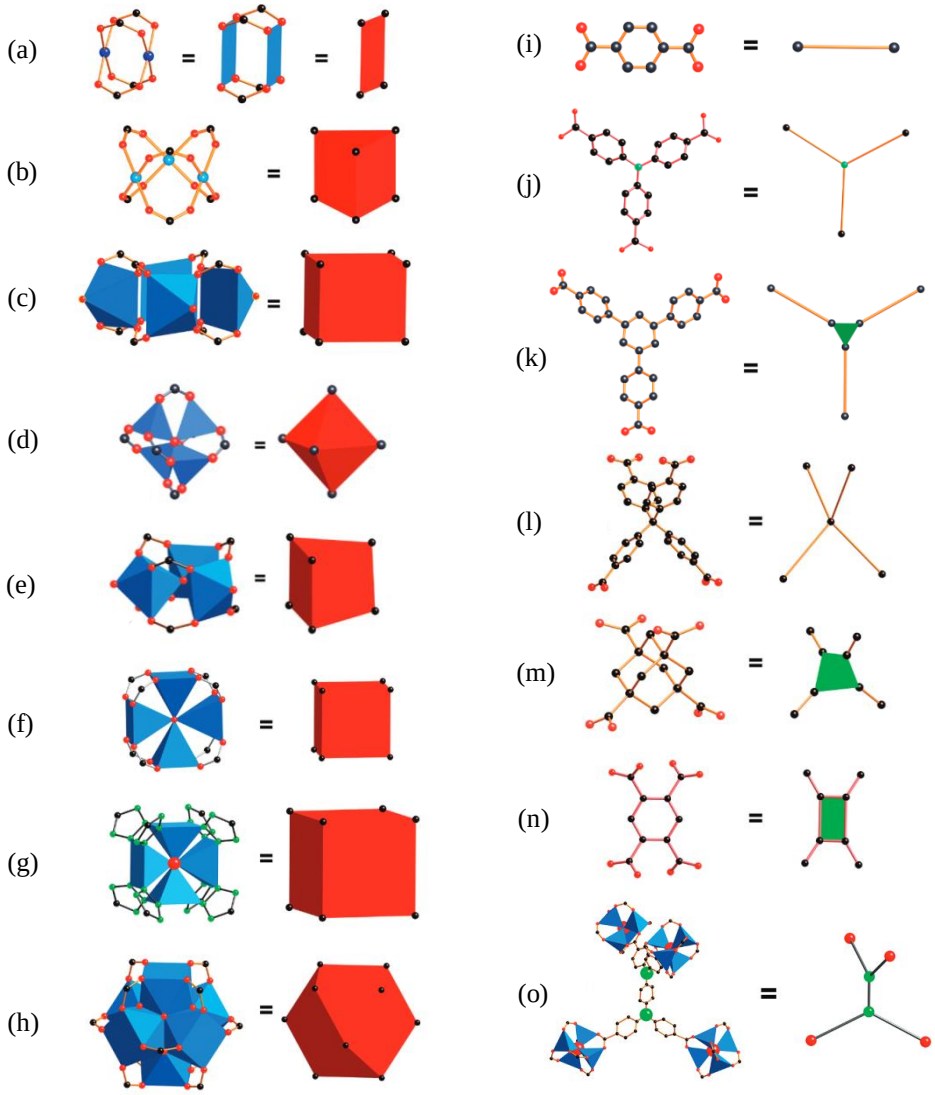

Figure 1.2: Illustration of common SBUs found within PCPs. SBUs for metal nodes are shown in red for (a) 2 square planar sites, (b) three square planar sites, (c) four square planar/square pyramidal sites, (d) the basic zinc acetate [$Zn_4O(CO_2)_6$] node, (e) the basic chromium acetate [$Cr_3O(CO_2)_6$] node, (f/g) 8 points of extension, and (h) 12 points of extension. SBUs for organic linkers are shown in orange and green for (i) ditopic, (j/k) tritopic, (l/m) tetrahedral, and (n) square ligands. (o) A combination of octahedral SBUs coordinated to a tetrahedral linker.[15]

Notable solid-state properties

PCPs have proven to be attractive candidates for a wide range of solid-state applications due to many of their inherent physical properties. Their highly ordered structures exhibit permanent porosity following the removal of uncoordinated solvent molecules, and they typically possess pore apertures that can accommodate the passage of light gases, ions, and small organic species into the interior of the PCP. However, synthesis with large organic linkers can lead to the formation of materials with unusually large pore openings and/or pore volumes. Extended ligands can also lead to framework interpenetration, *i.e.* when two or more independent networks form inside of one another, but the use of mixed-ligand systems has been shown to produce non-interpenetrated structures.[1] This technique has allowed for the incorporation of more complex molecules into PCPs with sufficiently large pore openings, for example, vitamin B_{12}, metal-organic polyhedron-18, myoglobin, and green fluorescent protein (GFP) within IRMOF-74-IV, -V, -VII, and -IX, respectively (Figure 1.3).[19] The largest pore aperture reported in a PCP thus far is 98 Å from Mg(II)-based IRMOF-74-XI,[19] and the largest pore volume is 4.40 $cm^3\ g^{-1}$ from Cu(II)-based NU-110 (Figure 1.4).[20]

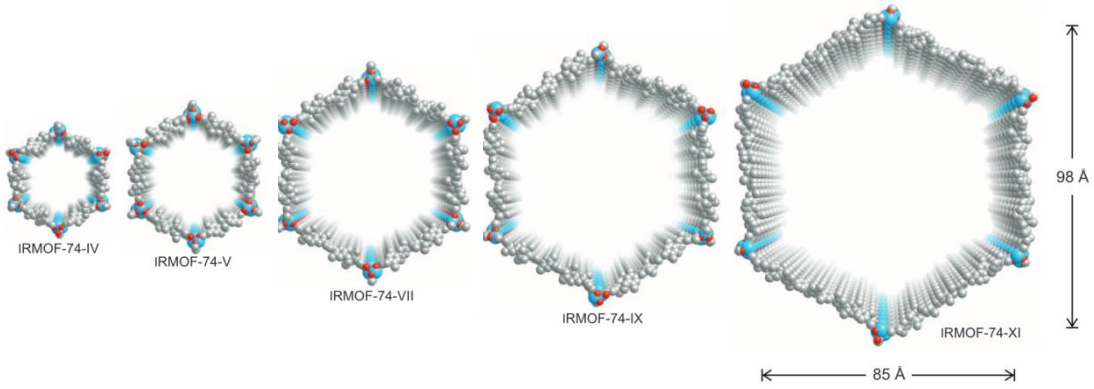

Figure 1.3: Perspective views of a single one-dimensional channel shown for IRMOF-74-IV, -V, -VII, and -IX, from left to right. Pore aperture is described by the length of the diagonal and the distance between the two opposite edges in the regular hexagonal cross section. Hexyl chains and hydrogen atoms are omitted for clarity. C = gray, O = red, Mg = blue.[19]

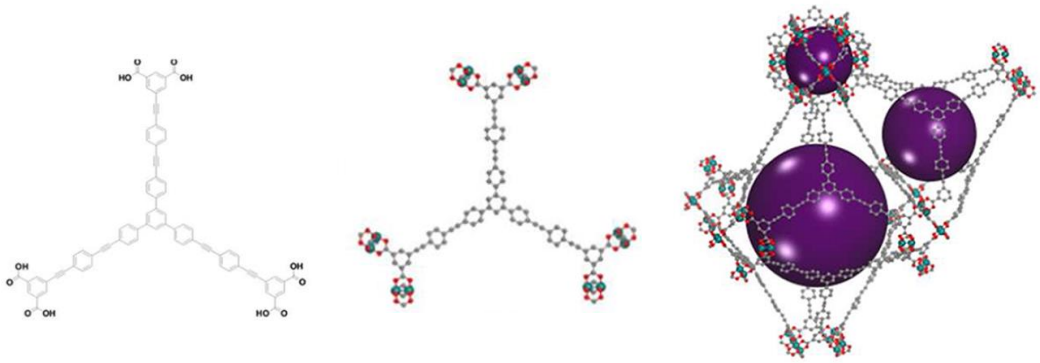

Figure 1.4: *(Left)* The hexatopic ligand LH_6 used in the synthesis of NU-110; *(center)* connectivity of LH_6 with the Cu(II) paddlewheel dimers; *(right)* the three different pore topologies within NU-110, shown with purple spheres for distinction. C = gray, O = red, Cu = teal.[20]

There are three main subclasses of porous solids that are based on the size of the pores within the materials: microporous, mesoporous, and macroporous. The majority of PCPs are microporous and contain pore diameters that are less than 2 nm in size, but there are also many examples of mesoporous PCPs that possess pore diameters between 2 and 50 nm. Macroporous materials contain pores that are greater than 50 nm and are beyond the realm of PCPs.

The most attractive feature of PCPs is undoubtedly their unsurpassed internal surface areas, which are of particular interest for applications in gas storage and gas separations. This measurement describes the degree to which guest molecules can be accommodated (adsorbed) within the pores of the material based on direct contact with the structure; higher surface areas lead to higher amounts of adsorbed guest molecules. Recent research aimed at the design of materials with record-breaking surface areas has achieved values of 4100 $m^2 g^{-1}$ (MIL-101) in 2005,[21] 5200 $m^2 g^{-1}$ (UMCM-2) in 2009,[22] and 6240 $m^2 g^{-1}$ (MOF-210) in 2010.[23] The highest recorded internal surface area was reported in 2012 for NU-110, which possesses a BET surface area of 7140 $m^2 g^{-1}$ (Figure 1.4).[20] Not only was this the highest internal surface area of a PCP, it was also the highest internal surface area amongst all known porous materials. Current computational studies have yielded a theoretical limit for PCP surface areas at 14,600 $m^2 g^{-1}$.[20]

It follows that the high porosity of PCPs also yields materials with low densities. This can lead to higher gas storage capacities, especially for H_2 at 77 K,[23,24] as well as lighter working devices, particularly with cylinders for gas storage. The lowest density achieved in a PCP to date is 0.126 g cm^{-3} from MOF-399, composed of sizable 4,4',4"-(benzene-1,3,5-triyl-tris(benzene-4,1-diyl))-tribenzoate linkers and Cu(II) paddlewheel dimers.[25]

PCPs also exhibit enhanced thermal stabilities due to the presence of covalent and strong coordination bonds. This typically leads to high decomposition temperatures, between 300–550 °C, for the vast majority of these materials. However, due to their tendency to undergo link-displacement reactions during solvent-exchange, much effort has been spent on improving the chemical stability of PCPs, especially in aqueous solutions or under humid conditions. Nevertheless, several materials have been shown to possess impressive chemical stabilities; Zn(II)-based ZIF-8 retains crystallinity after boiling in methanol, benzene, and water for seven days, as well as after submersion in a concentrated sodium hydroxide solution at 100 °C for 24 hours,[26] and Zr(II)-based UiO-66 is stable under both acidic and basic conditions, retaining crystallinity from pH = 1 to pH = 14.[27]

PCPs by design

With the above considerations in mind, it follows that new PCPs can be rationally constructed by careful selection of the organic and inorganic species. The organic linkers commonly contain acidic functional groups that deprotonate in solution or nitrogen functionalities that act as neutral lone-pair donors.[28,29] These groups form strong coordination bonds to the metal nodes, which can contain metals from Groups I or II, early transition metals, and/or lanthanides and range in composition from single metal ions to complex heteroatomic clusters.[28] Attention must be paid to the size and shape of the resulting pores with regard to the desired application, *e.g.* the use of short organic linkers will not facilitate the adsorption of large molecules. The chemical functionalities present in the resulting materials must also be considered with respect to the organic and inorganic precursors, such as the inclusion of catalytically-active metal species for

heterogeneous catalysis, chiral groups for chiral catalysis and/or chiral separations, and optically-active species for molecular sensing, *etc*.

Pre-synthetic modification

The organic linkers used in PCP development can be effectively fine-tuned by chemical modification either before or after polymerization with metal precursors; these two processes are referred to as *pre*-synthetic and *post*-synthetic modification, respectively. There are many examples in the literature of *post*-synthetic modification, which involves the direct reaction of substrates with *pre*-formed PCPs to tailor the pore functionality and solid-state properties of the materials.[30-33] This can include the addition of ligand functional groups, total ligand substitution, metal atom substitution, and/or ion-exchange of the materials, and it is especially useful if the modification would inhibit the initial formation of the framework. However, the materials must possess sufficient thermal and chemical stabilities to withstand the required reaction conditions for the modification to take place.

There are several synthetic benefits of employing *pre*-synthetic modification for PCP synthesis. Most importantly, it can allow for the presence of target functional groups within a material that would otherwise be impossible if the material could not withstand the reaction conditions necessary for *post*-synthetic incorporation. These groups can be designed to be located within the pores of a material or to help facilitate bonding to the metal nodes. *Pre*-synthetic modification can also be utilized to induce a higher degree of symmetry into an organic species and thus encourage the formation of a crystalline material; Zn(II)-based PCM-18 is formed by the solvothermal reaction of a *p*-carboxylated *bis*(phosphine) ligand that contains a *cis*-chelated $–MCl_2$ (M = Pd, Pd)

group (Figure 1.5).[34] Addition of this group effectively locks the phosphine atoms in place and inhibits free rotation of the P–C (backbone) bonds. This enforces a rigid geometry throughout the entire structure that is not present in the metal-free ligand. Efforts to obtain PCM-18 using the metal-free *bis*(phosphine) ligand have yet to be successful.

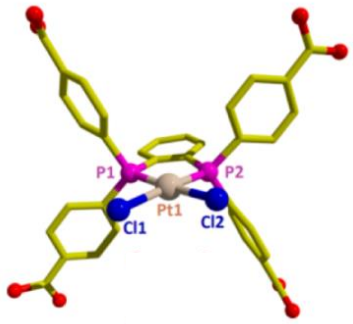

Figure 1.5: Crystal structure of the *pre*-synthetically modified BBCB-$PtCl_2$ ligand used for the synthesis of PCMs 18, 24, and 27.

APPLICATIONS OF PCPS

Due to their ultrahigh surface areas and permanent porosities, initial interest in PCPs focused on the development of new materials for gas storage and separations.[35-38] The size-exclusion effects offered by discreet and tunable pore dimensions, coupled with the abundance of available surface sites within the interior channels of the materials, has led to the selective adsorption of light gases (N_2, CO_2, CH_4, O_2, Ar), harmful gases (H_2S, SO_2, Cl_2, NH_3, NO_x, CO), vapor-phase solvent molecules, and gaseous hydrocarbons.[39] As the synthetic approach to new materials shifted its attention to the careful tailoring of organic ligands and functionalization of internal pore surfaces, these interests have advanced beyond the scope of adsorption and molecular sieving applications to include

the areas of molecular sensing,[40-44] magnetism,[45-48] drug delivery,[49-53] proton conductivity,[54-57] and catalysis.[58-61]

Gas storage and separations

Adsorption within a PCP describes the process by which gas molecules (the *adsorbate*) adhere to the surface of a material (the *adsorbent*). Adsorbate-adsorbent interactions can range from physisorption-based forces (van der Waals) to strong, chemisorption-based bonding. However, because chemisorption typically requires the breakage of adsorbate bonds prior to the formation of adsorbate-adsorbent bonds, this process does not favor the facile and reversible adsorption required for many working devices.

The adsorption capacity of a given PCP is determined by obtaining an adsorption/desorption isotherm of the target adsorbate over a range of pressures. This is achieved by the initial *activation* of the material by subjection to elevated temperatures (*ca*. 100–200 °C) under ultrahigh vacuum to remove guest molecules remaining from synthesis. This effectively liberates the pore surfaces from any impurities that may interfere with the target adsorbate, which is followed by stepwise dosing of the material with small amounts of the adsorbate under increasing pressures and a constant temperature. Once a given pressure has equilibrated within the sample apparatus, another dose of adsorbate is introduced and the process repeated. When the apparatus reaches the maximum desired pressure, the dosing is then reversed with a stepwise decrease in pressure to monitor the removal of the target adsorbate. These processes are referred to as adsorption and desorption, respectively, and the volumes of total adsorbed target molecules are calculated at each incremental pressure. These pressures typically range

from 0.05–1.0 bar for low pressure analyses, and can reach up to 100 bar for high pressure analyses.

Adsorption/desorption isotherms can describe how much gas can be adsorbed within a PCP, as well as the nature in which it occurs. Gating effects can take place in materials with small pore apertures, which is illustrated by hysteresis of the desorption isotherm. Surface areas are also calculated from the adsorption isotherms of PCPs and are reported according to two different methods, Langmuir and Brunauer-Emmett-Teller (BET).[62] Calculations using the Langmuir method assume a single monolayer of coverage within the material, while the BET method takes into account the formation of multiple layers. It follows that Langmuir calculations always produce higher surface area values, but it is widely accepted that BET estimations are the most accurate due to the complexity of surface molecule binding and the unlikelihood of perfect monolayer formation.

To achieve efficient gas separation within a PCP, the material must possess compatible functionalities and/or pore dimensions that will selectively bind a target adsorbate within a mixture of gases while excluding all other species. A material can be utilized for gas separations by exploiting its adsorptive properties, its molecular sieving properties, or a combination of the two.[39,65] An adsorptive (thermodynamic) separation is based on a difference in affinity of the gas molecules toward the pore surfaces, while a molecular sieving (kinetic) separation is based on size exclusion effects induced by the physical properties of the PCP. A selective separation can be achieved by fine-tuning a material to include both size exclusion and selective adsorption properties for a desired mixture of gases.

Materials can also exhibit temperature- or pressure-dependent sorption and/or selectivity. This effect is illustrated in Figure 1.6 with the temperature-dependent

adsorption of acetylene and CO_2 within $Cu_2(pzdc)_2(pyz)$.[63] Flexible or interpenetrated PCPs can also be subject to temperature-dependent gating effects.[64] These materials can be fine-tuned to adsorb a target species, followed by a controlled release of the species upon a change in temperature.

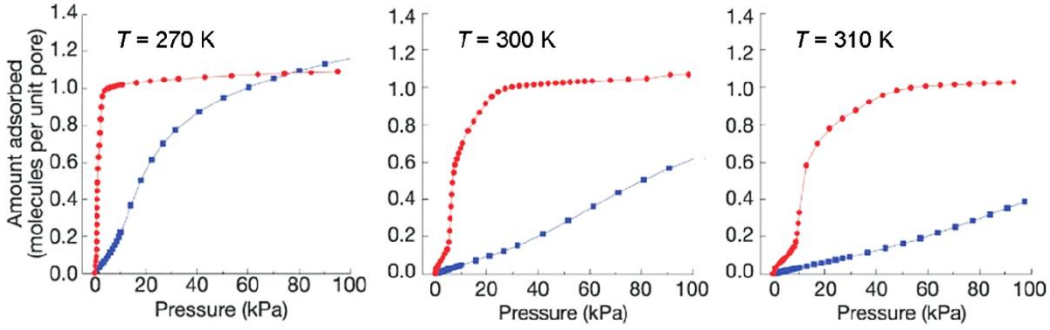

Figure 1.6: Adsorption isotherms illustrating the temperature-dependent selectivity of $Cu_2(pzdc)_2(pyz)$ for C_2H_2 (red) and CO_2 (blue).[63]

There are two methods used to define the adsorption capacity of a PCP. The *gravimetric capacity* refers to the amount of gas adsorbed per unit mass of the material, while the *volumetric capacity* refers to the amount of gas adsorbed per unit volume.[65] The latter also describes the packing density of the molecules within the material. Under low pressures ($\leq$ 1 bar), high adsorption capacities are primarily governed by the functionalities present on the pore surfaces, while the capacities at high pressures are largely dictated by the amount of available surfaces inside the material. This trend is illustrated by the highest CO_2 capacities to date in NU-100 (6143 $m^2\ g^{-1}$), MOF-200 (4530 $m^2\ g^{-1}$), and MOF-210 (6240 $m^2\ g^{-1}$), which adsorb 69.8, 73.9, and 74.2 wt % CO_2 at 298 K and 40, 50, and 50 bar, respectively.[23,24] However, Mg-MOF-74 adsorbs 68.9 wt % CO_2 at 287 K and 36 bar and possesses a markedly lower surface area of

1542 $m^2 g^{-1}$,[66] but this enhanced uptake is due to the availability open metal sites on the Mg(II) nodes, a phenomenon known to produce superior sorption capabilities.[67,68]

Another parameter used to describe the behavior of a material toward an adsorbate is enthalpy of adsorption (Q_{st}). The magnitude of Q_{st} describes the affinity of the pore surface of a material toward the adsorbate; high values denote a large release of energy upon the single, initial adsorption event, which is indicative of strong surface binding. In terms of gas storage, optimization of this parameter is crucial to providing a material that can effectively store a sufficient volume of gas without requiring an excessive amount of energy to expel it.

Q_{st} can be calculated by fitting a virial-type equation to two or more adsorption isotherms obtained at similar temperatures.[69] The $\ln(n/p)$ values for a given amount adsorbed (n) can then be calculated from the linear regressions of the virial equation analysis using the Equation 1:

$$ln(n/p) = A_0 + A_1 n + A_2 n^2 \qquad \text{(Equation 1)}$$

where p is pressure, n is amount adsorbed and A_0, A_1, *etc*. are virial coefficients. A_0 is related to the adsorbate-adsorbent interactions, while A_1 describes adsorbate-adsorbate interactions. The Henry's Law constant (K_H) is equal to $exp(A_0)$, and at low surface coverage, A_2 and higher terms can be ignored. Accordingly, a graph of $ln(n/p)$ versus n should give a straight line at low surface coverage. The virial method based on Equation 1 is preferred at low pressure because the linearity in the low pressure part of the isotherm provides direct confirmation of the accuracy of the interpolations. Also, the intercept of the graph gives A_0, where the Henry's Law constant $K_H = exp(A_0)$, which is a measure of the adsorbate surface interactions.

Carbon dioxide sequestration

Over the past several decades, much effort has been directed toward the development and utilization of alternative energy sources. The burning of coal and fossil fuels in automobiles and power plants results in increasing levels of atmospheric CO_2, releasing approximately 20 metric tons per capita in the United States per year.[70,71] Over 40 % of these emissions are due to electricity generation from coal- and natural gas-burning power plants.[72] This can negatively impact the environment by contributing to global warming and rising sea levels, as well as irreversibly increasing the acidity of sea water in the earth's oceans.[73] Accordingly, there has been increased interest for the development of CO_2 storage and sequestration materials in the field of PCPs.[74-77] Ideal candidates would exhibit a high selectivity for CO_2 over N_2, O_2, and H_2O, the most abundant components of flue gas emissions, and would be able to treat large volumes of gas while operating under ambient pressures and temperatures. A comprehensive review of the CO_2 adsorption capacities and selectivities of known PCPs, as well as the structural compositions and respective surface areas of each material, has been published by Sumida *et al*.[65]

Hydrogen storage

The decreasing supply of globally available fossil fuels has also generated considerable interest in hydrogen energy. Hydrogen is one of the most promising candidates for an alternative fuel source due to its high energy density and clean-burning emissions.[78] However, the feasibility of replacing fossil fuels with hydrogen gas in automobiles has yet to be realized. The amount of stored gas necessary to power a vehicle within the practical distance of 300 miles ranges between 5–13 kg,[79] which would require the use of large gas cylinders for pressurized gas or cryogenic liquid H_2 storage.

Both present unrealistic scenarios when refueling multiple times per day may be necessary. However, storage inside a PCP-packed gas cylinder can yield a considerably higher amount of stored H_2 within the same relative volume. Recently, a great deal of research has focused on the development of novel PCPs with unprecedented H_2 storage at ambient temperatures.[80-82] The 2017 DOE target for feasible H_2 storage within a PCP requires a gravimetric uptake of 5.5 wt%, a volumetric uptake of 40 g L^{-1}, and an operating temperature range of –40–60 °C with a maximum pressure of 100 atm.[83] A comprehensive review published by Lim and coworkers in 2012 details the impressive progress of high-capacity H_2 storage within the field of PCPs thus far.[79]

Molecular sensing

It is difficult to overstate the need for improved chemical sensors that can achieve lower limits of detection and tolerate a range of chemical environments. The demand for reliable, affordable, and portable sensors supports the development of many critical technologies that include medicine, environmental pollution control, food safety monitoring, and the detection of illicit substances and chemical weapons, among others.[84,85]

Chemical sensors provide analytical information about the chemical composition of a gaseous or liquid environment in a two-step process.[86-88] First, the target analyte species physically interacts with selective receptor sites in the sensor material, thus inducing a physical change in the state of the sensor. The analyte-sensor interactions should be reversible and can range from weak intermolecular interactions to the formation of strong chemical bonds. Second, the induced change in the sensor is converted into a measurable output signal. To date, the most popular mechanism

investigated for sensing by PCPs has relied on the monitoring of the solid-state luminescence modulation as a function of gas or liquid analyte interactions. These systems are each carefully designed to take advantage of certain physical properties that are unique to PCPs, which allows for a broad scope of chemical detection.

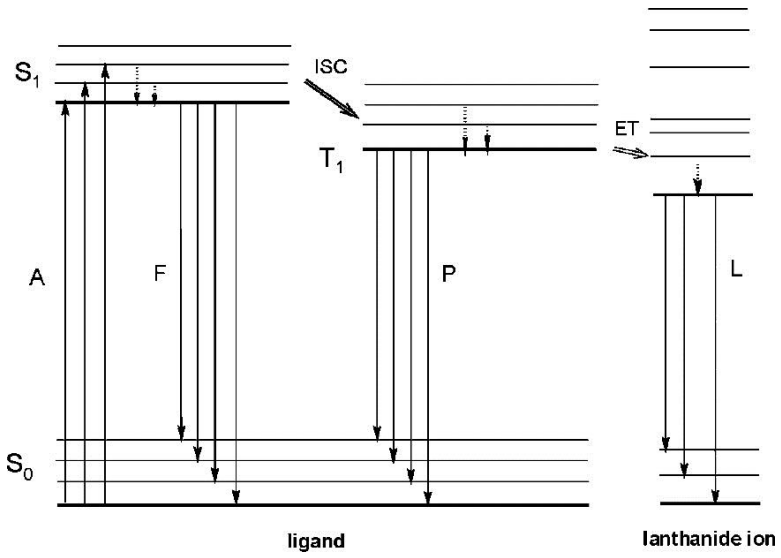

Figure 1.7: Schematic representation of photophysical processes in lanthanide(III) complexes (antenna effect). Abbreviations: A = absorption; F = fluorescence; P = phosphorescence; L = lanthanide-centered luminescence; S = singlet; T = triplet; ISC = intersystem crossing; ET = energy transfer. Full vertical lines indicate radiative transitions; dotted vertical lines indicate non-radiative transitions.[91]

Luminescence is the general term used to describe the process of light emission from a cold body, where photons are produced by processes other than heating.[89,90] Photoluminescence is the process by which light is emitted from a substance promoted by the prior absorption of incoming photons and is most relevant to the use of luminescent PCPs as sensor materials. Photoluminescence processes are usually further distinguished

as occurring *via* fluorescent or phosphorescent pathways (Figure 1.7).[91] Fluorescence is the process by which an incoming photon ($h\nu_{ex}$) excites an electron in a molecule to an excited state (S_1; Equation 2), followed by rapid (< 10 ns) relaxation of that electron back to its ground state (S_0) accompanied by emission of a secondary fluorescent photon ($h\nu_F$) (Figure 1.7, *left* and Equation 3). Notably, there is no change in the electron spin multiplicity during this process, which remains a singlet (*S*). Due to non-radiative (vibrational) energy losses, the energy of the emitted photon is lower than that of the incoming photon and the emission will be red shifted relative to the excitation wavelength. The fluorescence process is commonly summarized as:

Excitation: $S_0 + h\nu_{ex} \rightarrow S_1$ (Equation 2)

Emission: $S_1 \rightarrow S_0 + h\nu_F + \text{heat}$ (Equation 3)

In contrast, phosphorescence is a much slower emissive process that can occur over a period of microseconds, seconds, minutes or even hours.[42] The initial excitation is the same as that shown in Equation 2. However, instead of direct relaxation back to the ground state, the excited electron undergoes an intersystem crossing event (ISC) in which the electron undergoes a spin reversal into a triplet state (T_1) (Equation 4). The resulting T_1 electronic configuration must now relax back to an S_0 ground state (Figure 1.7, *center*). The relaxation is slower than fluorescence because a $T \rightarrow S$ transition is quantum mechanically forbidden. The relaxation is accompanied by emission of a phosphorescent photon ($h\nu_P$), which is typically of significantly lower energy than the incoming photon (Equation 5):

Excitation:	$S_0 + h\nu_{ex} \rightarrow S_1$	(Equation 2)
ISC:	$S_1 \rightarrow T_1$	(Equation 4)
Emission:	$T_1 \rightarrow S_0 + h\nu_{\mathrm{P}} + \mathrm{heat}$	(Equation 5)

A wide variety of compounds and materials exhibit photoluminescence because they have atomic or multi-body centers with electronic structures that are readily excited by incoming photons ($h\nu_{ex}$). These photons must possess energies comparable to the S_0–S_1 gap that occurs in the UV/visible portion of the electromagnetic spectrum. The luminescence efficiency of a given compound or material, otherwise known as its emissive quantum yield (φ), is a simple measure of the efficiency of a photoluminescent material based on the ratio of the number of photons emitted *versus* the number of photons absorbed. There are many factors that are known to affect the value of φ, as well as other related properties, such as the excited state lifetime, τ. These are beyond the scope of this discussion, but several detailed descriptions of chemical photoluminescence have been previously described.[84,92-95] Coordination compounds and organometallic complexes are often employed in photoluminescent devices because their electronic energy levels can be finely tuned by synthetic tailoring of the ligands, metals, and coordination modes. This allows not only for optimization of φ, but also tunability of the excitation and emission wavelengths and the lifetimes of the excited states.

Photoluminescence quenching results in a reduction in the overall luminescence intensity of a given material. Quenching is generally viewed as an unwanted effect in molecular systems and can be broadly defined as any non-radiative relaxation pathway that results in a reduction of the overall fluorescent and phosphorescent quantum yields. There are many causes of quenching, a common example of which is vibrational coupling of an excited state with neighboring molecules (*e.g.*, solvents), resulting in non-radiative

decay of the excited state.[96] Another common example is concentration-dependent quenching in the solid-state caused by *inter*-molecular energy transfer between closely-packed molecules. However, quenching can be exploited in PCPs for molecular sensing applications because the observed reduction of the luminescence intensity (or emission lifetime) may be proportional to the presence of a known quencher – thus providing a diagnostic signal.

With the above considerations in mind, there are a number of discernible reasons why PCPs are prime candidates for chemical sensing. The crystalline, periodic nature of PCPs results in structurally well-defined chemical moieties that are immobilized at regular intervals within the polymer networks. It is relatively straightforward to install a wide range of both organic and inorganic photoluminescent species into PCPs. As a result, their luminescence properties (φ, τ, $h\nu_{ex}$, $h\nu_{F}$, *etc.*) should be tunable, predictable, and easily optimizable. Furthermore, the inherent porosity and correspondingly high surface areas of PCPs make possible a number of additional opportunities that are not readily available to traditional amorphous inorganic complexes.[84] PCPs are generally obtained as microcrystalline powders with individual crystallites ranging between microns to millimeters in size. Therefore, the number of luminescent sensor receptor sites inside a given crystallite (and thus only accessible to analytes *via* the micropore structure) will always greatly dominate the number of equivalent sites on the crystallite exteriors. It follows that the PCP pore structures can be exploited to control which analytes are able to access the crystallite interiors. For example, using a given pore structure as a size- or chemically-selective filter assures that only certain analytes are permitted access to the pores, which results in a quantifiable sensor response. In this way, PCP sensors could be programmed with molecular specificity for diagnostic applications of complex mixtures of analytes without the need for prior separation or

purification steps. Microcrystalline PCPs are also mechanically robust, thus allowing for flexible processibility into various device formats.

It is appropriate to consider in more depth the types of chemical moieties that are useful in the construction of luminescent materials, and how these can be deliberately combined to create luminescent PCPs with multifunctional sensing capabilities. In isolation, metal ions are not commonly luminescent; only lanthanide ions and a few uranyl ($[UO_2]^{2+}$)-based complexes are luminescent.[97] The lanthanides, which generally exist as trivalent cations, each have their own unique emission spectra. However, only Sm(III), Eu(III), Tb(III) and Dy(III) display practically useful luminescence in the visible region of the electromagnetic spectrum. Most of the other Ln(III) ions are luminescent to varying degrees in the near-infrared (NIR) spectral region, and Gd(III) is emissive in the UV region.[84] Lanthanide-based luminescence has attracted much recent attention in advanced optics, partly because the spectral properties of Ln(III) ions are well defined and are not easily perturbed by external forces. This is because the 4*f* (valence) electrons that are involved in the optically-active transitions are contracted inside the radius of (and therefore shielded by) the filled $5s^2$ and $5p^6$ orbitals. As a result, Ln(III) ions do not engage in any substantial covalent bonding with ligands;[98] although they can be incorporated into a variety of charged ligands to form complexes, the stabilizing interactions are predominantly ionic and therefore the energy levels of the 4*f*-electrons remain largely unperturbed. This leads to inner shell 4*f*–4*f* transitions that are characteristically very sharp and easily identifiable (Figure 1.8).[99]

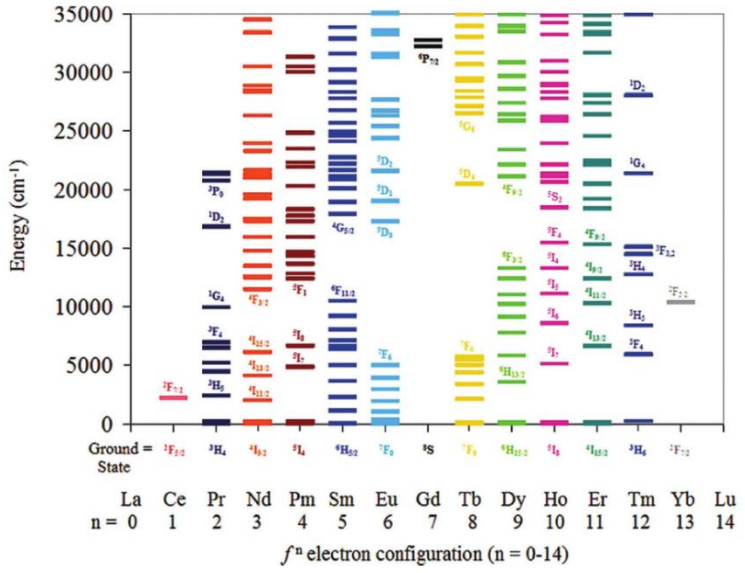

Figure 1.8: A summary of electronic excited-state energy levels for Ln(III) ions.[42]

Unfortunately, lanthanide luminescence is generally very weak for isolated Ln(III) ions because *f*–*f* transitions are classically forbidden. This issue can be overcome by coupling the Ln(III) ions to organic ligands that can facilitate energy transfer, a process commonly referred to as the antenna effect. The mechanism of this effect is summarized in Figure 1.7. First, light is absorbed by a conjugated organic ligand in close proximity to a Ln(III) ion to generate a T_1 excited state *via* the process of ISC. The energy of the excited state is transferred directly to the Ln(III) ion, which results in promotion of an electron to an excited state of the Ln(III) ion instead of resulting in ligand-based phosphorescence (ET; Figure 1.7). The 4*f*-centered excited state then undergoes radiative decay to the ground state.[42] The efficiency of this specific type of ligand-to-metal energy transfer is dependent on the relative energetic positions of the ligand and Ln(III) ion excited states, as well as strong vibronic coupling between the two

components. Therefore, it is important to ensure a good energy match between the ligand and Ln(III) ion excited states.

The development of improved Ln(III)-based organic materials is a topical field in its own right.[100] Specifically regarding PCP-based chemical sensors, the antenna effect presents an ideal opportunity to create more highly luminescent materials because Ln(III) ions are also able to act as the inorganic nodes. Classically, PCP chemistry has relied most heavily on the use of 3*d*-based metal ions as nodes, since they have somewhat predictable coordination geometries and numbers. The preparation of PCPs with desired structures using Ln(III) ions presents some additional challenges, due to the variable coordination numbers (6-12) and less defined geometries adopted by Ln(III) ions in complexes, which can result in the formation of denser, less porous materials.[101] However, recent research has shown that a careful choice of precursors can still result in stable, highly porous materials with associated luminescence quantum yields that compare to the best known molecular complexes.

PHOSPHINE COORDINATION MATERIALS (PCMS)

Over the past decade, a novel class of PCPs has been established based on the polymerization of organophosphine linkers. The development of Phosphine Coordination Materials (PCMs) was pioneered by the reaction of a *p*-carboxylated triphenylphosphine ($tctpH_3$) ligand and its subsequent phosphine oxide and methyl phosphonium derivatives with Zn(II) metal precursors. Reaction of $tctpH_3$ with $Zn(OAc)_2$ under slightly varied synthetic conditions (*e.g.* solvent composition and pH) yielded the first 2-dimensional materials, PCMs 1-3, which possessed remarkably similar crystal structures.[102] PCM-1 was composed of 3,3-connected hexagonal sheets containing single, tetrahedral Zn(II)

atoms capped by dimethylamine, generated *in situ*. The addition of pyrazine to the synthetic mixture prior to heating led to the formation of PCM-2, which contained pairs of 6,3-connected hexagonal sheets fused face-to-face *via* $Zn_4(OH)_2$ nodes. PCM-3 was virtually identical to PCM-2, but the substitution of ethylene diamine (en) for pyrazine produced the more ordered $Zn_4(OH)_2(en)_2$ metal clusters (Figure 1.9). Interestingly, all three materials were resistant to oxidation under aerobic synthetic conditions and resist decomposition at temperatures below 400 °C.

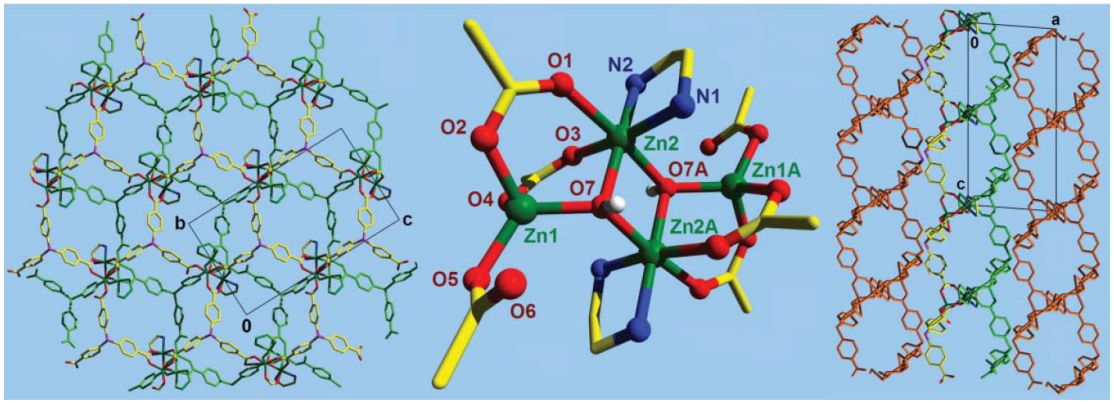

Figure 1.9: *(Left)* A single bilayer sheet of PCM-3 with $Zn_4(OH)_2$ clusters located on the inside of the bilayer; the relationship between PCM-2 and PCM-3 and two fused equivalents of PCM-1 is shown using full color and green to distinguish between the two sides of the bilayer; *(center)* connectivity within a single $Zn_4(OH)_2$ cluster in ethylene diamine-containing PCM-3; *(right)* view in the *ac* plane for PCM-3 showing the close-packed array of bilayers.

PCM-4 was developed by the *in situ* oxidation of $tctpH_3$ and subsequent reaction with $Zn(OAc)_2$ to produce a 3-dimensional, doubly interpenetrated PCP with phosphine oxide ($tctpo^{3-}$) moieties.[103] Oddly, the material could not be produced by the direct

reaction of the phosphine oxide ($tctpoH_3$) ligand with $Zn(OAc)_2$ under identical synthetic conditions. PCM-4 exhibits irreversible, hysteretic sorption of N_2, O_2, and Ar at 77, 90, and 87 K, respectively, shown from cyclic re-adsorption measurements. However, this effect could be reversed at 196 K, which is indicative of temperature-dependent gas trapping within the material.

PCMs 5-9 were synthesized from the *pre*-synthetically modified methyl-phosphonium (Me-$tctp^+H_3$) ligand and Zn(II) salts, yielding five topologically distinct materials.[102,104] PCM-5 was formed by the reaction of $Zn(NO_3)_2$ with Me-$tctp^+H_3$ upon the addition of 1 M KOH. Under identical synthetic conditions, and by altering the Zn(II) source, the formation of four structurally unique frameworks was made possible solely by varying the source of the OH^- ions. The addition of 1 M LiOH, NaOH, KOH, or CsOH to solutions of Me-$tctp^+H_3$ and $Zn(OAc)_2$ produced PCM-6, PCM-7, PCM-8, and PCM-9, respectively. An isostructural analog of PCM-8 can be formed by the addition of RbOH, however, all four materials possess different crystallographic features, internal surface areas, and gas sorption properties (Figure 1.10).

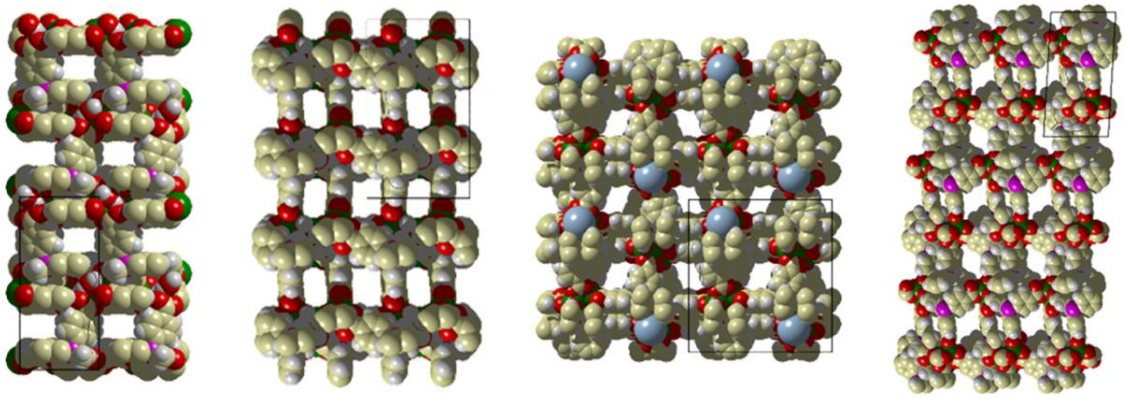

Figure 1.10: Space-filling models of PCM-6 (Li), PCM-7 (Na^+), PCM-8 (K^+ or Rb^+), and PCM-9 (Cs^+), shown from left to right.

PCM-10 was developed by the polymerization of $tctpH_3$ with $Ca(OH)_2$.[105] The phosphine sites remain uncoordinated within in the pores of the material, similar to PCMs 1-3, but the 3-dimensionality of PCM-10 led to superior chemical and thermal stabilities compared to the earlier PCMs. Accordingly, its solid-state properties have been extensively explored. *Post*-synthetic modification with Me_2SAuCl, H_2O_2, and MeI led to the formation of the corresponding Cl-Au-PCM-10, O=PCM-10, and [Me-PCM-10]I materials, as well as anion exchange of the latter with [*n*-Bu_4N]BF_4, [*n*-Bu_4]PF_6, and [*n*-Bu_4N]F to afford [Me-PCM-10]BF_4, [Me-PCM-10]PF_6, and [Me-PCM-10]F, respectively.[106] Adsorption/desorption isotherms illustrated the ability of *post*-synthetic modification to fine-tune the CO_2 capacities of each material at 196 K, as well as how the addition of a soft, catalytic metal could drastically increase the amount of adsorbed H_2 at 77 K, from 69.5 to 525 $cm^3\ g^{-1}$ in PCM-10 and Cl-Au-PCM-10, respectively.

The second material composed of phosphine oxide linkers was synthesized by the direct reaction of *tris*(*p*-carboxylated)triphenyl-phosphine oxide ($tctpoH_3$) with $Mg(OH)_2$ under slightly basic conditions.[107] PCM-11 is a thermally-robust 3-dimensional PCP

whose structure and gas sorption properties will be discussed at length in Chapter 2 of this dissertation. Lastly, PCM-12 was also synthesized from $Mg(OH)_2$ but utilized the free phosphine of the $tctpH_3$ ligand, similar to PCM-10. This 6,3-connected material contains 2-dimensional sheets with Mg(II) trimers linked by a μ^3-OH_2 group. Although PCM-12 is thermally stable up to 500 °C, desolvation that occurs under lower temperatures produces irreversible collapse of the framework lattice.

Following the development of the first twelve PCMs, an array of new materials have been constructed *via* polymerization of $tctpH_3$, $tctpoH_3$, and Me-$tctp^+H_3$ with Ca(II), Mg(II), and lanthanide(III) metal precursors.[108-112] A new monophosphine linker has been synthesized by reaction of *p*-iodobenzoic acid with $tctpH_3$ to produce a tetrahedral phosphonium zwitterion, $tctp^+H_3$, along with a *bis*(phosphine) ligand developed from a synthetic route analogous to that of $tctpH_3$.[34] These novel linkers have been reacted with trivalent lanthanides and divalent 3*d* transition metals, respectively, to afford materials with interesting solid-state applications that will be detailed in Chapters 3 and 4. To date, PCMs have shown promise in the areas of high pressure CO_2 storage,[107] molecular sensing,[109,110] magnetism,[112] and heterogeneous catalysis.[34,105]

Benefits of phosphine linkers

Organophosphine linkers offer several advantages over the more commonly used linear linkers (*e.g.* 1,4-benzenedicarboxylic acid, 4,4'-biphenyldicarboxylic acid, 4,4'-bipyridine, *etc.*) or flat linkers (*e.g.* 1,3,5-benzenetricarboxylic acid, 4,4',4"-benzene-1,3,5-triyl-benzoic acid, *etc.*) often utilized in PCPs. The tetrahedral electronic geometry of the phosphine site produces ligands that are inherently 3-dimensional, which have been known to promote the formation of 3-dimensional materials upon

polymerization. Although this degree of synthetic control is never guaranteed, the majority of the synthesized PCMs to date are 3-dimensional in nature.

Additionally, because phosphorus acts as a connector (node) between aromatic rings, incorporation of a *P*-node effectively replaces a portion of the metal atoms used for polymerization (Figure 1.11). This produces materials with lower densities, which is advantageous for incorporation of PCPs into working devices, particularly for gas cylinders.

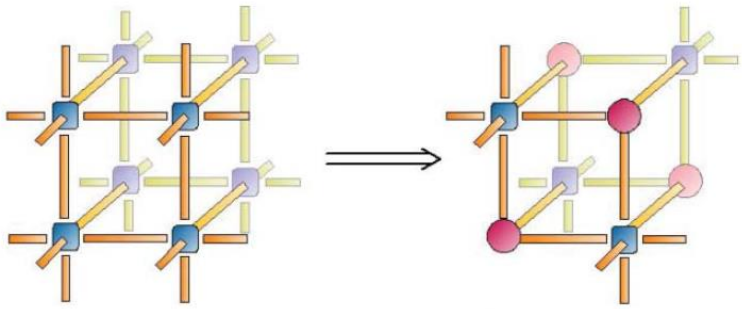

Figure 1.11: Comparison between a 6,6-connected cubic net *(left)* and the 6,3-connected phosphine analog *(right)*. Blue = metal nodes; pink = phosphorus atoms; orange = organic linkers.

Phosphorus also provides a "soft" binding site for *pre*- or *post*-synthetic functionalization with single atoms (chalcogens), aliphatic or aromatic hydrocarbons, or catalytically-active metal species. This allows for direct tunability of the internal pore surfaces away from the polymerization sites, which are commonly composed of "hard" metal nodes.

Modification of the phosphine site

Although the organophosphorus linkers are initially synthesized as free phosphines, *i.e.* the phosphorus atom possesses a lone pair of electrons, a majority of the subsequent PCMs contain functionalized phosphine sites. PCMs 1-3, 10, 12, and 22 are synthesized from the $tctpH_3$ ligand and are the only materials that retain the free phosphine site upon polymerization; all other PCMs either undergo *in situ* oxidation or utilize a *pre*-synthetically modified ligand. It is worth mentioning that the free phosphine sites within PCM-10 have been modified *post*-synthetically with a number of reagents to produce functionalized Cl-Au-PR_3, O=PR_3, and Me-PR_3 species within the pores of the material (R = *p*-$C_6H_4CO_2^-$). However, the variability of P(III) → P(V) chemistry allows for the incorporation of organic and inorganic species into the resulting PCPs both *pre*- and *post*-synthetically, which can directly affect the solid state-properties of the each material.

Reaction of hydrogen peroxide with lithium carboxylate salts, *e.g.* $tctpLi_3$ and BBCB-Li_4, under aqueous conditions affords the corresponding phosphine oxides. Protonation with HCl to pH = 3 yields the respective free acid (–CO_2H) phosphine oxide ligands, O=$tctpH_3$ and BBCB(=O)$_2$, in near-quantitative yields. Similarly, reaction of aqueous $tctpLi_3$ with S_8 or Se, followed by protonation with HCl, has afforded the respective S=$tctpH_3$ and Se=$tctpH_3$ ligands. While BBCB(=O)$_2$ has yet to be incorporated into a PCM, the O=$tctpH_3$, S=$tctpH_3$, and Se=$tctpH_3$ ligands have all been successfully polymerized (Figure 1.12).

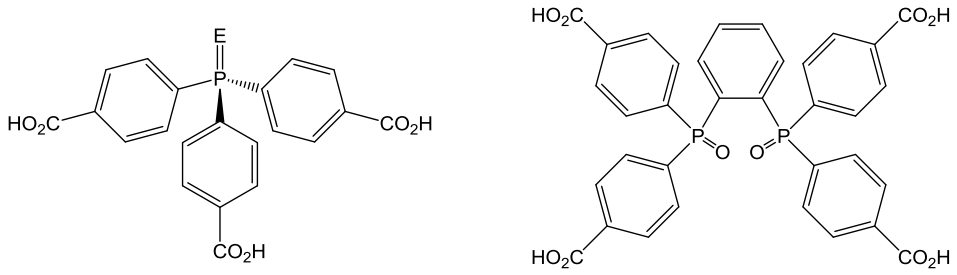

Figure 1.12: Structures of the *pre*-synthetically modified $tctpH_3$ *(left)* and BBCB *(right)* ligands. E = O, S, or Se.

Reaction of $tctpLi_3$ with methyl iodide in a biphasic H_2O:CH_2Cl_2 system at room temperature afforded the first of five phosphonium salts based on the $tctpH_3$ ligand. Vigorous stirring of this reaction produced an emulsion and allowed the hydrophilic and hydrophobic components to react, which was followed by protonation of the aqueous layer with HCl to yield the [Me-$tctp^+H_3$]Cl ligand. [Et-$tctp^+H_3$]Cl was synthesized in a similar manner by reaction of $tctpLi_3$ with ethyl iodide in a biphasic H_2O:THF system at 45 °C, followed by the removal of THF *in vacuo* and subsequent protonation of the aqueous solution with HCl. Propyl iodide and *sec*-butyl iodide have been also reacted with $tctpLi_3$ in a H_2O:MeCN (1:3) solution at 75 °C, followed by the removal of MeCN *in vacuo* and protonation with HCl, to afford the [Pr-$tctp^+H_3$]Cl and [*s*-Bu-$tctp^+H_3$]Cl ligands, respectively. Polymerization of these four phosphonium salts will result in the presence of hydrophobic moities inside the pores of the resulting PCMs, ranging in size from one to four carbons (Figure 1.13). This can influence the gas and vapor sorption properties, molecular sensing capabilities, and/or catalytic activities of the materials. Specifically, polymerization of [*s*-Bu-$tctp^+H_3$]Cl could lead to the development of a chiral PCM that could be used for chiral separations and/or chiral catalysis.

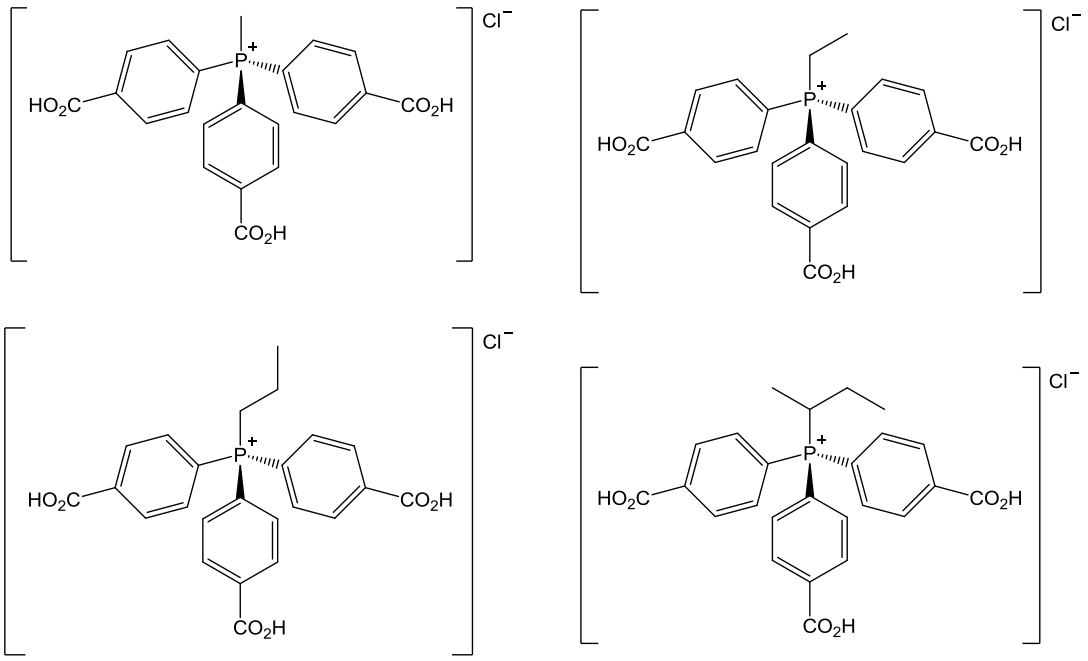

Figure 1.13: Structures of the *pre*-synthetically modified [Me-tctp^{+}H$_3$]Cl, [Et-tctp^{+}H$_3$]Cl, [*s*-Bu-tctp^{+}H$_3$]Cl, and [Pr-tctp^{+}H$_3$]Cl ligands (shown clockwise from the top left).

While the aforementioned phosphonium salts contain modifications that affect the chemical environment inside of the pores, a fifth ligand was synthesized with the specific intention of changing the connectivity of the linker itself. Tetraphenylphosphonium halides are well-known,[113-115] and the addition of carboxylic acids to the aromatic rings would allow for polymerization into a PCM. The synthesis of a tetrahedral *p*-carboxylated tetraphenylphosphonium salt was achieved by the Pd(II)-catalyzed reaction of tctpH$_3$ with *p*-iodobenzoic acid. This afforded the phosphonium zwitterion, tctp^{+}H$_3$, which effectively contained a 4-connected *P*-node following deprotonation of all

four carboxylic acid groups (Figure 1.14). This highly-symmetric linker is capable of producing highly-symmetric PCPs, including those with a 4,4-connected diamond-like topology.[116-118]

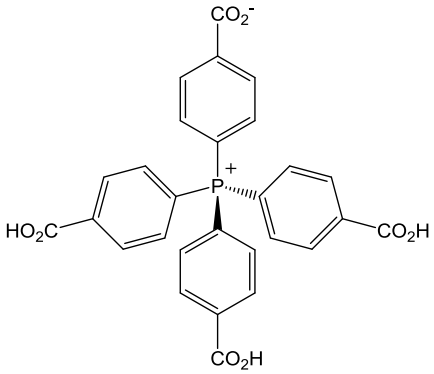

Figure 1.14: Structure of the *pre*-synthetically modified tctp$^{+}H_3$ ligand.

Lastly, the *pre*-synthetic modification of *bis*(phosphine) (BBCB) and PCP-pincer ligands with catalytic metals has been carried out by reaction with (COD)MCl_2 (M = Pd, Pt) precursors in THF under low-temperature conditions. The free-acid complexes of BBCB-$PdCl_2$, BBCB-$PtCl_2$, and PCP-PdCl were obtained in near-quantitative yields and can provide square planar M(II) moieties with available d_{z^2} orbitals within the pores of a material (Figure 1.15). PCMs based on these linkers could potentially be used for gas storage, gas separations, and heterogeneous catalysis.

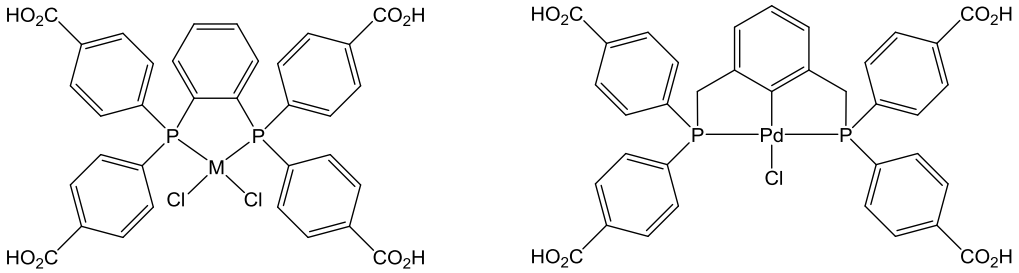

Figure 1.15: Structures of the *pre*-synthetically modified BBCB-MCl_2 (M = Pd, Pt) *(left)* and PCP-PdCl *(right)* ligands.

The ligands discussed above, coupled with the availability of a broad range of metal precursors, have allowed for the development of a diverse class of PCPs with novel topologies, pore functionalities, and solid-state properties.

REFERENCES

[1] H. Furukawa, K. E. Cordova, M. O'Keeffe, O. M. Yaghi, *Science* **2013**, *341*, 974.

[2] S. Kitagawa, R. Kitaura, S. Noro, *Angew. Chem. Int. Ed.* **2004**, *43*, 2334.

[3] P. Venuto, *Microporous Mater.* **1994**, *2*, 297.

[4] D. W. Breck, *Zeolite Molecular Sieves: Structure, Chemistry, and Use*, Wiley, New York, **1974**.

[5] J. Smith, *Chem. Rev.* **1988**, *88*, 149.

[6] P. Bénard, R. Chahine, *Langmuir* **2001**, *17*, 1950.

[7] N. Texier-Mandoki, J. Dentzer, T. Piquero, S. Saadallah, P. David, C. Vix-Guterl, *Carbon* **2004**, *42*, 2744.

[8] B. Hoskins, R. Robson, *J. Am. Chem. Soc.* **1990**, *112*, 1546.

[9] O. Yaghi, H. Li, *J. Am. Chem. Soc.* **1995**, *117*, 10401.

[10] H. Li, M. Eddaoudi, T. L. Groy, O. M. Yaghi, *J. Am. Chem. Soc.* **1998**, *120*, 8571.

[11] M. Kondo, T. Yoshitomi, K. Seki, H. Matsuzaka, S. Kitagawa, *Angew. Chem. Int. Ed.* **1997**, *36*, 1725.

[12] O. M. Yaghi, M. O'Keeffe, N. W. Ockwig, H. K. Chae, M. Eddaoudi, J. Kim, *Nature* **2003**, *423*, 705.

[13] H. Furukawa, J. Kim, N. W. Ockwig, M. O'Keeffe, O. M. Yaghi, *J. Am. Chem. Soc.* **2008**, *130*, 11650.

[14] D. J. Tranchemontagne, J. L. Mendoza-Cortés, M. O'Keeffe, O. M. Yaghi, *Chem. Soc. Rev.* **2009**, *38*, 1257.

[15] M. O'Keeffe, O. M. Yaghi, *Chem. Rev.* **2012**, *112*, 675.

[16] J. J. P. Iv, J. A. Perman, M. J. Zaworotko, *Chem. Soc. Rev.* **2009**, *38*, 1400.

[17] A. Rabenau, *Angew. Chem. Int. Ed. Engl.* **1985**, *24*, 1026.

[18] N. Stock, S. Biswas, *Chem. Rev.* **2012**, *112*, 933.

[19] H. Deng, S. Grunder, K. E. Cordova, C. Valente, H. Furukawa, M. Hmadeh, F. Gandara, A. C. Whalley, Z. Liu, S. Asahina, H. Kazumori, M. O'Keeffe, O. Terasaki, J. F. Stoddart, O. M. Yaghi, *Science* **2012**, *336*, 1018.

[20] O. K. Farha, I. Eryazici, N. C. Jeong, B. G. Hauser, C. E. Wilmer, A. A. Sarjeant, R. Q. Snurr, S. T. Nguyen, A. O. Yazaydin, J. T. Hupp, *J. Am. Chem. Soc.* **2012**, *134*, 15016.

[21] G. Ferey, C. Mellot-Draznieks, C. Serre, F. Millange, J. Dutour, S. Surble, I. Margiolaki, *Science* **2005**, *309*, 2040.

[22] K. Koh, A. G. Wong-Foy, A. J. Matzger, *J. Am. Chem. Soc.* **2009**, *131*, 4184.

[23] H. Furukawa, N. Ko, Y. B. Go, N. Aratani, S. B. Choi, E. Choi, A. O. Yazaydin, R. Q. Snurr, M. O'Keeffe, J. Kim, O. M. Yaghi, *Science* **2010**, *329*, 424.

[24] O. K. Farha, A. O. Yazaydin, I. Eryazici, C. D. Malliakas, B. G. Hauser, M. G. Kanatzidis, S. T. Nguyen, R. Q. Snurr, J. T. Hupp, *Nat. Chem.* **2010**, *2*, 944.

[25] H. Furukawa, Y. B. Go, N. Ko, Y. K. Park, F. J. Uribe-Romo, J. Kim, M. O'Keeffe, O. M. Yaghi, *Inorg. Chem.* **2011**, *50*, 9147.

[26] K. S. Park, Z. Ni, A. P. Cote, J. Y. Choi, R. Huang, F. J. Uribe-Romo, H. K. Chae, M. O'Keeffe, O. M. Yaghi, *Proc. Natl. Acad. Sci. U. S. A.* **2006**, *103*, 10186.

[27] J. H. Cavka, S. Jakobsen, U. Olsbye, N. Guillou, C. Lamberti, S. Bordiga, K. P. Lillerud, *J. Am. Chem. Soc.* **2008**, *130*, 13850.

[28] O. K. Farha, J. T. Hupp, *Acc. Chem. Res.* **2010**, *43*, 1166.

[29] A. Y. Robin, K. M. Fromm, *Coord. Chem. Rev.* **2006**, *250*, 2127.

[30] Z. Wang, S. M. Cohen, *Chem. Soc. Rev.* **2009**, *38*, 1315.

[31] A. D. Burrows, C. G. Frost, M. F. Mahon, C. Richardson, *Angew. Chem. Int. Ed.* **2008**, *47*, 8482.

[32] Z. Wang, K. K. Tanabe, S. M. Cohen, *Chem. Eur. J.* **2010**, *16*, 212.

[33] V. Valtchev, G. Majano, S. Mintova, J. Perez-Ramirez, *Chem. Soc. Rev.* **2013**, *42*, 263.

[34] A. M. Bohnsack, I. A. Ibarra, V. I. Bakhmutov, V. M. Lynch, S. M. Humphrey, *J. Am. Chem. Soc.* **2013**, *135*, 16038.

[35] B. L. Chen, C. D. Liang, J. Yang, D. S. Contreras, Y. L. Clancy, E. B. Lobkovsky, O. M. Yaghi, S. Dai, *Angew. Chem. Int. Ed.* **2006**, *45*, 1390.

[36] B. Chen, S. Ma, F. Zapata, F. R. Fronczek, E. B. Lobkovsky, H. -C. Zhou, *Inorg. Chem.* **2007**, *46*, 1233.

[37] J. -R. Li, R. J. Kuppler, H. -C. Zhou, *Chem. Soc. Rev.* **2009**, *38*, 1477.

[38] H. Furukawa, O. M. Yaghi, *J. Am. Chem. Soc.* **2009**, *131*, 8875.

[39] J. -R. Li, J. Sculley, H. -C. Zhou, *Chem. Rev.* **2012**, *112*, 869.

[40] M. D. Allendorf, C. A. Bauer, R. K. Bhakta, R. J. T. Houk, *Chem. Soc. Rev.* **2009**, *38*, 1330.

[41] B. Chen, S. Xiang, G. Qian, *Accounts Chem. Res.* **2010**, *43*, 1115.

[42] Y. Cui, Y. Yue, G. Qian, B. Chen, *Chem. Rev.* **2012**, *112*, 1126.

[43] Z. Hu, B. J. Deibert, J. Li, *Chem. Soc. Rev.* **2014**, *43*, 5815.

[44] L. E. Kreno, K. Leong, O. K. Farha, M. Allendorf, R. P. Van Duyne, J. T. Hupp, *Chem. Rev.* **2012**, *112*, 1105.

[45] E. Coronado, G. Minguez Espallargas, *Chem. Soc. Rev.* **2013**, *42*, 1525.

[46] M. -C. Dul, E. Pardo, R. Lescouëzec, Y. Journaux, J. Ferrando-Soria, R. Ruiz-García, J. Cano, M. Julve, F. Lloret, D. Cangussu, C. L. M. Pereira, H. O. Stumpf, J. Pasán, C. Ruiz-Pérez, *Coord. Chem. Rev.* **2010**, *254*, 2281.

[47] H. A. Habib, J. Sanchiz, C. Janiak, *Inorg. Chim. Act.* **2009**, *362*, 2452.

[48] M. Kurmoo, *Chem. Soc. Rev.* **2009**, *38*, 1353.

[49] J. Della Rocca, D. Liu, W. Lin, *Accounts Chem. Res.* **2011**, *44*, 957.

[50] P. Horcajada, T. Chalati, C. Serre, B. Gillet, C. Sebrie, T. Baati, J. F. Eubank, D. Heurtaux, P. Clayette, C. Kreuz, J. -S. Chang, Y. K. Hwang, V. Marsaud, P. -N. Bories, L. Cynober, S. Gil, G. Ferey, P. Couvreur, R. Gref, *Nat. Mater.* **2010**, *9*, 172.

[51] P. Horcajada, R. Gref, T. Baati, P. K. Allan, G. Maurin, P. Couvreur, G. Ferey, R. E. Morris, C. Serre, *Chem. Rev.* **2012**, *112*, 1232.

[52] W. J. Rieter, K. M. Pott, K. M. L. Taylor, W. Lin, *J. Am. Chem. Soc.* **2008**, *130*, 11584.

[53] K. M. L. Taylor-Pashow, J. Della Rocca, Z. Xie, S. Tran, W. Lin, *J. Am. Chem. Soc.* **2009**, *131*, 14261.

[54] N. C. Jeong, B. Samanta, C. Y. Lee, O. K. Farha, J. T. Hupp, *J. Am. Chem. Soc.* **2012**, *134*, 51.

[55] X. Liang, F. Zhang, W. Feng, X. Zou, C. Zhao, H. Na, C. Liu, F. Sun, G. Zhu, *Chem. Sci.* **2013**, *4*, 983.

[56] A. Shigematsu, T. Yamada, H. Kitagawa, *J. Am. Chem. Soc.* **2011**, *133*, 2034.

[57] G. K. H. Shimizu, J. M. Taylor, S. Kim, *Science* **2013**, *341*, 354.

[58] A. Corma, H. Garcia, F. X. L. I. Llabres i Xamena, *Chem. Rev.* **2010**, *110*, 4606.

[59] D. Farrusseng, S. Aguado, C. Pinel, *Angew. Chem. Int. Ed.* **2009**, *48*, 7502.

[60] J. Lee, O. K. Farha, J. Roberts, K. A. Scheidt, S. T. Nguyen, J. T. Hupp, *Chem. Soc. Rev.* **2009**, *38*, 1450.

[61] M. Yoon, R. Srirambalaji, K. Kim, *Chem. Rev.* **2012**, *112*, 1196.

[62] W. Lu, Z. Wei, Z. -Y. Gu, T. -F. Liu, J. Park, J. Park, J. Tian, M. Zhang, Q. Zhang, T. Gentle, M. Bosch, H. -C. Zhou, *Chem. Soc. Rev.* **2014**, *43*, 5561.

[63] Matsuda, R. Kitaura, S. Kitagawa, Y. Kubota, R. V. Belosludov, T. C. Kobayashi, H. Sakamoto, T. Chiba, M. Takata, Y. Kawazoe, Y. Mita, *Nature* **2005**, *436*, 238.

[64] D. Zhao, D. Yuan, R. Krishna, J. M. van Baten, H. -C. Zhou, *Chem. Commun.* **2010**, *46*, 7352.

[65] K. Sumida, D. L. Rogow, J. A. Mason, T. M. McDonald, E. D. Bloch, Z. R. Herm, T. -H. Bae, J. R. Long, *Chem. Rev.* **2012**, *112*, 724.

[66] P. D. C. Dietzel, V. Besikiotis, R. Blom, *J. Mater. Chem.* **2009**, *19*, 7362.

[67] A. Mallick, S. Saha, P. Pachfule, S. Roy, R. Banerjee, *J. Mater. Chem.* **2010**, *20*, 9073.

[68] S. R. Caskey, A. G. Wong-Foy, A. J. Matzger, *J. Am. Chem. Soc.* **2008**, *130*, 10870.

[69] I. P. O'koye, M. Benham, K. M. Thomas, *Langmuir* **1997**, *13*, 4054.

[70] D. Leaf, H. J. H. Verolme, W. F. Hunt, *Environ. Int.* **2003**, *29*, 303.

[71] M. Tucker, *Ecol. Econ.* **1995**, *15*, 215.

[72] U.S. Environmental Protection Agency: http://www.epa.gov/climatechange/emissions/co2_human.html

[73] R. K. Pachauri, A. Reisinger, Eds., *Climate Change 2007: Synthesis Report*, IPCC, Geneva, Switzerland, **2008**.

[74] D. M. D'Alessandro, B. Smit, J. R. Long, *Angew. Chem. Int. Ed.* **2010**, *49*, 6058.

[75] J. -R. Li, Y. Ma, M. C. McCarthy, J. Sculley, J. Yu, H. -K. Jeong, P. B. Balbuena, H. -C. Zhou, *Coord. Chem. Rev.* **2011**, *255*, 1791.

[76] M. Nandi, H. Uyama, *Chem. Rec.* **2014**, *14*, 1134.

[77] A. Phan, C. J. Doonan, F. J. Uribe-Romo, C. B. Knobler, M. O'Keeffe, O. M. Yaghi, *Accounts Chem. Res.* **2010**, *43*, 58.

[78] L. J. Murray, M. Dinca, J. R. Long, *Chem. Soc. Rev.* **2009**, *38*, 1294.

[79] M. P. Suh, H. J. Park, T. K. Prasad, D. -W. Lim, *Chem. Rev.* **2012**, *112*, 782.

[80] B. Kesanli, Y. Cui, M. R. Smith, E. W. Bittner, B. C. Bockrath, W. B. Lin, *Angew. Chem. Int. Ed.* **2005**, *44*, 72.

[81] D. J. Collins, H. -C. Zhou, *J. Mater. Chem.* **2007**, *17*, 3154.

[82] M. Dinca, J. R. Long, *Angew. Chem. Int. Ed.* **2008**, *47*, 6766.

[83] http://www1.eere.energy.gov/hydrogenandfuelcells/storage/current_technology.html

[84] J. -M. Zhou, W. Shi, N. Xu, P. Cheng, *Inorg. Chem.* **2013**, *52*, 8082.

[85] J. J. Perry IV, C. A. Bauer, M. D. Allendorf, *Metal-Organic Frameworks*, Wiley-VCH, Weinheim, **2011**, Chapter 12, pp. 267-308.

[86] G. Korotcenkov, *Chemical Sensors*, Momentum Press, New York, vol. 6, **2011**.

[87] P.-I. Gouma, *Nanomaterials for Chemical Sensors and Biotechnology*, Pan Stanford Publishing, Singapore, **2009**.

[88] P. Gründler, *Chemical Sensors*, Springer, Berlin, **2010**.

[89] L. Prodi, M. Montalti ,N. Zaccheroni, Eds., *Luminescence Applied in Sensor Science*, Springer, **2013**.

[90] R. C. Ropp, *Luminescence and the Solid State*, Elsevier Science, Amsterdam, 2 edition, **2004**.

[91] K. Binnemans, *Chem. Rev.* **2009**, *109*, 4283.

[92] V. Balzani, *Supramolecular Photochemistry*, D. Reidel Publishing Company, Anacapri, **1987**.

[93] N. J. Turro, J. C. Scaiano, V. Ramamurthy, *Modern Molecular Photochemistry of Organic Molecules*, University Science Books, Sausalito, **2010**.

[94] V. Ramamurthy, Y. Inoue, Eds., *Supramolecular Photochemistry: Controlling Photochemical Processes*, Wiley, Hoboken, **2011**.

[95] V. Ramamurthy, K. S. Schanze, *Solid State and Surface Photochemistry*, CRC Press, New York, **2000**.

[96] T. J. Penfold, S. Karlsson, G. Capano, F. A. Lima, J. Rittmann, M. Reinhard, M. H. Rittmann-Frank, O. Braem, E. Baranoff, R. Abela, I. Tavernelli, U. Rothlisberger, C. J. Milne, M. Chergui, *J. Phys. Chem. A*, **2013**, *117*, 4591.

[97] A. P. Demchenko, *Introduction to Fluorescence Sensing*, Springer, Netherlands, **2008**.

[98] E. G. Moore, A. P. S. Samuel, K. N. Raymond, *Acc. Chem. Res.*, **2009**, *42*, 542.

[99] S. V. Eliseeva, J. -C. G. Bünzli, *Chem. Soc. Rev.* **2009**, *39*, 189.

[100] Z. Liu, W. He, Z. Guo, *Chem. Soc. Rev.* **2013**, *42*, 1568.

[101] J. Rocha, L. D. Carlos, F. A. Almeida Paz, D. Ananias, *Chem. Soc. Rev.* **2011**, *40*, 926.

[102] S. M. Humphrey, P. K. Allan, S. E. Oungoulian, M. S. Ironside, E. R. Wise, *Dalton Trans.* **2009**, 2298.

[103] S. M. Humphrey, S. E. Oungoulian, J. W. Yoon, Y. K. Hwang, E. R. Wise, J. -S. Chang, *Chem. Commun.* **2008**, 2891.

[104] N. W. Waggoner, P. K. Allan, T. Kornfuehrer, S. M. Humphrey, *manuscript in prep.*

[105] A. J. Nunez, L. N. Shear, N. Dahal, I. A. Ibarra, J. Yoon, Y. K. Hwang, J. -S. Chang, S. M. Humphrey, *Chem. Commun.* **2011**, *47*, 11855.

[106] A. J. Nunez, M. S. Chang, I. A. Ibarra, S. M. Humphrey, *Inorg. Chem.* **2014**, *53*, 282.

[107] A. M. Bohnsack, I. A. Ibarra, P. W. Hatfield, J. W. Yoon, Y. K. Hwang, J. -S. Chang, S. M. Humphrey, *Chem. Commun.* **2011**, *47*, 4899.

[108] I. A. Ibarra, K. E. Tan, V. M. Lynch, S. M. Humphrey, *Dalton Trans.* **2012**, *41*, 3920.

[109] I. A. Ibarra, T. W. Hesterberg, B. J. Holliday, V. M. Lynch, S. M. Humphrey, *Dalton Trans.* **2012**, *41*, 8003.

[110] I. A. Ibarra, T. W. Hesterberg, J. -S. Chang, J. W. Yoon, B. J. Holliday, S. M. Humphrey, *Chem. Commun.* **2013**, *49*, 7156.

[111] I. A. Ibarra, J. W. Yoon, J. -S. Chang, S. K. Lee, V. M. Lynch, S. M. Humphrey, *Inorg. Chem.* **2012**, *51*, 12242.

[112] N. W. Waggoner, B. Saccoccia, I. A. Ibarra, V. M. Lynch, P. T. Wood, S. M. Humphrey, *Inorg. Chem.* **2014**, *53*, 12674.

[113] H. H. Willard, L. R. Perkins, *Anal. Chem.* **1953**, *25*, 1634.

[114] G. W. Kaatz, S. M. Seo, *J. Antimicrob. Chemother.* **2004**, *54*, 364.

[115] D. Marcoux, A. B. Charette, *J. Org. Chem.* **2008**, *73*, 590.

[116] H.-D. Guo, D.-F. Qiu, X.-M. Guo, G.-L. Zheng, X. Wang, S. Dang, H.-J. Zhang, *CrystEngComm* **2009**, *11*, 2425.

[117] L.-J. Li, G. Yuan, L. Chen, D.-Y. Du, X.-L. Wang, G.-J. Xu, H.-N. Wang, K.-Z. Shao, Z.-M. Su, *J. Coord. Chem.* **2011**, *64*, 1578.

[118] L. Carlucci, G. [] Ciani, D. M. Proserpio, *Coord. Chem. Rev.* **2003**, *246*, 247.

Chapter 2: A New PCM Based on a $R_3P{=}O$ Building Block

INTRODUCTION

PCPs that incorporate specialized organic substituents have proven to be attractive candidates for particular solid-state applications due to the ability to subsequently functionalize their internal pore surfaces.[119-123] For example, it has been demonstrated that the inclusion of polar substituents within a host framework may provide control over the selectivity, spatial orientation, and enthalpy of adsorption of certain guest adsorbates.[124-127] In addition, PCPs that contain available Lewis acid or base sites are key targets for *post*-synthetic modification, particularly with catalytic metal species.[30,58,128-132] Organophosphine ligands are ideal coordination polymer precursors for a number of reasons; notably, the 'soft' Lewis base nature of R_3P: species and the broad range of P(III) → P(V) chemistry provide access to polar (R_3PE (E = O, S, NR, BX_3…)) or ionic substituents ($[R_3PR']^+$) within the pores.[133] In addition, the trigonal geometry at P provides an organic building block that greatly favors the formation of 3-dimensional polymers, as opposed to the formation of lower dimensional (layered) solids.

Recent studies using *tris*(carboxylated) triphenylphosphine,[102] its oxide,[103] and several methylphosphonium derivatives[102] have provided the first examples of phosphine coordination materials (PCMs). A current extension of this work has focused in particular on the incorporation of early *s*-block metals into PCM materials. In comparison to 3*d*-metals, the lower atomic masses and associated higher metal–ligand bond stabilities of *s*-block metals have recently attracted significant attention.[68,134,135] In this study, a new Mg(II)-based material was identified that exhibits significant solid-state stability and a very high adsorption capacity of molecular CO_2 at 30 °C and 12 bar.

RESULTS AND DISCUSSION

Synthesis and structure

$[Mg_4(\mu_3\text{-}OH)_2(tctpo)_2(OH_2)_4]$, hereafter referred to as PCM-11, was obtained directly as pure crystalline product from the reaction of $Mg(OH)_2$ with *tris*(*p*-carboxylato)triphenyl phosphine oxide $[P(=O)(C_6H_4CO_2H)_3]$ ($tctpoH_3$)[136] at 90 °C in an ethanol:DMF:H_2O mixture (4:1:1) with excess OH^-. Unlike the synthesis of PCM-4 that contains Zn(II) and the same phosphine oxide ligand,[136] it was not possible to prepare PCM-11 by *in situ* oxidation of the free phosphine ligand, so the *pre*-oxidized ligand was employed directly.

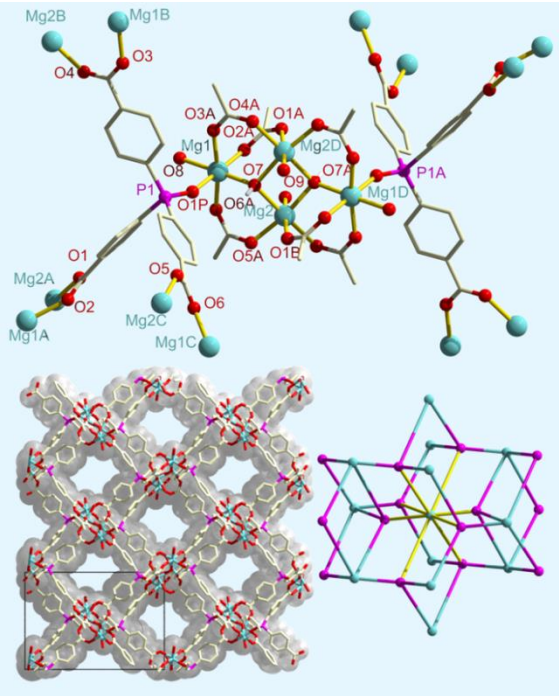

Figure 2.1: (*Top*) The bond connectivity within PCM-11: a single $[Mg_4(\mu_3\text{-}OH)_2(OH_2)_2]^{6+}$ inorganic node is shown along with all carboxylate bridging groups, in addition to two phosphine oxide-bound $tctpo^{3-}$ ligands with completed coordination spheres; (*bottom left*) view of the extended lattice of PCM-11 as viewed in the crystallographic *bc*-plane (space-filling model shown in grey); (*bottom right*) the basic $4^{12}.4^6$ net topology of PCM-11 (metal nodes = cyan; P nodes = magenta).

The solid-state structure of PCM-11 is shown in Figure 2.1 and is built upon 8-connected $[Mg_4(\mu_3\text{-}OH)_2(OH_2)_4]^{6+}$ inorganic nodes and 4-connected phosphine oxide organic nodes. The former 8-connected metal-based clusters are *syn,syn*-bridged on both faces by ligand carboxylate groups, and in addition, both Mg1 and Mg2 are singly hydrated. Notably, Mg1 is formally bound to the phosphine oxide moiety (Mg1–O1P = 2.073(3) Å, P1–O1P–Mg1 = 155.5(2)°; Figure 2.1, *top*). Thus, each ligand node is coordinated by seven Mg(II) equivalents and acts as a *pseudo*-tetrahedral building block.

The resulting PCM-11 lattice is based on a distorted cubic box-girder structure supported by isolated Mg_4 clusters. There are square pore openings in all three crystallographic directions with the largest openings having an accessible diagonal distance of 11.4 Å (Figure 2.1, *bottom left*). It is noteworthy that the relatively low symmetry of the ligands and metal nodes result in an open structure with 'corrugated' walls due to the staggering of adjacent aromatic groups. This topological facet has previously been shown to result in high mechanical stability and resistance to pore collapse upon desolvation compared to more highly-symmetric coordination polymers.[137-139] Consideration of the overall 8,4-connectivity within PCM-11 reveals a net topology that consists purely of 4-membered rings (Schläfli notation $4^{12}.4^3$; Figure 2.1, *bottom right*), which does not appear to have been previously categorized.

^{31}P-MAS NMR of PCM-11 also illustrated that the P=O moiety from the $tctpo^{3-}$ ligand is fully retained in the solid state (Figure 2.2).

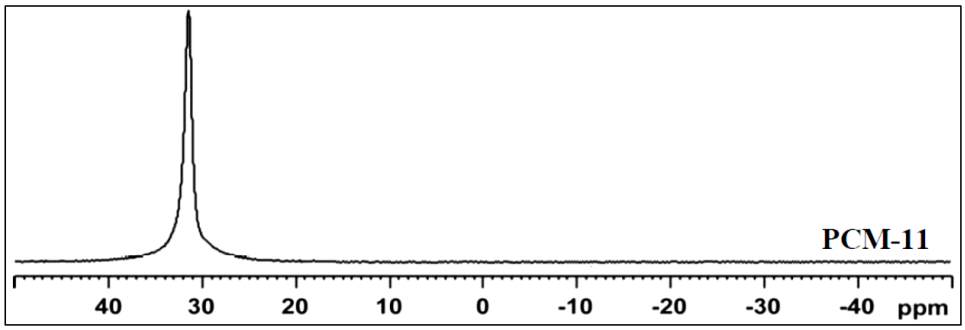

Figure 2.2: Solid-state ^{31}P-MAS NMR spectrum for as-synthesized PCM-11.

Gas adsorption

Initial adsorption studies on an as-synthesized crystalline sample of PCM-11 were performed using N_2 after outgassing at 200 °C for 5 h. Application of the standard Brunauer–Emmett–Teller (BET) model for N_2 adsorption in the p/p_0 range 0.05–0.3 gave a measured surface area of 810 m^2 g^{-1}, with a corresponding estimated micropore volume of 0.302 mL g^{-1} (*t*-plot analysis).[140] In contrast, a second crystalline sample that had first been treated with cycles of $CHCl_3$ to remove solvent of crystallization prior to outgassing under the same conditions gave inferior values of 380 m^2 g^{-1} and 0.125 mL g^{-1} (Figure 2.3).

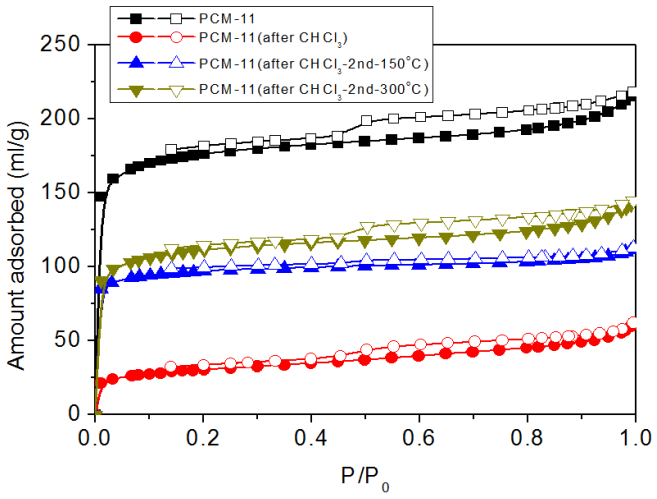

Figure 2.3: N_2 adsorption/desorption isotherms for $CHCl_3$ solvent-exchanged PCM-11 after outgassing for 5 h at 150 °C and after subsequent outgassing steps at higher temperature.

After confirming the permanently-porous nature of PCM-11, its potential for the sorption of CO_2 was studied in more detail. At 30 °C, the as-synthesized PCM-11 showed a linear uptake of CO_2 in the low pressure region (2.53 mmol g^{-1} or 11.1 wt % at 1 bar; Figure 2.4, *inset*), with no indication of saturation being reached. The linear uptake region was found to extend to over 3 bar, while saturation is still not achieved at 12 bar, corresponding to around 10.8 mmol g^{-1} or 47.5 wt% CO_2 (Figure 2.4). The CO_2 uptake of PCM-11 at 1 bar was higher than that of Mg-MOF-1 (0.6 mmol g^{-1})[67] but lower than that of Mg/DOBDC (8.0 mmol g^{-1}).[68] Most significantly, the CO_2 uptake of PCM-11 at 12 bar was considerably higher than that of MOF-210 (7.9 mmol g^{-1} or 34.7 wt%) at 25 °C and the same pressure,[23] which was considered the highest capacity to-date amongst such porous materials (S_{BET} = 6240 m^2 g^{-1}).[23,67,68,141-145]

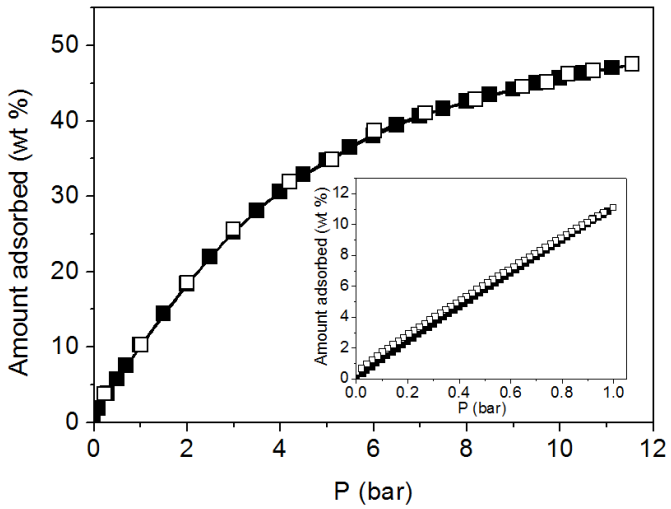

Figure 2.4: CO_2 isotherm for as-synthesized PCM-11 at 30 °C after outgasssing at 200 °C for 5 h: black squares = adsorption; white squares = desorption; *(inset)* low-pressure region at the same temperature.

Using additional as-synthesized samples of PCM-11, a range of additional small molecule adsorbates were employed, all of which showed reversible type-I isotherms with appreciable capacities at 1 bar: Ar (87 K; 390 mL g^{-1}), O_2 (77 K; 439 mL g^{-1}), and H_2 (77 K; 196 mL g^{-1}) (Figures 2.5 and 2.6).

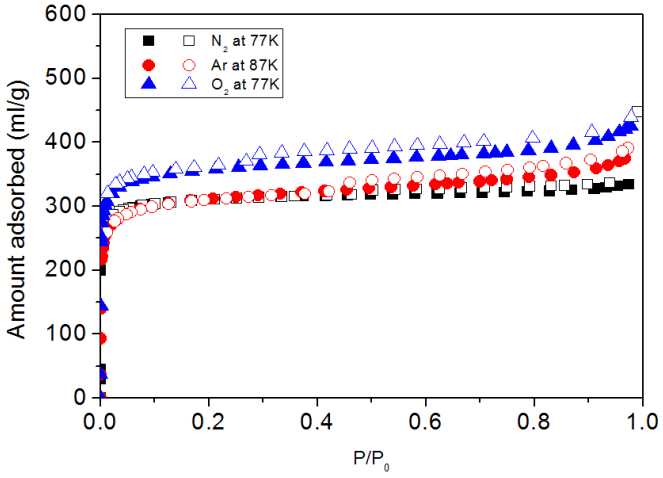

Figure 2.5: Adsorption/desorption isotherms for as-synthesized PCM-11 after outgassing for 5 h at 200 °C, for: N_2 (black squares; 77 K); Ar (red circles; 87 K); O_2 (blue triangles; 77 K).

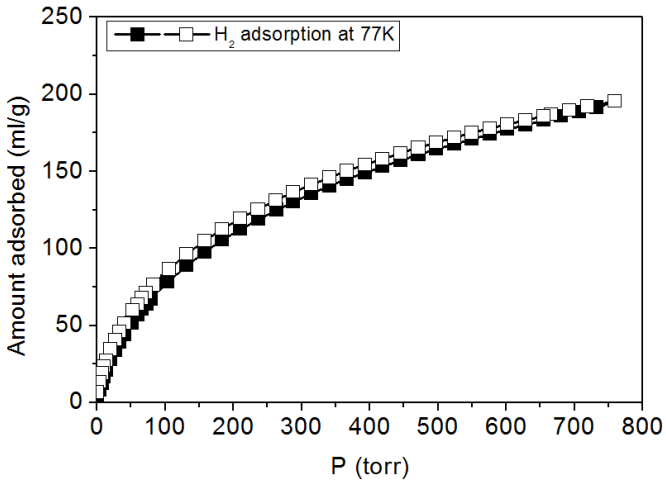

Figure 2.6: Corresponding H_2 adsorption/desorption isotherm for as-synthesized PCM-11 at 77 K after outgassing for 5 h at 200 °C.

Thermal stability

Thermogravimetric analysis of PCM-11 was used to help describe the observed gas sorption behavior under various conditions. First, an as-synthesized crystalline sample was studied using CO_2 as the carrier gas in order to specifically check the stability of PCM-11 in the presence of the adsorbate molecule of interest. The material underwent facile desolvation below 80 °C, after which it remained unchanged up to 460 °C when the onset of framework degradation was observed (Figure 2.7; red line).

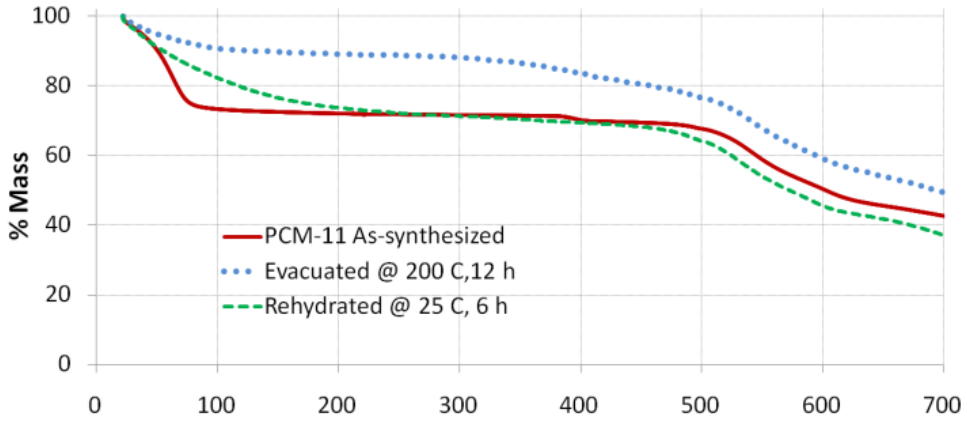

Figure 2.7: Comparison of thermogravimetric analyses of as-synthesized PCM-11, the same sample after evacuation at 200 °C, and after re-exposure to water (all under CO_2 purge).

This represents a significant enhancement of overall thermal stability in the desolvated material compared to transition metal-based coordination polymers, which commonly undergo irreversible structural collapse above 350 °C, and is a direct result of the influence of Mg(II). During the initial low temperature desolvation step on PCM-11, 27 % of the initial mass is lost *via* removal of all solvent molecules from the pores and coordinated H_2O molecules from the $[Mg_4(\mu_3\text{-}OH)_2]^{6+}$ clusters.

TGA of the same sample that had been *pre*-evacuated at 200 °C overnight indicated that both coordinated and lattice solvent had been successfully removed under these conditions without structural collapse (Figure 2.7; blue dashed line). These findings were further supported by *in situ* temperature-dependent FT-IR spectroscopy on the as-synthesized PCM-11, which showed the loss of the broad peak *ca.* 3500 cm^{-1} due to H_2O above 100 °C and was accompanied by retention of the expected hydroxide vibrational modes *ca.* 3675 cm^{-1} (Figure 2.8).

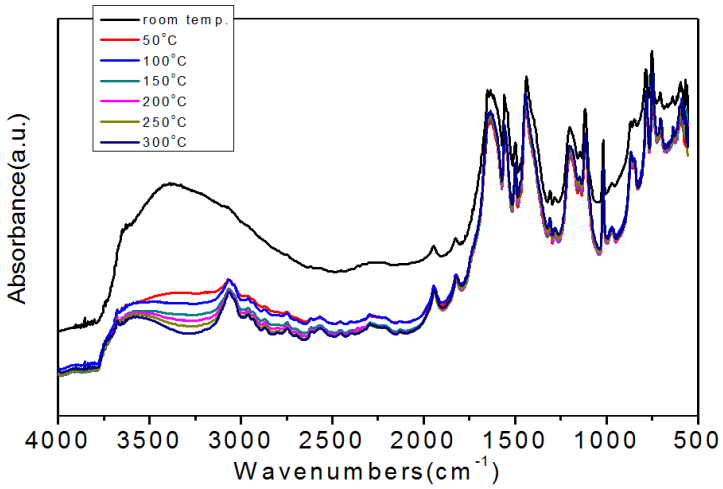

Figure 2.8: *In situ* temperature-dependent FT-IR spectra of as-synthesized PCM-11 upon heating under an inert atmosphere; loss of H_2O from the pores appears complete above 100 °C in agreement with TGA data.

More importantly, immersion of the desolvated sample in H_2O at 25 °C and slow evaporation to dryness resulted in a new TGA trace that closely matched the original sample, indicating that PCM-11 does not readily react with moisture when desolvated (Figure 2.7; green dashed line). These observations were also supported by the corresponding XRPD patterns (Figure 2.9) and justified the use of mild pretreatment conditions, such as those applied in the CO_2 uptake studies herein.

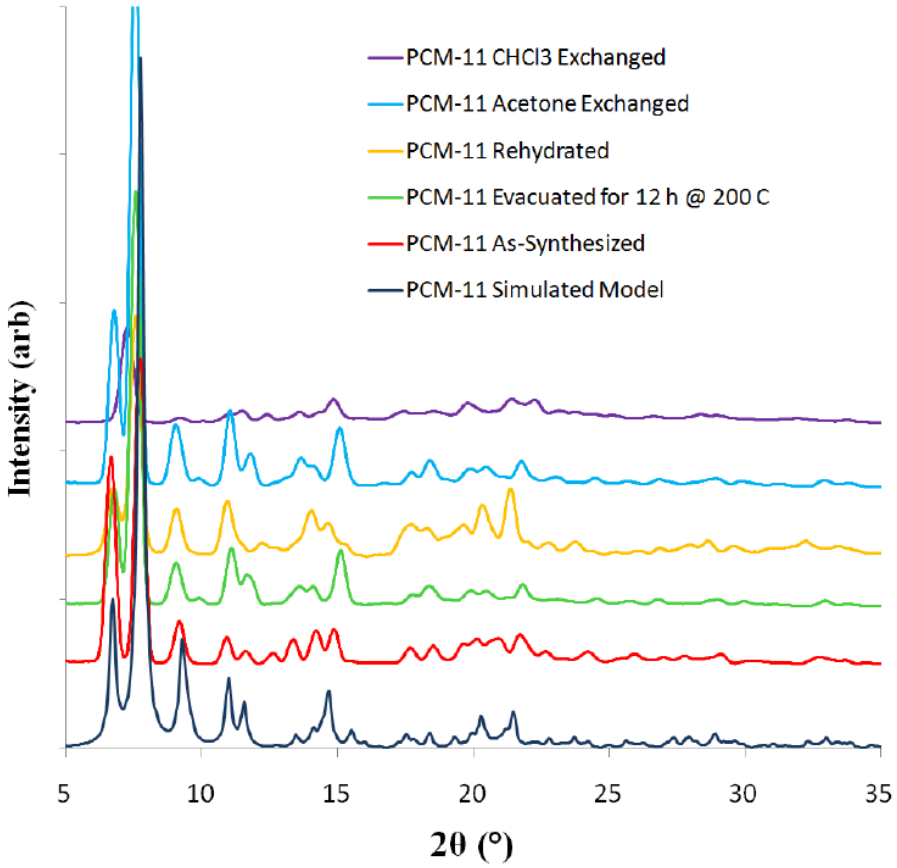

Figure 2.9: Comparative XRPD spectra for bulk samples of PCM-11 under various treatment conditions.

TGA also provided compelling evidence to explain the lower gas uptake capacities observed for various adsorbates in $CHCl_3$-exchanged PCM-11 samples: a distinct 7% mass loss was observed between 350–405 °C for PCM-11 that had been subjected to cycles of $CHCl_3$ solvent exchange over 5 days and was then evacuated at 100 °C (Figure 2.10). This mass loss corresponds closely to what should be observed for the removal of four equivalents of coordinated H_2O *per* $[Mg_4(\mu_3\text{-}OH)_2]^{6+}$ cluster. The relatively high onset temperature for this dehydration step at ambient pressure is similar

to those observed for other hydrated Mg(II) materials.[146,147] The same step was also observed, to a lesser extent, in a similar sample that had been outgassed at 200 °C overnight. However, this H_2O loss step was not observed in an acetone-exchanged sample of PCM-11 that had been subjected to vacuum at only 25 °C. This suggested that coordinated H_2O ligands were easily removed by polar, solubilizing solvents, but remained mostly coordinated to Mg(II) in the presence of apolar, H_2O-immiscible solvent, even upon application of a vacuum at 100 °C.

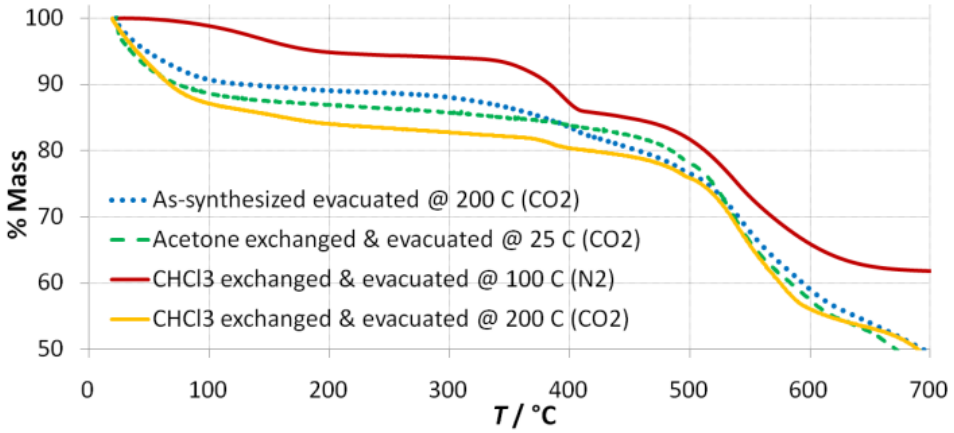

Figure 2.10: TGA of PCM-11 after solvent exchange with $CHCl_3$ and acetone and 12 h vacuum *pre*-activation (purge gas shown in parentheses).

Based on the mild gas sorption *pre*-treatment conditions employed in these studies, it is therefore most likely that the inferior sorption properties observed for $CHCl_3$-treated samples corresponded to a failure to generate a majority of 'open' sites on Mg(II); such vacant metal sites are known to promote high-capacity CO_2 uptake.[23,67,68,141-145] This finding may have potentially important consequences for determining a rational choice of activation conditions for other chemically-related coordination polymers.

CONCLUSIONS

A new porous phosphine coordination material, PCM-11, was formed by reaction of Mg(II) with *tris*(*p*-carboxylato)triphenylphosphine oxide under basic conditions. PCM-11 is an unusual 8,4-connected coordination polymer with an open 3-D pore structure, and the highly ionic nature of the metal–ligand bonding resulted in excellent thermal stability upon desolvation (>460 °C). PCM-11 was easily activated for small molecule sorption at low temperature without the requirement for solvent *pre*-exchange, and it adsorbed 47.5 wt% CO_2 at 11.6 bar and 30 °C.

EXPERIMENTAL TECHNIQUES

General

All ligand syntheses were performed under an N_2 atmosphere using standard schlenk techniques. 1,4-dibromobenzene (Alfa Aesar, ≥98%), phosphorus trichloride (Sigma-Aldrich, ≥99%), *n*-butyllithium (1.6 M in hexanes, Sigma-Aldrich), hydrogen peroxide (30% in H_2O, Fisher Chemical), and $Mg(OH)_2$ (Sigma-Aldrich, ≥95%) were used as received. Organic solvents (THF, DMF, ethanol, diethyl either) were obtained from Fisher Scientific. THF was dried/degassed using a Solvent Purification System (Innovative Technologies) and further degassed using freeze-thaw cycles prior to use. Diethyl ether, DMF, and all aqueous solutions were purged with N_2 for 30 min prior to use. ^{1}H-NMR, ^{13}C-NMR and ^{31}P-NMR were collected in-house using a Varian Unity 300 MHz spectrometer; FT-IR spectra were obtained directly from solid samples using a Nicolet iS*50 spectrophotometer fitted with an attenuated total reflectance apparatus; thermogravimetric analyses (TGA) were collected using a TA Instruments Q50 system. Elemental microanalyses were performed by Midwest Microlab LLC (Indianapolis).

X-ray crystallography

Crystals were mounted on thin glass fibers using perfluoropolyether oil, which was frozen *in situ* by a nitrogen gas Cryostream flow. Data for PCM-11 reported herein were collected on an Enraf Nonius Kappa CCD diffractometer using monochromated Mo$K\alpha$ radiation (λ = 0.71073 Å). Cell refinement and data reduction was performed using the HKL SCALEPACK & DENZO and COLLECT utilities. Absorption corrections were made based on ψ- and ω-scans using the SORTAV program. Structures were solved using direct methods and refined on F^2 using the program SIR-92 and then refined using SHELXTL-97 software. All non-hydrogen atoms were refined anisotropically for all structures, except for uncoordinated and disordered solvent molecules, which were refined with isotropic displacement parameters. Solvent molecules were refined with geometric restraints in order to stabilize the refinement process and free variables were initially applied in order to determine site occupancies, which were set to 1.0 or 0.5 in the final refinement cycle. The SQUEEZE utility in *PLATON* was applied to all structures *post*-refinement in order to remove residual peaks due to any remaining disordered solvent. In all instances, this resulted in only small improvements to the final statistics (included in CIF data). For all structures, hydrogen atoms were fixed based on idealized coordinates and were refined with values of U_{iso} set to 1.5 times that of the carrier atom. Solvent H_2O H-atoms were not directly located in the peak difference maps; compensatory alterations were made to final structural formula as required.

X-ray powder diffraction

Phase purity of the PCM-11 materials before and after solvent exchange and activation were confirmed by analysis of powdered crystalline samples that were sealed

inside borosilcate capillary tubes and spun *in situ* to prevent preferential orientation of the crystallites. Spectra were recorded on a Rigaku R-Axis Spider diffractometer with an image plate detector using a graphite monochromator and Cu$K\alpha$ radiation (λ = 1.5418Å). The instrument was controlled using Rapid/XRD Version 2.3.8 diffractometer control software. Reflection data was collected in the range 5.0–40.0° 2θ. Integration of the two dimensional data into a one dimensional pattern was accomplished using 2DP Version 1.0. The XRPD spectra were then compared directly to their corresponding simulated patterns that were generated using the SimPowPatt function in *PLATON* using the single crystal model for the hkl reflection data obtained in the single crystal experiment.

Ligand synthesis

Procedure for ttpBr$_3$

1,4-dibromobenzene (20.0 g; 84.8 mmol) was dissolved in THF (500 cm^3) in a 1000 cm^3 round bottomed flask and cooled to –78 °C. A solution of *n*-butyllithium (1.6 M in hexanes; 84.8 mmol) was added drop-wise to the reaction over a 30 min period. The resulting white slurry was stirred for 1 h at –78 °C. Phosphorus trichloride (2.47 cm^3; 28.3 mmol) was added drop-wise to the mixture over 30 min before slowly warming to room temperature with stirring overnight. The yellow solution was washed with degassed sat. NaCl (200 cm^3) and extracted twice with diethyl ether (100 cm^3). The combined organic extracts were dried over $MgSO_4$, and the solvent was removed *in vacuo* to yield a yellow oil. The product was purified by column chromatography (silica gel eluted with CH_2Cl_2:hexanes (1:1)) to afford a white powder (11.1 g; 22.2 mmol). Yield, 78.6 %. ^{1}H NMR ($CDCl_3$, 300.1 MHz) δ = 7.46 (dd, 6H), 7.10 (t, 6H); ^{13}C NMR ($CDCl_3$, 75.5 MHz) δ = 135.20 (d, Ar), 135.06 (d, Ar), 131.92 (d, Ar), 123.94 (s, Ar); ^{31}P NMR ($CDCl_3$,

121.5 MHz) δ = –7.41. FT-IR (ATR) ν_{max} (cm^{-1}) = 3041 (w), 2955 (w), 2927 (w), 1903 (w), 1790 (w), 1637 (w), 1569 (s), 1471 (s), 1382 (s), 1299 (m), 1260 (w), 1177 (m), 1106 (w), 1092 (m), 1064 (s), 1006 (s), 948 (w), 843 (m), 816 (s), 807 (s), 725 (s), 709 (w), 629 (w), 528 (m), 509 (s), 473 (m), 452 (m), 429 (w), 380 (w), 355 (m), 338 (m), 291 (w), 281 (w), 260 (m), 244 (m), 231 (w), 187 (w), 156 (m), 132 (w), 121 (w).

Procedure for tctpLi$_3$

$TtpBr_3$ (5.0 g; 10.0 mmol) was dissolved in THF (500 cm^3) in a 1000 cm^3 round bottomed flask and cooled to –78 °C. A solution of *n*-butyllithium (2.5 M in hexanes; 32.1 mmol) was added drop-wise to the reaction over a 30-minute period. The light orange slurry was stirred for 2 h at –78 °C, after which an excess of crushed dry ice (*ca.* 500 g) and diethyl either (200 cm^3) were added. The reaction was removed from the cooling bath and allowed to stir at room temperature overnight. The product was filtered in air and rinsed with fresh diethyl ether to afford an off-white powder (3.7 g; 9.1 mmol). Yield, 90.5 %. ^{1}H NMR (D_2O, 300.1 MHz) δ = 7.69 (dd, 6H), 7.27 (td, 6H); ^{31}P NMR (D_2O, 121.5 MHz) δ = –6.50.

Procedure for tctpoH$_3$

$TctpLi_3$ (1.0 g; 2.4 mmol) was dissolved in H_2O (10 cm^3) in a Teflon-lined screw cap vial and excess H_2O_2 (4.36 cm^3; 42.7 mmol) was added. The vial was sealed and stirred overnight at room temperature. The product was precipitated with HCl (1.0 M) to pH = 3 and filtered in air to afford a white powder (0.77 g; 2.0 mmol). Yield, 81.4 %. ^{1}H NMR (DMSO-*d$_6$*, 300.1 MHz) δ = 8.11 (dd, 6H), 7.80 (dd, 6H); ^{13}C NMR (DMSO-*d$_6$*, 75.5 MHz) δ = 166.67 (s, CO_2H), 136.19 (d, Ar), 134.37 (d, Ar), 132.02 (d, Ar), 129.68

(d, Ar); ^{31}P NMR (DMSO-d_6, 121.5 MHz) δ = 25.73. FT-IR (ATR) ν_{max} (cm^{-1}) = 3331 (m br), 3040 (w), 2917 (w), 2618 (m), 2491 (m), 1694 (s), 1603 (w), 1563 (m), 1497 (m), 1395 (s), 1314 (w), 1246 (s br), 1162 (m), 1101 (s), 1085 (w), 1016 (m), 966 (w), 856 (m), 813 (w), 767 (m), 692 (s), 632 (w), 571 (s).

PCP synthesis

Procedure for PCM-11

TctpoH$_3$ (41.0 mg, 0.10 mmol) was dissolved in ethanol:DMF:H$_2$O (1:1:1, 2.5 cm^3) and mixed with a second solution of Mg(OH)$_2$ (15.0 mg, 0.25 mmol) in DMF (2.5 cm^3). 1.0 M NaOH (0.1 mmol) was added to the resulting opaque slurry, which was heated in a 20 cm^3 scintillation vial at 90 °C for 5 d in a graphite thermal bath. The resulting solution and any amorphous white solids were decanted away from large clusters of colorless crystalline needles and rinsed with fresh ethanol:DMF:H$_2$O (1:4:1). Average yield, 40 mg (from six reactions). ^{31}P-MAS NMR (161.9 MHz) δ = 31.5 ppm (R$_3$P(=O)). FT-IR (ATR) ν_{max} (cm^{-1}) = 3675 (m), 3590 (w), 2974 (s), 2901 (s), 2372 (m), 2311 (m), 1619 (br m), 1555 (w), 1407 (s), 1250 (m), 1066 (s), 1051 (s), 879 (w), 778 (m), 736 (s), 700 (w), 635 (w). Crystal data for PCM-11: C$_{45}$H$_{33}$Mg$_4$NO$_{21}$P; MW = 1082.90, monoclinic, space group $P2_1/c$, a = 13.5792(4), b = 13.8958(4), c = 20.7478(6) Å, β = 104.882(1)°, V = 3783.7(2) Å^3, Z = 2, ρ = 0.951 g cm^{-3}, μ(Mo-Kα) = 0.144 mm^{-1}, R_1 = 0.078, 21285 measured reflections, (5893 independent reflections, $I > 2\sigma(I)$), wR_2 = 0.238 (all data), R_{int} = 0.088, GoF = 1.021; CCDC 788656.

[119] J. -R. Li, Y. Tao, Q. Yu, X. -H. Bu, H. Sakamoto, S. Kitagawa, *Chem. Eur. J.* **2008**, *14*, 2771.

[120] C. Ritchie, F. Li, C. P. Pradeep, D. -L. Long, L. Xu, L. Cronin, *Dalton Trans.* **2009**, 6483.

[121] A. J. Blake, N. R. Champness, T. L. Easun, D. R. Allan, H. Nowell, M. W. George, J. Jia, X. -Z. Sun, *Nat. Chem.* **2010**, *2*, 688.

[122] I. A. Riddell, M. M. J. Smulders, J. K. Clegg, J. R. Nitschke, *Chem. Commun.* **2011**, *47*, 457.

[123] L. Ma, C. -D. Wu, M. M. Wanderley, W. Lin, *Angew. Chem. Int. Ed.* **2010**, *49*, 8244.

[124] X. Lin, N. R. Champness, M. Schröder, "Functional Metal-Organic Frameworks: Gas Storage, Separation and Catalysis," *Top. Curr. Chem.* Springer Berlin Heidelberg: Berlin, Heidelberg, **2009**, *293*, pp. 35–76.

[125] J. Seo, N. Jin, H. Chun, *Inorg. Chem.* **2010**, *49*, 10833.

[126] S. Shimomura, M. Higuchi, R. Matsuda, K. Yoneda, Y. Hijikata, Y. Kubota, Y. Mita, J. Kim, M. Takata, S. Kitagawa, *Nat. Chem.* **2010**, *2*, 633.

[127] A. Demessence, J. R. Long, *Chem. Eur. J.* **2010**, *16*, 5902.

[128] M. J. Ingleson, J. P. Barrio, J. Bacsa, C. Dickinson, H. Park, M. J. Rosseinsky, *Chem. Commun.* **2008**, 1287.

[129] X. Zhang, F. X. Llabrés i Xamena, A. Corma, *J. Catal.* **2009**, *265*, 155.

[130] D. Dang, P. Wu, C. He, Z. Xie, C. Duan, *J. Am. Chem. Soc.* **2010**, *132*, 14321.

[131] K. K. Tanabe, S. M. Cohen, *Angew. Chem. Int. Ed.* **2009**, *48*, 7424.

[132] L. H. Wee, S. R. Bajpe, N. Janssens, I. Hermans, K. Houthoofd, C. E. A. Kirschhock, J. A. Martens, *Chem. Commun.* **2010**, *46*, 8186.

[133] W. E. McEwen, L. Maier, B. Miller, *Topics in Phosphorus Chemistry*, M. Grayson and E. J. Griffith, eds., Wiley, **1965**, *1–2*.

[134] Y. -Y. Liu, J. Zhang, F. Xu, L. -X. Sun, T. Zhang, W. -S. You, Y. Zhao, J. Zeng, Z. Cao, D. Yang, *Cryst. Growth Des.* **2008**, *8*, 3127.

[135] A. E. Platero-Prats, V. A. de la Peña-O'Shea, N. Snejko, Á. Monge, E. Gutiérrez-Puebla, *Chem. Eur. J.* **2010**, *16*, 11632.

[136] R. Amengual, E. Genin, V. Michelet, M. Savignac, J.-P. Genêt, *Adv. Synth. Catal.* **2002**, *344*, 393.

[137] Z. Zhang, S. Xiang, Y. -S. Chen, S. Ma, Y. Lee, T. Phely-Bobin, B. Chen, *Inorg. Chem.* **2010**, *49*, 8444.

[138] C. Volkringer, T. Loiseau, G. Férey, C. M. Morais, F. Taulelle, V. Montouillout, D. Massiot, *Micropor. Mesopor. Mater.* **2007**, *105*, 111.

[139] S. M. Humphrey, J. -S. Chang, S. H. Jhung, J. W. Yoon, P. T. Wood, *Angew. Chem. Int. Ed.* **2007**, *46*, 272.

[140] A. Galarneau, H. Cambon, F. Di Renzo, F. Fajula, *Langmuir* **2001**, *17*, 8328.

[141] Y. J. Choi, J. H. Choi, K. M. Choi, J. K. Kang, *J. Mater. Chem.* **2011**, *21*, 1073.

[142] L. Valenzano, B. Civalleri, S. Chavan, G. T. Palomino, C. O. Areán, S. Bordiga, *J. Phys. Chem. C* **2010**, *114*, 11185.

[143] Z. Bao, L. Yu, Q. Ren, X. Lu, S. Deng, *J. Colloid Interf. Sci.* **2011**, *353*, 549.

[144] R. Vaidhyanathan, S. S. Iremonger, K. W. Dawson, G. K. H. Shimizu, *Chem. Commun.* **2009**, 5230.

[145] M. Dincă, J. R. Long, *Journal of the American Chemical Society* **2005**, *127*, 9376.

[146] H. -K. Liu, T. -H. Tsao, Y. -T. Zhang, C. -H. Lin, *CrystEngComm* **2009**, *11*, 1462.

[147] B. R. Srinivasan, S. C. Sawant, *Thermochim. Acta* **2003**, *402*, 45.

Chapter 3: New PCMs Based on a Quaternary R_4P^+ Building Block

INTRODUCTION

Porous coordination polymers (PCPs) are a class of materials that have gained widespread attention over the past two and a half decades due to their unsurpassed internal surface areas, permanent porosities, and high thermal stabilities.[2,12,18,148] PCPs are infinite, crystalline lattices composed of organic linkers and metal nodes that react to form 1-, 2-, or 3-dimensional arrays. The latter, most highly coordinated class of nets has been shown to result in more thermally and chemically robust materials that are also more resistant to pore collapse, which typically leads to superior gas sorption properties. The organic linkers commonly contain nitrogen atoms or acidic functional groups (which deprotonate in solution) that form strong coordination bonds to the metal nodes.[16,28,29] These nodes can be prepared based on alkali earth metals, early transition metals, or lanthanides (Ln's), and may range from single metal ions to more complex heteroatomic clusters. Early efforts in PCP development were aimed at gas storage and separations,[35-39] notably hydrogen storage[78-82] and carbon dioxide sequestration,[65,74-77] and have since evolved to include the areas of magnetism,[45-48] drug delivery,[49-53] proton conductivity,[54-57] catalysis,[58-61] and molecular sensing.[149-153]

Ln's are commonly exploited for their luminescence properties due to their long lifetimes and narrow, characteristic emission bands, which show little dependence on coordination environments.[91,99,154] Ln-containing materials and complexes have found use in solid-state lighting,[155-158] optical devices,[159-161] biological imaging,[162-165] and chemical sensing applications.[100,166-168] Ln luminescence in PCPs has been well-studied; the mechanism for this phenomenon is attributed to the so-called antenna effect, whereby

energy transfer from the triplet (T_1) excited state of the organic species in the PCP to the excited electronic state of the metal node induces luminescence upon radiative relaxation (see *Molecular Sensing* in Chapter 1).[42,101,169,170] The lifetimes and quantum yields of these emissive processes have been shown to diminish in the presence of O–H oscillators, which can vibronically couple to the metal excited state and provide a non-radiative decay pathway.[171-173] This quenching effect frequently occurs in PCPs due to the presence of coordinated OH_2 molecules bound to the metal nodes. It follows that removal of these molecules can lead to increased luminescence properties; manipulation of this effect has been utilized previously to yield an effective sensory response. To date, Ln-based PCPs have been utilized for a broad range of sensing applications, including the detection of charged metal species,[174-179] gases and vapors,[109,110,180-184] solvents,[84,185-189] explosives,[190-194] and temperature.[195-199]

In this chapter, the synthesis and characterization of a tetrahedral phosphonium zwitterion, an ionic metal-free phosphonium PCM, and a new series of Ln(III)-based PCMs will be described. The gas sorption properties of all nine structurally analogous PCM-25 materials were studied, as well as the emissive characteristics of Tb-, Eu-, and Dy-PCM-25.

RESULTS AND DISCUSSION

Tetrahedral phosphonium zwitterion

Synthesis and structure

The Pd(II)-catalyzed reaction of the free phosphine tctpH_3 ligand with *p*-iodobenzoic acid was carried out by refluxing in DMF for 8-10 hours to afford the *tetrakis*(*p*-carboxylated)tetraphenylphosphonium salt, tctp$^+H_3$. A crystal structure of the ligand was obtained following purification by sonication in acetone and recrystallization in DMF. The absence of a counter ion within the crystal lattice and deprotonation of one carboxylic acid group led to the formation of a zwitterionic phosphonium species. Interestingly, tctp$^+H_3$ did not behave like a typical organic molecule in that the monomers were not tightly packed, presumably due to the conformational frustration of the T_d ligand. Hydrogen bonding between adjacent carboxylic acid groups promoted the formation of a material that was not only porous, but also lightweight due to the absence of heavy metal-based nodes. This metal-free, porous, *ionically*-bonded phosphine material has been named accordingly as iPCM-1.

iPCM-1 is a neutral PCP due to the charge balance of one deprotonated carboxylic acid group with the positively-charged *P*-node. The remaining three protonated carboxylic acids form hydrogen bonds with neighboring groups (Figure 3.1) to produce a 3-dimensional material. iPCM-1 contains accessible pores in 2 dimensions, the largest of which measure 7.2 Å in diameter (Figure 3.2).

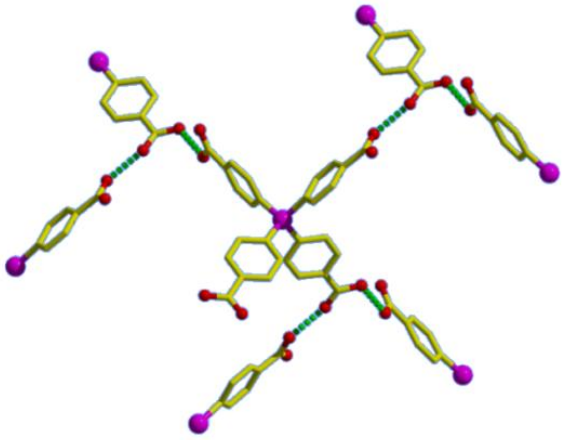

Figure 3.1: Hydrogen bonds (green) between neighboring carboxylic acid groups in iPCM-1. C = yellow, O = red, P = pink.

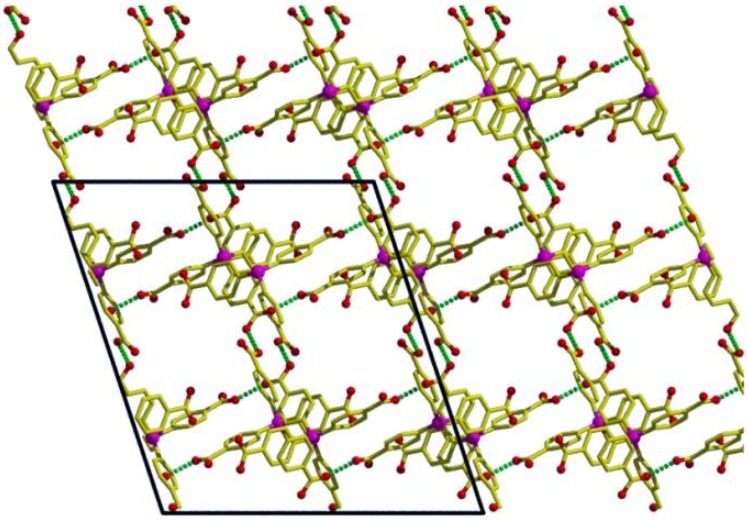

Figure 3.2: Crystal lattice of iPCM-1 shown in the *ac*-plane with a pore diameter of 7.2 Å.

iPCM-1 crystallized into the monoclinic space group *I*2/*a* with unit cell dimensions a = 22.753(3), b = 15.3561(19), c = 24.772(3) Å, β= 108.320(9)°. Two carboxylic acid groups are *syn*-connected and the third is *syn,anti*-connected to neighboring groups. The *P*-node is *pseudo*-tetrahedral with C–P–C bond angles ranging between 105.8(3)–113.4(3)°.

X-ray powder diffraction

X-ray powder diffraction (XRPD) was used to analyze samples of iPCM-1 that were solvent-exchanged and/or activated under ultrahigh vacuum at 150 °C (Figures 3.3 and 3.4). As-synthesized iPCM-1 closely matched the simulated powder pattern generated from the single crystal structure. XRPD analysis of acetone-exchanged iPCM-1 produced a powder pattern with considerably fewer reflections (Figure 3.3; light blue line), indicative of a phase change within the material to a space group of higher symmetry. XRPD of acetone-exchanged iPCM-1 remained virtually unchanged upon activation at 150 °C. However, activation of the as-synthesized material yielded a pattern that appeared to partially convert toward the pattern of higher symmetry seen in the acetone-exchanged materials. Efforts to obtain a single crystal structure of acetone-exchanged iPCM-1 are ongoing.

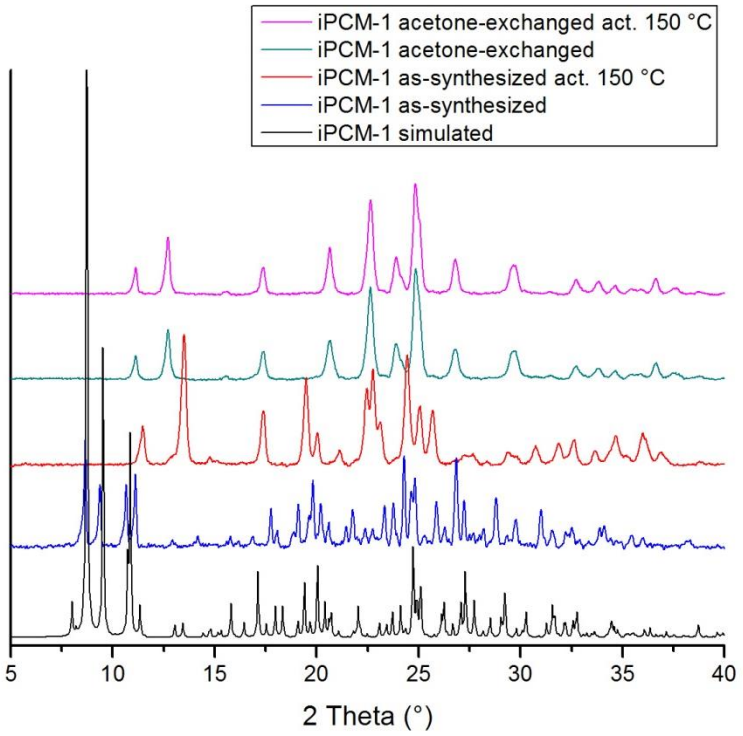

Figure 3.3: X-ray powder diffraction patterns for as-synthesized and acetone-exchanged iPCM-1 before and after activation at 150 °C.

The chemical stability of iPCM-1 was also monitored by solvent-exchange with H_2O and THF (Figure 3.4). The material exhibited no sign of dissolution in either solvent and also retained a high degree of crystallinity. The powder pattern of THF-exchanged iPCM-1 was similar to that of the as-synthesized material, indicating only minor effects induced by THF on the crystal lattice. However, H_2O-exchange resulted in a larger change in the structure of iPCM-1 due to the observed shifting of many low angle peaks in the powder pattern. Efforts to obtain a single crystal structure of the H_2O-exchanged material are also ongoing.

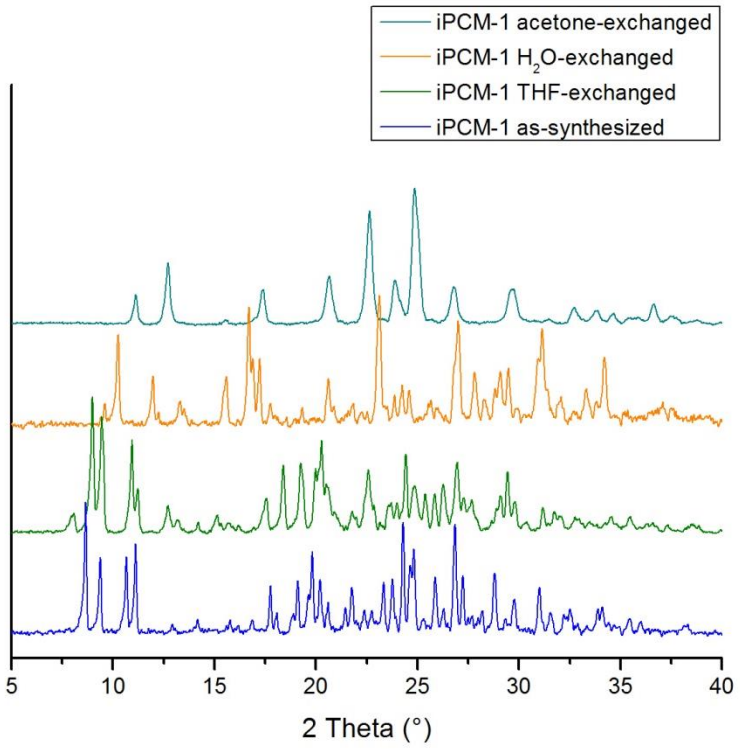

Figure 3.4: X-ray powder diffraction patterns for THF-, H_2O-, and acetone-exchanged samples of iPCM-1 compared with the as-synthesized material.

Not only was iPCM-1 highly crystalline upon solvent exchange, it was also chemically stable in a wide range of organic solvents ($CHCl_3$, CH_2Cl_2, MeOH, EtOH, iPrOH, MeCN, 1,4-dioxane, NMP, pyridine, ethyl acetate, ether, hexanes) and could only be dissolved under basic conditions (pH $\geq$ 9). This chemical robustness is a more characteristic property of PCPs and is highly unusual for crystallized organic molecules.

Thermal stability

Thermogravimetric analysis (TGA) was used to monitor the thermal stability of iPCM-1. The as-synthesized material exhibited a slight mass decrease of 3.2 % below 45 °C, which was attributed to the removal of uncoordinated solvent molecules, followed by the gradual loss of 5.8 % mass prior to decomposition at 330 °C (Figure 3.5). Acetone-exchanged iPCM-1 was highly stable with a gradual 3.3 % decrease in mass observed below 330 °C. A slight loss of 2.3 % was observed in the acetone-exchanged after activation at 150 °C, along with 7.4 % between 290–330 °C and decomposition at 340 °C.

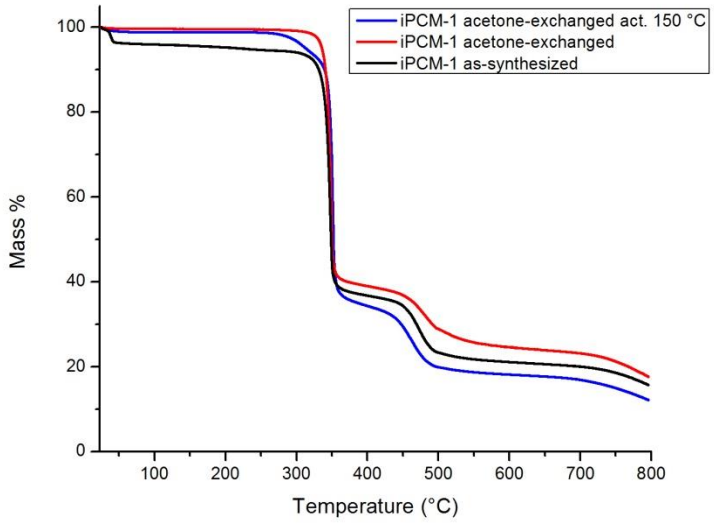

Figure 3.5: TGA of iPCM-1 as-synthesized and acetone-exchanged, before and after activation at 150 °C.

This high thermal stability is also more characteristic of PCPs rather than simple, recrystallized organic molecules, and serves to illustrate the robust, material-like nature of iPCM-1.

Gas adsorption

The gas sorption properties of iPCM-1 were probed by BET analysis. As with a number of PCMs, CO_2 was used to determine the internal surface area of iPCM-1 due to the low affinity of material toward N_2 gas. An as-synthesized sample activated at 150 °C yielded a surface area of 191 $m^2\ g^{-1}$, which was increased to 273 $m^2\ g^{-1}$ by acetone-exchange of the material prior to activation. iPCM-1 exhibited Type-I behavior with CO_2 sorption at 196 K, as-synthesized and acetone-exchanged samples of which adsorbed 81.68 and 107.79 $cm^3\ g^{-1}$ CO_2, respectively, and did not appear to reach saturation at 1 bar (Figures 3.6 and 3.7).

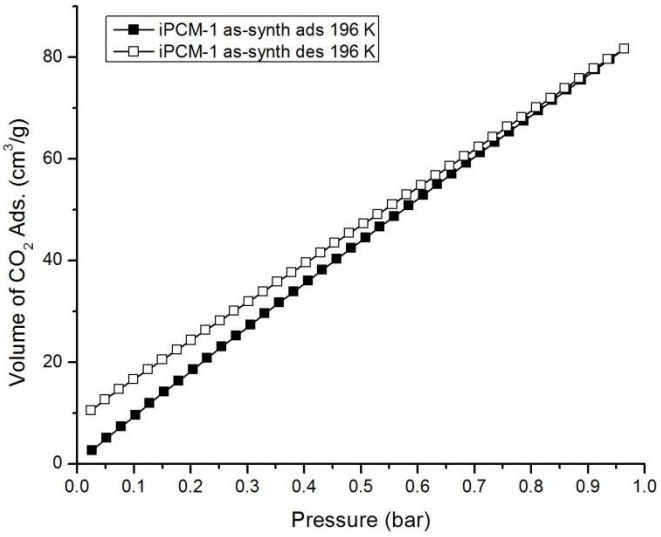

Figure 3.6: CO_2 sorption of as-synthesized iPCM-1 at 196 K after activation at 150 °C.

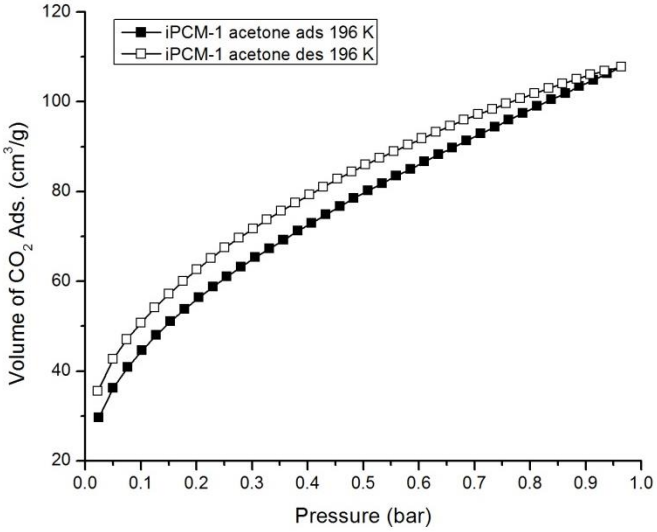

Figure 3.7: CO_2 sorption of acetone-exchanged iPCM-1 at 196 K after activation at 150 °C.

Ln(III)-based PCM-25

Synthesis and structure

($tctp^+H_3$) was reacted with Y(III) and a series of Ln(III) nitrate salts in DMF:ethanol:H_2O (1:1:1, 5 cm^3) to afford the material [$M(tctp^+)(OH_2)_4$], hereafter referred to as M-PCM-25 (M = Y, Eu, Gd, Tb, Dy, Ho, Er, Tm, Yb). Although iPCM-1 is chemically stable in the aforementioned 1:1:1 solution, the increased pH due to dissolution of the NO_3^- salts was sufficient to aid in dissolution of the ligand. M-PCM-25 crystallized into the monoclinic space group *I*2/*a* with unit cell dimensions *a* = 24.540(7), *b* = 14.812(4), *c* = 26.274(6) Å, β = 111.61(2)°. The *pseudo*-tetrahedral *P*-node contains C–P–C bond angles within the range of 107.0(4)–113.5(4)°. M-PCM-25 is 3-dimensional and contains accessible pores in 2 dimensions, the largest of which having a diameter of 13.9 Å in the *bc*-plane (Figure 3.8).

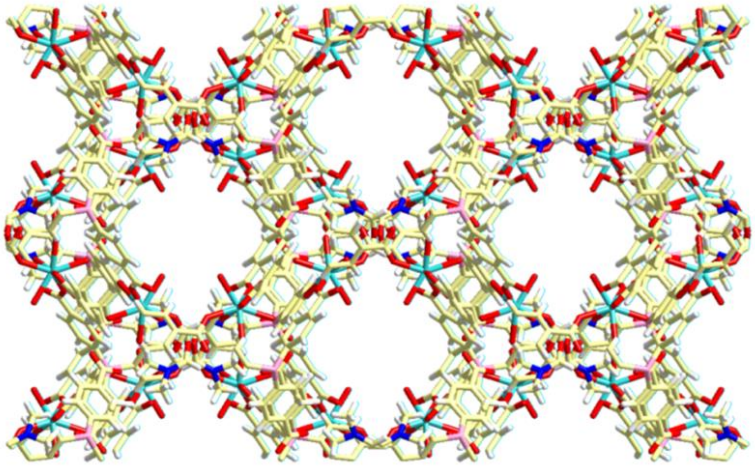

Figure 3.8: Crystal lattice of PCM-25 shown in the *bc*-plane with a pore diameter of 13.9 Å. O= red, P = pink, Ln = light blue.

PCM-25 is composed of 3-connected organic linkers with 3-connected metal nodes, each composed of a single $[Ln(OH_2)_4]^{3+}$ fragment. All four of the *p*-carboxylate/carboxylic acid moieties are deprotonated in the crystal lattice, two of which are *syn*-coordinated and a third η^2-coordinated to the metal nodes (Figure 3.9). The fourth carboxylate remains uncoordinated within the material. Each 8-coordinate metal center is bound to three carboxylate groups and four coordinated OH_2 molecules (Figure 3.9; green atoms) in an unusual asymmetric coordination geometry resembling a capped dodecahedron. As expected, the longest M–O bonds (2.392(6) and 2.480(5) Å) originate from the η^2-carboxylate group, compared to 2.303(6) and 2.339(6) Å from those that are *syn*-coordinated. The M–O bond lengths of the coordinated OH_2 molecules range between 2.321(7)–2.359(6) Å.

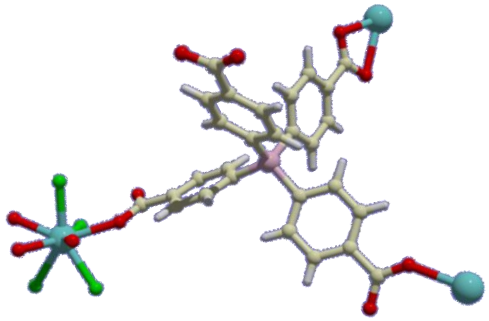

Figure 3.9: Linker connectivity of PCM-25 shown with one complete Ln(III) sphere containing four carboxylate oxygen atoms and four coordinated OH_2 molecules (green).

X-ray powder diffraction

All nine PCM-25 materials are isostructural as shown by X-ray powder diffraction (Figure 3.10). Although yttrium is not a 4*f* metal, it often behaves chemically similar to Ln(III) ions because its effective ionic radius (1.015 Å) is within the range of those from the selected Ln(III) ions (0.98–1.07 Å). Y-PCM-25 formed with a structure that was identical to the other Ln-PCM-25 materials.

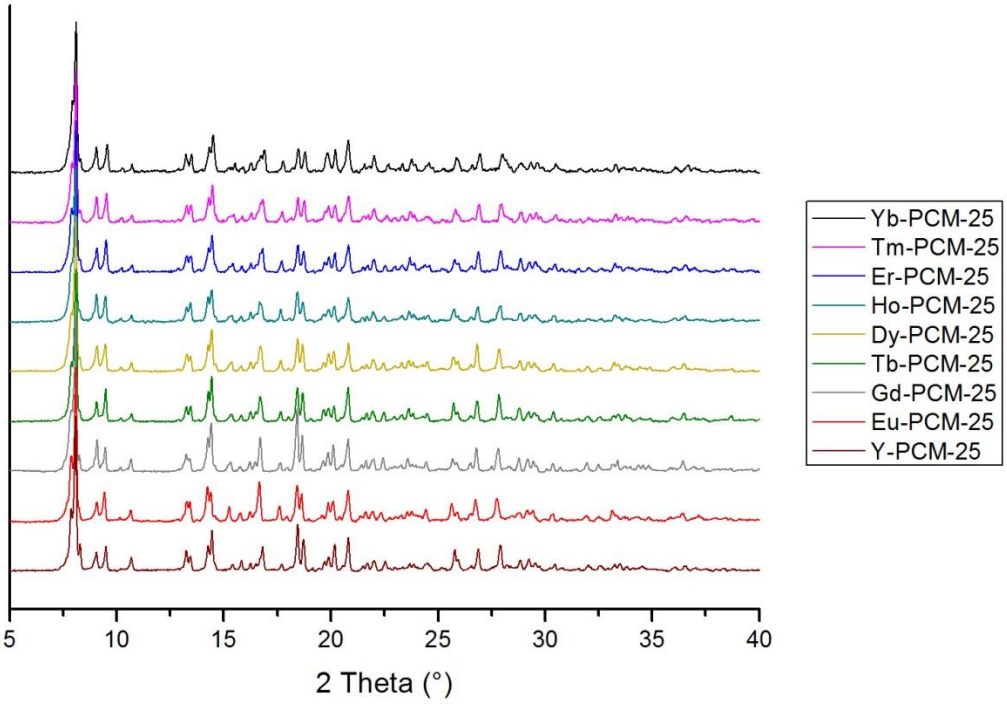

Figure 3.10: X-ray powder diffraction patterns of nine isostructural PCM-25 materials.

Gas adsorption

The gas adsorption properties of PCM-25 were investigated by BET analysis with activation at 200 °C ($p \leq 10^{-10}$ Torr) before each experiment. Due to the similar nature in which all nine materials behaved, only the results for Tb-PCM-25 will be discussed in detail. The full list of PCM-25 gas sorption results is shown in Table 3.1.

	Y^{3+}	Eu^{3+}	Gd^{3+}	Tb^{3+}	Dy^{3+}	Ho^{3+}	Er^{3+}	Tm^{3+}	Yb^{3+}
SA_{BET} ($m^2 g^{-1}$)	210	212	198	190	227	173	TBD	TBD	TBD
CO_2 196 K ($cm^3 g^{-1}$)	62.24	63.50	59.94	57.73	68.11	53.26	TBD	TBD	TBD
N_2 77 K ($cm^3 g^{-1}$)	9.24	5.94	7.76	10.23	10.01	6.07	TBD	TBD	TBD
H_2 77 K ($cm^3 g^{-1}$)	66.01	61.45	58.85	55.12	80.69	63.39	TBD	TBD	TBD

Table 3.1: Gas sorption properties of all PCM-25 materials.

The surface area of Tb-PCM-25 (190 $m^2 g^{-1}$) was determined by CO_2 adsorption at 196 K due to the low affinity of the material toward N_2 gas. The shape of the N_2 isotherm was slightly erratic with a maximum adsorption of 10.23 $cm^3 g^{-1}$ at 77 K and 1 bar (Figure 3.11). PCM-25 displayed Type-I behavior with CO_2 sorption at 196 K and appeared to be approaching saturation at 1 bar. At these conditions, Tb-PCM-25 adsorbed 57.73 $cm^3 g^{-1}$ CO_2 (Figure 3.12).

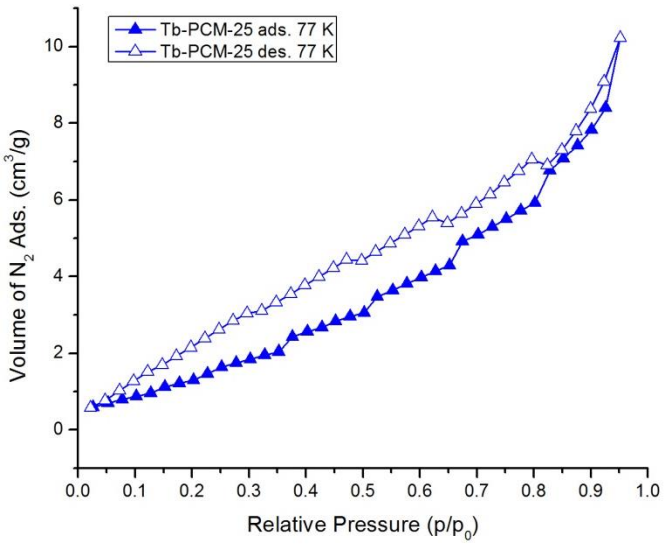

Figure 3.11: N_2 sorption of Tb-PCM-25 at 77 K.

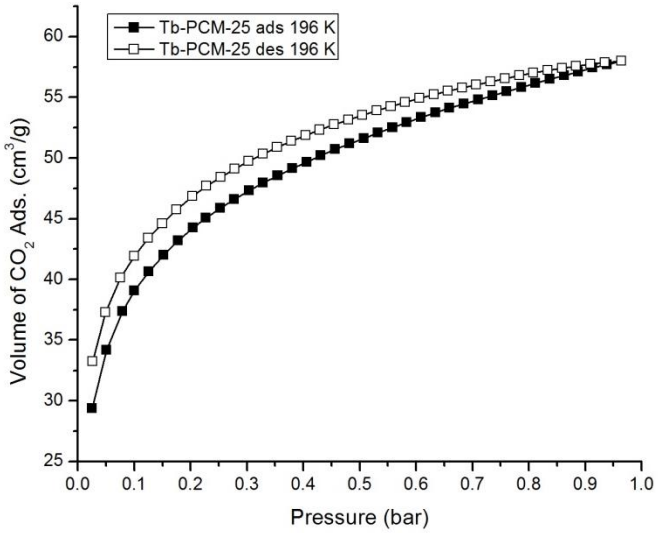

Figure 3.12: CO_2 sorption of Tb-PCM-25 at 196 K.

Tb-PCM-25 also displayed Type-I behavior with H_2 sorption at 77 K (Figure 3.13). Nearing saturation, the material adsorbed 55.12 $cm^3 g^{-1}$ H_2 at 77 K and 1 bar.

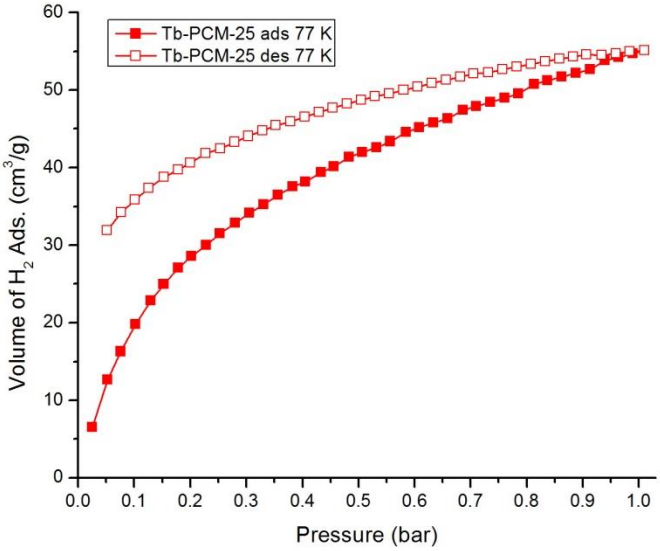

Figure 3.13: H_2 sorption of Tb-PCM-25 at 77 K.

Thermal stability

TGA was performed on the PCM-25 materials with as-synthesized samples (Figure 3.14) and with those after activation at 200 °C (Figure 3.15). Similarly, only the results for Tb-PCM-25 will be discussed in detail.

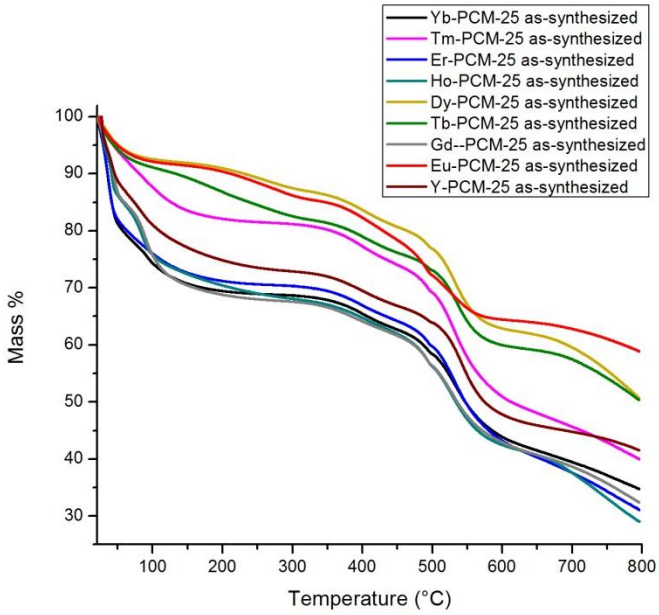

Figure 3.14: TGA of all as-synthesized PCM-25 materials.

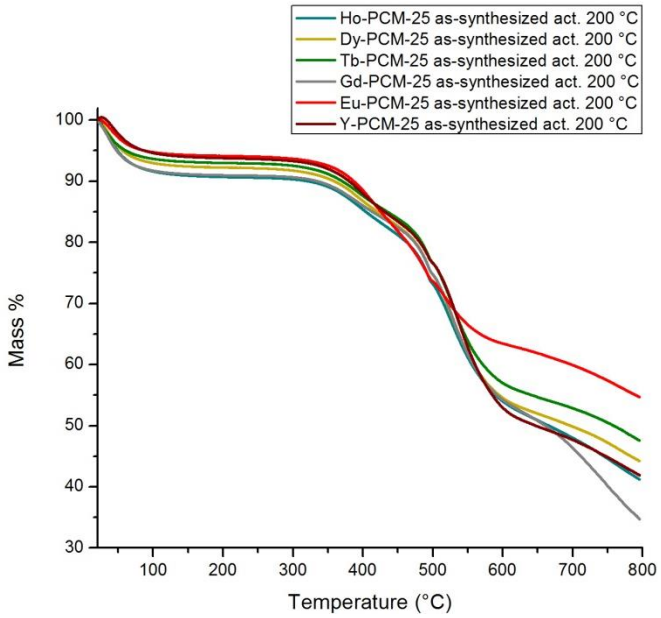

Figure 3.15: TGA of as-synthesized PCM-25 materials after activation at 200 °C.

Several mass losses were observed in an as-synthesized sample of Tb-PCM-25 prior to the onset of structural decomposition at 475 °C (Figure 3.16; black). These can be attributed to the removal of ambient moisture below 100 °C, accompanied by the removal of nonvolatile solvent plus one coordinated OH_2 molecule between 105–340 °C (9.2 %). The results obtained from elemental analysis confirmed the removal of one coordinated OH_2 molecule upon activation at 200 °C under vacuum. Setting the mass at 340 °C (81.7 %) to 100%, corresponding to the fully desolvated structure after the loss of one coordinated OH_2 molecule [$Tb(tctp^{+})(OH_2)_3$], yielded a mass loss of 7.2 % between 340–440 °C. This closely matched the expected decrease of 7.4 % due to the loss of the remaining three coordinated OH_2 molecules.

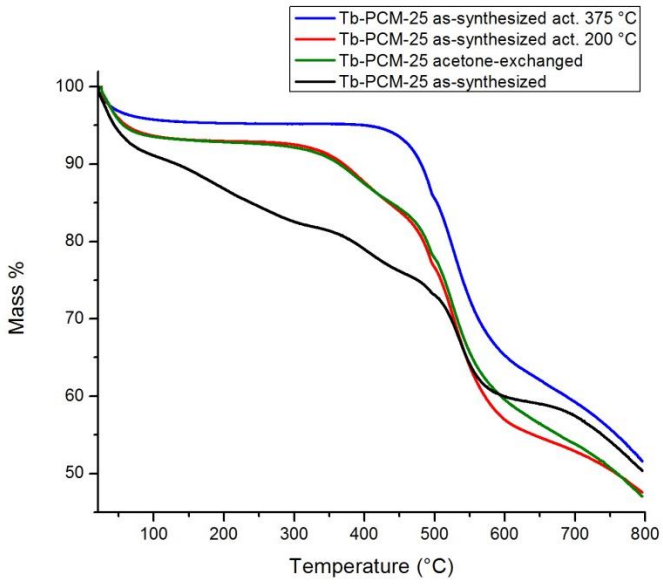

Figure 3.16: TGA of Tb-PCM-25 as-synthesized, acetone-exchanged, and activated under ultrahigh vacuum at 200 and 375 °C.

After activation at 200 °C, TGA of Tb-PCM-25 yielded comparable results to those obtained from the as-synthesized sample (Figure 3.16; red). The material lost 6.1 % mass below 100 °C presumably due to the uptake of ambient moisture into the pores of the material upon loading into the TGA. No decrease was observed in the range of 105–340 °C, indicating that the material had been successfully desolvated during activation. By setting the mass at 340 °C (94.6 %) to 100 % for the triply hydrated Tb-PCM-25 structure [Tb(tctp$^+$)$(OH_2)_3$], the decrease of 7.5 % from 340–440 °C was consistent with the as-synthesized sample and accounted for the loss of three coordinated OH_2 molecules.

Additionally, TGA was obtained on a sample of as-synthesized Tb-PCM-25 that had been activated at 375 °C (Figure 3.16; blue). This sample showed remarkable thermal stability up to 440 °C with only a slight, initial mass loss of 4.2 % below 100 °C,

attributable to the uptake of ambient moisture. Not only did this measurement illustrate that all four coordinated OH_2 molecules could be removed by activation at 375 °C (albeit for 12 hours at 10^{-10} Torr), but it also showed that re-coordination of OH_2 molecules to the Tb(III) sites did not readily occur upon exposure to ambient moisture; if this process were favored, the samples activated at 200 and 375 °C would have been indistinguishable. Furthermore, because the Tb(III) sites remained dehydrated upon exposure to air, this confirmed the removal of one coordinated OH_2 molecule upon activation at 200 °C shown by elemental analysis.

TGA was also performed on solvent-exchanged samples of Tb-PCM-25, namely, with acetone, $CHCl_3$, ethanol, H_2O, and THF (Figure 3.17). Acetone-exchange removed the majority of the nonvolatile solvent molecules prior to analysis and produced only a 6.2 % loss in mass below 100 °C. This was followed by a slight loss of 3.2 % up to 340 °C and a 7.5% loss from 340–440 °C (Figures 3.16 and 3.17; green). However, acetone-exchange yielded virtually identical results to those obtained from an as-synthesized sample that was activated directly at 200 °C. For this reason, no solvent-exchange was employed on any PCM-25 material prior to activation at 200 °C for gas sorption analyses.

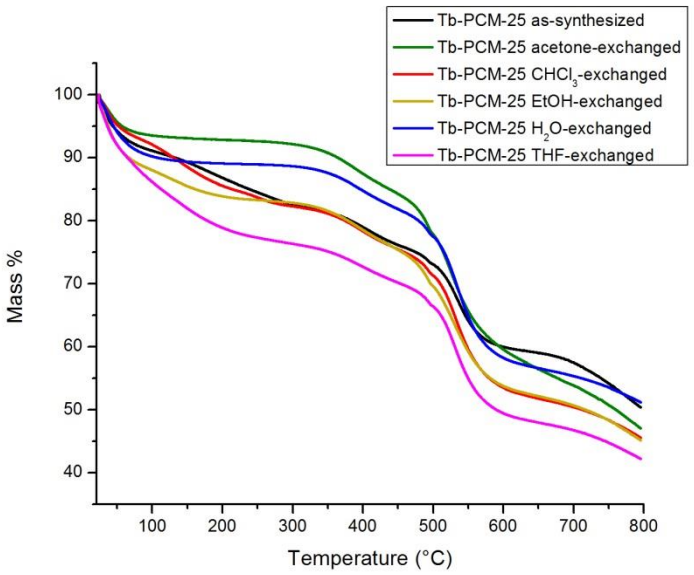

Figure 3.17: TGA of Tb-PCM-25 as-synthesized and after solvent-exchange with acetone, chloroform, ethanol, water, and THF.

Luminescence properties

Due to the presence of emissive Ln species within the materials, the luminescence properties of PCM-25 were investigated. The solid-state excitation and emission spectra for the $tctp^{+}H_3$ ligand (iPCM-1) are shown in Figure 3.18, obtained utilizing λ_{em} = 469 nm and λ_{ex} = 318 nm, respectively. The triplet excited state (T_1) of $tctp^{+}H_3$ was determined by taking the blue edge of the excitation peak (434 nm), yielding a T_1 energy level of 23,041 cm^{-1}. The proximity of the T_1 energy to that of the excited state energy levels of Ln(III) led us to believe that it would efficiently sensitize emission from these Ln's.

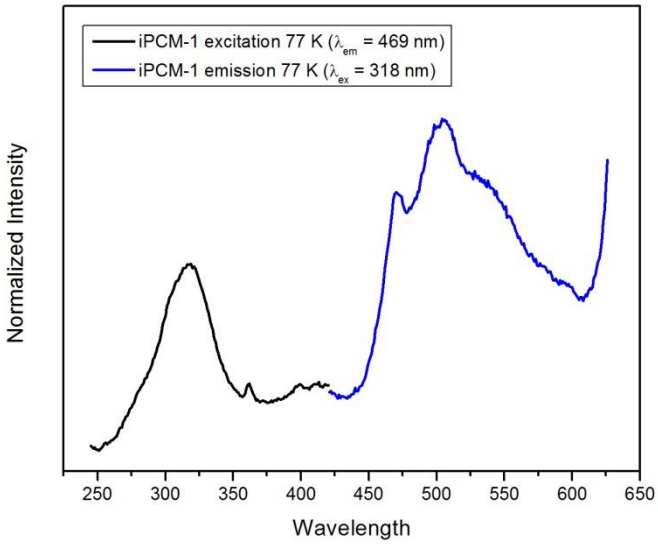

Figure 3.18: Solid-state excitation (λ_{em} = 469 nm) and emission (λ_{ex} = 318 nm) spectra of crystallized tctp$^{+}H_3$ ligand (iPCM-1).

The excitation spectra of Tb-, Eu-, and Dy-PCM-25 are shown in Figure 3.19, obtained by monitoring the emission bands at 545, 613, 576 nm, respectively.

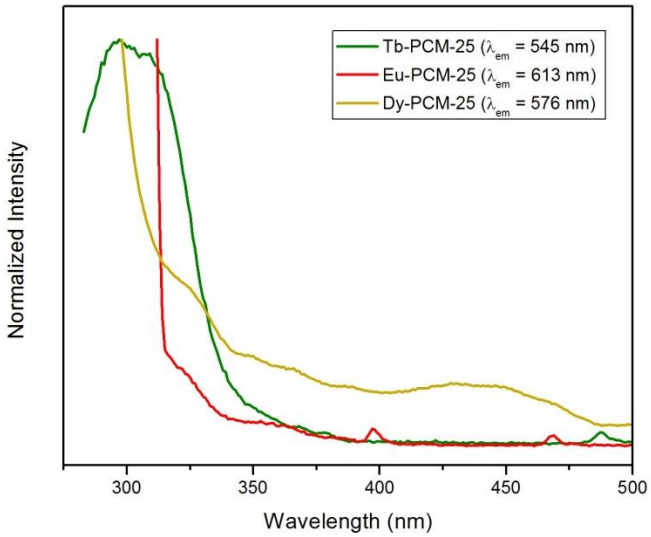

Figure 3.19: Excitation spectra of Tb-, Eu-, and Dy-PCM-25.

The emission spectra of Tb-, Eu-, and Dy-PCM-25 are shown in Figures 3.20-3.22. Tb-PCM-25 produced characteristic Tb(III) emission bands upon excitation at λ_{ex} = 295 nm, corresponding to the $^5D_4 \rightarrow {}^7F_6$ (490 nm), $^5D_4 \rightarrow {}^7F_5$ (545 nm), $^5D_4 \rightarrow {}^7F_4$ (586 nm), and $^5D_4 \rightarrow {}^7F_3$ (622 nm) transitions. Similarly, Eu-PCM-25 produced the expected $^5D_0 \rightarrow {}^7F_1$ (593 nm), $^5D_0 \rightarrow {}^7F_2$ (616 nm), $^5D_0 \rightarrow {}^7F_3$ (654 nm), and $^5D_0 \rightarrow {}^7F_4$ (701 nm) transitions, obtained by excitation at λ_{ex} = 300 nm. Although the intensity of the Dy-PCM-25 emission was the lowest of the three materials, three bands were observed at 484, 576, and 666 nm with excitation at λ_{ex} = 290 nm, corresponding to the $^4F_{9/2} \rightarrow {}^6H_{15/2}$, and $^4F_{9/2} \rightarrow {}^6H_{13/2}$, and $^4F_{9/2} \rightarrow {}^6H_{11/2}$ transitions, respectively.

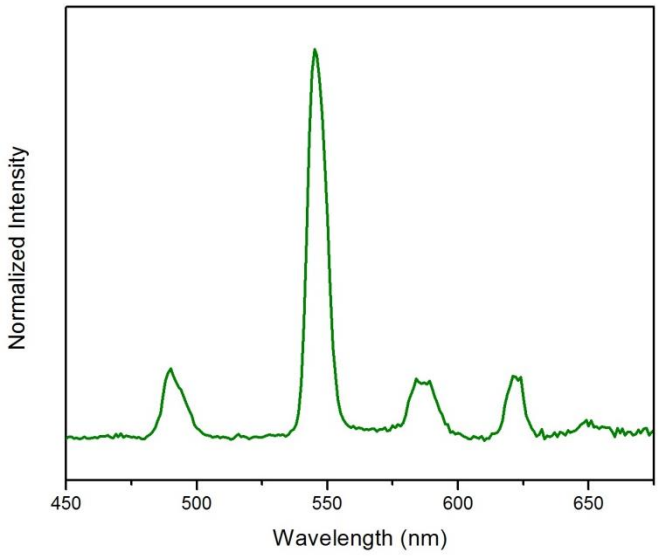

Figure 3.20: Emission spectrum of Tb-PCM-25 (λ_{ex} = 295 nm).

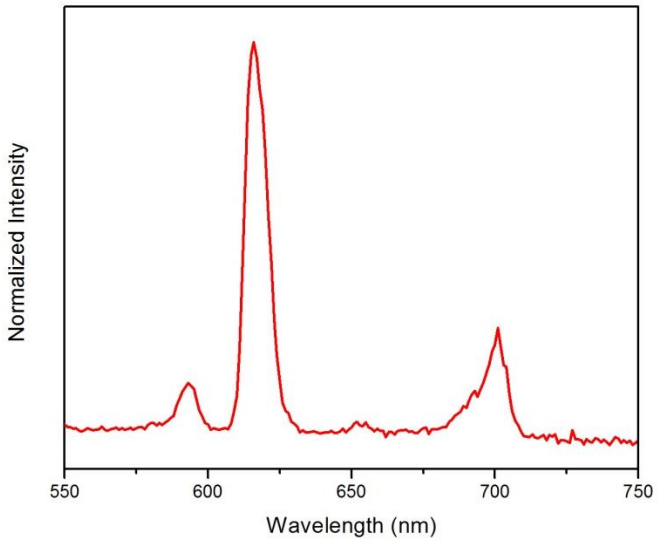

Figure 3.21: Emission spectrum of Eu-PCM-25 (λ_{ex} = 300 nm).

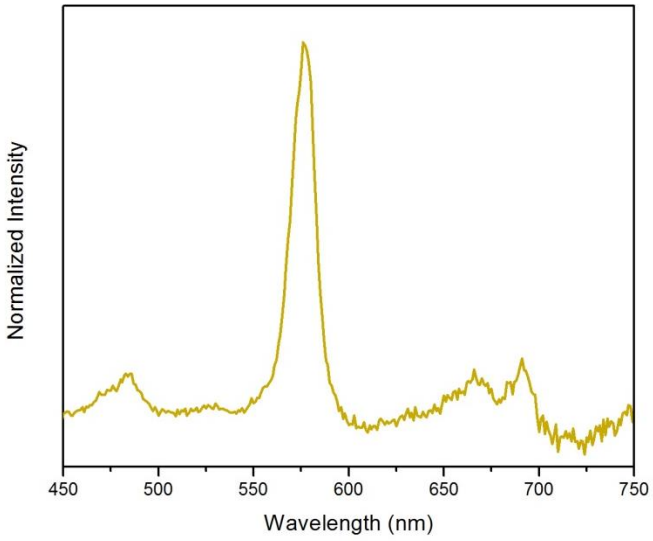

Figure 3.22: Emission spectrum of Dy-PCM-25 (λ_{ex} = 290 nm).

The luminescence properties of the materials were also probed by examining the correlation between activation temperature and the resulting emissive quantum yields and lifetimes. Due to the presence of coordinated OH_2 molecules on each Ln, and since O–H oscillators are known to quench Ln(III) emission, we wanted to determine whether the removal of one or more of these molecules *via* activation would increase the luminescence properties of each material. The solid-state quantum yields for as-synthesized Tb-, Eu-, and Dy-PCM-25 were first obtained using a spectrophotometer fitted with an integrating sphere collector, and then each was activated under ultrahigh vacuum at 25 and 200 °C in a custom air-free quartz tube. Changes in the quantum yields of the materials upon activation were monitored by changes in the emission intensities relative to the intensities of the as-synthesized materials. The quantum yield for as-synthesized Tb-PCM-25 was determined to be 3.7 ± 0.2 %, which experienced a slight increase to 4.6 ± 0.5 and 5 ± 2 % after activation at 25 and 200 °C, respectively. The normalized emission spectra representative of these results are shown in Figure 3.23.

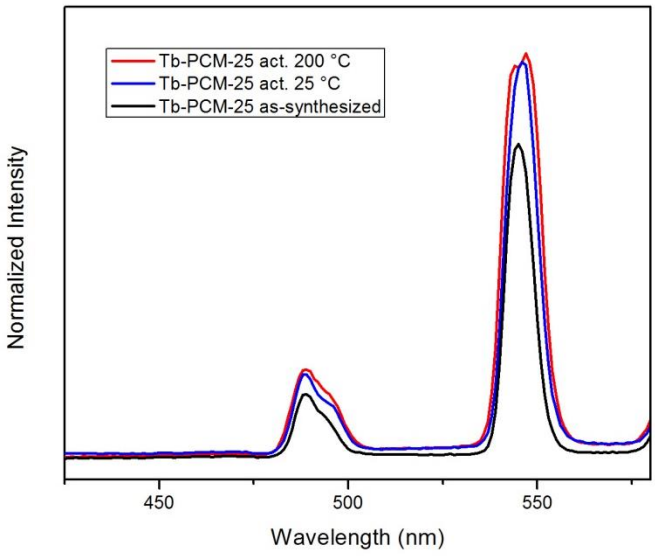

Figure 3.23: Emission intensity of Tb-PCM-25 monitored at 545 nm (λ_{ex} = 295 nm) for as-synthesized and activated samples.

The Eu-PCM-25 quantum yields obtained for the as-synthesized, activated at 25 °C, and activated at 200 °C samples did not correlate with the activation temperatures used for each experiment, resulting in values of 8.4 ± 0.3 %, 5.3 ± 0.4 %, and 6.5 ± 0.7 %, respectively (Figure 3.24).

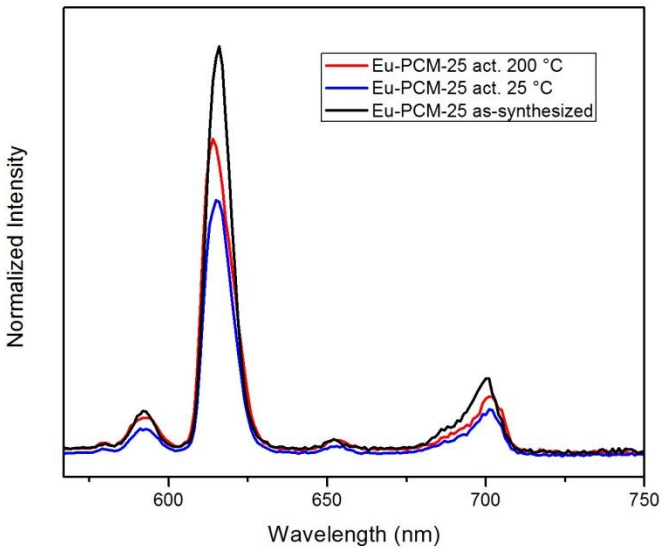

Figure 3.24: Emission intensity of Eu-PCM-25 monitored at 616 nm (λ_{ex} = 300 nm) for as-synthesized and activated samples.

Similarly, the quantum yield obtained for as-synthesized Dy-PCM-25 was 0.94 ± 0.08 %, which increased slightly to 1.36 ± 0.07 % upon activation at 25 °C, but then decreased further to 0.41 ± 0.02 % after activation at 200 °C (Figure 3.25).

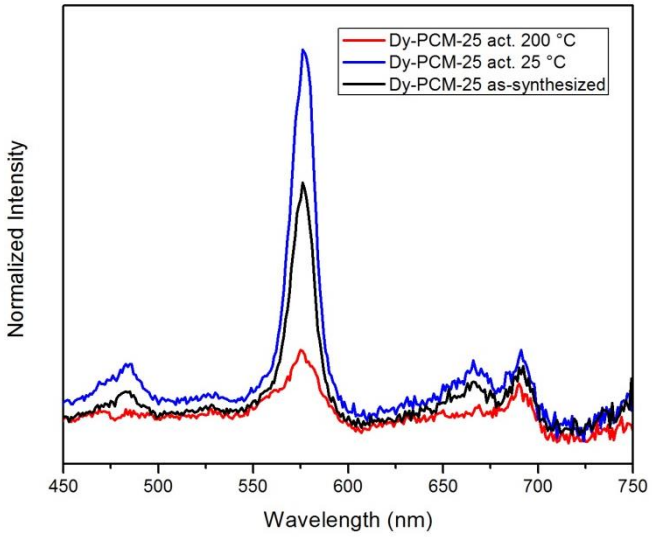

Figure 3.25: Emission intensity of Dy-PCM-25 monitored at 576 nm (λ_{ex} = 290 nm) for as-synthesized and activated samples.

The emission lifetimes for Tb-, Eu-, and Dy-PCM-25 were also determined under all three activation conditions. Unfortunately, none of the materials displayed any significant trend upon activation at 25 and 200 °C. The lifetime for as-synthesized Tb-PCM-25 was 57 ± 2 μs, followed by 20 ± 2 and 111 ± 1 μs after activation at 25 and 200 °C, respectively. Eu-PCM-25 exhibited a consistent decrease in lifetime upon activation with increasing temperature, yielding values of 181 ± 3, 79 ± 2, and 60 ± 2 μs for the as-synthesized, activated at 25 °C, and activated at 200 °C materials, respectively. The lifetime of emission from Dy-PCM-25 was unable to be determined due to the low intensity of luminescence from the material under all activation conditions. A summary of the quantum yields and lifetimes for all experiments is shown in Table 3.2.

	Tb-PCM-25	Eu-PCM-25	Dy-PCM-25
QY as-synthesized (%)	3.7 ± 0.2	8.4 ± 0.3	0.94 ± 0.08
QY act. 25 °C (%)	4.6 ± 0.5	5.3 ± 0.4	1.36 ± 0.07
QY act. 200 °C (%)	5 ± 2	6.5 ± 0.7	0.41 ± 0.02
Lifetime as-synthesized (μs)	57 ± 2	181 ± 3	n/a
Lifetime act. 25 °C (μs)	20 ± 2	79 ± 2	n/a
Lifetime act. 200 °C (μs)	111 ± 1	60 ± 2	n/a

Table 3.2: Summary of luminescence quantum yields (QY) and lifetimes of Tb-, Eu-, and Dy-PCM-25.

TGA results confirmed that all four coordinated OH_2 molecules could be removed with activation at 375 °C under ultrahigh vacuum. It was expected that the complete removal of the O–H oscillators on the Ln(III) nodes should have led to an increase in the luminescence properties of the material. Regrettably, a sample of Tb-PCM-25 activated at 375 °C did not exhibit any detectable luminescence. It is possible that elimination of the OH_2 molecules allowed for other quenching events to occur, namely, photo-induced electron transfer involving the ligand carboxylate groups.[200] Another explanation could be that the material is no longer porous; it is common for PCPs to collapse following the removal of coordinated solvent molecules, especially in cases where they comprise a sizeable fraction of the coordination sphere.[148,201] However, Tb-PCM-25 activated at 375 °C still exhibited crystallinity as shown by XRPD (Figure 3.26; light blue).

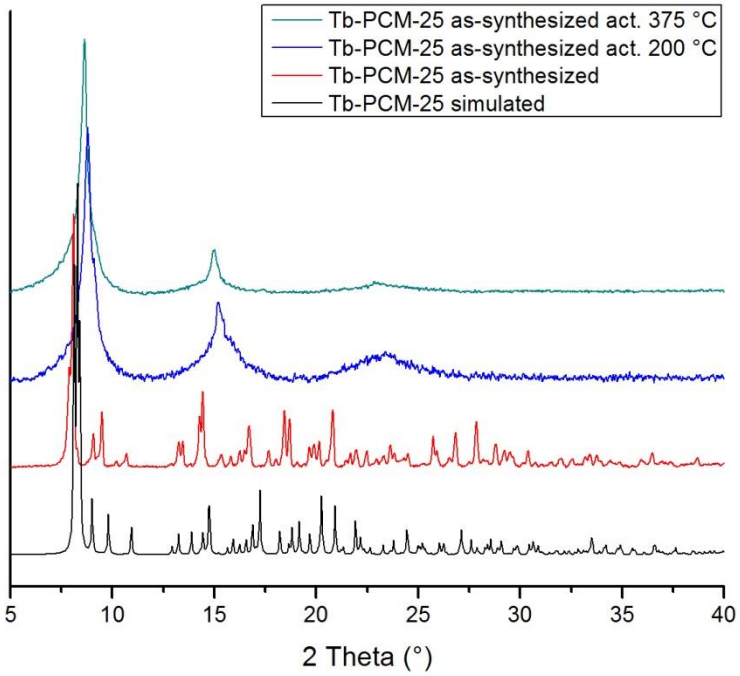

Figure 3.26: X-ray powder diffraction patterns of Tb-PCM-25 as-synthesized and after activation at 200 and 375 °C.

It is possible is that the two *syn*-carboxylates can re-coordinate η^2- to the metal nodes following the removal of all coordinated OH_2 groups, stabilizing the lattice with 6-coordinate Ln(III) species. This transition could induce a change in cell symmetry within the material due to contortions of the $[tctp^+]^{3-}$ ligand, which may also explain the presence of only two XRPD peaks at these temperatures. Nevertheless, identical powder patterns and measurable surface areas by BET analysis confirmed that the porosity of Tb-PCM-25 was retained after activation at both 200 and 375 °C. Efforts to obtain a single crystal structure of Tb-PCM-25 following the removal of the coordinated OH_2 molecules are ongoing.

CONCLUSIONS

We have synthesized a new series of Ln(III)-based coordination polymers from a tetrahedral phosphonium zwitterion. All nine PCM-25 materials are isostructural and exhibit comparable thermal stabilities and gas sorption properties. Their surface areas range from 173–212 $m^2 g^{-1}$, and each adsorbs a moderate amount of H_2 at 77 K, between 55.12–80.69 $cm^3 g^{-1}$. The luminescence lifetimes and quantum yields of Tb-, Eu-, and Dy-PCM-25 were investigated under three different activation conditions and showed no correlation between activation temperature and increased luminescence properties, despite the removal of all four coordinated OH_2 molecules and the retained porosity of the material. Ongoing research with this system involves the synthesis of new Ln(III)-based materials from the $tctp^+H_3$ ligand, including those from high-pressure, high-temperature water-based syntheses, in an effort to design new, thermally-stable, luminescent materials from this highly-symmetric organophosphonium ligand.

EXPERIMENTAL TECHNIQUES

General

All ligand syntheses were performed under an N_2 atmosphere using standard schlenk techniques. 1,4-dibromobenzene (Alfa Aesar, ≥98%), phosphorus trichloride (Sigma-Aldrich, ≥99%), *n*-butyllithium (1.6 M in hexanes, Sigma-Aldrich), 4-iodobenzoic acid (Sigma-Aldrich, ≥98%), $Pd(OAc)_2$ (Strem, ≥99.9%-Pd), $Y(NO_3)_3 \cdot 6H_2O$ (Alfa Aesar, ≥99.9%), $Tb(NO_3)_3 \cdot nH_2O$ (Alfa Aesar, ≥99.9%), $Ln(NO_3)_3 \cdot nH_2O$ (Ln = Eu, Gd, Er, Tm, Yb) (Strem, ≥99.9%), and $Ln(NO_3)_3 \cdot nH_2O$ (Ln = Dy, Ho) (Sigma-Aldrich, ≥99.9%) were used as received. Organic solvents (THF, DMF, ethanol, diethyl ether) were obtained from Fisher Scientific. THF was dried/degassed

using a Solvent Purification System (Innovative Technologies) and further degassed using freeze-thaw cycles prior to use. Diethyl ether, DMF, and all aqueous solutions were purged with N_2 for 30 min prior to use. ^{1}H-NMR, ^{13}C-NMR and ^{31}P-NMR were collected in-house using a Varian Unity 300 MHz spectrometer; FT-IR spectra were obtained directly from solid samples using a Nicolet iS*50 spectrophotometer fitted with an attenuated total reflectance apparatus; thermogravimetric analyses (TGA) were collected using a TA Instruments Q50 system. Elemental microanalyses were performed by Midwest Microlab LLC (Indianapolis).

X-Ray Crystallography

Suitable crystals were mounted on thin glass fibers using perfluoropolyether oil, which were frozen *in situ* by a nitrogen gas Cryostream flow. Data for the structures reported were collected on a Rigaku Saturn CCD diffractometer using monochromated Mo$K\alpha$ radiation (λ = 0.71073 Å). Absorption corrections were made based on multiple ψ- and ω-scans using the SORTAV program. Structures were solved using direct methods and refined on F^2 then refined using SHELXTL-97 software. All non-hydrogen atoms were refined anisotropically for all structures, except for uncoordinated and disordered solvent molecules, which were refined with isotropic displacement parameters. The SQUEEZE utility in *PLATON* was applied *post*-refinement in order to remove residual peaks due to any remaining disordered solvent. In all instances, this resulted in only small improvements to the final statistics (included in CIF data). For all structures, hydrogen atoms were fixed based on idealized coordinates and were refined with values of U_{iso} set to 1.5 times that of the carrier atom.

X-ray powder diffraction

Phase purity of iPCM-1 and all PCM-25 materials before and after activation were confirmed by analysis of powdered crystalline samples that were sealed inside borosilcate capillary tubes and spun *in situ* to prevent preferential orientation of the crystallites. Spectra were recorded on a Stoe Stadi-P diffractometer, operating in Debye-Scherrer geometry using Co*K*α radiation (1.7902 Å). Reflection data was collected in the range 5.0–40.0° 2θ using multiple scans, which were subsequently averaged. The XRPD spectra were then compared directly to their corresponding simulated patterns that were generated using the SimPowPatt function in *PLATON* using the single crystal model for the hkl reflection data obtained in the single crystal experiment.

Fluorimetry

Luminescence measurements were recorded on a Photon Technology International QM 4 spectrophotometer equipped with a calibrated 6-in. diameter K Sphere-B integrating sphere, which was used for as-synthesized absolute quantum yield measurements. The as-synthesized absolute quantum yields of all materials were calculated by dividing the area under the emission peaks of the materials by the difference between the area under the excitation peak of the sample and that of a blank solution. Subsequent quantum yields of evacuated materials were determined by comparing the intensity of the main luminescent transition of each Ln-PCM-25 in a custom air-free quartz cell to that of the as-synthesized material; all intensities were standardized to the λ_{em} = 575 nm emission intensity of an external perylene diimide reference utilizing λ_{ex} = 525 nm, which was stored in a sealed quartz tube. Luminescence lifetimes were determined by monitoring the main luminescent transition under excitation at the optimal wavelength inherent to each material, and utilized a quartz tube containing

$BaSO_4$ to determine the instrument response function (IRF). Luminescence decays were modeled as single-exponential functions in all cases using FeliX32 Analysis software v. 1.2.

Ligand synthesis

Procedure for ttpBr$_3$

1,4-dibromobenzene (20.0 g; 84.8 mmol) was dissolved in THF (500 cm^3) in a 1000 cm^3 round bottomed flask and cooled to –78 °C. A solution of *n*-butyllithium (1.6 M in hexanes; 84.8 mmol) was added drop-wise to the reaction over a 30-minute period. The resulting white slurry was stirred for 1 h at –78 °C. PCl_3 (2.47 cm^3; 28.3 mmol) was added drop-wise to the mixture over 30 min before slowly warming to room temperature with stirring overnight. The yellow solution was washed with degassed sat. NaCl (200 cm^3) and extracted twice with diethyl ether (100 cm^3). The combined organic extracts were dried over $MgSO_4$, and the solvent was removed *in vacuo* to yield a yellow oil. The product was purified by column chromatography (silica gel eluted with CH_2Cl_2:hexanes (1:1)) to afford a white powder (11.1 g; 22.2 mmol). Yield, 78.6 %. ^{1}H NMR ($CDCl_3$, 300.1 MHz) δ = 7.46 (dd, 6H), 7.10 (t, 6H); ^{13}C NMR ($CDCl_3$, 75.5 MHz) δ = 135.20 (d, Ar), 135.06 (d, Ar), 131.92 (d, Ar), 123.94 (s, Ar); ^{31}P NMR ($CDCl_3$, 121.5 MHz) δ = –7.41. FT-IR (ATR) ν_{max} (cm^{-1}) = 3041 (w), 2955 (w), 2927 (w), 1903 (w), 1790 (w), 1637 (w), 1569 (s), 1471 (s), 1382 (s), 1299 (m), 1260 (w), 1177 (m), 1106 (w), 1092 (m), 1064 (s), 1006 (s), 948 (w), 843 (m), 816 (s), 807 (s), 725 (s), 709 (w), 629 (w), 528 (m), 509 (s), 473 (m), 452 (m), 429 (w), 380 (w), 355 (m), 338 (m), 291 (w), 281 (w), 260 (m), 244 (m), 231 (w), 187 (w), 156 (m), 132 (w), 121 (w).

Procedure for tctpLi$_3$

$TtpBr_3$ (5.0 g; 10.0 mmol) was dissolved in THF (500 cm^3) in a 1000 cm^3 round bottomed flask and cooled to –78 °C. A solution of *n*-butyllithium (2.5 M in hexanes; 32.1 mmol) was added drop-wise to the reaction over a 30-minute period. The light orange slurry was stirred for 2 h at –78 °C, after which an excess of crushed dry ice (*ca*. 500 g) and diethyl ether (200 cm^3) were added. The reaction was removed from the cooling bath and allowed to stir at room temperature overnight. The product was filtered in air and rinsed with fresh diethyl ether to afford an off-white powder (3.7 g; 9.1 mmol). Yield, 90.5 %. ^{1}H NMR (D_2O, 300.1 MHz) δ = 7.69 (dd, 6H), 7.27 (td, 6H); ^{31}P NMR (D_2O, 121.5 MHz) δ = –6.50.

Procedure for tctpH$_3$

$TctpLi_3$ (2.0 g; 4.9 mmol) was dissolved in H_2O (400 cm^3) in a 600 cm^3 beaker and precipitated with HCl (1.0 M) to pH = 3. The product was isolated by centrifugation, rinsed twice with H_2O, and dried under N_2 to afford a white powder (1.8 g; 4.7 mmol). Yield, 96.4 %. ^{1}H NMR (DMSO-d_6, 300.1 MHz) δ = 7.96 (dd, 6H), 7.38 (t, 6H); ^{13}C NMR (DMSO-d_6, 75.5 MHz) δ = 167.63 (s, CO_2H), 141.66 (d, Ar), 134.17 (d, Ar), 132.32 (s, Ar), 130.33 (d, Ar); ^{31}P NMR (DMSO-d_6, 121.5 MHz) δ = –5.30. FT-IR (ATR) ν_{max} (cm^{-1}) = 3392 (br), 3015 (br), 2658 (w), 2537 (w), 1685 (s), 1593 (s), 1558 (m), 1493 (w), 1413 (m), 1394 (m), 1311 (m), 1288 (w), 1269 (m), 1230 (m), 1181 (m), 1128 (w), 1108 (w), 1085 (m), 1016 (s), 919 (w), 851 (m), 813 (w), 794 (w), 760 (s), 693 (s), 633 (w), 519 (s), 477 (m), 353 (w), 300 (m), 273 (w), 174 (w), 149 (w), 133 (w).

Procedure for tctp$^{+}H_3$

TctpH_3 (0.20 g; 0.51 mmol), 4-iodobenzoic acid (0.19 g; 0.76 mmol), and palladium (II) acetate (5.7 mg; 0.025 mmol) were dissolved in DMF (30 cm^3) in a 50 cm^3 round bottomed flask. The yellow solution was stirred at room temperature overnight followed by heating at 150 °C until the solution turned a deep red color (8-12 h). The reaction was then cooled to room temperature and the solvent reduced to *ca*. 5 cm^3. The product was precipitated with cold H_2O (100 cm^3), isolated by centrifugation, and dried under N_2 to afford a brown solid. The product was washed with acetone (2 x 10 cm^3) and dried under N_2 to afford a light brown powder (0.22 g; 0.43 mmol). Yield, 84.3 %. Analysis after dehydration under vacuum at 50 °C for 18 h, found: C 62.78, H 3.59; $C_{28}H_{19}O_8P \cdot H_2O$ requires: C 63.16, H 3.98. ^{1}H NMR (DMSO-d_6, 300.1 MHz) δ = 8.26 (dd, 8H), 7.89 (dd, 8H); ^{13}C NMR (D_2O, NaOH, 75.5 MHz) δ = 173.81 (s, CO_2^-), 143.06 (d, Ar), 135.14 (d, Ar), 129.88 (d, Ar), 119.73 (d, Ar); ^{31}P NMR (DMSO-d_6, 121.5 MHz) δ = 23.63. FT-IR (ATR) ν_{max} (cm^{-1}) = 3449 (br), 3041 (w), 2800 (w), 2607 (w), 2489 (w), 1702 (s), 1600 (w), 1561 (w), 1545 (w), 1494 (w), 1392 (s), 1313 (w), 1244 (m), 1182 (w), 1128 (w), 1097 (s), 1012 (m), 859 (m), 813 (w), 763 (m), 709 (s), 690 (w), 632 (m), 567 (s), 512 (w), 476 (w), 384 (s), 314 (w), 271 (s), 177 (w), 138 (w), 122 (m).

PCP synthesis

Procedure for Y-PCM-25

Tctp$^{+}H_3$ (30.0 mg, 0.058 mmol) was dissolved in ethanol:DMF:H_2O (1:1:1, 5.0 cm^3), to which solid $Y(NO_3)_3 \cdot 6H_2O$ (87.7 mg, 0.23 mmol) was added. The yellow solution was heated in a 20 cm^3 scintillation vial at 45 °C for 7 d in a graphite thermal bath. Brown platelets were isolated by decantation of the mother liquor and brief

sonication (5 s) in fresh ethanol:DMF:H_2O (1:1:1, 10 cm^3). Average yield, 65 mg (from six reactions). Analysis after dehydration under vacuum at 100 °C for 18 h, found: C 51.5, H 3.00; $C_{28}H_{16}O_8PY \cdot 3H_2O$ requires: C 51.4, H 3.39. FT-IR (ATR) ν_{max} (cm^{-1}) = 3216 (br s), 2934 (w), 1651 (s), 1585 (s), 1534 (s), 1497 (w), 1377 (s), 1308 (w), 1254 (m), 1187 (w), 1145 (w), 1102 (s), 1064 (w), 1014 (m), 863 (m), 775 (m), 727 (s), 692 (w), 661 (w) 633 (w), 572 (m), 542 (w), 475 (m), 400 (m).

Procedure for Eu-PCM-25

$Tctp^+H_3$ (30.0 mg, 0.058 mmol) was dissolved in ethanol:DMF:H_2O (1:1:1, 5.0 cm^3), to which solid $Eu(NO_3)_3 \cdot 6H_2O$ (102 mg, 0.23 mmol) was added. The yellow solution was heated and the resulting brown platelets were isolated by processes analogous to those mentioned above (*Y-PCM-25*). Average yield, 100 mg (from six reactions). Analysis after dehydration under vacuum at 100 °C for 18 h, found: C 46.8, H 2.96; $C_{28}H_{16}O_8PEu \cdot 3H_2O$ requires: C 46.9, H 3.09. FT-IR (ATR) ν_{max} (cm^{-1}) = 3357 (br m), 3064 (w), 2931 (w), 1651 (w), 1585 (s), 1537 (s), 1495 (w), 1371 (s), 1254 (w), 1187 (w), 1142 (w), 1098 (s), 1013 (m), 854 (m), 773 (m), 728 (s), 691 (m), 631 (w), 569 (m), 541 (w), 471 (m), 400 (s).

Procedure for Gd-PCM-25

$Tctp^+H_3$ (30.0 mg, 0.058 mmol) was dissolved in ethanol:DMF:H_2O (1:1:1, 5.0 cm^3), to which solid $Gd(NO_3)_3 \cdot 6H_2O$ (103 mg, 0.23 mmol) was added. The yellow solution was heated and the resulting brown platelets were isolated by processes analogous to those mentioned above (*Y-PCM-25*). Average yield, 100 mg (from six reactions). Analysis after dehydration under vacuum at 100 °C for 18 h, found: C 48.0, H

2.70; $C_{28}H_{16}O_8PGd \cdot 2H_2O$ requires: C 47.7, H 2.86. FT-IR (ATR) ν_{max} (cm^{-1}) = 3373 (br m), 3065 (w), 2930 (w), 1652 (w), 1585 (s), 1537 (s), 1495 (w), 1371 (s), 1311 (w), 1254 (w), 1188 (w), 1142 (w), 1098 (s), 1013 (m), 857 (m), 843 (w), 773 (m), 729 (s), 691 (m), 662 (w), 631 (w), 569 (m), 544 (w), 468 (m), 400 (m).

Procedure for Tb-PCM-25

$Tctp^+H_3$ (30.0 mg, 0.058 mmol) was dissolved in ethanol:DMF:H_2O (1:1:1, 5.0 cm^3), to which solid $Tb(NO_3)_3 \cdot nH_2O$ (104 mg, 0.23 mmol) was added. The yellow solution was heated and the resulting brown platelets were isolated by processes analogous to those mentioned above (*Y-PCM-25*). Average yield, 100 mg (from six reactions). Analysis after dehydration under vacuum at 100 °C for 18 h, found: C 47.2, H 2.52; $C_{28}H_{16}O_8PTb \cdot 2.5H_2O$ requires: C 47.0, H 2.96. FT-IR (ATR) ν_{max} (cm^{-1}) = 3362 (br m), 3065 (w), 2929 (w), 1652 (m), 1585 (s), 1537 (s), 1494 (w), 1371 (s), 1310 (w), 1253 (w), 1188 (w), 1142 (w), 1098 (s), 1013 (m), 857 (m), 843 (w), 773 (m), 728 (s), 691 (m), 661 (w), 631 (w), 569 (m), 544 (w), 472 (m), 400 (m).

Procedure for Dy-PCM-25

$Tctp^+H_3$ (30.0 mg, 0.058 mmol) was dissolved in ethanol:DMF:H_2O (1:1:1, 5.0 cm^3), to which solid $Dy(NO_3)_3 \cdot nH_2O$ (105 mg, 0.23 mmol) was added. The yellow solution was heated and the resulting brown platelets were isolated by processes analogous to those mentioned above (*Y-PCM-25*). Average yield, 100 mg (from six reactions). Analysis after dehydration under vacuum at 100 °C for 18 h, found: C 46.5, H 2.84; $C_{28}H_{16}O_8PDy \cdot 3H_2O$ requires: C 46.2, H 3.05. FT-IR (ATR) ν_{max} (cm^{-1}) = 3371 (br m), 3066 (w), 2934 (w), 1651 (w), 1585 (s), 1537 (s), 1495 (w), 1370 (s), 1311 (w), 1255

(w), 1188 (w), 1142 (w), 1098 (s), 1013 (m), 858 (m), 844 (w), 773 (m), 729 (s), 691 (m), 631 (w), 569 (m), 545 (w), 468 (m), 400 (m).

Procedure for Ho-PCM-25

Tctp^{+}H$_3$ (30.0 mg, 0.058 mmol) was dissolved in ethanol:DMF:H_2O (1:1:1, 5.0 cm^3), to which solid $Ho(NO_3)_3 \cdot 5H_2O$ (101 mg, 0.23 mmol) was added. The yellow solution was heated and the resulting brown platelets were isolated by processes analogous to those mentioned above (*Y-PCM-25*). Average yield, 100 mg (from six reactions). Analysis after dehydration under vacuum at 100 °C for 18 h, found: C 46.9, H 3.20; $C_{28}H_{16}O_8PHo \cdot 2.5H_2O$ requires: C 46.6, H 2.93. FT-IR (ATR) ν_{max} (cm^{-1}) = 3334 (br w), 3061 (w), 2928 (w), 2859 (w), 1655 (s), 1589 (s), 1540 (s), 1493 (m), 1412 (w), 1381 (s), 1308 (w), 1252 (m), 1186 (w), 1140 (w), 1099 (s), 1062 (w), 1013 (m), 857 (m), 776 (m), 735 (s), 693 (m), 658 (w), 632 (w), 573 (m), 548 (w), 482 (m), 402 (m).

Procedure for Er-PCM-25

Tctp^{+}H$_3$ (30.0 mg, 0.058 mmol) was dissolved in ethanol:DMF:H_2O (1:1:1, 5.0 cm^3), to which solid $Er(NO_3)_3 \cdot nH_2O$ (106 mg, 0.23 mmol) was added. The yellow solution was heated and the resulting brown platelets were isolated by processes analogous to those mentioned above (*Y-PCM-25*). Average yield, 100 mg (from six reactions). Analysis after dehydration under vacuum at 100 °C for 18 h, found: C 45.8, H 2.61; $C_{28}H_{16}O_8PEr \cdot 3H_2O$ requires: C 45.9, H 3.03. FT-IR (ATR) ν_{max} (cm^{-1}) = 3366 (br s), 2933 (w), 1652 (m), 1585 (s), 1534 (s), 1497 (w), 1378 (s), 1308 (w), 1254 (w), 1187 (w), 1143 (w), 1102 (s), 1064 (w), 1013 (m), 972 (w), 863 (m), 816 (w), 775 (m), 727 (s), 691 (m), 661 (w), 633 (w), 572 (m), 541 (w), 479 (m), 402 (m).

Procedure for Tm-PCM-25

$Tctp^{+}H_3$ (30.0 mg, 0.058 mmol) was dissolved in ethanol:DMF:H_2O (1:1:1, 5.0 cm^3), to which solid $Tm(NO_3)_3 \cdot 6H_2O$ (106 mg, 0.23 mmol) was added. The yellow solution was heated and the resulting brown platelets were isolated by processes analogous to those mentioned above (*Y-PCM-25*). Average yield, 100 mg (from six reactions). Analysis after dehydration under vacuum at 100 °C for 18 h, found: C 45.5, H 2.99; $C_{28}H_{16}O_8PTm \cdot 3H_2O$ requires: C 45.8, H 3.02. FT-IR (ATR) ν_{max} (cm^{-1}) = 3365 (br m), 2933 (w), 1652 (m), 1585 (s), 1537 (s), 1497 (w), 1378 (s), 1308 (w), 1254 (w), 1187 (w), 1143 (w), 1102 (s), 1064 (w), 1013 (m), 971 (w), 864 (m), 815 (w), 774 (m), 728 (s), 692 (m), 661 (w), 632 (w), 572 (m), 544 (w), 479 (m), 402 (m).

Procedure for Yb-PCM-25

$Tctp^{+}H_3$ (30.0 mg, 0.058 mmol) was dissolved in ethanol:DMF:H_2O (1:1:1, 5.0 cm^3), to which solid $Yb(NO_3)_3 \cdot 5H_2O$ (103 mg, 0.23 mmol) was added. The yellow solution was heated and the resulting brown platelets were isolated by processes analogous to those mentioned above (*Y-PCM-25*). Average yield, 100 mg (from six reactions). Analysis after dehydration under vacuum at 100 °C for 18 h, found: C 44.2, H 2.92; $C_{28}H_{16}O_8PYb \cdot 4H_2O$ requires: C 44.5, H 3.20. FT-IR (ATR) ν_{max} (cm^{-1}) = 3362 (br m), 2933 (w), 1652 (m), 1586 (s), 1537 (s), 1497 (w), 1378(s), 1308 (w), 1254 (w), 1187 (w), 1144 (w), 1102 (s), 1064 (w), 1013 (m), 971 (w), 865 (m), 818 (w), 775 (m), 728 (s), 692 (m), 661 (w), 633 (w), 573 (m), 544 (w), 479 (m), 402 (m).

[148] O. K. Farha, I. Eryazici, N. C. Jeong, B. G. Hauser, C. E. Wilmer, A. A. Sarjeant, R. Q. Snurr, S. T. Nguyen, A. O. Yazaydin, J. T. Hupp, *J. Am. Chem. Soc.* **2012**, *134*, 15016.

[149] Y. -Q. Chen, G. -R. Li, Z. Chang, Y. -K. Qu, Y. -H. Zhang, X. -H. Bu, *Chem. Sci.* **2013**, *4*, 3678.

[150] Z. -F. Wu, B. Tan, M. -L. Feng, A. -J. Lan, X. -Y. Huang, *J. Mater. Chem. A* **2014**, *2*, 6426.

[151] B. V. Harbuzaru, A. Corma, F. Rey, J. L. Jorda, D. Ananias, L. D. Carlos, J. Rocha, *Angew. Chem. Int. Ed.* **2009**, *48*, 6476.

[152] R. -B. Lin, F. Li, S. -Y. Liu, X. -L. Qi, J. -P. Zhang, X. -M. Chen, *Angew. Chem. Int. Ed.* **2013**, *52*, 13429.

[153] X. Wei, L. Zheng, F. Luo, Z. Lin, L. Guo, B. Qiu, G. Chen, *J. Mater. Chem. B* **2013**, *1*, 1812.

[154] J. C. G. Bunzli, C. Piguet, *Chem. Soc. Rev.* **2005**, *34*, 1048.

[155] A. de Bettencourt-Dias, *Dalton Trans.* **2007**, 2229.

[156] Q. Dai, M. E. Foley, C. J. Breshike, A. Lita, G. F. Strouse, *J. Am. Chem. Soc.* **2011**, *133*, 15475.

[157] J. Kido, Y. Okamoto, *Chem. Rev.* **2002**, *102*, 2357.

[158] A. -L. Penard, T. Gacoin, J. -P. Boilot, *Accounts Chem. Res.* **2007**, *40*, 895.

[159] L. D. Carlos, R. A. S. Ferreira, V. de Z. Bermudez, S. J. L. Ribeiro, *Adv. Mater.* **2009**, *21*, 509.

[160] K. Kuriki, Y. Koike, Y. Okamoto, *Chem. Rev.* **2002**, *102*, 2347.

[161] L. Wang, Y. Li, *Chem. Mater.* **2007**, *19*, 727.

[162] Y. Fan, P. Yang, S. Huang, J. Jiang, H. Lian, J. Lin, *J. Phys. Chem. C* **2009**, *113*, 7826.

[163] B. Andes Hess, A. Kędziorski, L. Smentek, D. J. Bornhop, *J. Phys. Chem. A* **2008**, *112*, 2397.

[164] C. P. Montgomery, B. S. Murray, E. J. New, R. Pal, D. Parker, *Acc. Chem. Res.* **2009**, *42*, 925.

[165] B. Song, V. Sivagnanam, C. D. B. Vandevyver, I. Hemmilä, H. -A. Lehr, M. A. M. Gijs, J. -C. G. Bünzli, *Analyst* **2009**, *134*, 1991.

[166] T. Gunnlaugsson, J. P. Leonard, *Chem. Commun.* **2005**, 3114.

[167] H. Tsukube, S. Shinoda, *Chem. Rev.* **2002**, *102*, 2389.

[168] O. S. Wolfbeis, A. Durkop, M. Wu, Z. H. Lin, *Angew. Chem. Int. Ed.* **2002**, *41*, 4495.

[169] B. D. Chandler, D. T. Cramb, G. K. H. Shimizu, *J. Am. Chem. Soc.* **2006**, *128*, 10403.

[170] J. -C. G. Bunzli, *J. Coord. Chem.* **2014**, *67*, 3706.

[171] W. Horrocks, D. Sudnick, *Accounts Chem. Res.* **1981**, *14*, 384.

[172] Y. Yu, J.-P. Ma, Y. -B. Dong, *Crystengcomm* **2012**, *14*, 7157.

[173] C. -Y. Sun, X. -L. Wang, C. Qin, J. -L. Jin, Z. -M. Su, P. Huang, K. -Z. Shao, *Chem. Eur. J.* **2013**, *19*, 3639.

[174] Y. Xiao, Y. Cui, Q. Zheng, S. Xiang, G. Qian, B. Chen, *Chem. Commun.* **2010**, *46*, 5503.

[175] B. Chen, L. Wang, Y. Xiao, F. R. Fronczek, M. Xue, Y. Cui, G. Qian, *Angew. Chem. Int. Ed.* **2009**, *48*, 500.

[176] X. -H. Zhou, L. Li, H. -H. Li, A. Li, T. Yang, W. Huang, *Dalton Trans.* **2013**, *42*, 12403.

[177] K. Jayaramulu, R. P. Narayanan, S. J. George, T. K. Maji, *Inorg. Chem.* **2012**, *51*, 10089.

[178] B. Liu, C. Sun, Y. Chen, *J. Mater. Chem. B* **2014**, *2*, 1661.

[179] Q. -B. Bo, H. -T. Zhang, H. -Y. Wang, J. -L. Miao, Z. -W. Zhang, *Chem. Eur. J.* **2014**, *20*, 3712.

[180] S. Mohapatra, B. Rajeswaran, A. Chakraborty, A. Sundaresan, T. K. Maji, *Chem. Mater.* **2013**, *25*, 1673.

[181] T. -F. Liu, W. Zhang, W. -H. Sun, R. Cao, *Inorg. Chem.* **2011**, *50*, 5242.

[182] W. -H. Zhu, Z. -M. Wang, S. Gao, *Inorg. Chem.* **2007**, *46*, 1337.

[183] Z. Dou, J. Yu, Y. Cui, Y. Yang, Z. Wang, D. Yang, G. Qian, *J. Am. Chem. Soc.* **2014**, *136*, 5527.

[184] J. Demel, P. Kubat, F. Millange, J. Marrot, I. Cisarova, K. Lang, *Inorg. Chem.* **2013**, *52*, 2779.

[185] Z. Hao, G. Yang, X. Song, M. Zhu, X. Meng, S. Zhao, S. Song, H. Zhang, *J. Mater. Chem. A* **2014**, *2*, 237.

[186] C. Zhan, S. Ou, C. Zou, M. Zhao, C.-D. Wu, *Anal. Chem.* **2014**, *86*, 6648.

[187] Z. Guo, H. Xu, S. Su, J. Cai, S. Dang, S. Xiang, G. Qian, H. Zhang, M. O'Keeffe, B. Chen, *Chem. Commun.* **2011**, *47*, 5551.

[188] K. A. White, D. A. Chengelis, K. A. Gogick, J. Stehman, N. L. Rosi, S. Petoud, *J. Am. Chem. Soc.* **2009**, *131*, 18069.

[189] J. -J. Wu, Y. -X. Ye, Y. -Y. Qiu, Z. -P. Qiao, M. -L. Cao, B. -H. Ye, *Inorg. Chem.* **2013**, *52*, 6450.

[190] Y. -N. Gong, L. Jiang, T. -B. Lu, *Chem. Commun.* **2013**, *49*, 11113.

[191] H. Xu, F. Liu, Y. Cui, B. Chen, G. Qian, *Chem. Commun.* **2011**, *47*, 3153.

[192] X. Zhou, H. Li, H. Xiao, L. Li, Q. Zhao, T. Yang, J. Zuo, W. Huang, *Dalton Trans.* **2013**, *42*, 5718.

[193] J. -D. Xiao, L. -G. Qiu, F. Ke, Y. -P. Yuan, G. -S. Xu, Y. -M. Wang, X. Jiang, *J. Mater. Chem. A* **2013**, *1*, 8745.

[194] S. -B. Ding, W. Wang, L. -G. Qiu, Y. -P. Yuan, F. -M. Peng, X. Jiang, A. -J. Xie, Y. -H. Shen, J. -F. Zhu, *Mater. Lett.* **2011**, *65*, 1385.

[195] X. Rao, T. Song, J. Gao, Y. Cui, Y. Yang, C. Wu, B. Chen, G. Qian, *J. Am. Chem. Soc.* **2013**, *135*, 15559.

[196] Y. Cui, H. Xu, Y. Yue, Z. Guo, J. Yu, Z. Chen, J. Gao, Y. Yang, G. Qian, B. Chen, *J. Am. Chem. Soc.* **2012**, *134*, 3979.

[197] K. Miyata, Y. Konno, T. Nakanishi, A. Kobayashi, M. Kato, K. Fushimi, Y. Hasegawa, *Angew. Chem. Int. Ed.* **2013**, *52*, 6413.

[198] R. F. D'Vries, S. Alvarez-Garcia, N. Snejko, L. E. Bausa, E. Gutierrez-Puebla, A. de Andres, M. Angeles Monge, *J. Mater. Chem. C* **2013**, *1*, 6316.

[199] A. Cadiau, C. D. S. Brites, P. M. F. J. Costa, R. A. S. Ferreira, J. Rocha, L. D. Carlos, *ACS Nano* **2013**, *7*, 7213.

[200] M. D. Ward, *Chem. Soc. Rev.* **1997**, *26*, 365.

[201] A. P. Nelson, O. K. Farha, K. L. Mulfort, J. T. Hupp, *J. Am. Chem. Soc.* **2009**, *131*, 458.

Chapter 4: New PCMs Based on *Bis*(phosphine) Building Blocks

INTRODUCTION

PCPs that contain unsaturated 4*d*- or 5*d*-transition-metal sites remain somewhat exceptional. Their rarity may be due to difficulties in the preparation of stable networks using heavier transition metal precursors while simultaneously being able to control the extent of coordination. However, such materials would be useful for specific solid-state applications because guest molecules could access the structurally-defined, 'soft' open metal coordination sites inside the micropores.[54,79,202] This would allow for adsorbates to engage in moderate or strong bonding interactions with the unsaturated metal centers (UMCs), potentially resulting in pore-confined chemical reactivity. Some examples of pertinent solid-state applications include catalysis,[58,61] enhanced binding of gas molecules *via* elevated enthalpies of adsorption,[203-205] molecular sensing,[44] and *post*-synthetic coordination and/or exchange of organic species.[206-208]

In some instances, it is possible to generate UMCs in PCPs based on 3*d* transition metals, *s*-block cations, or lanthanides *via* the removal of labile solvate ligands (*e.g.*, OH_2 or *N,N*-dimethylformaldehyde (DMF)) by heating under vacuum. Examples of this type of activation have shown significantly increased gas adsorption enthalpies and capacities, indicative of direct metal-guest interactions.[66,82,209,210] However, synthetic control over the degree of metal solvation during PCP synthesis is limited. Alternatively, installation of unsaturated metal sites into PCPs has shown recent promise. Notable examples include the incorporation of $Cr(CO)_3$ *via* η^6-coordination to aromatic structures in the pores,[211] the addition of carbene-bound Pd(II) organometallics,[212] and uptake of metal cations into *pre*- or *post*-synthetically installed chelating groups.[105,131,213-215]

The incorporation of unsaturated metal species into PCPs using *pre*-formed coordination complexes or organometallic species with known and desirable chemical reactivity, especially those based on heavier transition metals, remains a much more significant synthetic challenge. This research details the construction of PCPs based on organophosphine ligands, where the available soft P: donor sites can be used to coordinate catalytic metals, either *pre*- or *post*-synthetically. Phosphine ligands are ubiquitous in homogeneous catalysis and are well-suited for coordination of a broad range of heavier transition metals that have not previously been incorporated into PCPs. The coordination of Au(I) to individual P: sites in PCM-10 has already been demonstrated.[105] A recent extension of this work has concentrated on the synthesis of *pre*-formed metalated building blocks based on *bis*(phosphines) that would potentially exhibit enhanced chemical stability due to the chelate effect, thus preventing loss or exchange of the metal site upon construction of a PCM in the presence of secondary metal species. Moreover, 1,2-substituted *bis*(phosphines) are excellent ligands for the activation of soft transition-metal centers toward chemical reactivity and catalysis.[216-219] The preparation of the previously unreported tetra-*p*-carboxylated *bis*(phosphine) (BBCB) was specifically targeted to provide a versatile building block for the preparation of isostructural coordination polymers in which numerous different unsaturated metal species may be incorporated. The metalated complexes, BBCB-MCl_2 (M = Pd, Pt), are structurally rigid. This greatly increases the possibility of readily obtaining porous coordination polymers *via* the formation of coordination bonds between secondary metal salts and the ancillary *p*-carboxylate moieties.

RESULTS AND DISCUSSION

Bis(phosphine) complexes

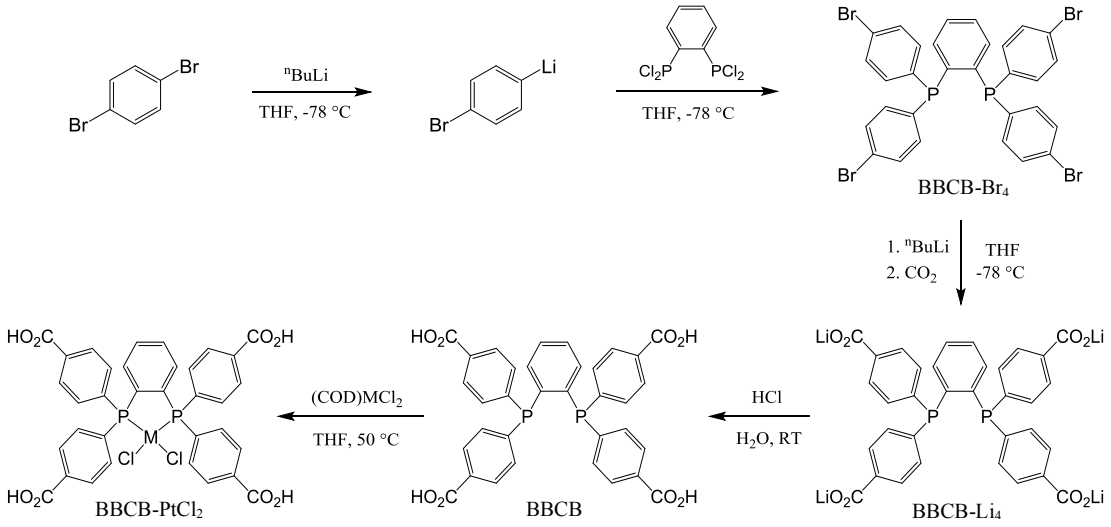

Scheme 4.1: Synthetic route to obtain the BBCB-MCl_2 complexes.

The BBCB ligand was prepared as shown in Scheme 4.1: low temperature treatment of 1,2-*bis*(dichlorophosphino)benzene with 1-lithio-4-bromobenzene in tetrahydrofuran (THF) produced the tetra-*p*-brominated intermediate (BBCB-Br_4) in 64−87% yield. BBCB-Li_4 was then prepared in cold THF using excess *n*-butyllithium, followed by *in situ* treatment with solid CO_2 to afford the lithium carboxylate salt in near-quantitative yield. The free acid (BBCB) was obtained by protonation with HCl in degassed H_2O. BBCB is insoluble in most apolar organic solvents, but it has reasonable solubility in polar solvents, including alcohols. Initial coordination chemistry studies focused on the use of Pd(II) and Pt(II) precursors to incorporate square-planar UMCs, which would, importantly, lock the resulting metalloligand building block into a rigid orientation. Metal precursors with basic ligands (*e.g.*, acetates) were unsuitable since

these tended to favor deprotonation of the ancillary carboxylic acid groups. Instead, reaction of BBCB in THF with $M(COD)Cl_2$ precursors (M = Pd, Pt) resulted in the desired P_2-coordination complexes, which were recrystallized from EtOH.

Zn(II)-based PCM-18

Synthesis and structure

The single crystal structure of BBCB-$PtCl_2$ confirms that when complexed, each phosphine-*P* is *pseudo*-tetrahedral. The complex has approximate C_2-symmetry in which the four *p*-aryl carboxylic acids project above and below the planar P_2MCl_2 core (Figure 4.1). As building blocks for the formation of coordination polymers, BBCB-MCl_2 may be considered a planar four-connected node (Figure 4.1, *left*, inset) that incorporates open metal species at its center. BBCB-MCl_2 is structurally similar to several tetratopic organic ligands commonly found in PCP systems, such as biphenyl-3,5,3′,5′-tetracarboxylate used by Schröder *et al.* for the NOTT-x series,[220] and the larger 4,4′,4″,4‴-benzene-1,2,4,5-tetrayltetrabenzoate employed by Hupp and Farha,[221] all of which have proven great utility in the construction of highly porous and stable framework materials.

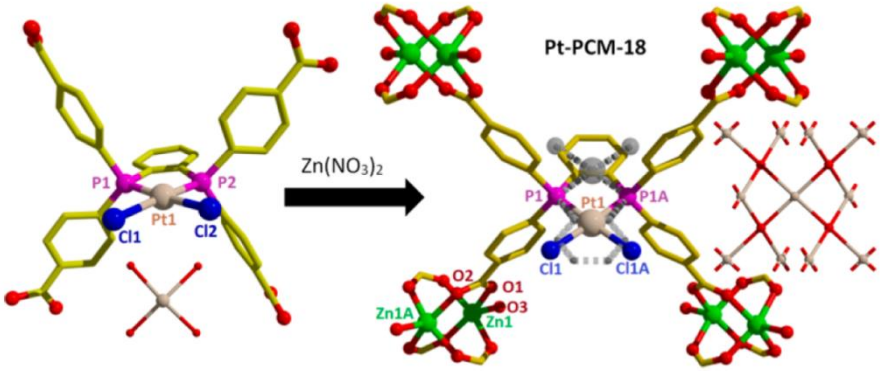

Figure 4.1: (*Left)* Crystal structure of BBCB-$PtCl_2$ with simplified node structure (inset); *(right)* the corresponding Pt-PCM-18 crystal structure with Zn(II) paddlewheel nodes and puckered square grid net (inset). Disorder associated with individual monomers is shown in dashed gray bonds.

Milligram quantities of BBCB-MCl_2 were subsequently reacted with Zn(II) salts in solvent mixtures that have been previously established as ideal for the formation of other PCMs.[102,105] Direct treatment of $Zn(NO_3)_2$ with BBCB-MCl_2 in EtOH/DMF mixtures resulted in deprotonation of the carboxylic acids and Zn−O coordination to give crystalline products. Single crystal XRD analysis revealed two isostructural porous PCMs with the formula unit $[Zn_2(BBCB\text{-}MCl_2)(OH_2)_2]\cdot solv$, hereafter referred to as M-PCM-18 (M = Pd, Pt). The most immediately striking feature of the polymer structures was their significantly high symmetry compared to the monomeric precursors. M-PCM-18 crystallized into the body-centered orthorhombic space group *Imma*, whereas the monomer BBCB-$PtCl_2$ was solved in the much lower-symmetry monoclinic space group, $P2_1/c$. A direct comparison of the structures shows that configurational freedom in the molecular species (originating from rotation of P-aryl groups around P−C bonds) has been removed upon insertion into the polymer. In fact, the high symmetry of the polymeric metalated *bis*(phosphine) complex imposes a site symmetry of 2/*m* at the

center of the chelate ring, which is higher than the inherent symmetry of the ligand itself. As a result, each monomer can be inverted and superimposed upon itself while maintaining the geometry of the P-aryl groups (Figure 4.1; gray dashed bonds). This induces disorder in the lattice of PCM-18 such that monomers are randomly arranged in one of the two possible orientations. PCM-18 has infinite 3D connectivity in which each carboxylate group is coordinated to Zn(II) paddlewheel dimers with axial OH_2 ligands. The result is an unusual puckered square grid topology based on two different 4-connected square-planar nodes (Figure 4.1, *right*, inset). There are large pore openings in all three crystallographic planes (Figure 4.2); the largest pore windows in the ac-plane have maximum accessible dimensions of 1.7 × 2.0 nm.

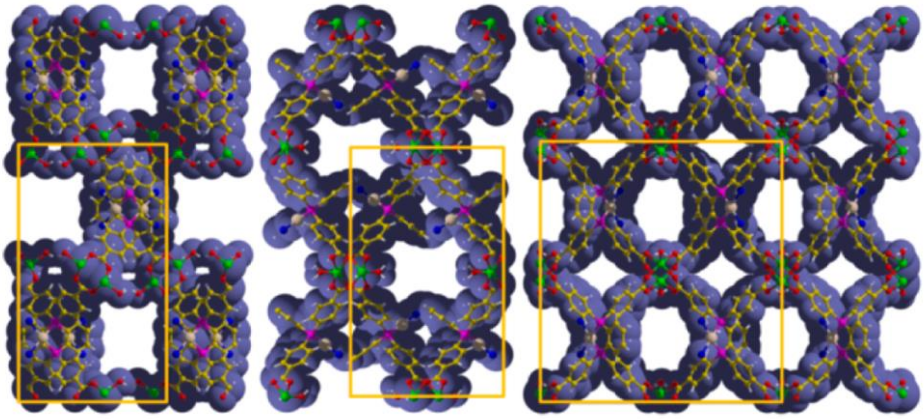

Figure 4.2: Space-filling representations of Pt-PCM-18 viewed normal to the bc- (left), ac- (center), and ab-planes (right).

Thermal stability

The ability to construct isostructural and non-interpenetrated frameworks using the BBCB-MCl_2 building blocks offers a range of interesting opportunities to compare and contrast their resulting solid-state properties and reactivity. According to TGA, the as-synthesized M-PCM-18 materials were thermally stable at temperatures up to 300 °C after removal of uncoordinated DMF and H_2O solvent molecules from the pores (Figures 4.3 and 4.4).

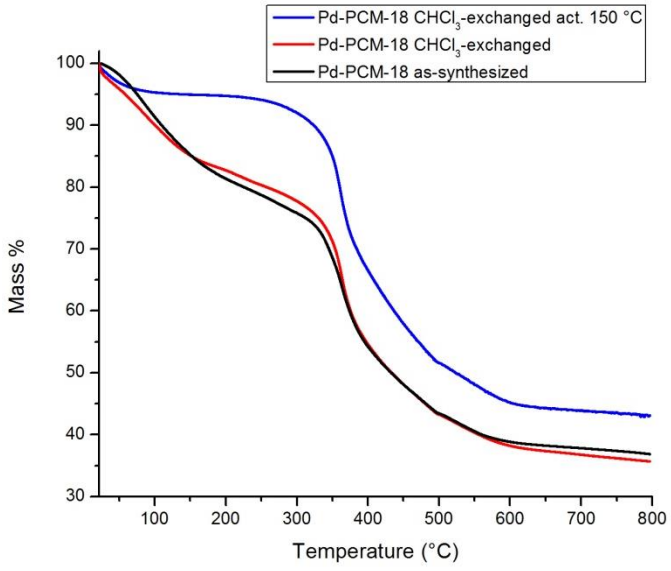

Figure 4.3: TGA of Pd-PCM-18 with various solvent *pre*-treatment and activation conditions.

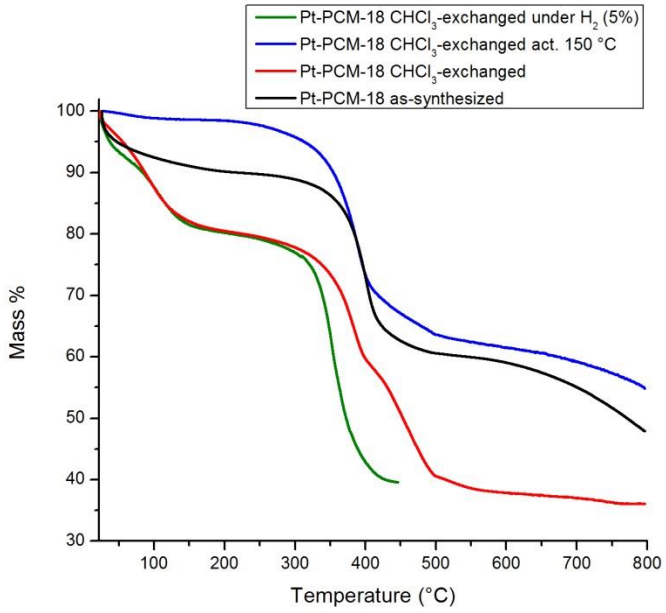

Figure 4.4: TGA of Pt-PCM-18 with various solvent *pre*-treatment and activation conditions.

X-ray powder diffraction

XRPD confirmed that the crystalline products were stable in air for weeks or upon solvent exchange with $CHCl_3$ and subsequent suspension in fresh DMF/EtOH mixtures (Figures 4.5 and 4.6). The $CHCl_3$-exchanged samples appeared to be amorphous when analyzed directly by XRPD; however, if re-solvated in DMF, the materials exhibited crystallinity comparable to the as-synthesized samples.

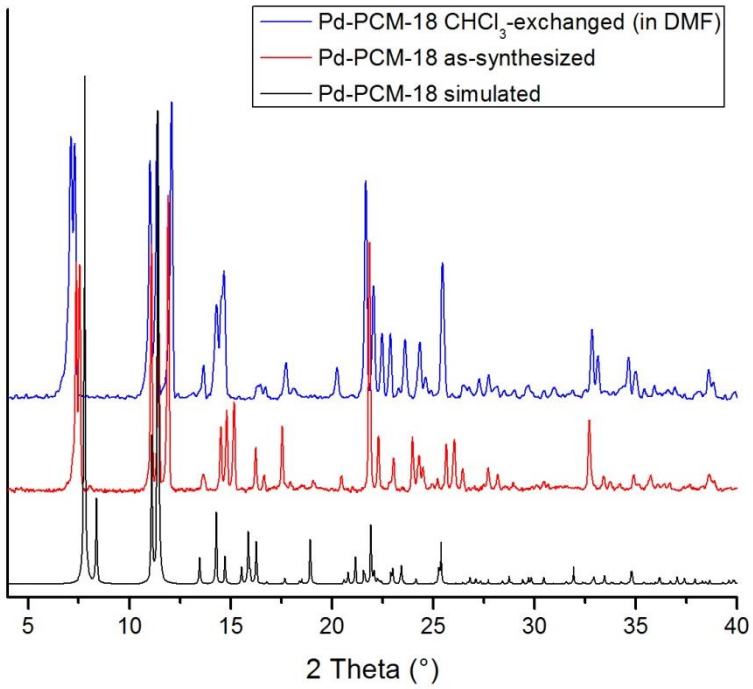

Figure 4.5: X-ray powder diffraction patterns of as-synthesized and $CHCl_3$-exchanged Pd-PCM-18.

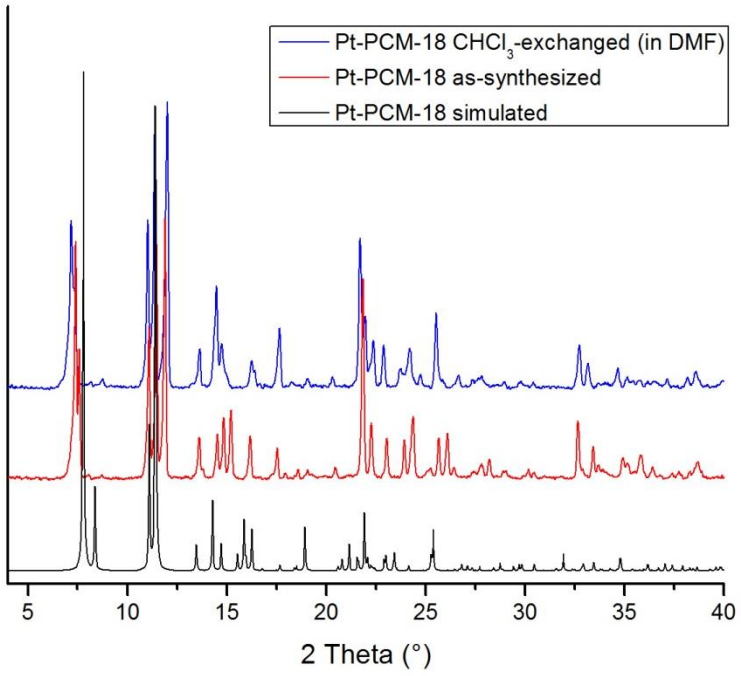

Figure 4.6: X-ray powder diffraction patterns of as-synthesized and $CHCl_3$-exchanged Pt-PCM-18.

Gas adsorption

To probe the bulk surface areas of the M-PCM-18 materials, samples were subjected to repeated cycles of solvent exchange by suspension in $CHCl_3$ over 3 days, followed by evacuation at 423 K for 12 h. N_2 was not significantly adsorbed inside the pores of either Pd- or Pt-PCM-18. However, CO_2 was found to be an appropriate probe gas, revealing BET surface areas of 211 and 244 $m^2\ g^{-1}$ at 196 K (for Pd and Pt, respectively); at this temperature, CO_2 was reversibly adsorbed inside M-PCM-18 (Figure 4.7).

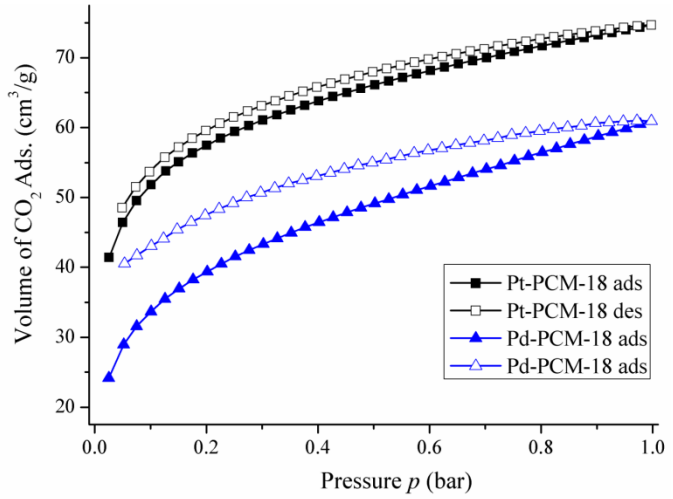

Figure 4.7: CO_2 sorption of $CHCl_3$-exchanged M-PCM-18 at 196 K after activation at 150 °C.

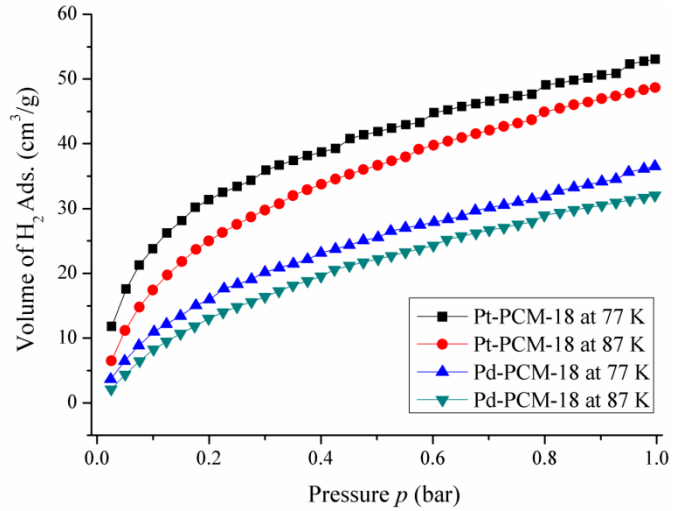

Figure 4.8: H_2 adsorption isotherms for $CHCl_3$-exchanged M-PCM-18 at 77 and 87 K after activation at 150 °C.

Next, the H_2 sorption properties of the M-PCM-18 materials were assessed. At 77 K, both Pd- and Pt-containing materials showed modest H_2 uptakes of 36 and 53 $cm^3\ g^{-1}$ with reversible type I isotherms (Figure 4.8). The isosteric heats of H_2 adsorption (Q_{st}) were obtained using the accepted virial expansion method,[69] yielding values of 2.75 and 4.82 kJ mol^{-1} for Pd- and Pt-PCM-18, respectively (Figures 4.9–4.13). The relatively low magnitude of these values did not suggest any significant interaction of H_2 with the metals at 78 K.

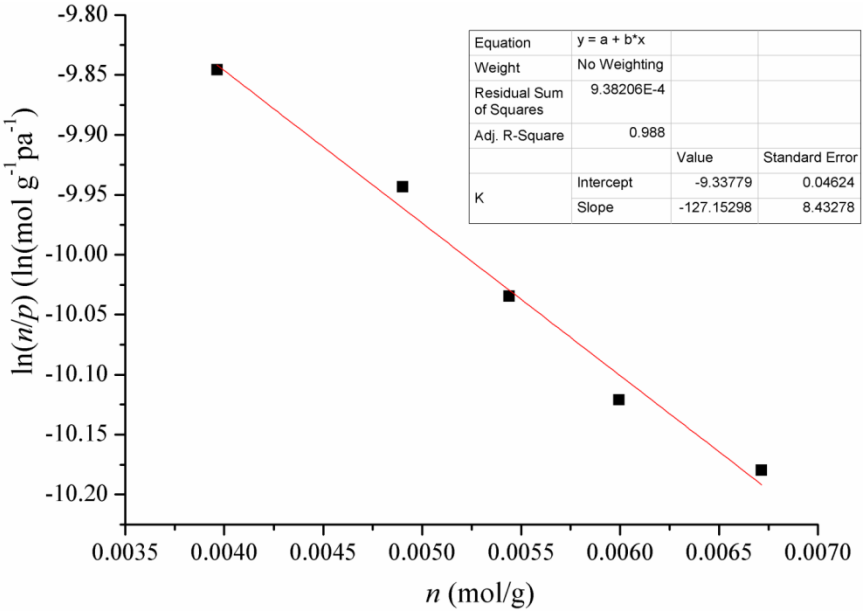

Figure 4.9: Virial plot for the adsorption of H_2 on activated Pd-PCM-18 at 77 K.

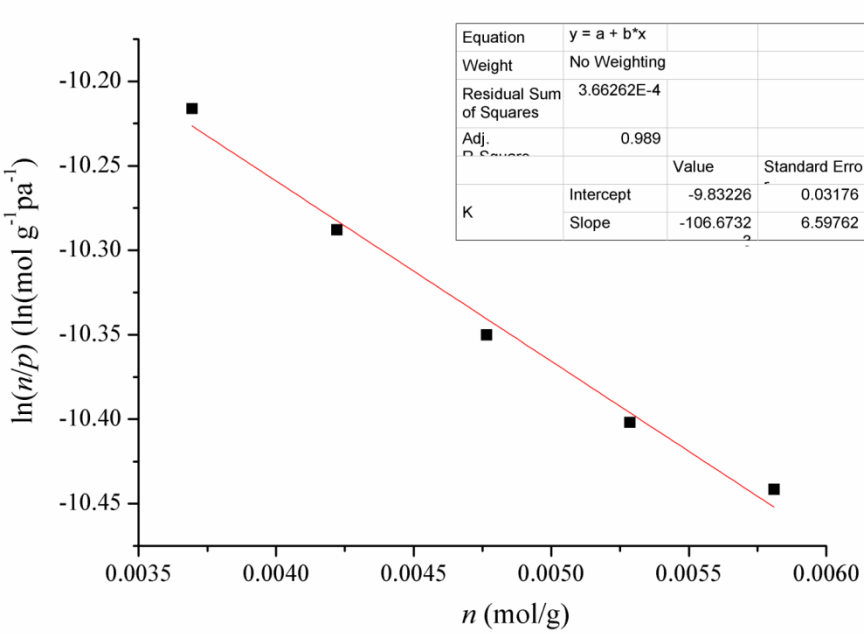

Figure 4.10: Virial plot for the adsorption of H_2 on activated Pd-PCM-18 at 87 K.

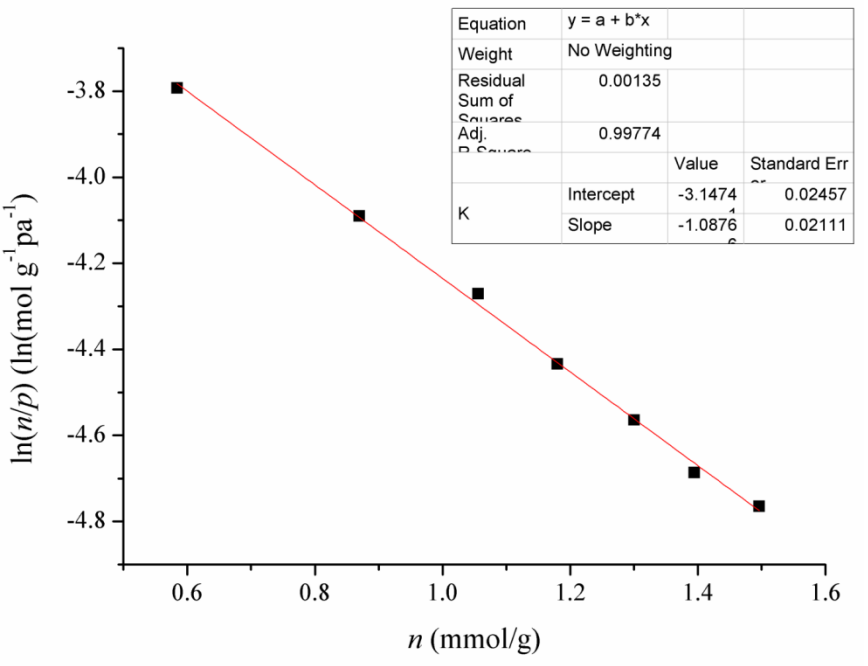

Figure 4.11: Virial plot for the adsorption of H_2 on activated Pt-PCM-18 at 77 K.

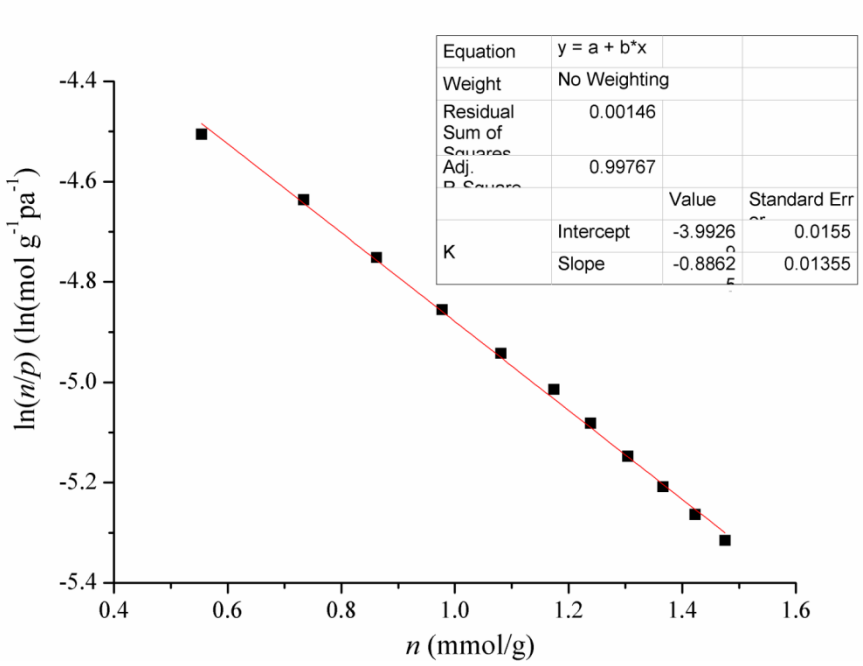

Figure 4.12: Virial plot for the adsorption of H_2 on activated Pt-PCM-18 at 87 K.

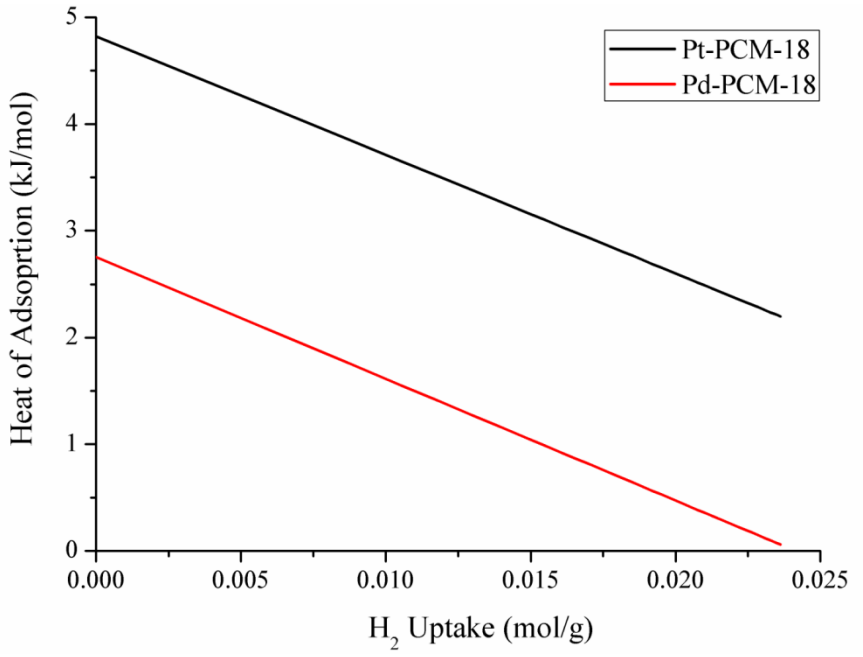

Figure 4.13: Variation of the Q_{st} of H_2 at low loading for activated M-PCM-18.

However, it is known that open Pd(II) or Pt(II) sites can interact with the filled 1σ and empty 1σ* orbitals of H_2 *via* their d_{z^2} and d_{xz} orbitals, perpendicular to the P_2MCl_2 plane,[216,222-229] or can induce H_2 clevage.[230] A number of reports that show Kubas-type η^2–H_2 interactions are commonly observed at ambient or elevated temperatures for transition-metal centers that contain *bis*(phosphine) ligands.[222,223] For example, the isolable complex trans-[Ru(L)$_2$H(η^2-H_2)] (L = η^2-*bis*(phosphinoethane)) is formed at 358 K under 24.1 bar of H_2.[224] Recent theoretical studies have also predicted moderately strong $PdCl_2$–H_2 interactions in modified COF-301[227] and axial η^2-H_2 bonding at vacant Ni(II) sites in other PCPs.[228] So, it was decided to study H_2 adsorption in M-PCM-18 over a wider temperature range. Interestingly, at temperatures above 300 K, both Pd- and Pt-PCM-18 showed marked increases in H_2 adsorption between 0–1 bar. Adsorption–desorption isotherms were collected on freshly activated samples at 25 K increments, which revealed maximum H_2 sorption occurred at ~425 K and 1.0 bar H_2 for both materials (Figures 4.14 and 4.15).

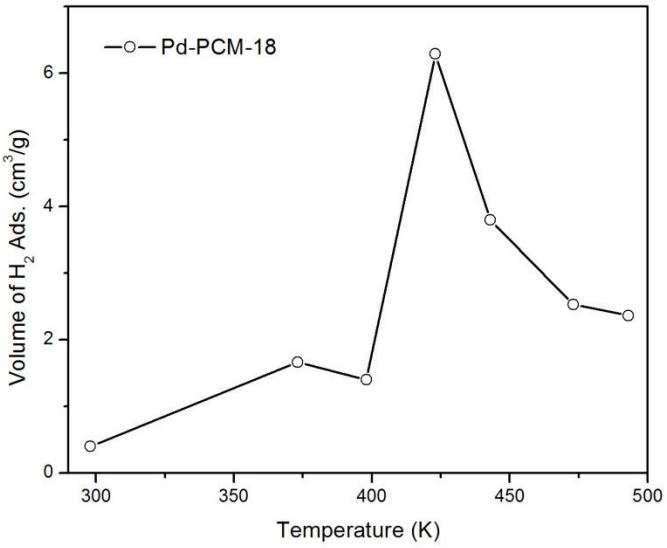

Figure 4.14: Temperature-dependence of H_2 adsorption in Pd-PCM-18.

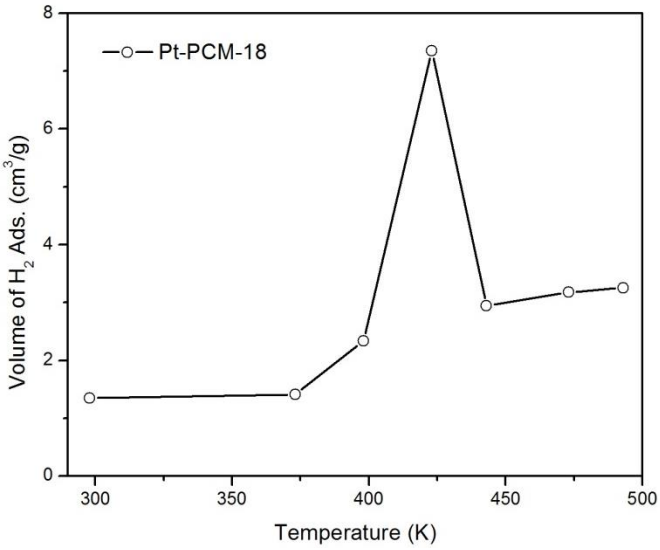

Figure 4.15: Temperature-dependence of H_2 adsorption in Pt-PCM-18.

Between 425−500 K the total amount of adsorbed H_2 was diminished but remained higher than at ambient temperature. The high-temperature H_2 adsorption isotherms were always linear, suggesting that saturation was not reached at 1.0 bar (Figure 4.16).

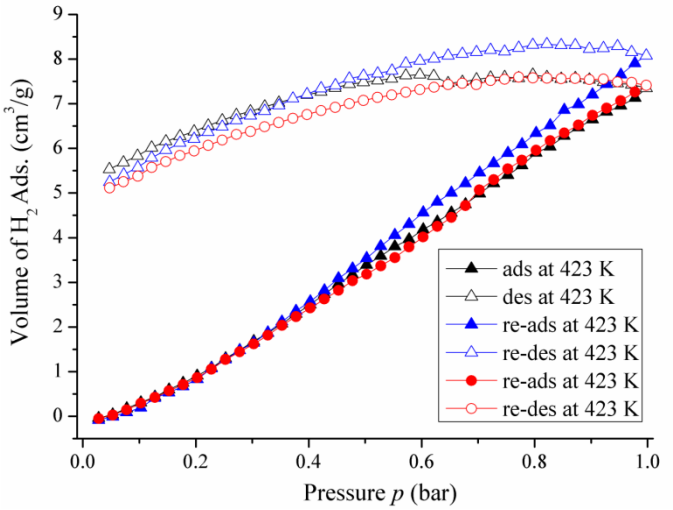

Figure 4.16: Repeated 425 K H_2 adsorption on the same Pt-PCM-18 sample after reactivation at 425 K *in vacuo*.

Desorption phases showed marked hysteresis, indicative of relatively strong H_2 binding inside the materials, even at 423 K (Figure 4.16). In addition, if the same samples were reactivated *in situ* by prolonged evacuation (4 h; also at 425 K), it was possible to obtain the original hysteretic adsorption−desorption profiles over repeated cycles without any decrease in H_2 capacity (Figure 4.16).

To further investigate the nature of the high-temperature H_2 adsorption observed in M-PCM-18, a number of control adsorption measurements were performed under otherwise identical conditions. First, three other previously reported PCPs were studied in an attempt to confirm the role of the accessible *bis*(phosphine)MCl_2 sites in the H_2 adsorption. These materials were specifically chosen because they each contain structural subunits that are also present in M-PCM-18: PCM-3[102] contains free R_3P: sites and Zn(II) metal nodes; MOF-2[231] is constructed entirely of 1,4-terephthalate and Zn_2 paddlewheels with axial OH_2 groups, structurally identical to the nodes in M-PCM-18; CUK-1[139] is a highly robust 3D PCP based on Co(II) and pyridine-2,4-dicarboxylate that adsorbs 1.6 wt % H_2 at 77 K with characteristic reversible type-I behavior. None of these materials showed any measurable H_2 adsorption across the entire temperature range 300−500 K when activated and measured using the same methods and apparatus as for M-PCM-18 (Figures 4.17 and 4.18).

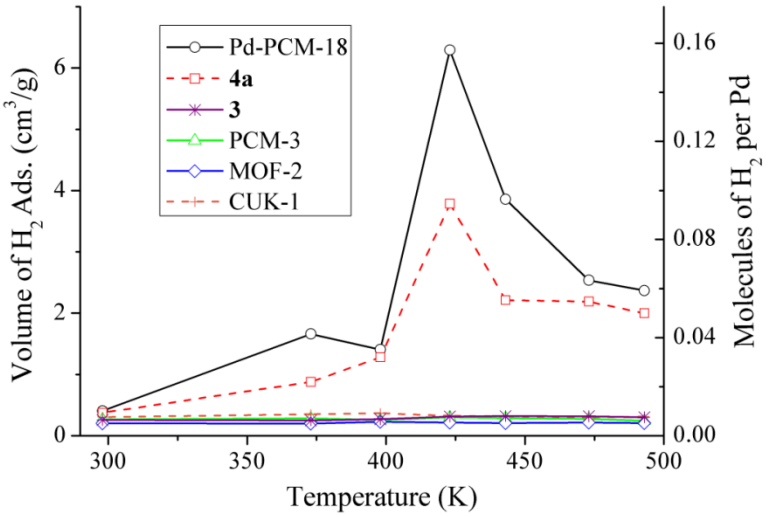

Figure 4.17: Temperature-dependence of H_2 adsorption in Pd-PCM-18, BBCB-$PdCl_2$ (4a), BBCB (3), and other PCP materials at elevated temperatures.

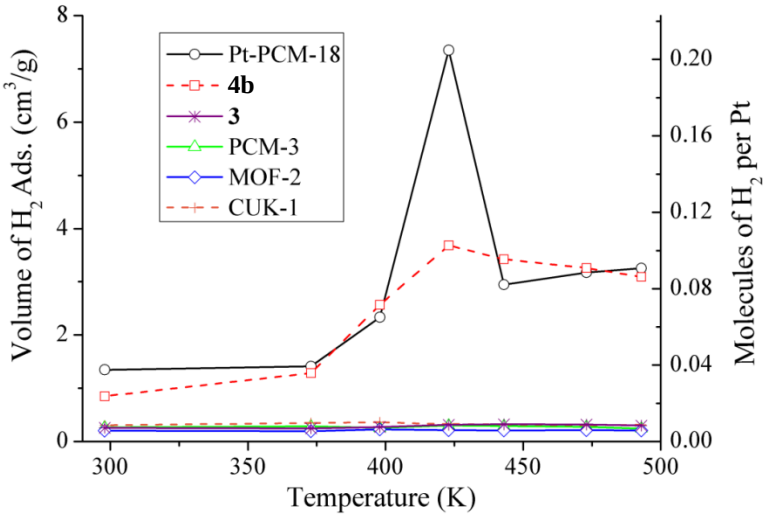

Figure 4.18: Temperature-dependence of H_2 adsorption in Pt-PCM-18, BBCB-$PtCl_2$ (4b), BBCB (3), and other PCP materials at elevated temperatures.

It can be reasonably deduced that neither the phosphine moieties nor the Zn_2 paddlewheel nodes were responsible for the observed H_2 sorption behavior of M-PCM-18. In comparison, when the amorphous metalated ligands (BBCB-MCl_2) were studied under identical conditions, significant H_2 adsorption was observed above 300 K, also with a peak around 425 K (Figures 4.17 and 4.18; red dashed lines). The overall w/w H_2 uptakes were slightly lower compared with the crystalline PCMs, which is reasonable because the ligands did not contain open pore networks to permit easy movement of H_2 throughout the samples. Moreover, the metal-free ligand BBCB showed no H_2 uptake at elevated temperatures (Figures 4.17 and 4.18; purple lines). Thus, the analogous behavior of the complexes and M-PCM-18 materials, but not BBCB, strongly indicates the role of the Pd(II) or Pt(II) *bis*(phosphine) sites in the high-temperature H_2 binding behavior.

In absolute terms, the maximum H_2 adsorption observed at 425 K was equivalent to 0.16 or 0.22 H_2 molecules per Pd or Pt site, respectively. This is similar in magnitude to what has been recently observed for Kubas-type H_2 adsorption at 298 K in coordinatively unsaturated V(III)-based PCPs (albeit under 85 bar H_2), in which 0.25−0.88 H_2/V were reported.[229] Further analysis of the M-PCM-18 materials *post*-H_2 adsorption at high temperature was performed to check for stability and reversibility. The 77 K H_2 sorption characteristics were recollected for each sample after consecutive high-temperature sorption runs, which also gave sorption behavior that was unchanged from the as-synthesized materials (Figure 4.19).

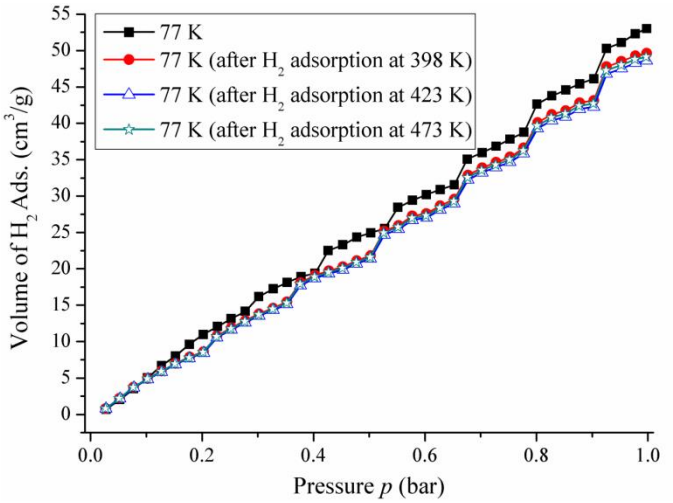

Figure 4.19: 77 K H_2 adsorption in Pt-PCM-18 before and after consecutive high-temperature H_2 adsorption experiments.

The ^{1}H- and $^{31}P\{^{1}H\}$CP-MAS NMR spectra of Pt-PCM-18 were collected for the as-synthesized material and *post*-H_2 addition at 425 K (Figures 4.20 and 4.21). The spectra were unchanged in both cases, and no hydride signals were observed in the ^{1}H spectrum of the *post*-H_2 addition sample at room temperature.

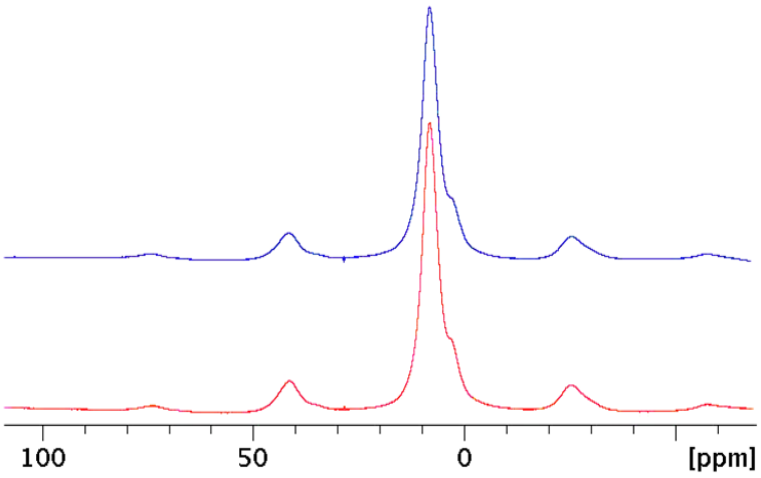

Figure 4.20: ^{1}H-MAS NMR for as-synthesized Pt-PCM-18 (blue) and 425 K H_2-loaded (red).

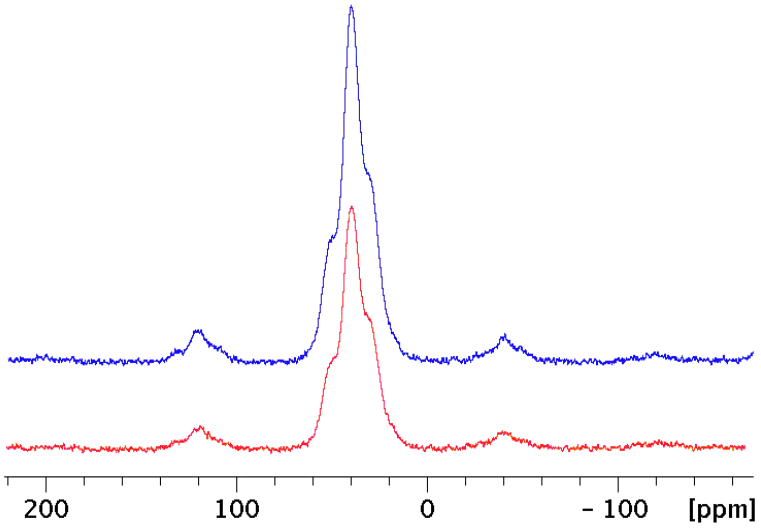

Figure 4.21: ^{31}P{^{1}H}CP-MAS NMR for as-synthesized Pt-PCM-18 (blue) and 425 K H_2-loaded (red).

The %Cl elemental microanalysis was also unchanged after repeated cycles of 425 K H_2 adsorption−desorption, and there was no visible change in the far-IR spectra of the materials. Hence, it appears that Pt−Cl bonds were not activated, which would be the case for chemisorption of H_2 followed by reductive elimination of HCl to form new Pt–H bonds. Furthermore, TGA studies in which samples were heated in a 5% H_2 atmosphere did not reveal any unusual decomposition versus the same measurement when carried out under pure He (see Figure 4.4 above).

Post-synthetic modification

To explore the potential of the M-PCM-18 materials for catalytic applications, reactions to *post*-synthetically activate the Group 10 metal sites *via* substitution of the chloride ligands were also attempted. Initial studies in this regard focused on reactions that can be conducted at low temperature using reagents that are selective for M−Cl bonds. Pringle *et al*. demonstrated that similar *bis*(phosphine)$PtCl_2$ complexes could be employed to prepare organometallic metal−alkyl species by direct treatment of the Pt−Cl bond with diazoalkanes, resulting in α-migration of the chloride at ambient temperature.[232] The platinum(II)-alkyls thus obtained could be employed in catalytic reductive elimination reactions with alkynes.[233] In a control study, BBCB-$PtCl_2$ was easily converted into the racemic organometallic complex [BBCB-PtCl($CHClCO_2Et$)] by reaction of excess ethyl diazoacetate in EtOH/CH_2Cl_2 at 303 K over 48 h (see Experimental Techniques). Similar treatment of Pt-PCM-18 was then attempted by covering single crystals with a solution of the ethyl diazoacetate in CH_2Cl_2 and standing for 3 days at ambient temperature. The crystals were washed several times with fresh CH_2Cl_2 and air-dried.

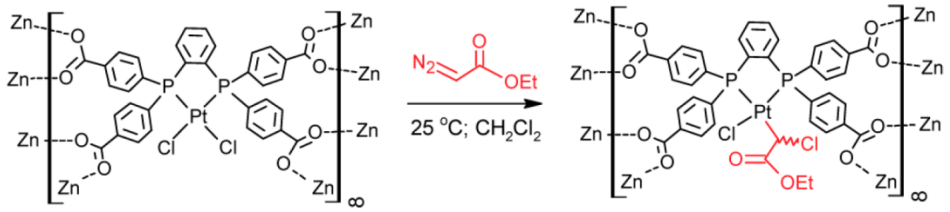

Scheme 4.2: Reaction of Pt-PCM-18 with ethyl diazoacetate to form new Pt–C bonds.

Detailed solid-state NMR studies on the product confirmed near-quantitative conversion of $PtCl_2$ sites inside the crystallites (Scheme 4.2). In comparison to the parent Pt-PCM-18, the ^{1}H-MAS NMR revealed a new resonance at 1.1 ppm corresponding to aliphatic protons in the structure (Figure 4.22). The $^{13}C\{^{1}H\}$CP-MAS NMR spectrum showed two clear resonances at 12.8 and 60.1 ppm corresponding to the CH_3CH_2 group, while resonances were also observed at 183 and 166 ppm due to the ester C=O groups. In addition, the broad resonance at 73.9 ppm corresponds to the chiral Pt−C fragment (Figure 4.23). The $^{31}P\{^{1}H\}$CP-MAS NMR spectrum, obtained at a regular contact time of 5000 μs, revealed a broad and nonsymmetrical resonance due to overlapping of at least two resonances, as expected due to lowering of symmetry at the Pt center (Figure 4.24). The peaks were more resolved at a contact time of 100 μs, yielding chemical shift values of 46.1 and 40.6 ppm, which correspond closely to what was observed for the BBCB-$PtCl_2$ monomer (45.3 and 40.9 ppm), and in the original work.[232,233] In contrast, the precursor Pt-PCM-18 spectrum only showed a single, symmetrical peak *ca*. 42 ppm (Figure 4.21). Additional peaks were also observed in the FT-IR spectrum *ca*. 1689 and 355 cm^{-1}, corresponding to the ester and Pt−C moieties, respectively (Figures 4.25 and 4.26).

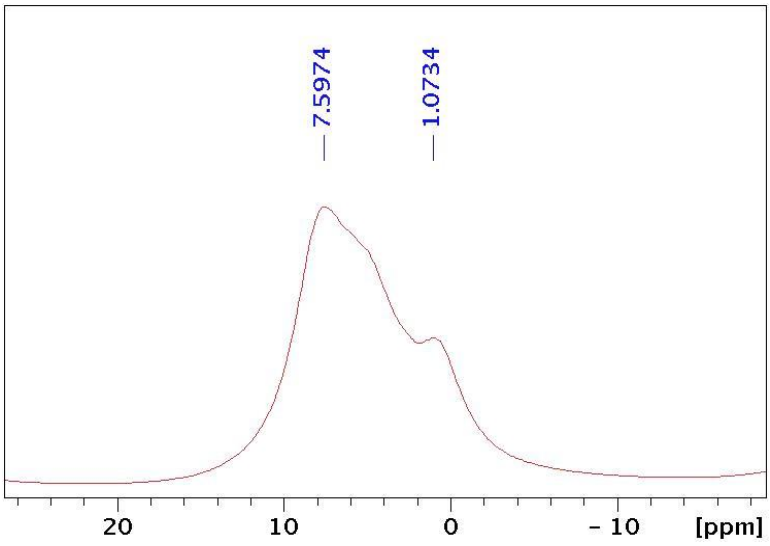

Figure 4.22: ^{1}H-MAS NMR spectrum for the organometallic functionalized Pt-PCM-18, recorded at a spinning rate of 12 kHz.

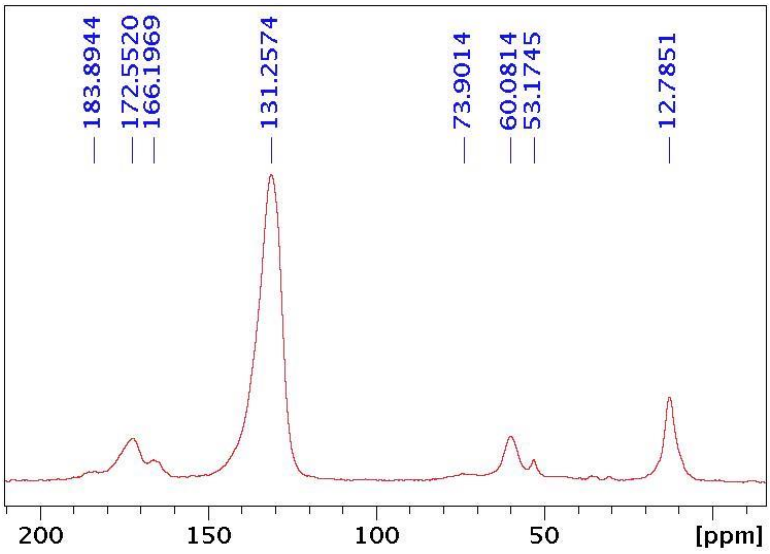

Figure 4.23: ^{13}C{^{1}H}CP-MAS-NMR spectrum for the organometallic functionalized Pt-PCM-18, recorded at a spinning rate of 12 kHz.

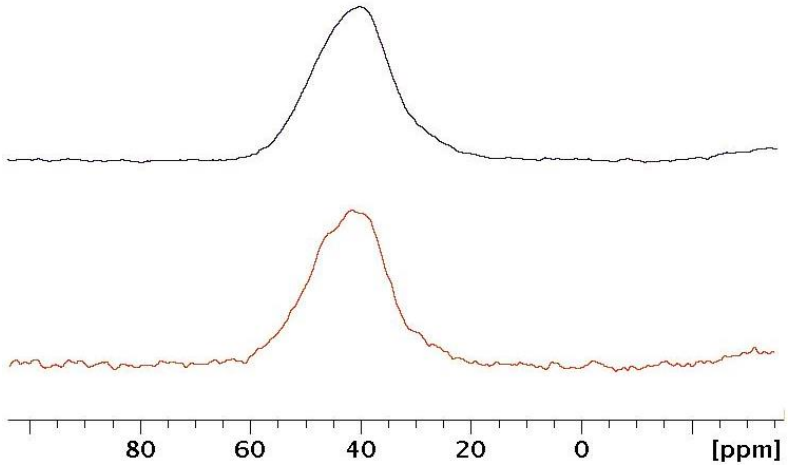

Figure 4.24: $^{31}P\{^{1}H\}$CP-MAS NMR spectrum for the organometallic functionalized Pt-PCM-18, recorded at a contact time of 5000 μs (black) and 100 μs (red).

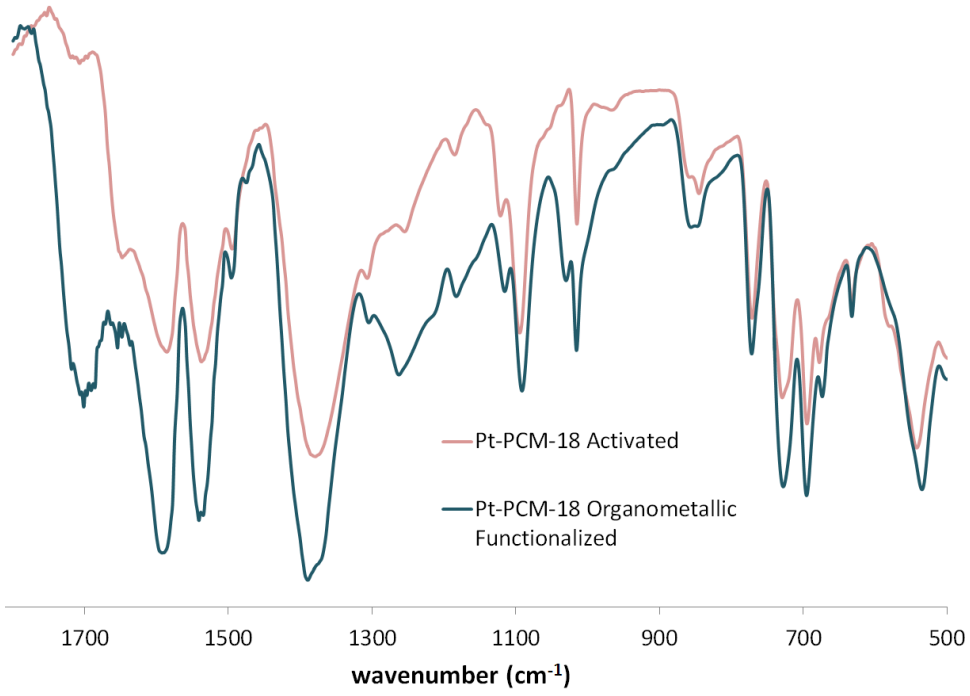

Figure 4.25: FT-IR spectral comparisons for activated Pt-PCM-18 and after 4d treatment with ethyl diazoacetate to generate the organometallic derivative.

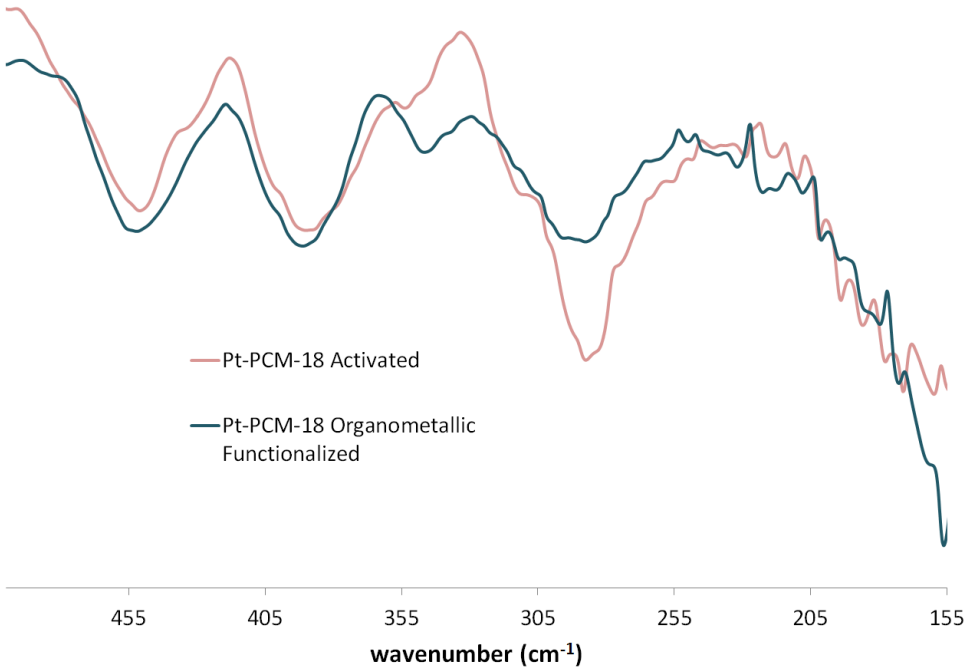

Figure 4.26: Far-IR spectral comparisons for activated Pt-PCM-18 and after 4d treatment with ethyl diazoacetate to generate the organometallic functionalized material.

Co(II)-based PCM-24 and PCM-27

Synthesis and structure

The BBCB-MCl_2 complexes were reacted with $Co(NO_3)_2$ in 2:1 EtOH:DMF under solvothermal conditions similar to those of M-PCM-18 to yield the Co(II)-based materials, M-PCM-24 (M = Pd, Pt). Due to severe twinning issues in crystals of both M-PCM-24 analogs, a finalized crystal structure has yet to be solved. Data obtained from the most recent attempt is included (Appendix I), as well as all characterization data for TGA, XRPD, and gas sorption analyses. However, the crystal structure of a polymorph that formed simultaneously during Pt-PCM-24 synthesis has been obtained.

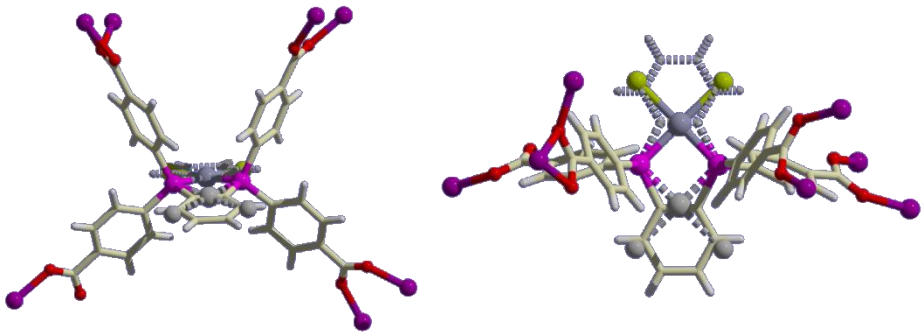

Figure 4.27: Connectivity of BBCB-$PtCl_2$ in Pt-PCM-27 with identical site disorder as seen in PCM-18 (dashed gray bonds).

$[Co_2(BBCB\text{-}PtCl_2)(OH_2)_2(DMF)]\cdot solv$, hereafter referred to as Pt-PCM-27, crystallized into the monoclinic space group *C*2/*c* with unit cell dimensions a = 36.833(3), b = 12.1094(9), c = 35.282(2) Å, β= 98.635(8)°. One carboxylate group is η^2-coordinated, one is *syn*-coordinated, and the remaining two are *syn,syn*-coordinated to the $[Co(OH_2)_2(DMF)]^{4+}$ nodes with bond lengths ranging between 2.006(7)–2.169(6) Å. Each *P*-node is *pseudo*-tetrahedral with bond angles of 104.2(5)–118.8(4)°, and the BBCB-$PtCl_2$ monomer exhibits identical site disorder as seen in M-PCM-18 (Figure 4.27; dashed grey bonds). Pt-PCM-27 is 3-dimensional and also exhibits porosity in 2 dimensions. The largest pores measure 14.2 Å, shown in Figure 4.28 in the *ac*-plane.

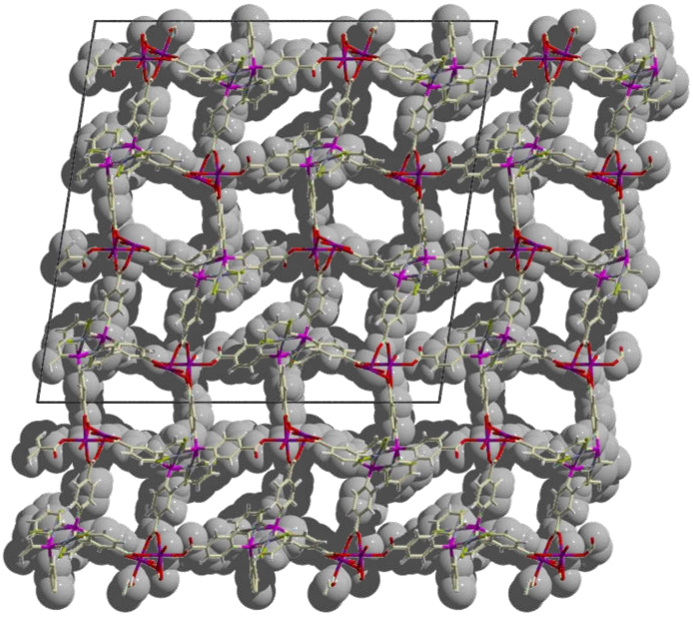

Figure 4.28: Space-filling representation of Pt-PCM-27 viewed normal to the *ac*-plane.

Thermal stability

TGA was performed on as-synthesized, solvent-exchanged, and activated samples of M-PCM-24 (Figures 4.29 and 4.30), and both exhibited thermal stability up to 330 °C. Several mass losses were observed in as-synthesized M-PCM-24 prior to decomposition. These were attributed to the removal of ambient moisture and uncoordinated solvent below 45 °C, accompanied by the removal of nonvolatile solvent between 45–150 °C for Pd-PCM-24 (10.8 %) and Pt-PCM-24 (10.7 %) (Figures 4.29 and 4.30; pink).

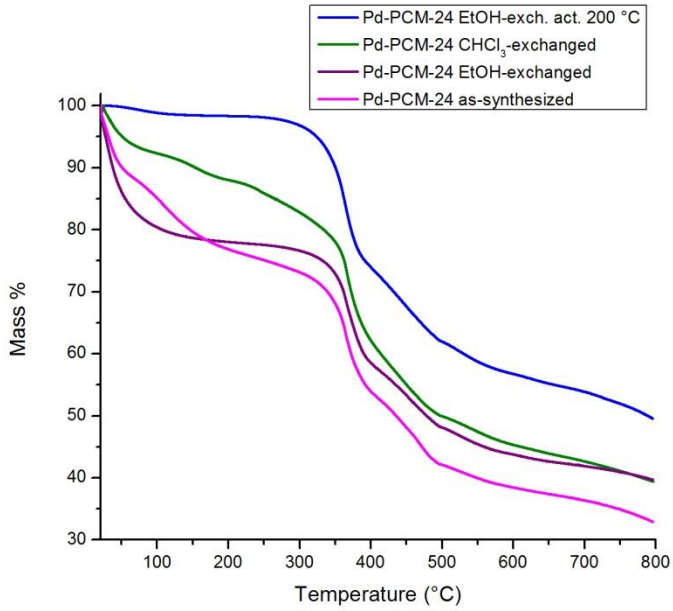

Figure 4.29: TGA of Pd-PCM-24 with various solvent *pre*-treatment and activation conditions.

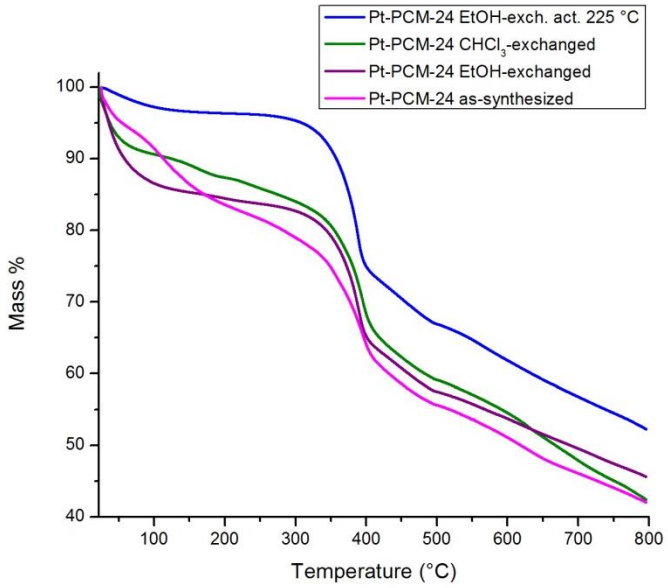

Figure 4.30: TGA of Pt-PCM-24 with various solvent *pre*-treatment and activation conditions.

EtOH-exchanged Pd- and Pt-PCM-24 each exhibited a single, large decrease below 110 °C of 20.2 and 13.9 %, respectively, attributed to the removal of ambient moisture and residual EtOH prior to decomposition at 340 °C (Figures 4.29 and 4.30; purple). TGA of M-PCM-24 after high-temperature activation illustrated complete desolvation of the materials with initial losses of <3.0 % below 100 °C due to ambient moisture (Figures 4.29 and 4.30; blue). A minor 2.5 % decrease was observed in activated Pd-PCM-24 between 110–260 °C prior to the earlier-onset decomposition at 310 °C, along with 1.3 % between 130–295 °C in activated Pt-PCM-24.

TGA was also obtained on $CHCl_3$-exchanged samples of M-PCM-24 (Figures 4.29 and 4.30; green). As seen in PCM-11,[107] solvent-exchange with a polar, hydrophilic solvent (acetone) facilitated the removal of coordinated OH_2 molecules within the material, while the use of a hydrophobic solvent ($CHCl_3$) did not. There are two distinct decreases in the $CHCl_3$-exchanged samples between 90–175 and 200–250 °C, with a total loss of 6.7 % in Pd-PCM-24 and 5.0 % in Pt-PCM-24 between 90–250 °C. These were absent in the EtOH-exchanged and activated samples, indicating that exchange with polar solvent sufficiently removed the coordinated OH_2 molecules without the need for activation at high temperature.

X-ray powder diffraction

XRPD illustrated that crystalline M-PCM-24 is stable in a solution of fresh 2:1 EtOH:DMF and upon solvent-exchange in pure EtOH for several weeks (Figures 4.31 and 4.32).

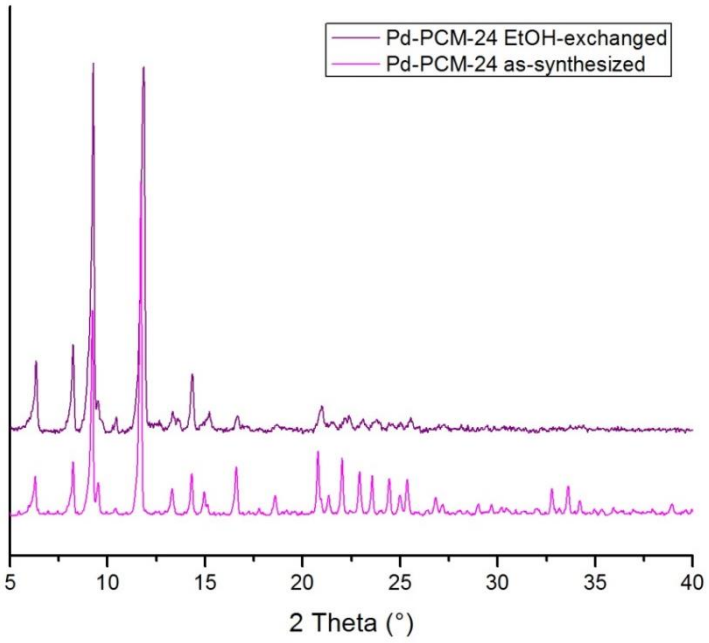

Figure 4.31: X-ray powder diffraction patterns of as-synthesized and EtOH-exchanged Pd-PCM-24.

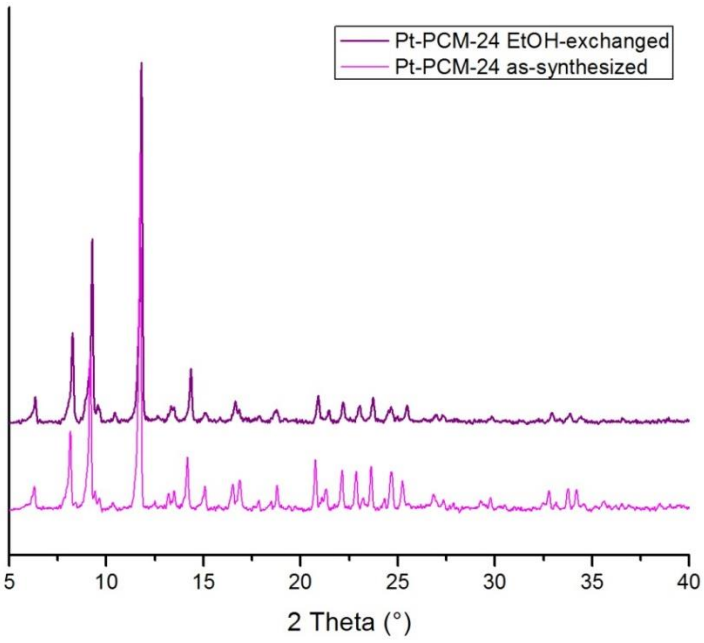

Figure 4.32: X-ray powder diffraction patterns of as-synthesized and EtOH-exchanged Pt-PCM-24.

Gas adsorption

The gas adsorption properties of M-PCM-24 were investigated by BET analyses upon activation at 75 °C and 10^{-10} Torr. Due to the low affinity of the materials toward N_2 gas, the surface areas of Pd- and Pt-PCM-24 were calculated by CO_2 adsorption at 196 K, yielding values of 184 and 136 $m^2\ g^{-1}$, respectively. Both exhibited Type-I behavior and appeared to be approaching saturation at 1 bar. At these conditions, Pd- and Pt-PCM-24 adsorbed 59.70 and 48.74 $cm^3\ g^{-1}$ CO_2, respectively (Figure 4.33).

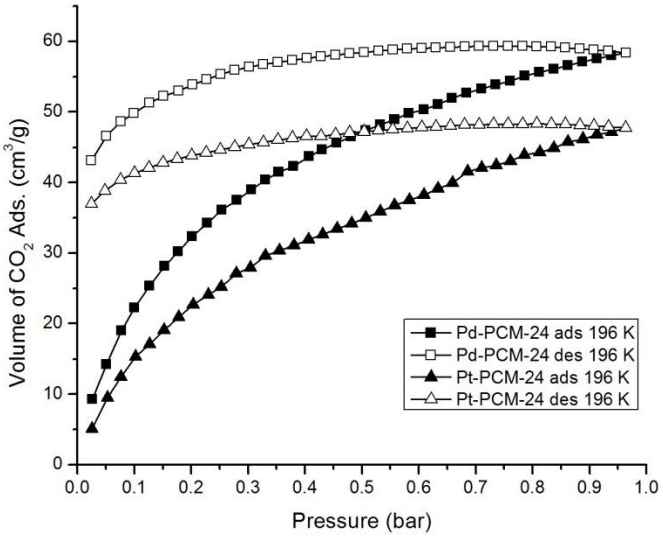

Figure 4.33: CO_2 sorption of EtOH-exchanged M-PCM-24 at 196 K after activation at 75 °C.

Due to the high-temperature H_2 sorption observed in the M-PCM-18 materials, M-PCM-24 was studied for similar trends under identical conditions. Unlike M-PCM-18, M-PCM-24 did not adsorb an appreciable amount of H_2 at 77 K (Figure 4.34), adsorbing only 5.93 and 6.18 $cm^3\ g^{-1}$ H_2 at 1 bar for Pd- and Pt-PCM-24, respectively.

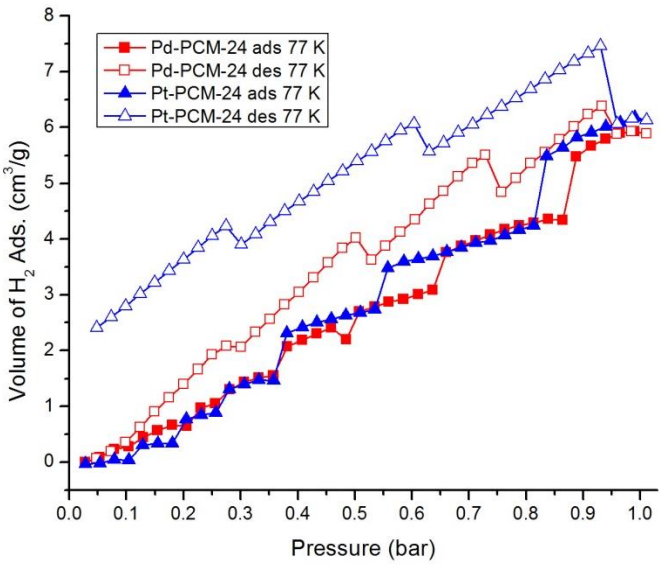

Figure 4.34: H_2 sorption of EtOH-exchanged M-PCM-24 at 77 K after activation at 75 °C. The stepwise behavior is likely not real and can be attributed to instrument drift due to low overall uptake.

However, Pt-PCM-24 exhibited Type-I H_2 sorption under high-temperature conditions that did not appear to be nearing saturation, shown in Figure 4.35 for H_2 sorption at 150 °C. Isotherms collected between 100–225 °C revealed a steady increase in the H_2 sorption at 1 bar, compared to the distinct maximum observed at 150 °C in the M-PCM-18 materials (Figure 4.36).

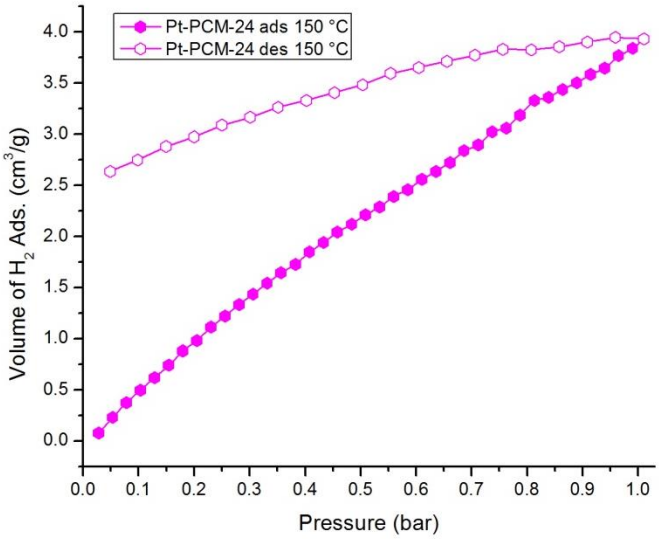

Figure 4.35: H_2 sorption of EtOH-exchanged Pt-PCM-24 at 150 °C.

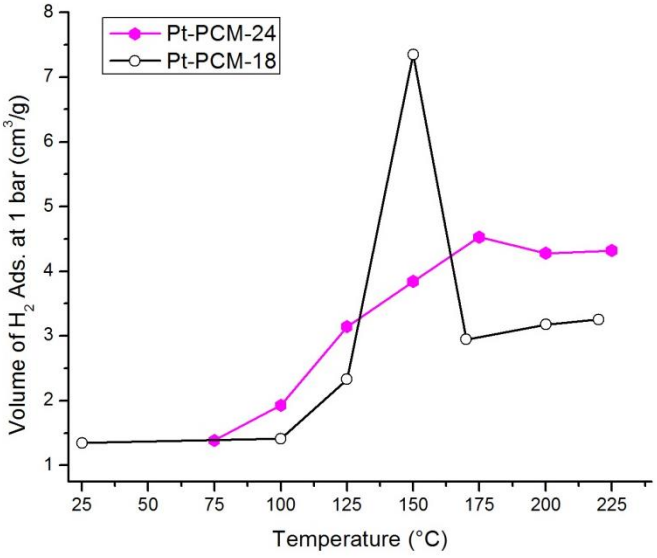

Figure 4.36: H_2 adsorption in Pt-PCM-24 and Pt-PCM-18 at elevated temperatures.

Although this trend did not mirror that of M-PCM-18, it provided a second example of a PCM composed of *bis*(phosphine)MCl_2 linkers with the ability to adsorb H_2 at elevated temperatures. We have recently begun a collaboration with the Head-Gordon Group at UC Berkeley, who have performed computational H_2 sorption studies on similar systems,[234] in an attempt to discover the origin of this unusual high-temperature behavior.

Structural transition

M-PCM-24 exhibited a reversible characteristic cobalt(II) color change upon solvent exchange and activation at 75 °C. The pink as-synthesized material became bright purple upon solvent exchange with either $CHCl_3$ or EtOH, which could be reverted back to pink if exchanged with 2:1 EtOH:DMF or 100 % DMF (Figure 4.37).

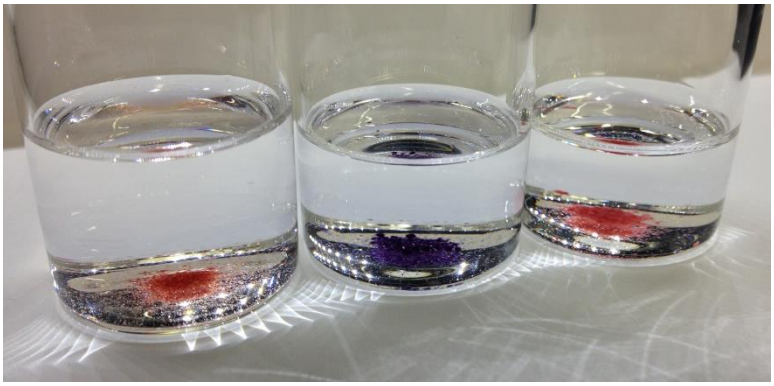

Figure 4.37: Visible color changes of Pt-PCM-24 in solutions of *(left)* 2:1 EtOH: DMF, *(center)* EtOH or $CHCl_3$, and *(right)* 2:1 EtOH:DMF or 100 % DMF.

For gas sorption analyses, EtOH-exchanged M-PCM-24 materials were activated at 75 °C prior to each experiment. A dried sample of EtOH-exchanged Pt-PCM-24 is

shown in Figure 4.38 before *(left)* and after *(center)* activation. The material retained the purple color after drying under N_2 but became dark blue after activation at 75 °C for 12 h.

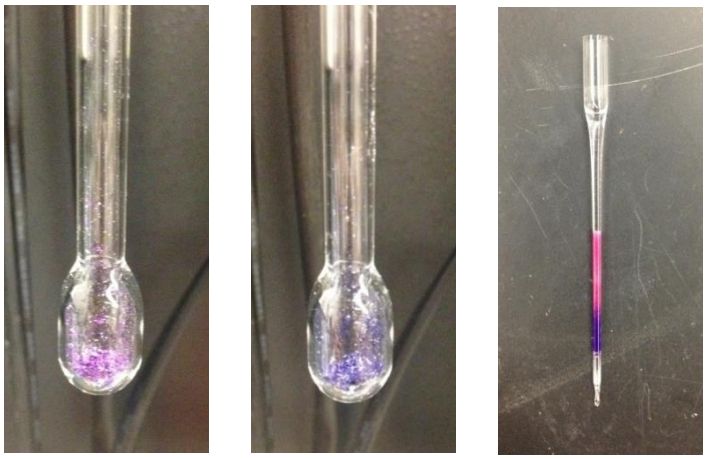

Figure 4.38: Visible color changes of Pt-PCM-24 after EtOH-exchange *(left)* at room temperature and *(center)* after evacuation at 75 °C for 12 hr; *(right)* A sample of Pt-PCM-24 submerged in EtOH in a borosilicate capillary tube after exposure to ambient moisture for 3 days.

Cobalt(II)-based materials that exhibit a pink or blue color are known to contain metal centers in an octahedral (O_h) or tetrahedral (T_d) coordination environment, respectively.[235-237] This is in agreement with the initial results from single crystal X-ray diffraction; each Co(II) center in the as-synthesized material is *pseudo*-octahedral with coordination to 6 oxygen atoms, four from the ligand carboxylates and two from coordinated OH_2 molecules. Solvent-exchange and activation under ultrahigh vacuum at elevated temperatures are two processes commonly used to remove coordinated solvent molecules within PCPs. It is most likely that the OH_2 molecules on the Co(II) centers were removed following EtOH-exchange and activation at 75 °C. This would decrease

the coordination number from six to four for each Co(II) node, enabling a transition of the nodes to a geometry that is more T_d in nature. This phenomenon would explain the color change of Pt-PCM-24 from pink to blue after activation, and the purple color of the EtOH-exchanged sample could be attributed to an incomplete transition containing a mixture of both O_h and T_d centers. This effect was also demonstrated by the color change of a Pt-PCM-24 sample submerged in EtOH inside a borosilicate capillary tube (Figure 4.38, *right*). After exposure to ambient moisture for three days, the top of the sample returned to a pink color, presumably from the re-coordination of OH_2 molecules to the Co(II) nodes. Efforts to obtain a crystal structure of the blue, activated M-PCM-24 materials are ongoing.

FTIR analysis of Pt-PCM-24 also illustrated that EtOH-exchange and activation at 75 °C produced a structural transition within the material (Figure 4.39); the bands at 1646, 1252, 828, and 663 cm^{-1} disappeared in the as-synthesized sample after EtOH-exchange, and a new band at 1040 cm^{-1} in the EtOH-exchanged sample disappeared after activation.

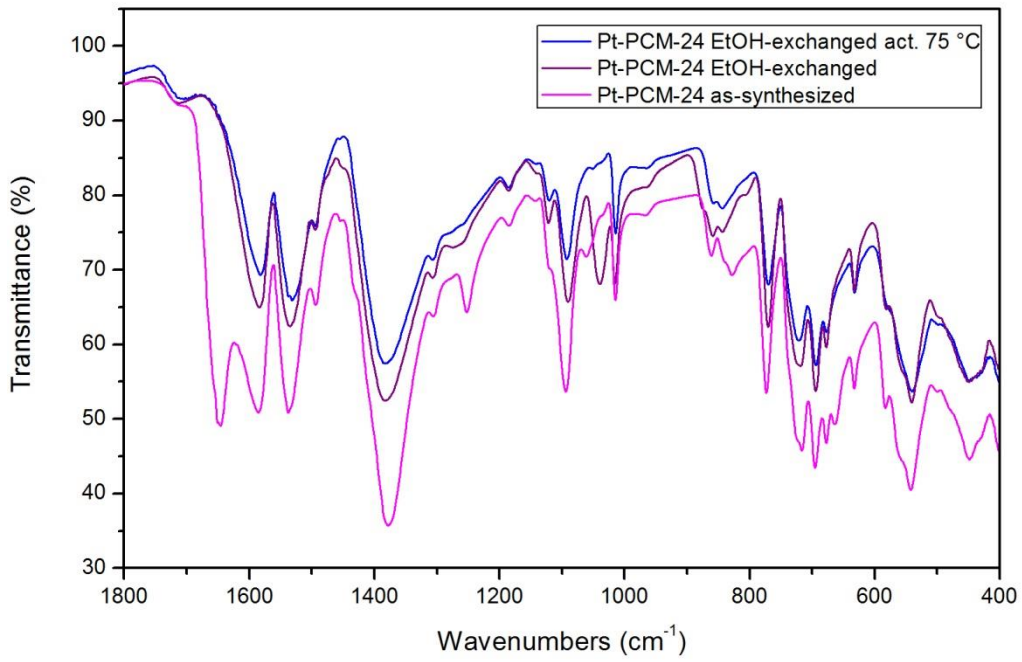

Figure 4.39: FTIR of as-synthesized, EtOH-exchanged, and activated Pt-PCM-24.

CONCLUSIONS

In summary, a versatile *bis*(phosphine) ligand has been developed that can be used to construct coordination polymers containing a variety of UMCs as a means to impart unusual chemical reactivity by rational design. We are presently investigating further the catalytic properties of the M-PCM-18 materials, in addition to the incorporation of earlier 4*d* and 5*d* transition metals, such as Rh(CO)Cl into similar polymers, to access fundamental catalytic reactions, such as hydroformylation. Further analyses of the M-PCM-24 materials are ongoing, including the high-temperature H_2 sorption properties of Pd-PCM-24 and X-ray diffraction studies of the blue, activated materials.

EXPERIMENTAL TECHNIQUES

General

All ligand syntheses were performed under an N_2 atmosphere using standard schlenk techniques. 1,4-dibromobenzene (Alfa Aesar, ≥98%), 1,2-*bis*(dichlorophosphino)benzene (Strem Chemicals Inc., ≥97%), *n*-butyllithium (1.6 M in hexanes, Sigma-Aldrich), $Zn(NO_3)_2 \cdot 6H_2O$ (Sigma-Aldrich, ≥98%) and ethyl diazoacetate (≥13% CH_2Cl_2; Sigma-Aldrich) were used as received. Organic solvents (THF, DMF, EtOH) were obtained from Fisher Scientific and dried/degassed using a Solvent Purification System (Innovative Technologies) and further degassed using freeze-thaw cycles prior to use. Chloroform, diethyl either, and all aqueous solutions were purged with N_2 for 30 min prior to use. Solution ^{1}H-NMR, ^{13}C-NMR and ^{31}P-NMR were collected in-house using a Varian Unity 300 MHz spectrometer; FT-IR spectra and Far-IR spectra were obtained directly from solid samples using a Nicolet iS*50 spectrophotometer fitted with an attenuated total reflectance apparatus; thermogravimetric analyses (TGA) were collected using a TA Instruments Q50 system. Elemental microanalyses were performed by QTI Intertek (New Jersey) or Midwest Microlab LLC (Indianapolis).

Solid-state NMR

The solid-state ^{1}H, ^{13}C{^{1}H} cross-polarization (CP), and ^{31}P{^{1}H}CP-MAS NMR spectra have been obtained with a Bruker Avance-400 spectrometer (400 MHz for protons) equipped by a standard 4-mm MAS probe head. A standard 4mm zirconium oxide rotor has been used at a spinning rate of 12 kHz. The ^{1}H, ^{13}C and ^{31}P shifts have been referred to external TMS and H_3PO_4, respectively. A contact time of 2000 μs was

applied for the ^{13}C-CP-MAS NMR experiment. In the ^{31}P-CP experiments, a contact time was varied between 5000 and 100 μs. The relaxation delays in all of these experiments were 5s.

X-Ray crystallography

Crystals were mounted on thin glass fibers using perfluoropolyether oil, which was frozen *in situ* by a nitrogen gas Cryostream flow. Data for the structures reported were either collected on an Enraf Nonius Kappa CCD diffractometer (BBCB-$PtCl_2$ and Pt-PCM-18) or a Rigaku Saturn CCD diffractometer (Pd-PCM-18) using monochromated Mo$K\alpha$ radiation (λ = 0.71073 Å). Absorption corrections were made based on multiple ψ- and ω-scans using the SORTAV program. Structures were solved using direct methods and refined on F^2 then refined using SHELXTL-97 software. All non-hydrogen atoms were refined anisotropically for all structures, except for uncoordinated and disordered solvent molecules, which were refined with isotropic displacement parameters. The SQUEEZE utility in *PLATON* was applied to Pd-PCM-18 and Pt-PCM-18 *post*-refinement in order to remove residual peaks due to any remaining disordered solvent. In all instances, this resulted in only small improvements to the final statistics (included in CIF data). For all structures, hydrogen atoms were fixed based on idealized coordinates and were refined with values of U_{iso} set to 1.5 times that of the carrier atom.

Powder X-ray diffraction (PXRD)

Phase purity of the PCM-18 materials before and after $CHCl_3$ solvent exchange and activation were confirmed by analysis of powdered crystalline samples that were sealed inside borosilcate capillary tubes and spun *in situ* to prevent preferential

orientation of the crystallites. Spectra were recorded on a Stoe Stadi-P diffractometer, operating in Debye-Scherrer geometry using Co*K*α radiation (1.7902 Å). Reflection data was collected in the range 5.0–40.0° 2θ using multiple scans, which were subsequently averaged. The XRPD spectra were then compared directly to their corresponding simulated patterns that were generated using the SimPowPatt function in *PLATON* using the single crystal model for the hkl reflection data obtained in the single crystal experiment.

Ligand synthesis

Procedure for BBCB-Br$_4$

1,4-dibromobenzene (7.1 g; 30.0 mmol) was dissolved in THF (100 cm^3) in a 250 cm^3 round bottomed flask and cooled to –78 °C. A solution of *n*-butyllithium (1.6 M in hexanes; 30.0 mmol) was added dropwise to the reaction over 30 min. The resulting white slurry was stirred for 1 h at –78 °C. 1,2-*bis*(dichlorophosphino)benzene (2.0 g; 7.1 mmol) was added drop-wise to the mixture over 30 min before slowly warming to room temperature and then stirring overnight. The orange solution was washed with NH_4Cl (10%, 100 cm^3) then dried over $MgSO_4$ and the solvent was removed *in vacuo* to yield an orange oil. The product was purified by column chromatography (silica gel eluted with CH_2Cl_2:hexanes (1:1)) to afford a white powder (3.5 g; 9.2 mmol). Yield, 87.7 %. ^{1}H-NMR ($CDCl_3$, 300.1 MHz): δ = 7.38 (d, 8H), 7.34 (m, 2H), 7.05 (m, 2H), 6.99 (m, 8H)); ^{13}C-NMR ($CDCl_3$, 75.5 MHz): δ = 142.85 (t, Ar), 135.65 (t, Ar), 135.30 (t, Ar), 134.25 (t, Ar), 131.95 (t, Ar), 129.92 (s, Ar), 123.94 (s, Ar); ^{31}P-NMR ($CDCl_3$, 121.5 MHz): δ = –15.33. FT-IR (ATR) ν_{max} (cm^{-1}) = 3044 (w), 2954 (w), 2925 (w), 2852 (w), 1638 (w), 1568 (m), 1554 (w), 1473 (s), 1438 (m), 1424 (w), 1382 (s), 1343 (w), 1297 (w), 1261

(m), 1181 (m), 1107 (w), 1094 (m), 1068 (s), 1007 (s), 944 (w), 808 (s), 757 (m), 735 (m), 723 (s), 702 (w), 663 (w), 628 (w), 568 (w), 553 (w), 512 (s), 501 (s), 436 (w), 401 (w), 375 (m), 364 (w), 351 (w), 330 (w), 307 (w), 278 (m), 267 (w), 230 (m), 182 (w), 174 (w).

Procedure for BBCB-Li$_4$

BBCB-Br$_4$ (1.0 g; 1.3 mmol) was dissolved in THF (100 cm^3) in a 250 cm^3 round bottomed flask and cooled to –78 °C. A solution of *n*-butyllithium (1.6 M in hexanes; 5.9 mmol) was added drop-wise to the reaction over 30 min. The resulting orange slurry was stirred for at least 2 h at –78 °C, after which an excess of crushed dry ice (*ca.* 200 g) and diethyl either (40 cm^3) were added, causing the reaction to immediately lose color. The mixture was removed from the cooling bath and allowed to reach room temperature with stirring overnight. The product was isolated on a D4 frit under nitrogen to afford an off-white powder (0.66 g; 1.0 mmol). ^{1}H-NMR (D_2O, 300.1 MHz): δ = 7.62 (d, 8H), 7.28 (m, 2H), 7.13 (m, 8H), 7.05 (m, 2H); ^{31}P-NMR (D_2O, 121.5 MHz): δ = –14.63.

Procedure for BBCB

BBCB-Li$_4$ (1.0 g; 1.5 mmol) was dissolved in carefully degassed H_2O (100 cm^3) in a 200 cm^3 schlenk flask, cooled to 0 °C in an ice-water bath and precipitated with degassed HCl (1.0 M) to pH = 3. The product was isolated by centrifugation, rinsed twice with degassed H_2O, and dried under flowing N_2 to afford a light yellow powder (0.72 g, 1.2 mmol). Yield, 94.6 % based on BBCB-Br$_4$. ^{1}H-NMR (DMSO-d_6, 300.1 MHz): δ = 13.07 (s, broad, 4H), 7.88 (d, 8H), 7.46 (m, 2H), 7.24 (m, 8H), 7.02 (m, 2H); ^{13}C-NMR (DMSO-d_6, 125.6 MHz): δ = 166.88 (s, CO_2H), 141.86 (t, Ar), 141.41 (s, Ar), 134.03 (s,

Ar), 133.31 (t, Ar), 131.16 (s, Ar), 130.44 (s, Ar), 129.35 (s, Ar); ^{31}P-NMR (DMSO-d_6, 121.5 MHz): δ = –11.79. FT-IR (ATR) ν_{max} (cm^{-1}) = 3436 (br), 3164 (br), 3044 (w), 2961 (w), 2654 (w), 2537 (w), 1683 (s), 1592 (s), 1557 (m), 1495 (w), 1413 (m), 1395 (s), 1313 (w), 1288 (m), 1261 (m), 1225 (s), 1179 (s), 1126 (w), 1109 (m), 1085 (m), 1016 (s), 912 (w), 850 (m), 793 (m), 759 (s), 731 (w), 694 (s), 677 (s), 632 (w), 514 (s), 387 (br), 272 (br), 185 (br), 176 (w), 134 (m).

Procedure for BBCB-PdCl$_2$

BBCB (0.50 g; 0.80 mmol) was dissolved in THF (100 cm^3) in a 200 cm^3 schlenk flask. A separate solution of (COD)PdCl$_2$ (0.25 g; 0.88 mmol) in the same solvent (15 cm^3) was added *via* cannula to the ligand solution and was stirred overnight at 50 °C. The solvent was subsequently removed *in vacuo* and the resulting yellow solid was dissolved in EtOH, filtered through celite, and concentrated to dryness on a rotary evaporator to afford a yellow powder (0.63 g; 0.79 mmol). Yield, 98.5 %. Analysis found: C 49.1, H 3.04, Cl 9.3. $C_{34}H_{24}Cl_2O_8P_2Pd{\cdot}2H_2O$ requires: C 48.9, H 3.37, Cl 8.5. ^{1}H-NMR (DMSO-d_6, 599.8 MHz): δ = 8.09 (dd, 8H), 7.92 (dd, 8H), 7.89 (m, 2H), 7.85 (m, 2H); ^{13}C-NMR (DMSO-d_6, 125.7 MHz): δ = 166.81 (s, CO_2H), 139.47 (m, Ar), 135.19 (s, Ar), 134.56 (s, Ar), 133.42 (s, Ar), 132.95 (s, Ar), 130.08 (s, Ar), 128.76 (s, Ar); ^{31}P-NMR (DMSO-d_6, 121.5 MHz): δ = 64.77. FT-IR (ATR) ν_{max} (cm^{-1}) = 3449 (br), 3148 (br), 3060 (w), 2952 (w), 2870 (w), 2645 (w), 2610 (w), 2506 (w), 1703 (s), 1601 (m), 1562 (m), 1495 (w), 1453 (w), 1426 (w), 1394 (s), 1316 (w), 1258 (w), 1220 (s), 1183 (m), 1122 (m), 1089 (s), 1048 (w), 1016 (s), 962 (w), 916 (w), 856 (m), 793 (w), 761 (s), 737 (m), 689 (s), 674 (w), 634 (m), 540 (s), 451 (w), 420 (w), 364 (w), 320 (m), 290 (s), 270 (br), 228 (w), 186 (br).

Procedure for BBCB-$PtCl_2$

The same procedure was employed as for the preparation of BBCB-$PdCl_2$ above, using (COD)$PtCl_2$ (0.33 g; 0.88 mmol), which gave an off-white powder (0.70 g; 0.78 mmol). Yield, 98.0 %. Analysis found: C 46.0, H 2.95, Cl 7.9, P 6.62. $C_{34}H_{24}Cl_2O_8P_2Pt$ requires: C 46.0, H 2.72, Cl 8.0, P 6.97. ^{1}H-NMR (DMSO-d_6, 599.8 MHz): δ = 8.08 (dd, 8H), 7.93 (m, 2H), 7.88 (dd, 8H), 7.78 (m, 2H); ^{13}C-NMR (DMSO-d_6, 125.7 MHz): δ = 167.19 (s, CO_2H), 139.83 (m, Ar), 135.23 (s, Ar), 134.98 (s, Ar), 134.71 (d, Ar), 132.98 (s, Ar), 132.46 (s, Ar), 130.36 (d, Ar); ^{31}P-NMR (DMSO-d_6, 121.5 MHz): δ = 41.98 (s; Pt satellites, J = 3556 Hz). FT-IR (ATR) ν_{max} (cm^{-1}) = 3459 (br), 3148 (br), 3044 (w), 2971 (w), 2949 (w), 2873 (w), 2629 (w), 2518 (w), 1715 (s), 1694 (s), 1599 (m), 1561 (m), 1495 (w), 1452 (w), 1431 (w), 1396 (s), 1315 (w), 1257 (s), 1227 (m), 1183 (w), 1121 (m), 1091 (s), 1047 (m), 1014 (m), 963 (w), 914 (w), 878 (w), 854 (m), 808 (w), 794 (w), 762 (s), 737 (m), 693 (s), 675 (s), 633 (m), 579 (m), 560 (w), 545 (s), 459 (br), 425 (w), 368 (w), 318 (m), 291 (s), 190 (br), 151 (m).

Procedure for organometallic functionalized BBCB-$PtCl_2$

BBCB-$PtCl_2$ (150 mg, 0.17 mmol) was dissolved in CH_2Cl_2:EtOH (1:1; 30 cm^3), to which was added $N_2CHCO_2C_2H_5$ (15 equiv.; 0.32 cm^3) over a period of 30 min at room temp. The mixture was stirred under N_2 for 4 d, then concentrated to dryness under vacuum. The residue was washed with diethyl ether (2 x 30 cm^3) and dried. Yield, 85.6 %. ^{1}H-NMR (DMSO-d_6, 300.1 MHz): δ = 8.05 – 7.69 (m, 20H), 4.95 (s, 1H), 4.11 (m, 2H), 1.16 (m, 3H); ^{31}P-NMR (DMSO-d_6, 121.5 MHz): δ = 45.36 (d, $J_{P\text{-}P}$ = 4.6 Hz; Pt satellites, $J_{Pt\text{-}P}$ = 2068 Hz,), 40.98 (d, $J_{P\text{-}P}$ = 4.6 Hz; Pt satellites, $J_{Pt\text{-}P}$ = 3957 Hz). FT-IR (ATR) ν_{max} (cm^{-1}) = 3429 (br), 3060 (w), 2978 (w), 2931 (w), 2902 (w), 2628 (br), 2510 (br), 1694 (s), 1599 (m), 1562 (m), 1496 (w), 1395 (m), 1371 (w), 1313 (w), 1258 (w),

1225 (br), 1180 (m), 1116 (w), 1090 (m), 1030 (w), 1016 (m), 856 (m), 799 (m), 764 (m), 736 (w), 690 (s), 633 (w), 575 (w), 540 (s), 452 (w), 421 (w), 366 (w), 346 (w), 300 (m), 273 (w).

PCP synthesis

Procedure for Pd-PCM-18

BBCB-$PdCl_2$ (16.0 mg, 0.020 mmol) was dissolved in EtOH (4.0 cm^3), to which a second solution of $Zn(NO_3)_2 \cdot 6H_2O$ (17.6 mg, 0.059 mmol) in DMF (4.0 cm^3) was added. The yellow solution was heated in a 20 cm^3 scintillation vial at 45 °C for 10 d in a graphite thermal bath. Yellow needles were isolated by decantation of the mother liquor and brief sonication (2 x 5 s) in fresh EtOH:DMF (2:1, 10 cm^3). Average yield, 40 mg (from ten reactions). Analysis found: C 38.3, H 2.41, Cl 14.6; $C_{34}H_{24}Cl_2O_{10}P_2PdZn_2 \cdot CHCl_3$ requires: C 38.8, H 2.33, Cl 16.3. FT-IR (ATR) ν_{max} (cm^{-1}) = 3395 (br), 3063 (w), 2933 (w), 2873 (w), 1647 (s), 1546 (m), 1492 (m), 1435 (w), 1384 (s), 1305 (w), 1254 (m), 1183 (w), 1092 (s), 1061 (w), 1015 (m), 968 (w), 866 (w), 845 (m), 776 (s), 733 (s), 696 (m), 678 (w), 660 (m) 634 (w), 541 (m), 454 (m), 397 (w), 357 (s), 320 (m), 291 (s), 183 (w), 139 (w).

Procedure for Pt-PCM-18

BBCB-$PtCl_2$ (15.0 mg, 0.017 mmol) was dissolved in EtOH (9.0 cm^3) and mixed with a second solution of $Zn(NO_3)_2 \cdot 6H_2O$ (17.6 mg, 0.059 mmol) in DMF (4.0 cm^3). The colorless solution was heated and the resulting colorless needles were isolated by processes analogous to those for Pd-PCM-18. Average yield, 40 mg (from ten reactions). Analysis found: C 38.3, H 1.72, Cl 6.9, P 5.63; $C_{34}H_{20}Cl_2O_{10}P_2PtZn_2$ requires: C 38.8, H

2.30, Cl 6.7, P 5.89. FT-IR (ATR) ν_{max} (cm^{-1}) = 3379 (br), 3062 (w), 2930 (w), 1647 (s), 1546 (m), 1495 (w), 1433 (w), 1382 (s), 1309 (w), 1254 (m), 1185 (w), 1094 (s), 1062 (w), 1015 (m), 966 (w), 865 (w), 844 (m), 776 (s), 731 (m), 697 (m), 679 (w), 659 (m), 634 (w), 586 (w), 546 (m), 453 (m), 400 (w), 357 (s), 317 (m), 292 (s), 175 (w), 145 (m), 137 (m), 130 (w).

Procedure for organometallic-functionalized Pt-PCM-18

Freshly-prepared Pt-PCM-18 (40 mg) was subjected to the same solvent exchange procedure used for surface area analysis, involving exchange with $CHCl_3$, rinsed 4-5 times over 24 h. The Pt-PCM-18 was then exchanged with CH_2Cl_2 (3 x 20 cm^3) over 4 h, and a solution of $N_2CHCO_2C_2H_5$ (15 equiv.; 0.07 cm^3) diluted into CH_2Cl_2 (5.0 cm^3) was added over 30 min with intermittent swirling. The mixture and solids were allowed to stand in a closed vial for 4 d with intermittent agitation. The product was isolated by decanting away the solution and then washing the crystals by exchanging with fresh CH_2Cl_2 (3 x 20 cm^3) over 2 h. FT-IR (ATR) ν_{max} (cm^{-1}) = 3346 (br), 3197 (br), 3059 (w), 2980 (w), 2934 (w), 1694 (m), 1590 (s), 1539 (s), 1495 (w), 1473 (w), 1392 (s), 1373 (w), 1306 (w), 1262 (m), 1183 (w), 1116 (w), 1091 (m), 1029 (w), 1015 (m), 858 (m), 848 (m), 772 (s), 728 (s), 695 (m), 674 (w), 632 (w), 535 (m), 453 (m), 392 (m), 347 (w), 297 (w), 287 (m).

Procedure for Pd-PCM-24

BBCB-$PdCl_2$ (16.0 mg, 0.020 mmol) was dissolved in EtOH (3.0 cm^3), to which a second solution of $Co(NO_3)_2 \cdot 6H_2O$ (18.0 mg, 0.062 mmol) in DMF (1.5 cm^3) was added. The pink solution was heated in a 20 cm^3 scintillation vial at 45 °C for 30 d in a graphite

thermal bath. Pink hexagonal prisms were isolated by decantation of the mother liquor and brief sonication (2 x 5 s) in fresh EtOH:DMF (1:1, 10 cm^3). Average yield, 50 mg (from twenty reactions). FT-IR (ATR) ν_{max} (cm^{-1}) = 3392 (br m), 3064 (w), 2928 (m), 2875 (w), 1646 (s), 1596 (w), 1543 (m), 1494 (m), 1435 (w), 1379 (s), 1306 (w), 1253 (m), 1184 (w), 1143 (w), 1094 (s), 1062 (w), 1015 (m), 968 (w), 863 (m), 828 (m), 774 (s), 726 (m), 715 (m), 695 (m), 677 (w), 660 (m), 633 (w), 574 (w), 555 (w), 539 (m), 498 (w), 479 (w), 449 (m), 425 (w), 381 (w), 355 (s), 318 (m), 290 (s), 245 (w), 175 (br, m).

Procedure for Pt-PCM-24

BBCB-$PtCl_2$ (15.0 mg, 0.017 mmol) was dissolved in EtOH (3.0 cm^3) and mixed with a second solution of $Co(NO_3)_2 \cdot 6H_2O$ (18.0 mg, 0.062 mmol) in DMF (1.5 cm^3). The pink solution was heated and the resulting pink hexagonal prisms were isolated by processes analogous to those for Pd-PCM-24. Average yield, 55 mg (from twenty reactions). FT-IR (ATR) ν_{max} (cm^{-1}) = 3334 (br, m), 3064 (w), 2929 (w), 1646 (s), 1537 (m), 1494 (w), 1378 (s), 1306 (w), 1252 (m), 1185 (w), 1142 (w), 1094 (s), 1061 (w), 1015 (m), 967 (w), 861 (w), 828 (w), 773 (s), 727 (m), 716 (m), 695 (m), 677 (w), 663 (w), 633 (w), 582 (w), 561 (w), 542 (m), 448 (m), 370 (m), 351 (w), 315 (m), 288 (s), 170 (br).

[202] P. D. C. Dietzel, P. A. Georgiev, J. Eckert, R. Blom, T. Strässle, T. Unruh, *Chem. Commun.* **2010**, *46*, 4962.

[203] S. Barman, H. Furukawa, O. Blacque, K. Venkatesan, O. M. Yaghi, H. Berke, *Chem. Commun.* **2010**, *46*, 7981.

[204] D. -C. Zhong, J.-B. Lin, W. -G. Lu, L. Jiang, T.-B. Lu, *Inorg. Chem.* **2009**, *48*, 8656.

[205] R. Sanz, F. Martínez, G. Orcajo, L. Wojtas, D. Briones, *Dalton Trans.* **2013**, *42*, 2392.

[206] H. Fei, J. F. Cahill, K. A. Prather, S. M. Cohen, *Inorg. Chem.* **2013**, *52*, 4011.

[207] S. Kim, K. W. Dawson, B. S. Gelfand, J. M. Taylor, G. K. H. Shimizu, *J. Am. Chem. Soc.* **2013**, *135*, 963.

[208] M. Kim, J. F. Cahill, H. Fei, K. A. Prather, S. M. Cohen, *J. Am. Chem. Soc.* **2012**, *134*, 18082.

[209] X. -S. Wang, S. Ma, P. M. Forster, D. Yuan, J. Eckert, J. J. López, B. J. Murphy, J. B. Parise, H. -C. Zhou, *Angew. Chem. Int. Ed.* **2008**, *47*, 7263.

[210] H. Wu, W. Zhou, T. Yildirim, *J. Am. Chem. Soc.* **2009**, *131*, 4995.

[211] S. S. Kaye, J. R. Long, *J. Am. Chem. Soc.* **2008**, *130*, 806.

[212] K. Oisaki, Q. Li, H. Furukawa, A. U. Czaja, O. M. Yaghi, *J. Am. Chem. Soc.* **2010**, *132*, 9262.

[213] T. Jacobs, R. Clowes, A. I. Cooper, M. J. Hardie, *Angew. Chem. Int. Ed.* **2012**, *51*, 5192.

[214] C. J. Doonan, W. Morris, H. Furukawa, O. M. Yaghi, *J. Am. Chem. Soc.* **2009**, *131*, 9492.

[215] K. C. Szeto, K. O. Kongshaug, S. Jakobsen, M. Tilset, K. P. Lillerud, *Dalton Trans.* **2008**, 2054.

[216] J. L. Crossland, D. M. Young, L. N. Zakharov, D. R. Tyler, *Dalton Trans.* **2009**, 9253.

[217] K. K. Majumdar, H. V. Nanishankar, B. R. Jagirdar, *Eur. J. Inorg. Chem.* **2001**, *2001*, 1847.

[218] G. Minghetti, A. Albinati, A. L. Bandini, G. Banditelli, *Angew. Chem. Int. Ed.* **1985**, *24*, 120.

[219] A. L. Bandini, G. Banditelli, M. Manassero, A. Albinati, D. Colognesi, J. Eckert, *Eur. J. Inorg. Chem.* **2003**, *2003*, 3958.

[220] X. Lin, I. Telepeni, A. J. Blake, A. Dailly, C. M. Brown, J. M. Simmons, M. Zoppi, G. S. Walker, K. M. Thomas, T. J. Mays, P. Hubberstey, N. R. Champness, M. Schröder, *J. Am. Chem. Soc.* **2009**, *131*, 2159.

[221] A. M. Shultz, O. K. Farha, J. T. Hupp, S. T. Nguyen, *J. Am. Chem. Soc.* **2009**, *131*, 4204.

[222] G. J. Kubas, *J. Organomet. Chem.* **2001**, *635*, 37.

[223] G. J. Kubas, *J. Organomet. Chem.* **2009**, *694*, 2648.

[224] N. K. Szymczak, D. A. Braden, J. L. Crossland, Y. Turov, L. N. Zakharov, D. R. Tyler, *Inorg. Chem.* **2009**, *48*, 2976.

[225] D. M. Heinekey, J. K. Law, S. M. Schultz, *J. Am. Chem. Soc.* **2001**, *123*, 12728.

[226] M. Findlater, K. M. Schultz, W. H. Bernskoetter, A. Cartwright-Sykes, D. M. Heinekey, M. Brookhart, *Inorg. Chem.* **2012**, *51*, 4672.

[227] J. L. Mendoza-Cortes, W. A. Goddard, H. Furukawa, O. M. Yaghi, *J. Phys. Chem. Lett.* **2012**, *3*, 2671.

[228] M. Kosa, M. Krack, A. K. Cheetham, M. Parrinello, *J. Phys. Chem. C* **2008**, *112*, 16171.

[229] T. K. A. Hoang, A. Hamaed, G. Moula, R. Aroca, M. Trudeau, D. M. Antonelli, *J. Am. Chem. Soc.* **2011**, *133*, 4955.

[230] K. Q. Almeida Leñero, Y. Guari, P. C. J. Kamer, P. W. N. M. van Leeuwen, B. Donnadieu, S. Sabo-Etienne, B. Chaudret, M. Lutz, A. L. Spek, *Dalton Trans.* **2013**, *42*, 6495.

[231] P.-Z. Li, Y. Maeda, Q. Xu, *Chem. Comm.* **2011**, *47*, 8436.

[232] P. Bergamini, E. Costa, S. Sostero, A. G. Orpen, P. G. Pringle, *Organometallics* **1991**, *10*, 2989.

[233] G. L. Casty, J. M. Stryker, *Organometallics* **1997**, *16*, 3083.

[234] E. Tsivion, J. R. Long, M. Head-Gordon, *J. Am. Chem. Soc.* **2014**, *136*, 17827.

[235] Q. Chen, Z. Chang, W. -C. Song, H. Song, H.-B. Song, T. -L. Hu, X. -H. Bu, *Angew. Chem. Int. Ed.* **2013**, *52*, 11550.

[236] X. -N. Cheng, W. -X. Zhang, Y. -Y. Lin, Y. -Z. Zheng, X. -M. Chen, *Adv. Mater.* **2007**, *19*, 1494.

[237] L. Wang, S. Lu, Y. Zhou, X. Guo, Y. Lu, J. He, D. G. Evans, *Chem. Commun.* **2011**, *47*, 11002.

Chapter 5: Summary of Key Results

1. A new coordination polymer (PCM-11) was synthesized from tctpoH_3 and $Mg(OH)_2$ under slightly basic solvothermal conditions.
2. PCM-11 adsorbed 47.5 wt % CO_2 at room temperature and 12 bar, the highest amount to date at those conditions, due to the generation of open metal sites on the $[Mg_4(\mu^3\text{-}OH)_2(OH_2)_4]^{6+}$ nodes during activation.
3. A highly symmetric tetrahedral phosphonium zwitterion (tctp$^+H_3$) was synthesized by reaction of tctpH_3 with *p*-iodobenzoic acid.
4. Crystallization of tctp$^+H_3$ afforded a metal-free ionic coordination polymer (iPCM-1) due to hydrogen-bonding between neighboring carboxylic acid groups.
5. Thermally and chemically robust iPCM-1 resisted decomposition up to 330 °C and retained crystallinity in a vast range of organic solvents.
6. Nine isostructural lanthanide-based PCMs were developed from the tctp$^+H_3$ ligand and $Ln(NO_3)_3$ salts (Ln-PCM-25).
7. Tb-, Eu-, and Dy-PCM-25 exhibited characteristic lanthanide luminescence due to the antenna effect, but the emission is significantly quenched by the O–H oscillators of coordinated solvent molecules.
8. The luminescence quantum yields and emission lifetimes of Tb-, Eu-, and Dy-PCM-25 could not be increased by the removal of one or four coordinated OH_2 molecules.
9. A novel *bis*(phosphine) ligand (BBCB) and its subsequent $-MCl_2$ (M = Pt, Pd) complexes were developed by a synthetic route analogous to that of tctpH_3.

10. Two coordination polymers were synthesized by reaction of the BBCB-MCl_2 complexes with $Zn(NO_3)_2$ under low-temperature solvothermal conditions (M-PCM-18).
11. M-PCM-18 exhibited unusual high-temperature H_2 physisorption at 150 °C and 1 bar; Pd- and Pt-PCM-18 adsorb 6.29 and 7.35 $cm^3\ g^{-1}$, respectively, corresponding to 0.16 and 0.22 H_2 molecules per metal site.
12. Pt-PCM-18 was *post*-synthetically modified by reaction with ethyl diazoacetate to afford the –$PtCl(CHClCO_2C_2H_5)$ organometallic moiety within the pores of the material.
13. Two cobalt(II)-based coordination polymers were synthesized from the BBCB-MCl_2 complexes with $Co(NO_3)_2$ under similar low-temperature conditions (M-PCM-24).
14. M-PCM-24 exhibited high-temperature H_2 sorption similar to M-PCM-18 between 125–225 °C.
15. A reversible color change was observed in M-PCM-24 upon solvent-exchange and activation at 75 °C, indicative of a transformation in the Co(II) coordination mode from O_h (pink) to T_d (blue) due to the removal of two coordinated OH_2 molecules.

Appendix I: Crystallographic Data

Table A1.1: Crystal data and structure refinement for PCM-11.

Identification code	sh0803b	
Empirical formula	C45 H33 Mg4 N O21 P2	
Formula weight	1082.90	
Temperature	180(2) K	
Wavelength	0.71073 Å	
Crystal system	monoclinic	
Space group	P2(1)/c	
Unit cell dimensions	a = 13.5792(4) Å	a= 90°.
	b = 13.8958(4) Å	b= 104.8821(13)°.
	c = 20.7478(6) Å	g = 90°.
Volume	3783.66(19) $Å^3$	
Z	2	
Density (calculated)	0.951 Mg/m^3	
Absorption coefficient	0.144 mm^{-1}	
F(000)	1112	
Crystal size	0.20 x 0.05 x 0.05 mm^3	
Theta range for data collection	3.56 to 24.00°.	
Index ranges	-15<=h<=15, -15<=k<=15, -23<=l<=23	
Reflections collected	21285	
Independent reflections	5893 [R(int) = 0.0880]	
Completeness to theta = 24.00°	99.2 %	
Absorption correction	Semi-empirical from equivalents	
Max. and min. transmission	0.995 and 0.889	
Refinement method	Full-matrix least-squares on F^2	
Data / restraints / parameters	5893 / 3 / 328	
Goodness-of-fit on F^2	1.021	
Final R indices [I>2sigma(I)]	R1 = 0.0783, wR2 = 0.2160	
R indices (all data)	R1 = 0.1098, wR2 = 0.2384	

Largest diff. peak and hole 1.410 and -0.296 e.Å^{-3}

Table A1.2: Atomic coordinates (x 10^4) and equivalent isotropic displacement parameters (Å^{2}x 10^3) for PCM-11. U(eq) is defined as one third of the trace of the orthogonalized U^{ij} tensor.

	x	y	z	U(eq)
P1	7360(1)	-371(1)	-1815(1)	25(1)
Mg1	6539(1)	-1340(1)	-495(1)	27(1)
Mg2	4051(1)	-430(1)	-517(1)	30(1)
O1P	6788(2)	-623(2)	-1316(1)	31(1)
O1	6285(2)	-4169(2)	-3926(1)	38(1)
O2	6305(2)	-2970(2)	-4647(1)	40(1)
O3	12143(2)	774(2)	-114(1)	37(1)
O4	12482(2)	-558(2)	-621(2)	44(1)
O5	6084(2)	3709(2)	-3652(2)	48(1)
O6	4616(2)	2857(2)	-3897(1)	35(1)
O7	5600(2)	-238(2)	-398(1)	27(1)
O8	7481(3)	-2498(3)	-613(2)	52(1)
O9	4168(3)	-1781(2)	12(2)	52(1)
C1	7159(3)	-1256(3)	-2473(2)	29(1)
C2	6826(4)	-2157(4)	-2361(2)	46(1)
C3	6598(4)	-2827(4)	-2870(2)	47(1)
C4	6692(3)	-2594(3)	-3504(2)	29(1)
C5	7049(4)	-1700(4)	-3606(2)	50(1)
C6	7287(4)	-1019(4)	-3103(2)	50(1)
C7	6408(3)	-3315(3)	-4066(2)	32(1)
C8	8707(3)	-229(3)	-1461(2)	26(1)
C9	9413(4)	-833(4)	-1625(3)	50(1)
C10	10442(4)	-742(4)	-1308(3)	51(1)

C11	10766(3)	-51(3)	-834(2)	32(1)
C12	10069(3)	565(4)	-676(2)	40(1)
C13	9035(3)	475(3)	-980(2)	40(1)
C14	11901(3)	61(3)	-495(2)	33(1)
C15	6886(3)	727(3)	-2254(2)	31(1)
C16	7491(3)	1392(4)	-2460(3)	49(1)
C17	7057(3)	2147(4)	-2871(2)	47(1)
C18	6007(3)	2228(3)	-3099(2)	33(1)
C19	5399(3)	1558(3)	-2885(2)	42(1)
C20	5827(3)	830(3)	-2462(2)	42(1)
C21	5529(3)	3002(3)	-3592(2)	35(1)
N100	9729(14)	-2517(15)	1758(9)	139(6)
O100	9123(10)	-3144(11)	494(7)	135(4)
C100	8965(18)	-2575(17)	981(11)	154(8)
C101	10360(20)	-3320(20)	1780(13)	206(13)
C102	9456(12)	-1868(12)	2132(8)	100(5)

Table A1.3: Bond lengths [Å] and angles [°] for PCM-11.

P1-O1P	1.488(3)	Mg1-Mg2#4	3.4583(19)
P1-C8	1.799(4)	Mg1-Mg2	3.5966(19)
P1-C1	1.806(4)	Mg2-O7#4	2.056(3)
P1-C15	1.808(4)	Mg2-O5#2	2.068(3)
Mg1-O7	2.034(3)	Mg2-O7	2.072(3)
Mg1-O3#1	2.063(3)	Mg2-O1#5	2.083(3)
Mg1-O6#2	2.069(3)	Mg2-O4#6	2.093(3)
Mg1-O1P	2.073(3)	Mg2-O9	2.159(4)
Mg1-O2#3	2.099(3)	Mg2-Mg2#4	3.136(3)
Mg1-O8	2.109(3)	Mg2-Mg1#4	3.4583(19)

O1-C7	1.243(5)	C12-C13	1.390(6)
O1-Mg2#2	2.083(3)	C12-H12A	0.9500
O2-C7	1.272(5)	C13-H13A	0.9500
O2-Mg1#7	2.099(3)	C15-C16	1.375(6)
O3-C14	1.258(5)	C15-C20	1.399(6)
O3-Mg1#1	2.063(3)	C16-C17	1.385(7)
O4-C14	1.239(5)	C16-H16A	0.9500
O4-Mg2#8	2.093(3)	C17-C18	1.387(6)
O5-C21	1.263(6)	C17-H17A	0.9500
O5-Mg2#5	2.068(3)	C18-C19	1.391(6)
O6-C21	1.255(5)	C18-C21	1.511(6)
O6-Mg1#5	2.069(3)	C19-C20	1.367(6)
O7-Mg2#4	2.056(3)	C19-H19A	0.9500
O7-H7	1.0000	C20-H20A	0.9500
C1-C2	1.372(6)	N100-C102	1.31(2)
C1-C6	1.401(6)	N100-C101	1.40(3)
C2-C3	1.382(6)	N100-C100	1.68(3)
C2-H2A	0.9500	O100-C100	1.34(2)
C3-C4	1.392(6)	C100-H10B	0.9500
C3-H3A	0.9500	C101-H10C	0.9800
C4-C5	1.370(7)	C101-H10D	0.9800
C4-C7	1.511(6)	C101-H10E	0.9800
C5-C6	1.384(7)	C102-H10F	0.9800
C5-H5A	0.9500	C102-H10G	0.9800
C6-H6A	0.9500	C102-H10H	0.9800
C8-C9	1.380(6)	O1P-P1-C8	113.55(17)
C8-C13	1.386(6)	O1P-P1-C1	111.18(18)
C9-C10	1.389(6)	C8-P1-C1	108.85(19)
C9-H9A	0.9500	O1P-P1-C15	111.62(18)
C10-C11	1.365(6)	C8-P1-C15	107.84(19)
C10-H10A	0.9500	C1-P1-C15	103.22(19)
C11-C12	1.376(6)	O7-Mg1-O3#1	96.88(12)
C11-C14	1.528(6)	O7-Mg1-O6#2	94.07(12)

O3#1-Mg1-O6#2	168.92(13)	O5#2-Mg2-O4#6	89.74(13)
O7-Mg1-O1P	87.66(12)	O7-Mg2-O4#6	177.31(14)
O3#1-Mg1-O1P	91.22(13)	O1#5-Mg2-O4#6	86.71(14)
O6#2-Mg1-O1P	90.95(12)	O7#4-Mg2-O9	87.39(13)
O7-Mg1-O2#3	91.57(12)	O5#2-Mg2-O9	84.22(15)
O3#1-Mg1-O2#3	87.40(13)	O7-Mg2-O9	96.36(13)
O6#2-Mg1-O2#3	90.58(13)	O1#5-Mg2-O9	171.80(14)
O1P-Mg1-O2#3	178.33(13)	O4#6-Mg2-O9	85.35(14)
O7-Mg1-O8	178.60(13)	O7#4-Mg2-Mg2#4	40.75(8)
O3#1-Mg1-O8	84.52(13)	O5#2-Mg2-Mg2#4	132.22(12)
O6#2-Mg1-O8	84.53(13)	O7-Mg2-Mg2#4	40.36(8)
O1P-Mg1-O8	92.27(13)	O1#5-Mg2-Mg2#4	94.77(11)
O2#3-Mg1-O8	88.54(14)	O4#6-Mg2-Mg2#4	137.64(12)
O7-Mg1-Mg2#4	32.46(7)	O9-Mg2-Mg2#4	92.48(10)
O3#1-Mg1-Mg2#4	69.95(9)	O7#4-Mg2-Mg1#4	32.08(8)
O6#2-Mg1-Mg2#4	119.79(10)	O5#2-Mg2-Mg1#4	158.92(11)
O1P-Mg1-Mg2#4	105.63(9)	O7-Mg2-Mg1#4	102.85(9)
O2#3-Mg1-Mg2#4	73.01(9)	O1#5-Mg2-Mg1#4	71.77(9)
O8-Mg1-Mg2#4	148.73(10)	O4#6-Mg2-Mg1#4	74.61(10)
O7-Mg1-Mg2	29.14(8)	O9-Mg2-Mg1#4	107.95(11)
O3#1-Mg1-Mg2	122.57(10)	Mg2#4-Mg2-Mg1#4	65.89(5)
O6#2-Mg1-Mg2	67.66(9)	O7#4-Mg2-Mg1	98.87(8)
O1P-Mg1-Mg2	99.90(9)	O5#2-Mg2-Mg1	71.86(10)
O2#3-Mg1-Mg2	80.08(10)	O7-Mg2-Mg1	28.57(8)
O8-Mg1-Mg2	149.62(12)	O1#5-Mg2-Mg1	111.92(10)
Mg2#4-Mg1-Mg2	52.74(4)	O4#6-Mg2-Mg1	154.09(11)
O7#4-Mg2-O5#2	168.84(14)	O9-Mg2-Mg1	75.01(10)
O7#4-Mg2-O7	81.11(12)	Mg2#4-Mg2-Mg1	61.37(5)
O5#2-Mg2-O7	92.50(13)	Mg1#4-Mg2-Mg1	127.26(4)
O7#4-Mg2-O1#5	95.61(12)	P1-O1P-Mg1	155.45(18)
O5#2-Mg2-O1#5	93.70(14)	C7-O1-Mg2#2	134.2(3)
O7-Mg2-O1#5	91.65(13)	C7-O2-Mg1#7	128.2(3)
O7#4-Mg2-O4#6	96.92(13)	C14-O3-Mg1#1	137.0(3)

C14-O4-Mg2#8	127.3(3)	C8-C9-C10	120.4(4)
C21-O5-Mg2#5	127.2(3)	C8-C9-H9A	119.8
C21-O6-Mg1#5	135.7(3)	C10-C9-H9A	119.8
Mg1-O7-Mg2#4	115.46(12)	C11-C10-C9	120.3(4)
Mg1-O7-Mg2	122.29(14)	C11-C10-H10A	119.9
Mg2#4-O7-Mg2	98.89(12)	C9-C10-H10A	119.9
Mg1-O7-H7	106.3	C10-C11-C12	119.6(4)
Mg2#4-O7-H7	106.3	C10-C11-C14	120.3(4)
Mg2-O7-H7	106.3	C12-C11-C14	120.1(4)
C2-C1-C6	119.9(4)	C11-C12-C13	120.9(4)
C2-C1-P1	119.1(3)	C11-C12-H12A	119.6
C6-C1-P1	121.0(3)	C13-C12-H12A	119.6
C1-C2-C3	120.3(4)	C8-C13-C12	119.3(4)
C1-C2-H2A	119.9	C8-C13-H13A	120.3
C3-C2-H2A	119.9	C12-C13-H13A	120.3
C2-C3-C4	120.5(4)	O4-C14-O3	126.9(4)
C2-C3-H3A	119.7	O4-C14-C11	117.0(4)
C4-C3-H3A	119.7	O3-C14-C11	116.1(4)
C5-C4-C3	118.8(4)	C16-C15-C20	119.0(4)
C5-C4-C7	120.8(4)	C16-C15-P1	124.0(3)
C3-C4-C7	120.5(4)	C20-C15-P1	116.5(3)
C4-C5-C6	121.7(4)	C15-C16-C17	120.4(4)
C4-C5-H5A	119.2	C15-C16-H16A	119.8
C6-C5-H5A	119.2	C17-C16-H16A	119.8
C5-C6-C1	118.9(4)	C16-C17-C18	120.7(4)
C5-C6-H6A	120.6	C16-C17-H17A	119.7
C1-C6-H6A	120.6	C18-C17-H17A	119.7
O1-C7-O2	126.3(4)	C17-C18-C19	118.6(4)
O1-C7-C4	118.5(4)	C17-C18-C21	120.9(4)
O2-C7-C4	115.2(4)	C19-C18-C21	120.4(4)
C9-C8-C13	119.4(4)	C20-C19-C18	120.8(4)
C9-C8-P1	122.1(3)	C20-C19-H19A	119.6
C13-C8-P1	118.4(3)	C18-C19-H19A	119.6

C19-C20-C15	120.5(4)	N100-C101-H10C	109.5
C19-C20-H20A	119.8	N100-C101-H10D	109.5
C15-C20-H20A	119.8	H10C-C101-H10D	109.5
O6-C21-O5	127.8(4)	N100-C101-H10E	109.5
O6-C21-C18	115.0(4)	H10C-C101-H10E	109.5
O5-C21-C18	117.2(4)	H10D-C101-H10E	109.5
C102-N100-C101	142.8(19)	N100-C102-H10F	109.5
C102-N100-C100	113.8(15)	N100-C102-H10G	109.5
C101-N100-C100	102.4(15)	H10F-C102-H10G	109.5
O100-C100-N100	124.8(18)	N100-C102-H10H	109.5
O100-C100-H10B	117.6	H10F-C102-H10H	109.5
N100-C100-H10B	117.6	H10G-C102-H10H	109.5

Symmetry transformations used to generate equivalent atoms:

#1 -x+2,-y,-z #2 -x+1,y-1/2,-z-1/2 #3 x,-y-1/2,z+1/2
#4 -x+1,-y,-z #5 -x+1,y+1/2,-z-1/2 #6 x-1,y,z
#7 x,-y-1/2,z-1/2 #8 x+1,y,z

Table A1.4: Anisotropic displacement parameters ($Å^2 x\ 10^3$) for PCM-11. The anisotropic displacement factor exponent takes the form: $-2\pi^2[h^2 a^{*2} U^{11} + ... + 2\ h\ k\ a^*\ b^*\ U^{12}]$.

	U^{11}	U^{22}	U^{33}	U^{23}	U^{13}	U^{12}
P1	25(1)	26(1)	23(1)	0(1)	3(1)	-1(1)
Mg1	30(1)	27(1)	22(1)	-1(1)	4(1)	1(1)
Mg2	28(1)	28(1)	31(1)	-4(1)	3(1)	0(1)
O1P	34(2)	30(2)	28(1)	0(1)	9(1)	0(1)
O1	49(2)	34(2)	29(2)	-5(1)	7(1)	-9(1)
O2	55(2)	34(2)	26(2)	-5(1)	5(1)	-3(2)
O3	30(2)	42(2)	34(2)	-12(1)	0(1)	0(1)
O4	27(2)	45(2)	55(2)	-11(2)	2(2)	2(1)

O5	43(2)	43(2)	52(2)	21(2)	0(2)	-3(2)
O6	36(2)	31(2)	35(2)	6(1)	4(1)	4(1)
O7	26(1)	29(2)	25(1)	-1(1)	5(1)	0(1)
O8	54(2)	50(2)	48(2)	-7(2)	7(2)	20(2)
O9	53(2)	40(2)	60(2)	4(2)	10(2)	-1(2)
C1	29(2)	30(2)	26(2)	-2(2)	5(2)	-3(2)
C2	70(3)	40(3)	30(2)	-3(2)	18(2)	-9(2)
C3	74(3)	32(3)	35(2)	-8(2)	14(2)	-15(2)
C4	30(2)	29(2)	28(2)	-4(2)	6(2)	-2(2)
C5	78(4)	44(3)	30(2)	-4(2)	18(2)	-14(3)
C6	82(4)	37(3)	33(2)	-4(2)	21(2)	-25(3)
C7	28(2)	38(3)	28(2)	-3(2)	4(2)	-1(2)
C8	23(2)	29(2)	23(2)	1(2)	2(2)	3(2)
C9	37(3)	49(3)	58(3)	-25(3)	1(2)	-4(2)
C10	32(2)	56(3)	62(3)	-23(3)	6(2)	4(2)
C11	28(2)	35(3)	30(2)	2(2)	-1(2)	1(2)
C12	32(2)	45(3)	38(2)	-20(2)	2(2)	-3(2)
C13	34(2)	41(3)	44(3)	-12(2)	5(2)	8(2)
C14	25(2)	41(3)	29(2)	0(2)	3(2)	1(2)
C15	31(2)	27(2)	30(2)	1(2)	2(2)	4(2)
C16	29(2)	48(3)	62(3)	23(3)	-3(2)	-6(2)
C17	36(2)	44(3)	57(3)	20(2)	5(2)	-8(2)
C18	35(2)	33(3)	30(2)	6(2)	4(2)	4(2)
C19	32(2)	46(3)	46(3)	19(2)	9(2)	7(2)
C20	29(2)	43(3)	53(3)	17(2)	10(2)	1(2)
C21	36(3)	37(3)	32(2)	1(2)	8(2)	6(2)

Table A1.5: Hydrogen coordinates (x 10^4) and isotropic displacement parameters ($Å^2$ x 10^3) for PCM-11.

	x	y	z	U(eq)
H7	5671	262	-729	32
H2A	6752	-2322	-1931	55
H3A	6375	-3452	-2786	56
H5A	7136	-1543	-4034	60
H6A	7532	-402	-3183	59
H9A	9193	-1314	-1956	60
H10A	10923	-1162	-1423	61
H12A	10298	1057	-355	48
H13A	8557	893	-861	48
H16A	8212	1333	-2319	59
H17A	7482	2613	-2999	56
H19A	4678	1606	-3035	50
H20A	5401	392	-2307	50
H10B	8378	-2175	878	185
H10C	10844	-3363	2220	309
H10D	10737	-3258	1437	309
H10E	9944	-3906	1697	309
H10F	9924	-1883	2579	150
H10G	8761	-2002	2164	150
H10H	9477	-1230	1935	150

Table A1.6: Crystal data and structure refinement for iPCM-1.

Identification code	sh13009fs	
Empirical formula	C34 H32 Cl0 N2 O11.25 P	
Formula weight	679.59	
Temperature	393(2) K	
Wavelength	0.71073 Å	
Crystal system	?	
Space group	?	
Unit cell dimensions	a = 22.753(3) Å	α= 90°.
	b = 15.3561(19) Å	β= 108.320(9)°.
	c = 24.772(3) Å	γ = 90°.
Volume	8216.5(17) $Å^3$	
Z	8	
Density (calculated)	1.099 Mg/m^3	
Absorption coefficient	0.119 mm^{-1}	
F(000)	2840	
Crystal size	0.10 x 0.10 x 0.10 mm^3	
Theta range for data collection	3.55 to 25.00°.	
Index ranges	-27<=h<=27, -18<=k<=18, -29<=l<=29	
Reflections collected	39712	
Independent reflections	7198 [R(int) = 0.0753]	
Completeness to theta = 25.00°	99.5 %	
Max. and min. transmission	0.9882 and 0.9882	
Refinement method	Full-matrix least-squares on F^2	
Data / restraints / parameters	7198 / 14 / 393	
Goodness-of-fit on F^2	1.341	
Final R indices [I>2sigma(I)]	R1 = 0.1573, wR2 = 0.3827	
R indices (all data)	R1 = 0.2201, wR2 = 0.4227	
Largest diff. peak and hole	1.013 and -0.395 $e.Å^{-3}$	

Table A1.7: Atomic coordinates (x 10^4) and equivalent isotropic displacement parameters ($Å^2$x 10^3) for iPCM-1. U(eq) is defined as one third of the trace of the orthogonalized U^{ij} tensor.

	x	y	z	U(eq)
P1	454(1)	5719(1)	2282(1)	53(1)
C1	-179(3)	6463(4)	2122(3)	61(2)
C2	-576(4)	6556(4)	1569(3)	70(2)
C3	-1089(4)	7069(6)	1475(4)	99(3)
C4	-1215(4)	7505(5)	1922(5)	93(3)
C5	-820(5)	7392(5)	2472(5)	95(3)
C6	-307(4)	6881(5)	2562(3)	80(2)
C7	-1799(7)	8075(8)	1813(11)	150(6)
C8	339(3)	4980(4)	2809(2)	56(2)
C9	-222(3)	4579(4)	2700(3)	64(2)
C10	-312(3)	4010(4)	3092(3)	61(2)
C11	135(3)	3836(3)	3589(2)	55(2)
C12	693(3)	4254(4)	3696(3)	65(2)
C13	804(3)	4818(4)	3314(3)	63(2)
C14	34(4)	3172(4)	4011(3)	71(2)
C15	1204(3)	6244(4)	2568(2)	61(2)
C16	1259(3)	7099(4)	2753(3)	64(2)
C17	1844(4)	7432(4)	3000(3)	68(2)
C18	2359(3)	6933(4)	3068(3)	57(2)
C19	2290(4)	6066(5)	2873(3)	72(2)
C20	1722(3)	5740(4)	2628(3)	66(2)
C21	2991(4)	7294(5)	3359(3)	72(2)
C22	465(3)	5139(3)	1650(2)	53(2)
C23	665(4)	5554(4)	1259(3)	73(2)
C24	686(4)	5097(4)	780(3)	77(2)
C25	521(3)	4240(4)	705(3)	64(2)
C26	305(4)	3843(5)	1106(3)	89(2)

C27	278(4)	4277(4)	1575(3)	78(2)
C28	575(4)	3748(6)	200(3)	82(2)
O1	-2127(5)	8125(7)	1316(7)	204(5)
O2	-1880(5)	8440(6)	2221(6)	189(5)
O3	-464(2)	2781(3)	3896(2)	86(2)
O4	491(3)	3071(3)	4449(2)	92(2)
O5	3067(2)	8046(3)	3517(2)	93(2)
O6	3429(3)	6722(4)	3418(3)	87(2)
O7	796(3)	4059(4)	-132(2)	108(2)
O8	366(4)	2953(4)	171(3)	122(2)
O100	-3068(7)	9057(11)	1789(7)	293(7)
N100	-3909(6)	9355(8)	949(5)	184(5)
C100	-3258(8)	9277(16)	1187(11)	304(12)
C101	-4101(10)	9919(13)	479(9)	288(11)
C102	-4289(9)	8868(13)	1117(9)	269(10)
O110	1506(6)	9559(8)	3367(6)	229(5)
N110	2382(6)	10404(9)	3480(6)	200(5)
C110	1855(8)	10090(12)	3133(8)	235(8)
C111	2619(11)	10064(14)	4042(8)	310(12)
C112	2728(8)	11071(11)	3373(7)	224(7)
O1W	2500	2660(20)	5000	228(13)
O2W	749(6)	7018(7)	3899(5)	209(4)

Table A1.8: Bond lengths [Å] and angles [°] for iPCM-1.

P1-C1	1.782(7)	C15-C16	1.382(9)
P1-C22	1.808(6)	C16-C17	1.378(9)
P1-C8	1.810(6)	C16-H16A	0.9300
P1-C15	1.819(7)	C17-C18	1.365(9)
C1-C6	1.373(9)	C17-H17A	0.9300
C1-C2	1.390(9)	C18-C19	1.408(9)
C2-C3	1.367(12)	C18-C21	1.499(10)
C2-H2A	0.9300	C19-C20	1.340(9)
C3-C4	1.399(12)	C19-H19A	0.9300
C3-H3A	0.9300	C20-H20A	0.9300
C4-C5	1.387(12)	C21-O5	1.214(8)
C4-C7	1.542(15)	C21-O6	1.302(9)
C5-C6	1.366(11)	C22-C23	1.352(9)
C5-H5A	0.9300	C22-C27	1.386(8)
C6-H6A	0.9300	C23-C24	1.394(9)
C7-O2	1.22(2)	C23-H23A	0.9300
C7-O1	1.225(19)	C24-C25	1.365(9)
C8-C9	1.365(9)	C24-H24A	0.9300
C8-C13	1.384(8)	C25-C26	1.380(10)
C9-C10	1.369(8)	C25-C28	1.499(10)
C9-H9A	0.9300	C26-C27	1.357(9)
C10-C11	1.354(8)	C26-H26A	0.9300
C10-H10A	0.9300	C27-H27A	0.9300
C11-C12	1.372(9)	C28-O7	1.190(9)
C11-C14	1.530(9)	C28-O8	1.303(10)
C12-C13	1.365(9)	O4-H4*	1.50(16)
C12-H12A	0.9300	O6-H6*	0.7(3)
C13-H13A	0.9300	O100-C100	1.46(2)
C14-O3	1.234(9)	N100-C102	1.307(14)
C14-O4	1.253(9)	N100-C101	1.406(14)
C15-C20	1.379(9)	N100-C100	1.417(16)

C100-H10B	0.9300	C5-C4-C3	119.1(8)
C101-H10C	0.9600	C5-C4-C7	120.0(12)
C101-H10D	0.9600	C3-C4-C7	120.8(12)
C101-H10E	0.9600	C6-C5-C4	119.3(8)
C102-H10F	0.9600	C6-C5-H5A	120.4
C102-H10G	0.9600	C4-C5-H5A	120.3
C102-H10H	0.9600	C5-C6-C1	121.5(8)
O110-C110	1.386(18)	C5-C6-H6A	119.3
N110-C110	1.327(15)	C1-C6-H6A	119.2
N110-C112	1.367(13)	O2-C7-O1	126.9(15)
N110-C111	1.426(16)	O2-C7-C4	117.5(17)
C110-H11A	0.9300	O1-C7-C4	115.6(17)
C111-H11B	0.9600	C9-C8-C13	120.0(6)
C111-H11C	0.9600	C9-C8-P1	118.5(5)
C111-H11D	0.9600	C13-C8-P1	121.5(5)
C112-H11E	0.9600	C8-C9-C10	119.1(6)
C112-H11F	0.9600	C8-C9-H9A	120.4
C112-H11G	0.9600	C10-C9-H9A	120.5
C1-P1-C22	110.7(3)	C11-C10-C9	122.3(6)
C1-P1-C8	105.8(3)	C11-C10-H10A	118.9
C22-P1-C8	111.1(3)	C9-C10-H10A	118.9
C1-P1-C15	113.4(3)	C10-C11-C12	118.0(6)
C22-P1-C15	106.8(3)	C10-C11-C14	121.5(6)
C8-P1-C15	109.1(3)	C12-C11-C14	120.4(6)
C6-C1-C2	120.0(7)	C13-C12-C11	121.6(6)
C6-C1-P1	118.8(5)	C13-C12-H12A	119.2
C2-C1-P1	120.9(5)	C11-C12-H12A	119.2
C3-C2-C1	118.9(7)	C12-C13-C8	119.1(6)
C3-C2-H2A	120.6	C12-C13-H13A	120.5
C1-C2-H2A	120.6	C8-C13-H13A	120.5
C2-C3-C4	121.2(8)	O3-C14-O4	126.2(7)
C2-C3-H3A	119.4	O3-C14-C11	119.4(7)
C4-C3-H3A	119.4	O4-C14-C11	114.4(7)

C20-C15-C16	120.8(6)	C27-C26-C25	121.5(6)
C20-C15-P1	117.3(5)	C27-C26-H26A	119.3
C16-C15-P1	121.8(5)	C25-C26-H26A	119.2
C17-C16-C15	118.3(6)	C26-C27-C22	119.2(7)
C17-C16-H16A	120.9	C26-C27-H27A	120.4
C15-C16-H16A	120.9	C22-C27-H27A	120.4
C18-C17-C16	121.3(6)	O7-C28-O8	124.3(7)
C18-C17-H17A	119.4	O7-C28-C25	122.5(8)
C16-C17-H17A	119.4	O8-C28-C25	113.2(8)
C17-C18-C19	119.3(6)	C14-O4-H4*	118(6)
C17-C18-C21	120.6(6)	C21-O6-H6*	142(10)
C19-C18-C21	120.1(7)	C102-N100-C101	123.6(13)
C20-C19-C18	119.8(7)	C102-N100-C100	121.9(13)
C20-C19-H19A	120.1	C101-N100-C100	114.1(13)
C18-C19-H19A	120.1	N100-C100-O100	112.4(17)
C19-C20-C15	120.6(6)	N100-C100-H10B	123.8
C19-C20-H20A	119.7	O100-C100-H10B	123.8
C15-C20-H20A	119.7	N100-C101-H10C	109.5
O5-C21-O6	125.4(7)	N100-C101-H10D	109.5
O5-C21-C18	121.6(7)	H10C-C101-H10D	109.5
O6-C21-C18	112.9(6)	N100-C101-H10E	109.4
C23-C22-C27	120.9(6)	H10C-C101-H10E	109.5
C23-C22-P1	119.1(4)	H10D-C101-H10E	109.5
C27-C22-P1	120.0(5)	N100-C102-H10F	109.5
C22-C23-C24	118.8(6)	N100-C102-H10G	109.4
C22-C23-H23A	120.6	H10F-C102-H10G	109.5
C24-C23-H23A	120.6	N100-C102-H10H	109.5
C25-C24-C23	121.3(6)	H10F-C102-H10H	109.5
C25-C24-H24A	119.3	H10G-C102-H10H	109.5
C23-C24-H24A	119.3	C110-N110-C112	127.3(14)
C24-C25-C26	118.2(6)	C110-N110-C111	119.1(13)
C24-C25-C28	120.6(7)	C112-N110-C111	113.6(12)
C26-C25-C28	121.2(6)	N110-C110-O110	117.7(15)

N110-C110-H11A	121.2	H11C-C111-H11D	109.5
O110-C110-H11A	121.2	N110-C112-H11E	109.4
N110-C111-H11B	109.4	N110-C112-H11F	109.4
N110-C111-H11C	109.6	H11E-C112-H11F	109.5
H11B-C111-H11C	109.5	N110-C112-H11G	109.6
N110-C111-H11D	109.4	H11E-C112-H11G	109.5
H11B-C111-H11D	109.5	H11F-C112-H11G	109.5

Symmetry transformations used to generate equivalent atoms:

Table A1.9: Anisotropic displacement parameters ($Å^2 x\ 10^3$) for iPCM-1. The anisotropic displacement factor exponent takes the form: $-2\pi^2[h^2\ a^{*2}U^{11} + ... + 2\ h\ k\ a^*\ b^*\ U^{12}]$.

	U^{11}	U^{22}	U^{33}	U^{23}	U^{13}	U^{12}
P1	67(1)	45(1)	45(1)	-1(1)	16(1)	-7(1)
C1	70(5)	49(3)	64(4)	-1(3)	20(4)	-5(3)
C2	75(5)	64(4)	65(4)	11(3)	12(4)	4(4)
C3	91(7)	93(6)	101(7)	20(5)	12(5)	-11(5)
C4	78(6)	76(5)	132(8)	27(5)	43(6)	14(4)
C5	109(7)	69(5)	132(8)	-5(5)	74(7)	2(5)
C6	95(6)	74(4)	70(5)	-4(4)	24(4)	11(4)
C7	98(10)	103(8)	250(20)	32(11)	54(11)	20(7)
C8	70(4)	49(3)	51(4)	-5(3)	22(3)	-7(3)
C9	67(5)	67(4)	55(4)	12(3)	13(3)	-14(3)
C10	55(4)	64(4)	60(4)	4(3)	13(3)	-14(3)
C11	69(4)	45(3)	50(4)	1(3)	19(3)	1(3)
C12	68(5)	63(4)	51(4)	7(3)	1(3)	-4(4)
C13	65(4)	56(3)	58(4)	9(3)	4(3)	-10(3)
C14	78(6)	63(4)	72(5)	14(3)	24(4)	22(4)

C15	76(5)	58(4)	50(4)	5(3)	21(3)	-8(3)
C16	65(5)	53(4)	66(4)	-2(3)	12(3)	-3(3)
C17	92(6)	49(3)	67(4)	-12(3)	28(4)	-12(4)
C18	65(4)	54(3)	55(4)	-6(3)	22(3)	-5(3)
C19	73(5)	75(4)	70(4)	-8(4)	28(4)	2(4)
C20	55(4)	58(4)	88(5)	-22(3)	25(4)	-10(3)
C21	84(6)	81(5)	55(4)	1(4)	31(4)	-11(5)
C22	67(4)	49(3)	37(3)	-4(3)	9(3)	0(3)
C23	113(6)	56(4)	58(4)	-3(3)	37(4)	-5(4)
C24	120(6)	65(4)	53(4)	-1(3)	38(4)	-11(4)
C25	80(5)	61(4)	47(4)	-9(3)	14(3)	3(3)
C26	126(7)	65(4)	83(5)	-23(4)	44(5)	-28(4)
C27	121(7)	56(4)	67(4)	-13(3)	42(4)	-21(4)
C28	96(6)	87(6)	61(5)	-10(4)	22(4)	13(5)
O1	118(8)	192(9)	267(14)	12(9)	9(8)	52(7)
O2	211(11)	140(7)	266(13)	41(7)	149(10)	73(7)
O3	62(3)	87(3)	111(4)	36(3)	31(3)	2(3)
O4	99(4)	86(3)	80(3)	36(3)	12(3)	-4(3)
O5	79(4)	74(3)	115(4)	-26(3)	15(3)	-16(3)
O6	68(4)	90(4)	104(4)	-18(3)	27(3)	-8(3)
O7	159(6)	100(4)	70(4)	-14(3)	45(4)	4(4)
O8	184(7)	94(4)	109(5)	-51(4)	76(5)	-42(4)

Table A1.10: Hydrogen coordinates (x 10^4) and isotropic displacement parameters ($Å^2$ x 10^3) for iPCM-1.

	x	y	z	U(eq)
H2A	-493	6274	1269	85
H3A	-1360	7128	1107	119

H5A	-903	7662	2776	114
H6A	-38	6814	2930	96
H9A	-539	4691	2364	77
H10A	-693	3733	3014	73
H12A	1003	4149	4038	78
H13A	1187	5090	3392	76
H16A	910	7440	2711	76
H17A	1889	8007	3124	82
H19A	2637	5721	2915	86
H20A	1677	5169	2497	80
H23A	787	6135	1310	88
H24A	815	5382	505	92
H26A	176	3266	1053	107
H27A	135	3998	1843	94
H10B	-2983	9356	981	365
H10C	-4545	9931	336	433
H10D	-3940	9717	186	433
H10E	-3948	10495	594	433
H10F	-4707	8980	883	404
H10G	-4248	9000	1506	404
H10H	-4192	8265	1086	404
H11A	1724	10222	2747	283
H11B	3015	10322	4231	465
H11C	2664	9444	4025	465
H11D	2338	10198	4249	465
H11E	2549	11263	2987	336
H11F	3143	10872	3429	336
H11G	2735	11546	3627	336
H6*	3730(120)	6680(150)	3420(110)	440(140)
H4*	380(70)	2730(100)	4980(70)	240(60)

Table A1.11: Crystal data and structure refinement for Ho-PCM-25.

Identification code	sh13014	
Empirical formula	C20.50 H0 Ho N O6 P	
Formula weight	552.11	
Temperature	100(2) K	
Wavelength	0.71073 Å	
Crystal system	?	
Space group	?	
Unit cell dimensions	a = 24.540(7) Å	α= 90°.
	b = 14.812(4) Å	β= 111.61(2)°.
	c = 26.274(6) Å	γ = 90°.
Volume	8879(4) $Å^3$	
Z	16	
Density (calculated)	1.652 Mg/m^3	
Absorption coefficient	3.669 mm^{-1}	
F(000)	4160	
Crystal size	0.10 x 0.10 x 0.10 mm^3	
Theta range for data collection	3.57 to 25.00°.	
Index ranges	-29<=h<=28, -17<=k<=17, -31<=l<=31	
Reflections collected	42730	
Independent reflections	7790 [R(int) = 0.0603]	
Completeness to theta = 25.00°	99.7 %	
Max. and min. transmission	0.7105 and 0.7105	
Refinement method	Full-matrix least-squares on F^2	
Data / restraints / parameters	7790 / 0 / 425	
Goodness-of-fit on F^2	1.008	
Final R indices [I>2sigma(I)]	R1 = 0.0752, wR2 = 0.2320	
R indices (all data)	R1 = 0.0789, wR2 = 0.2366	
Largest diff. peak and hole	1.909 and -1.008 $e.Å^{-3}$	

Table A1.12: Atomic coordinates (x 10^4) and equivalent isotropic displacement parameters ($Å^2$x 10^3) for Ho-PCM-25. U(eq) is defined as one third of the trace of the orthogonalized U^{ij} tensor.

	x	y	z	U(eq)
Ho1	1976(1)	1707(1)	1284(1)	39(1)
P1	4569(1)	6036(2)	2772(1)	41(1)
O3	6307(3)	6262(5)	5428(3)	49(2)
O4W	2520(3)	1221(4)	2184(3)	43(1)
O6	2821(3)	2556(5)	1600(3)	51(2)
O8	6058(3)	8136(5)	1399(3)	48(2)
O7	6758(3)	7210(4)	1904(2)	41(1)
O3W	2570(3)	1185(6)	827(3)	70(2)
O2W	1747(4)	212(5)	1381(3)	66(2)
O4	5987(4)	4837(5)	5414(3)	71(2)
O5	3369(3)	2520(5)	1083(3)	61(2)
O1	2272(4)	8861(6)	1934(4)	86(3)
O2	2842(4)	9644(5)	2654(3)	71(2)
C11	5649(4)	5663(7)	4591(4)	46(2)
C19	3436(4)	3972(7)	2209(4)	46(2)
C20	3740(4)	4699(6)	2512(4)	48(2)
C27	4904(4)	7236(6)	2135(4)	47(2)
C15	4228(4)	5038(6)	2414(4)	44(2)
C8	4991(4)	5847(7)	3483(4)	45(2)
C22	5058(4)	6464(7)	2471(4)	47(2)
C25	5817(4)	7132(6)	2002(3)	40(2)
C1	3998(4)	6843(6)	2690(4)	44(2)
C18	3610(4)	3582(7)	1811(4)	42(2)
C26	5298(4)	7558(7)	1908(4)	49(2)
C14	6004(4)	5573(8)	5186(4)	53(2)
C16	4409(4)	4629(6)	2026(4)	44(2)
C13	4870(4)	5147(7)	3775(4)	49(2)

C5	3664(6)	8221(7)	2951(5)	67(3)
C21	3245(4)	2825(6)	1475(4)	42(2)
C28	6238(4)	7506(6)	1754(3)	39(2)
C17	4091(4)	3890(7)	1724(4)	47(2)
C12	5205(4)	5048(7)	4331(4)	52(2)
C24	5967(4)	6354(7)	2316(4)	50(2)
C10	5764(4)	6367(8)	4294(4)	53(2)
C3	3099(5)	7503(8)	2129(5)	64(3)
C6	4087(5)	7547(8)	3067(4)	61(3)
C23	5588(4)	6035(7)	2558(4)	49(2)
C4	3173(5)	8196(6)	2483(5)	52(2)
C9	5441(4)	6457(8)	3744(4)	54(2)
C2	3505(5)	6832(7)	2220(5)	59(3)
C7	2728(6)	8966(8)	2352(5)	65(3)
O1W	1712(4)	3064(5)	788(3)	63(2)
O100	2715(6)	95(10)	76(7)	68(4)
N100	3322(12)	-1099(18)	602(11)	94(7)
C100	3013(12)	-673(19)	123(12)	79(7)
C101	3730(20)	-1900(30)	770(20)	133(14)
C102	3462(15)	-770(20)	1137(14)	100(9)
O50	3095(6)	10197(11)	3731(6)	138(5)
O51	1778(10)	7829(16)	946(9)	100(6)
O52	3431(11)	3595(18)	240(11)	112(7)
O53	4365(11)	-1924(16)	-486(10)	113(7)
O54	60(15)	2550(20)	425(14)	154(11)
O55	2416(16)	6080(30)	821(15)	177(13)

Table A1.13: Bond lengths [Å] and angles [°] for Ho-PCM-25.

Ho1-O6	2.303(6)	C20-H20A	0.9500
Ho1-O2W	2.321(7)	C27-C26	1.395(12)
Ho1-O3W	2.336(7)	C27-C22	1.408(14)
Ho1-O3#1	2.339(6)	C27-H27A	0.9500
Ho1-O4W	2.359(6)	C15-C16	1.390(13)
Ho1-O1W	2.354(8)	C8-C13	1.385(13)
Ho1-O8#2	2.392(6)	C8-C9	1.395(13)
Ho1-O7#2	2.480(5)	C22-C23	1.389(14)
Ho1-C28#2	2.794(9)	C25-C26	1.359(13)
P1-C15	1.786(9)	C25-C24	1.386(14)
P1-C22	1.779(9)	C25-C28	1.515(12)
P1-C8	1.796(9)	C1-C2	1.375(14)
P1-C1	1.793(10)	C1-C6	1.400(14)
O3-C14	1.285(12)	C18-C17	1.362(13)
O3-Ho1#3	2.339(6)	C18-C21	1.501(13)
O6-C21	1.267(10)	C26-H26A	0.9500
O8-C28	1.277(10)	C16-C17	1.407(13)
O8-Ho1#4	2.392(6)	C16-H16A	0.9500
O7-C28	1.268(10)	C13-C12	1.394(14)
O7-Ho1#4	2.480(5)	C13-H13A	0.9500
O4-C14	1.252(13)	C5-C4	1.370(16)
O5-C21	1.257(11)	C5-C6	1.389(16)
O1-C7	1.255(15)	C5-H5A	0.9500
O2-C7	1.247(14)	C28-Ho1#4	2.794(9)
C11-C12	1.392(13)	C17-H17A	0.9500
C11-C10	1.393(14)	C12-H12A	0.9500
C11-C14	1.489(13)	C24-C23	1.387(13)
C19-C20	1.382(13)	C24-H24A	0.9500
C19-C18	1.391(13)	C10-C9	1.375(14)
C19-H19A	0.9500	C10-H10A	0.9500
C20-C15	1.408(13)	C3-C4	1.351(15)

C3-C2	1.365(15)	O4W-Ho1-O1W	139.0(2)
C3-H3A	0.9500	O6-Ho1-O8#2	131.8(2)
C6-H6A	0.9500	O2W-Ho1-O8#2	78.6(3)
C23-H23A	0.9500	O3W-Ho1-O8#2	153.2(2)
C4-C7	1.528(15)	O3#1-Ho1-O8#2	77.9(2)
C9-H9A	0.9500	O4W-Ho1-O8#2	96.6(2)
C2-H2A	0.9500	O1W-Ho1-O8#2	84.7(3)
O100-O100#5	0.98(3)	O6-Ho1-O7#2	78.1(2)
O100-C100	1.33(3)	O2W-Ho1-O7#2	115.2(3)
N100-C100	1.36(4)	O3W-Ho1-O7#2	151.4(2)
N100-C102	1.41(4)	O3#1-Ho1-O7#2	124.7(2)
N100-C101	1.50(5)	O4W-Ho1-O7#2	73.6(2)
C100-H10B	0.9500	O1W-Ho1-O7#2	74.3(2)
C101-H10F	0.9800	O8#2-Ho1-O7#2	54.1(2)
C101-H10G	0.9800	O6-Ho1-C28#2	104.9(2)
C101-H10H	0.9800	O2W-Ho1-C28#2	97.3(3)
C102-H10C	0.9800	O3W-Ho1-C28#2	173.7(3)
C102-H10D	0.9800	O3#1-Ho1-C28#2	101.7(2)
C102-H10E	0.9800	O4W-Ho1-C28#2	84.5(2)
O6-Ho1-O2W	134.7(3)	O1W-Ho1-C28#2	78.3(3)
O6-Ho1-O3W	73.5(2)	O8#2-Ho1-C28#2	27.1(2)
O2W-Ho1-O3W	87.9(3)	O7#2-Ho1-C28#2	27.0(2)
O6-Ho1-O3#1	136.0(2)	C15-P1-C22	108.9(4)
O2W-Ho1-O3#1	74.0(2)	C15-P1-C8	113.5(4)
O3W-Ho1-O3#1	76.2(3)	C22-P1-C8	107.0(4)
O6-Ho1-O4W	72.7(2)	C15-P1-C1	107.2(4)
O2W-Ho1-O4W	70.8(2)	C22-P1-C1	109.6(5)
O3W-Ho1-O4W	100.6(3)	C8-P1-C1	110.8(5)
O3#1-Ho1-O4W	144.7(2)	C14-O3-Ho1#3	140.6(6)
O6-Ho1-O1W	76.2(3)	C21-O6-Ho1	142.7(6)
O2W-Ho1-O1W	147.9(3)	C28-O8-Ho1#4	94.3(5)
O3W-Ho1-O1W	95.4(3)	C28-O7-Ho1#4	90.4(5)
O3#1-Ho1-O1W	75.8(3)	C12-C11-C10	119.8(9)

C12-C11-C14	120.5(9)	O4-C14-C11	118.1(9)
C10-C11-C14	119.7(8)	O3-C14-C11	117.1(9)
C20-C19-C18	120.5(8)	C15-C16-C17	119.5(8)
C20-C19-H19A	119.8	C15-C16-H16A	120.3
C18-C19-H19A	119.7	C17-C16-H16A	120.3
C19-C20-C15	119.2(8)	C8-C13-C12	119.6(9)
C19-C20-H20A	120.4	C8-C13-H13A	120.2
C15-C20-H20A	120.4	C12-C13-H13A	120.2
C26-C27-C22	118.5(9)	C4-C5-C6	121.2(10)
C26-C27-H27A	120.7	C4-C5-H5A	119.4
C22-C27-H27A	120.8	C6-C5-H5A	119.4
C16-C15-C20	120.1(8)	O5-C21-O6	124.6(8)
C16-C15-P1	122.2(7)	O5-C21-C18	118.6(8)
C20-C15-P1	117.7(7)	O6-C21-C18	116.8(8)
C13-C8-C9	120.4(9)	O7-C28-O8	121.2(8)
C13-C8-P1	122.3(7)	O7-C28-C25	120.5(8)
C9-C8-P1	117.3(7)	O8-C28-C25	118.2(8)
C23-C22-C27	119.6(8)	O7-C28-Ho1#4	62.6(4)
C23-C22-P1	120.6(8)	O8-C28-Ho1#4	58.6(4)
C27-C22-P1	119.8(8)	C25-C28-Ho1#4	176.5(6)
C26-C25-C24	121.3(8)	C18-C17-C16	120.1(9)
C26-C25-C28	119.6(8)	C18-C17-H17A	120.0
C24-C25-C28	119.0(8)	C16-C17-H17A	120.0
C2-C1-C6	120.1(10)	C11-C12-C13	119.9(9)
C2-C1-P1	119.3(8)	C11-C12-H12A	120.0
C6-C1-P1	120.1(8)	C13-C12-H12A	120.1
C17-C18-C19	120.7(9)	C23-C24-C25	118.6(9)
C17-C18-C21	121.1(8)	C23-C24-H24A	120.7
C19-C18-C21	118.2(8)	C25-C24-H24A	120.7
C25-C26-C27	120.9(9)	C9-C10-C11	120.4(9)
C25-C26-H26A	119.5	C9-C10-H10A	119.8
C27-C26-H26A	119.6	C11-C10-H10A	119.8
O4-C14-O3	124.8(9)	C4-C3-C2	122.0(11)

C4-C3-H3A	119.0	O100#5-O100-C100	120.6(14)
C2-C3-H3A	119.0	C100-N100-C102	128(3)
C5-C6-C1	118.1(10)	C100-N100-C101	136(3)
C5-C6-H6A	120.9	C102-N100-C101	95(3)
C1-C6-H6A	120.9	O100-C100-N100	126(3)
C24-C23-C22	121.0(9)	O100-C100-H10B	117.2
C24-C23-H23A	119.5	N100-C100-H10B	117.2
C22-C23-H23A	119.5	N100-C101-H10F	109.4
C3-C4-C5	119.2(10)	N100-C101-H10G	109.5
C3-C4-C7	120.5(11)	H10F-C101-H10G	109.5
C5-C4-C7	120.2(10)	N100-C101-H10H	109.5
C10-C9-C8	119.9(9)	H10F-C101-H10H	109.5
C10-C9-H9A	120.1	H10G-C101-H10H	109.5
C8-C9-H9A	120.1	N100-C102-H10C	109.4
C3-C2-C1	119.5(10)	N100-C102-H10D	109.5
C3-C2-H2A	120.3	H10C-C102-H10D	109.5
C1-C2-H2A	120.3	N100-C102-H10E	109.5
O2-C7-O1	125.2(11)	H10C-C102-H10E	109.5
O2-C7-C4	118.8(11)	H10D-C102-H10E	109.5
O1-C7-C4	115.9(11)		

Symmetry transformations used to generate equivalent atoms:

#1 x-1/2,y-1/2,z-1/2 #2 x-1/2,-y+1,z #3 x+1/2,y+1/2,z+1/2
#4 x+1/2,-y+1,z #5 -x+1/2,y,-z

Table A1.14: Anisotropic displacement parameters ($Å^2 x\ 10^3$) for Ho-PCM-25. The anisotropic displacement factor exponent takes the form: $-2\pi^2[h^2 a^{*2} U^{11} + ... + 2\ h\ k\ a^*\ b^*\ U^{12}]$.

	U^{11}	U^{22}	U^{33}	U^{23}	U^{13}	U^{12}
Ho1	39(1)	46(1)	34(1)	-9(1)	16(1)	-2(1)
P1	37(1)	50(1)	38(1)	-2(1)	15(1)	-9(1)
O3	52(4)	53(4)	38(3)	-7(3)	12(3)	-8(3)
O4W	39(3)	50(4)	40(3)	1(3)	13(3)	3(3)
O6	50(4)	59(4)	52(4)	-18(3)	28(3)	-20(3)
O8	43(4)	63(4)	43(4)	16(3)	20(3)	8(3)
O7	40(3)	46(3)	40(3)	11(3)	18(3)	0(3)
O3W	58(4)	85(6)	80(5)	-38(4)	41(4)	-14(4)
O2W	72(5)	50(4)	58(4)	-7(3)	1(4)	-9(4)
O4	84(5)	65(5)	46(4)	4(3)	5(4)	-33(4)
O5	55(4)	71(5)	66(5)	-22(4)	33(4)	-13(4)
O1	73(6)	60(5)	104(7)	-3(5)	8(5)	2(4)
O2	80(5)	64(5)	66(5)	-4(4)	24(4)	15(4)
C11	40(5)	60(6)	37(5)	-10(4)	12(4)	-10(4)
C19	37(4)	66(6)	41(5)	-2(4)	21(4)	-8(4)
C20	50(5)	48(5)	53(5)	-13(4)	28(5)	-12(4)
C27	44(5)	49(5)	53(5)	5(4)	23(4)	-3(4)
C15	50(5)	48(5)	38(4)	1(4)	20(4)	-4(4)
C8	39(4)	58(6)	37(5)	-1(4)	13(4)	-6(4)
C22	44(5)	63(6)	37(5)	-4(4)	17(4)	-18(4)
C25	43(5)	44(5)	35(4)	0(4)	18(4)	-5(4)
C1	41(5)	51(5)	44(5)	-2(4)	19(4)	-14(4)
C18	43(5)	49(5)	38(5)	1(4)	19(4)	0(4)
C26	44(5)	58(6)	50(5)	7(4)	25(4)	-3(4)
C14	47(5)	68(7)	49(5)	0(5)	23(5)	-5(5)
C16	36(4)	54(5)	46(5)	2(4)	21(4)	-6(4)
C13	43(5)	55(6)	47(5)	-7(4)	15(4)	-13(4)

C5	74(8)	59(7)	56(7)	-15(5)	10(6)	6(5)
C21	34(4)	49(5)	45(5)	-4(4)	16(4)	-2(4)
C28	39(4)	42(5)	34(4)	-4(4)	11(4)	-2(4)
C17	40(5)	62(6)	44(5)	-1(4)	22(4)	4(4)
C12	55(6)	65(6)	40(5)	3(4)	20(4)	-10(5)
C24	46(5)	59(6)	46(5)	6(5)	20(4)	3(5)
C10	41(5)	68(6)	45(5)	-2(5)	9(4)	-23(5)
C3	56(6)	66(7)	63(7)	-10(5)	13(5)	-6(5)
C6	58(6)	68(7)	45(5)	-15(5)	7(5)	8(5)
C23	40(5)	60(6)	50(5)	16(4)	22(4)	-1(4)
C4	58(6)	47(5)	54(6)	-2(4)	24(5)	-3(4)
C9	51(6)	69(6)	39(5)	1(5)	12(4)	-21(5)
C2	50(6)	58(6)	57(7)	-14(5)	4(5)	8(5)
C7	71(8)	61(7)	62(7)	7(6)	23(6)	4(6)
O1W	86(6)	57(4)	45(4)	-3(3)	24(4)	6(4)

Table A1.15: Hydrogen coordinates (x 10^4) and isotropic displacement parameters (Å^2 x 10^3) for Ho-PCM-25.

	x	y	z	U(eq)
H19A	3107	3737	2273	56
H20A	3620	4967	2782	57
H27A	4539	7530	2065	56
H26A	5203	8084	1685	58
H16A	4744	4847	1966	52
H13A	4560	4737	3598	58
H5A	3717	8707	3200	80
H17A	4212	3607	1459	56
H12A	5130	4561	4531	63

H24A	6322	6045	2364	60
H10A	6067	6786	4472	64
H3A	2755	7483	1808	77
H6A	4426	7564	3393	73
H23A	5693	5516	2785	58
H9A	5524	6934	3542	65
H2A	3447	6361	1960	71
H10B	3009	-946	-205	95
H10F	3863	-1969	1172	200
H10G	4065	-1801	666	200
H10H	3517	-2443	596	200
H10C	3675	-1233	1402	150
H10D	3100	-613	1194	150
H10E	3708	-229	1189	150

Table A1.16: Crystal data and structure refinement for BBCB-$PtCl_2$.

Identification code	sh11005	
Empirical formula	C42 H48 Cl2 O12 P2 Pt	
Formula weight	1072.73	
Temperature	180(2) K	
Wavelength	0.71073 Å	
Crystal system	Monoclinic	
Space group	P2(1)/c	
Unit cell dimensions	a = 9.8367(4) Å	α= 90°.
	b = 16.3797(8) Å	β= 90.435(3)°.
	c = 27.5565(14) Å	γ = 90°.
Volume	4439.8(4) $Å^3$	
Z	4	
Density (calculated)	1.605 Mg/m^3	
Absorption coefficient	3.413 mm^{-1}	

F(000)	2152
Crystal size	0.25 x 0.25 x 0.02 mm^3
Theta range for data collection	3.55 to 24.00°.
Index ranges	-11<=h<=11, -18<=k<=18, -31<=l<=31
Reflections collected	28641
Independent reflections	6911 [R(int) = 0.0943]
Completeness to theta = 24.00°	99.0 %
Absorption correction	Semi-empirical from equivalents
Max. and min. transmission	0.937 and 0.645
Refinement method	Full-matrix least-squares on F^2
Data / restraints / parameters	6911 / 0 / 536
Goodness-of-fit on F^2	1.162
Final R indices [I>2sigma(I)]	R1 = 0.0912, wR2 = 0.1951
R indices (all data)	R1 = 0.1248, wR2 = 0.2050
Largest diff. peak and hole	2.767 and -2.373 e.$Å^{-3}$

Table A1.17: Atomic coordinates (x 10^4) and equivalent isotropic displacement parameters ($Å^2$x 10^3) for BBCB-$PtCl_2$. U(eq) is defined as one third of the trace of the orthogonalized U^{ij} tensor.

	x	y	z	U(eq)
Pt1	3457(1)	5676(1)	2826(1)	50(1)
Cl1	2692(5)	6838(3)	3243(2)	71(1)
Cl2	5691(4)	6175(2)	2856(2)	63(1)
P1	1317(4)	5242(2)	2748(2)	48(1)
P2	4099(4)	4520(2)	2489(2)	46(1)
O1	-1438(18)	4475(11)	4921(6)	116(6)
O2	-2320(20)	5715(14)	4804(7)	138(7)
O3	-2829(18)	6764(10)	1015(7)	131(7)
O4	-1500(20)	7820(10)	1079(7)	122(7)

O5	6620(15)	5045(9)	269(5)	89(4)
O6	7997(18)	4020(11)	492(6)	115(6)
O7	7945(14)	2732(7)	4208(5)	80(4)
O8	6828(14)	1615(8)	3980(5)	84(4)
C1	1391(12)	4171(10)	2447(5)	42(4)
C2	2586(18)	3936(9)	2304(6)	53(4)
C3	2675(18)	3243(10)	2020(7)	67(5)
C4	1540(20)	2805(10)	1914(8)	74(6)
C5	300(20)	3077(13)	2091(9)	87(7)
C6	210(20)	3774(11)	2368(7)	77(6)
C7	331(19)	5148(10)	3288(7)	62(5)
C8	640(20)	4560(12)	3610(7)	72(6)
C9	-50(20)	4529(12)	4069(8)	83(6)
C10	-990(20)	5104(12)	4180(8)	70(5)
C11	-1360(30)	5659(15)	3835(9)	109(9)
C12	-700(30)	5686(15)	3409(9)	106(8)
C13	-1620(20)	5117(16)	4653(9)	83(6)
C14	360(16)	5864(9)	2320(6)	51(4)
C15	-992(18)	5646(12)	2201(8)	78(6)
C16	-1733(18)	6109(13)	1855(8)	81(6)
C17	-1108(18)	6713(10)	1614(6)	56(4)
C18	146(17)	6952(11)	1741(7)	64(5)
C19	881(17)	6526(10)	2092(6)	54(4)
C20	-1870(20)	7171(15)	1223(9)	86(7)
C21	5118(16)	4570(8)	1946(6)	49(4)
C22	4762(19)	5122(9)	1600(7)	61(5)
C23	5402(18)	5122(10)	1163(8)	62(5)
C24	6412(19)	4557(11)	1056(7)	61(5)
C25	6779(19)	4005(11)	1405(7)	67(5)
C26	6157(19)	3989(11)	1841(8)	71(6)
C27	7060(20)	4519(12)	593(8)	72(5)
C28	5009(17)	3819(9)	2902(7)	53(4)
C29	6100(20)	4100(10)	3142(8)	81(7)

C30	6760(20)	3649(11)	3476(8)	82(7)
C31	6333(18)	2864(10)	3588(6)	59(5)
C32	5260(20)	2590(11)	3336(8)	79(6)
C33	4640(20)	3049(11)	2989(8)	84(7)
C34	7067(18)	2342(11)	3954(6)	59(5)
O100	2303(15)	5218(9)	572(5)	91(4)
C100	940(30)	4970(20)	680(11)	132(11)
C101	900(40)	4670(20)	1127(11)	154(13)
O110	747(17)	6896(10)	153(6)	102(5)
C110	-110(40)	7430(20)	-132(15)	183(19)
C111	460(80)	7680(30)	-553(17)	390(60)
O120	3870(40)	2575(17)	4726(11)	254(18)
C120	4760(50)	2370(30)	5062(19)	230(30)
C121	4270(60)	2160(30)	5508(19)	270(30)
O130	2970(30)	5700(20)	4276(9)	207(12)
C130	4540(40)	5290(50)	4246(15)	290(40)
C131	3550(60)	4320(60)	4280(30)	490(80)

Table A1.18: Bond lengths [Å] and angles [°] for BBCB-$PtCl_2$.

Pt1-P2	2.205(4)	P2-C21	1.808(18)
Pt1-P1	2.231(4)	P2-C2	1.837(16)
Pt1-Cl2	2.345(4)	P2-C28	1.844(16)
Pt1-Cl1	2.350(4)	O1-C13	1.30(3)
P1-C7	1.79(2)	O1-H1A	0.8400
P1-C14	1.816(15)	O2-C13	1.27(3)
P1-C1	1.943(16)	O3-C20	1.29(2)

O3-H13	0.8400	C16-C17	1.34(3)
O4-C20	1.19(3)	C16-H16	0.9500
O5-C27	1.31(2)	C17-C18	1.34(2)
O5-H5A	0.8400	C17-C20	1.51(3)
O6-C27	1.27(2)	C18-C19	1.39(2)
O7-C34	1.28(2)	C18-H18	0.9500
O7-H7A	0.8400	C19-H19	0.9500
O8-C34	1.22(2)	C21-C22	1.36(2)
C1-C2	1.30(2)	C21-C26	1.43(2)
C1-C6	1.34(2)	C22-C23	1.36(3)
C2-C3	1.38(2)	C22-H22	0.9500
C3-C4	1.36(2)	C23-C24	1.39(2)
C3-H3	0.9500	C23-H23	0.9500
C4-C5	1.38(3)	C24-C25	1.37(2)
C4-H4	0.9500	C24-C27	1.43(3)
C5-C6	1.38(3)	C25-C26	1.35(3)
C5-H5	0.9500	C25-H25	0.9500
C6-H6	0.9500	C26-H26	0.9500
C7-C8	1.34(2)	C28-C33	1.33(2)
C7-C12	1.38(3)	C28-C29	1.34(2)
C8-C9	1.44(3)	C29-C30	1.34(2)
C8-H8	0.9500	C29-H29	0.9500
C9-C10	1.35(3)	C30-C31	1.39(2)
C9-H9	0.9500	C30-H30	0.9500
C10-C11	1.36(3)	C31-C32	1.34(2)
C10-C13	1.45(3)	C31-C34	1.50(2)
C11-C12	1.35(3)	C32-C33	1.36(2)
C11-H11	0.9500	C32-H32	0.9500
C12-H12	0.9500	C33-H33	0.9500
C14-C19	1.36(2)	O100-C100	1.43(3)
C14-C15	1.41(2)	O100-H10	0.8400
C15-C16	1.42(2)	C100-C101	1.33(3)
C15-H15	0.9500	C100-H10A	0.9900

C100-H10B	0.9900	Cl2-Pt1-Cl1	90.26(16)
C101-H10C	0.9800	C7-P1-C14	107.9(8)
C101-H10D	0.9800	C7-P1-C1	107.4(7)
C101-H10E	0.9800	C14-P1-C1	104.5(7)
O110-C110	1.45(3)	C7-P1-Pt1	117.6(6)
O110-H11C	0.8400	C14-P1-Pt1	111.6(6)
C110-C111	1.35(6)	C1-P1-Pt1	106.9(4)
C110-H11A	0.9900	C21-P2-C2	104.4(8)
C110-H11B	0.9900	C21-P2-C28	105.6(8)
C111-H11D	0.9800	C2-P2-C28	103.6(7)
C111-H11E	0.9800	C21-P2-Pt1	118.2(5)
C111-H11F	0.9800	C2-P2-Pt1	109.3(6)
O120-C120	1.31(4)	C28-P2-Pt1	114.4(6)
O120-H12B	0.8400	C13-O1-H1A	109.5
C120-C121	1.37(5)	C20-O3-H13	109.5
C120-H12F	0.9900	C27-O5-H5A	109.5
C120-H12G	0.9900	C34-O7-H7A	109.5
C121-H12C	0.9800	C2-C1-C6	126.0(17)
C121-H12D	0.9800	C2-C1-P1	115.7(10)
C121-H12E	0.9800	C6-C1-P1	118.1(13)
O130-C130	1.70(5)	C1-C2-C3	118.4(15)
O130-H13A	0.8400	C1-C2-P2	119.6(12)
C130-C131	1.86(10)	C3-C2-P2	122.0(14)
C130-H13E	0.9900	C4-C3-C2	120.0(18)
C130-H13F	0.9900	C4-C3-H3	120.0
C131-H13B	0.9800	C2-C3-H3	120.0
C131-H13C	0.9800	C3-C4-C5	118.5(19)
C131-H13D	0.9800	C3-C4-H4	120.8
P2-Pt1-P1	87.62(15)	C5-C4-H4	120.8
P2-Pt1-Cl2	92.43(15)	C6-C5-C4	122(2)
P1-Pt1-Cl2	176.01(17)	C6-C5-H5	119.2
P2-Pt1-Cl1	174.90(18)	C4-C5-H5	119.2
P1-Pt1-Cl1	90.00(16)	C1-C6-C5	116(2)

C1-C6-H6	122.2	C18-C17-C20	119.5(17)
C5-C6-H6	122.2	C16-C17-C20	119.6(17)
C8-C7-C12	117(2)	C17-C18-C19	120.6(17)
C8-C7-P1	119.3(15)	C17-C18-H18	119.7
C12-C7-P1	123.2(16)	C19-C18-H18	119.7
C7-C8-C9	120.0(19)	C14-C19-C18	121.8(16)
C7-C8-H8	120.0	C14-C19-H19	119.1
C9-C8-H8	120.0	C18-C19-H19	119.1
C10-C9-C8	120(2)	O4-C20-O3	122(2)
C10-C9-H9	120.0	O4-C20-C17	122.3(19)
C8-C9-H9	120.0	O3-C20-C17	115(2)
C9-C10-C11	119(2)	C22-C21-C26	118.8(18)
C9-C10-C13	121(2)	C22-C21-P2	118.1(13)
C11-C10-C13	120(2)	C26-C21-P2	122.7(14)
C12-C11-C10	120(2)	C21-C22-C23	120.2(17)
C12-C11-H11	120.0	C21-C22-H22	119.9
C10-C11-H11	120.0	C23-C22-H22	119.9
C11-C12-C7	123(2)	C22-C23-C24	121.6(18)
C11-C12-H12	118.4	C22-C23-H23	119.2
C7-C12-H12	118.4	C24-C23-H23	119.2
O2-C13-O1	121(2)	C25-C24-C23	118.4(18)
O2-C13-C10	123(2)	C25-C24-C27	118.9(18)
O1-C13-C10	116(2)	C23-C24-C27	122.7(19)
C19-C14-C15	117.0(15)	C26-C25-C24	121.3(17)
C19-C14-P1	123.6(13)	C26-C25-H25	119.4
C15-C14-P1	119.4(13)	C24-C25-H25	119.4
C14-C15-C16	119.9(18)	C25-C26-C21	119.8(18)
C14-C15-H15	120.0	C25-C26-H26	120.1
C16-C15-H15	120.0	C21-C26-H26	120.1
C17-C16-C15	119.5(17)	O6-C27-O5	121(2)
C17-C16-H16	120.2	O6-C27-C24	124(2)
C15-C16-H16	120.2	O5-C27-C24	115.8(19)
C18-C17-C16	120.7(16)	C33-C28-C29	117.1(16)

C33-C28-P2	124.6(14)	C110-O110-H11C	109.5
C29-C28-P2	118.3(12)	C111-C110-O110	114(4)
C28-C29-C30	122.1(17)	C111-C110-H11A	108.8
C28-C29-H29	119.0	O110-C110-H11A	108.8
C30-C29-H29	119.0	C111-C110-H11B	108.8
C29-C30-C31	120.9(16)	O110-C110-H11B	108.8
C29-C30-H30	119.5	H11A-C110-H11B	107.7
C31-C30-H30	119.5	C110-C111-H11D	109.5
C32-C31-C30	115.9(16)	C110-C111-H11E	109.5
C32-C31-C34	122.1(17)	H11D-C111-H11E	109.5
C30-C31-C34	122.0(16)	C110-C111-H11F	109.5
C31-C32-C33	121.9(18)	H11D-C111-H11F	109.5
C31-C32-H32	119.0	H11E-C111-H11F	109.5
C33-C32-H32	119.0	C120-O120-H12B	109.5
C28-C33-C32	121.9(18)	O120-C120-C121	117(5)
C28-C33-H33	119.1	O120-C120-H12F	107.9
C32-C33-H33	119.1	C121-C120-H12F	107.9
O8-C34-O7	125.9(17)	O120-C120-H12G	107.9
O8-C34-C31	120.4(17)	C121-C120-H12G	107.9
O7-C34-C31	113.7(16)	H12F-C120-H12G	107.2
C100-O100-H10	109.5	C120-C121-H12C	109.5
C101-C100-O100	109(3)	C120-C121-H12D	109.5
C101-C100-H10A	109.8	H12C-C121-H12D	109.5
O100-C100-H10A	109.8	C120-C121-H12E	109.5
C101-C100-H10B	109.8	H12C-C121-H12E	109.5
O100-C100-H10B	109.8	H12D-C121-H12E	109.5
H10A-C100-H10B	108.3	C130-O130-H13A	109.5
C100-C101-H10C	109.5	O130-C130-C131	82(2)
C100-C101-H10D	109.5	O130-C130-H13E	115.0
H10C-C101-H10D	109.5	C131-C130-H13E	115.0
C100-C101-H10E	109.5	O130-C130-H13F	115.0
H10C-C101-H10E	109.5	C131-C130-H13F	115.0
H10D-C101-H10E	109.5	H13E-C130-H13F	112.0

C130-C131-H13B	109.5	C130-C131-H13D	109.5
C130-C131-H13C	109.5	H13B-C131-H13D	109.5
H13B-C131-H13C	109.5	H13C-C131-H13D	109.5

Symmetry transformations used to generate equivalent atoms:

Table A1.19: Anisotropic displacement parameters ($Å^2 x\ 10^3$) for BBCB-$PtCl_2$. The anisotropic displacement factor exponent takes the form: $-2\pi^2[h^2\ a^{*2}U^{11} + ... + 2\ h\ k\ a^*\ b^*\ U^{12}]$.

	U^{11}	U^{22}	U^{33}	U^{23}	U^{13}	U^{12}
Pt1	46(1)	30(1)	74(1)	-3(1)	-9(1)	0(1)
Cl1	63(3)	48(2)	103(4)	-24(2)	-23(3)	14(2)
Cl2	46(2)	38(2)	104(4)	3(2)	-9(2)	-9(2)
P1	44(2)	36(2)	65(3)	0(2)	-2(2)	2(2)
P2	46(2)	22(2)	71(3)	-1(2)	-2(2)	-1(2)
O1	140(15)	111(14)	98(13)	9(11)	28(11)	0(12)
O2	151(17)	156(19)	108(14)	-6(14)	43(12)	9(16)
O3	122(14)	97(12)	174(18)	24(12)	-93(13)	-1(11)
O4	153(16)	74(11)	139(16)	28(11)	-49(13)	-29(11)
O5	99(11)	86(10)	83(10)	2(9)	7(8)	11(9)
O6	124(14)	121(14)	100(12)	-1(10)	17(10)	54(12)
O7	102(10)	48(7)	89(10)	1(7)	-27(8)	-12(7)
O8	90(10)	56(8)	106(11)	21(8)	-29(8)	-18(7)
C1	13(6)	62(10)	50(9)	7(8)	-11(6)	-19(7)
C2	68(12)	26(8)	63(11)	-10(8)	-16(9)	-10(7)
C3	58(11)	40(10)	102(15)	-8(10)	4(10)	-6(8)
C4	85(15)	32(9)	104(16)	3(10)	-9(12)	-17(10)
C5	65(14)	68(14)	130(20)	-8(14)	-28(13)	1(11)

C6	105(17)	45(11)	80(15)	-10(10)	-11(12)	15(11)
C7	74(12)	44(10)	68(12)	2(9)	-10(10)	-2(9)
C8	87(14)	69(13)	60(12)	12(10)	29(11)	4(10)
C9	92(15)	61(13)	96(17)	13(12)	-7(13)	3(11)
C10	69(13)	58(12)	82(15)	4(11)	-1(11)	-10(10)
C11	140(20)	96(18)	93(18)	-1(15)	31(16)	65(17)
C12	140(20)	79(15)	101(18)	7(14)	52(16)	52(16)
C13	80(16)	83(17)	86(18)	-1(14)	-5(13)	-1(13)
C14	49(9)	38(9)	67(11)	-6(8)	-11(8)	12(7)
C15	54(11)	50(10)	130(18)	12(12)	-22(11)	3(9)
C16	42(10)	79(14)	122(18)	20(13)	-24(11)	5(10)
C17	64(12)	44(10)	61(11)	12(9)	-10(9)	6(9)
C18	53(11)	58(11)	83(14)	9(10)	2(10)	-8(9)
C19	48(9)	47(10)	66(12)	11(9)	0(8)	-13(8)
C20	75(14)	75(15)	107(18)	-26(14)	-8(13)	-17(12)
C21	51(9)	23(8)	72(12)	-5(7)	-6(8)	0(6)
C22	66(12)	32(9)	84(14)	-9(9)	-31(11)	10(8)
C23	58(11)	43(10)	85(15)	4(10)	-3(10)	6(8)
C24	73(12)	51(11)	59(12)	-10(9)	2(10)	-4(9)
C25	69(12)	55(11)	76(14)	-6(10)	14(11)	17(9)
C26	68(12)	55(11)	89(16)	-2(10)	-12(11)	29(9)
C27	77(14)	58(13)	81(15)	-3(11)	0(12)	-6(10)
C28	55(10)	24(8)	79(12)	-2(8)	-4(9)	12(7)
C29	90(15)	26(9)	127(19)	3(10)	-35(14)	1(9)
C30	77(13)	53(11)	114(17)	2(11)	-53(13)	-19(10)
C31	64(11)	48(10)	64(12)	-4(9)	-10(9)	15(9)
C32	87(15)	44(10)	105(17)	12(11)	-38(13)	-6(10)
C33	90(15)	51(12)	110(17)	21(12)	-42(13)	-20(11)
C34	65(12)	56(12)	56(11)	0(9)	-1(9)	-4(9)
O100	101(11)	85(10)	87(10)	-16(8)	9(9)	-17(9)
C100	130(20)	150(30)	120(20)	20(20)	-10(20)	-70(20)
C101	180(30)	180(30)	100(20)	20(20)	-20(20)	20(30)
O110	126(13)	92(11)	88(11)	-15(9)	-16(10)	20(10)

C110	200(40)	160(30)	190(40)	-80(30)	-80(30)	110(30)
C111	830(160)	180(50)	170(40)	90(40)	150(70)	290(70)
O120	370(50)	180(30)	210(30)	30(20)	-180(30)	-70(30)
C120	190(40)	310(70)	200(50)	90(50)	-80(40)	-50(40)
C121	350(70)	230(50)	230(50)	100(40)	80(50)	130(50)
O130	180(30)	260(30)	180(20)	80(20)	-3(19)	-50(20)
C130	90(30)	650(130)	130(30)	30(50)	20(20)	-60(50)
C131	240(60)	730(170)	490(110)	-520(130)	-110(70)	160(90)

Table A1.20: Hydrogen coordinates (x 10^4) and isotropic displacement parameters ($Å^2$ x 10^3) for BBCB-$PtCl_2$.

	x	y	z	U(eq)
H1A	-1843	4535	5186	139
H13	-3205	7056	802	158
H5A	7050	4980	9	107
H7A	8320	2411	4405	96
H3	3530	3073	1898	80
H4	1585	2323	1723	88
H5	-498	2775	2020	104
H6	-625	3963	2495	92
H8	1318	4166	3536	86
H9	152	4105	4294	99
H11	-2085	6026	3895	130
H12	-948	6094	3181	127
H15	-1404	5190	2354	94
H16	-2665	5993	1793	97
H18	538	7417	1591	77
H19	1773	6703	2175	64

H22	4066	5509	1662	73
H23	5153	5516	926	74
H25	7485	3626	1341	80
H26	6411	3593	2076	85
H29	6421	4635	3073	97
H30	7534	3871	3639	98
H32	4921	2058	3402	95
H33	3917	2816	2804	101
H10	2335	5394	286	136
H10A	323	5448	652	158
H10B	636	4553	445	158
H10C	-20	4484	1196	231
H10D	1157	5103	1359	231
H10E	1541	4218	1155	231
H11C	410	6835	429	153
H11A	-974	7150	-206	219
H11B	-326	7921	65	219
H11D	-171	8049	-723	589
H11E	639	7204	-757	589
H11F	1310	7967	-484	589
H12B	4269	2627	4459	381
H12F	5389	2841	5106	277
H12G	5301	1911	4939	277
H12C	5024	1999	5720	402
H12D	3629	1708	5473	402
H12E	3799	2632	5651	402
H13A	3017	6210	4232	310
H13E	5139	5400	4530	350
H13F	5022	5378	3936	350
H13B	4173	3857	4269	729
H13C	2913	4296	4007	729
H13D	3046	4311	4586	729

Table A1.21: Crystal data and structure refinement for Pt-PCM-18.

Identification code	sh11020	
Empirical formula	C34 H24 Cl2 O10 P2 Pt Zn2	
Formula weight	1051.20	
Temperature	120(2) K	
Wavelength	0.710747 Å	
Crystal system	Orthorhombic	
Space group	Imma	
Unit cell dimensions	a = 24.574(5) Å	α= 90°.
	b = 26.507(5) Å	β= 90°.
	c = 15.152(3) Å	γ = 90°.
Volume	9869(3) $Å^3$	
Z	4	
Density (calculated)	0.707 Mg/m^3	
Absorption coefficient	2.003 mm^{-1}	
F(000)	2040	
Crystal size	0.20 x 0.20 x 0.20 mm^3	
Theta range for data collection	1.5265 to 24.5414°.	
Index ranges	-28<=h<=28, -30<=k<=30, -17<=l<=17	
Reflections collected	16428	
Independent reflections	16428 [R(int) = 0.0770]	
Completeness to theta = 24.5414°	9950.00 %	
Absorption correction	Semi-empirical from equivalents	
Max. and min. transmission	1.0000 and 0.7737	
Refinement method	Full-matrix least-squares on F^2	
Data / restraints / parameters	4304 / 117 / 128	
Goodness-of-fit on F^2	1.077	
Final R indices [I>2sigma(I)]	R1 = 0.0588, wR2 = 0.1523	
R indices (all data)	R1 = 0.0729, wR2 = 0.1608	
Largest diff. peak and hole	0.487 and -0.479 e.$Å^{-3}$	

Table A1.22: Atomic coordinates (x 10^4) and equivalent isotropic displacement parameters ($Å^2$ x 10^3) for Pt-PCM-18. U(eq) is defined as one third of the trace of the orthogonalized U^{ij} tensor.

	x	y	z	U(eq)
Pt1	2094(6)	2500	1595(11)	84(6)
Cl1	1690(40)	3140(30)	690(60)	120(30)
Zn1	5000	4651(7)	-812(13)	71(7)
P1	2500	3086(16)	2500	82(13)
O1	4410(40)	4280(40)	-60(70)	110(30)
O2	4410(40)	4810(40)	1130(70)	100(30)
O3W	5000	4210(60)	-1870(100)	130(50)
C1	2990(50)	3500(40)	1950(90)	80(30)
C2	3220(50)	3350(50)	1110(90)	90(40)
C3	3630(50)	3650(50)	710(90)	90(40)
C4	3810(50)	4100(50)	1130(90)	90(30)
C5	3590(50)	4250(50)	1960(100)	100(40)
C6	3180(50)	3950(40)	2380(90)	90(40)
C7	4250(50)	4430(50)	710(100)	90(40)
C8	2860(90)	2770(80)	3340(170)	130(80)
C9	3160(90)	3040(110)	4000(180)	130(80)
C10	3450(100)	2770(70)	4660(180)	130(80)

Table A1.23: Bond lengths [Å] and angles [°] for Pt-PCM-18.

Pt1-P1	2.30(3)	Zn1-O3W	1.98(15)
Pt1-P1#1	2.30(3)	Zn1-O1#3	2.08(9)
Pt1-Cl1#2	2.39(9)	Zn1-O1	2.08(9)
Pt1-Cl1	2.39(9)	Zn1-O2#4	2.08(9)

Zn1-O2#5	2.08(9)	O3W-Zn1-O1	100(5)
Zn1-Zn1#5	3.08(4)	O1#3-Zn1-O1	88(6)
P1-C8#6	1.8(3)	O3W-Zn1-O2#4	102(5)
P1-C8	1.8(3)	O1#3-Zn1-O2#4	158(4)
P1-C1#6	1.84(11)	O1-Zn1-O2#4	88(4)
P1-C1	1.84(11)	O3W-Zn1-O2#5	102(5)
P1-Pt1#1	2.30(3)	O1#3-Zn1-O2#5	88(4)
O1-C7	1.30(16)	O1-Zn1-O2#5	158(4)
O2-C7	1.25(16)	O2#4-Zn1-O2#5	88(6)
O2-Zn1#5	2.08(9)	O3W-Zn1-Zn1#5	179(5)
O3W-H3W	0.8200	O1#3-Zn1-Zn1#5	81(3)
C1-C6	1.43(16)	O1-Zn1-Zn1#5	81(3)
C1-C2	1.44(17)	O2#4-Zn1-Zn1#5	77(3)
C2-C3	1.42(15)	O2#5-Zn1-Zn1#5	77(3)
C2-H2	0.9300	C8#6-P1-C8	123(10)
C3-C4	1.41(17)	C8#6-P1-C1#6	106(7)
C3-H3	0.9300	C8-P1-C1#6	107(7)
C4-C5	1.42(17)	C8#6-P1-C1	107(7)
C4-C7	1.54(16)	C8-P1-C1	106(7)
C5-C6	1.43(16)	C1#6-P1-C1	106(8)
C5-H5	0.9300	C8#6-P1-Pt1	14(8)
C6-H6	0.9300	C8-P1-Pt1	109(8)
C8-C8#2	1.4(4)	C1#6-P1-Pt1	113(4)
C8-C9	1.4(3)	C1-P1-Pt1	115(4)
C9-C10	1.4(3)	C8#6-P1-Pt1#1	109(8)
C9-H9	0.9300	C8-P1-Pt1#1	14(8)
C10-C10#2	1.4(4)	C1#6-P1-Pt1#1	115(4)
C10-H10	0.9300	C1-P1-Pt1#1	113(4)
P1-Pt1-P1#1	85.0(17)	Pt1-P1-Pt1#1	95.0(17)
P1-Pt1-Cl1	92(2)	C7-O1-Zn1	124(9)
P1#1-Pt1-Cl1	177(2)	C7-O2-Zn1#5	130(9)
Cl1#2-Pt1-Cl1	90(5)	Zn1-O3W-H3W	109.5
O3W-Zn1-O1#3	100(5)	C6-C1-C2	120(10)

C6-C1-P1	120(9)	C5-C6-H6	120.4
C2-C1-P1	119(9)	C1-C6-H6	120.4
C3-C2-C1	119(10)	O2-C7-O1	128(10)
C3-C2-H2	120.3	O2-C7-C4	118(10)
C1-C2-H2	120.3	O1-C7-C4	114(10)
C4-C3-C2	120(10)	C8#2-C8-C9	120(10)
C4-C3-H3	119.8	C8#2-C8-P1	118(8)
C2-C3-H3	119.8	C9-C8-P1	122(10)
C3-C4-C5	121(10)	C10-C9-C8	120(10)
C3-C4-C7	121(10)	C10-C9-H9	119.9
C5-C4-C7	118(10)	C8-C9-H9	119.9
C4-C5-C6	120(10)	C9-C10-C10#2	120(10)
C4-C5-H5	119.9	C9-C10-H10	120.1
C6-C5-H5	119.9	C10#2-C10-H10	120.1
C5-C6-C1	119(10)		

Symmetry transformations used to generate equivalent atoms:

#1 -x+1/2,-y+1/2,-z+1/2 #2 x,-y+1/2,z #3 -x+1,y,z
#4 x,-y+1,-z #5 -x+1,-y+1,-z #6 -x+1/2,y+0,-z+1/2

Table A1.24: Anisotropic displacement parameters ($Å^2$ x 10^3) for Pt-PCM-18. The anisotropic displacement factor exponent takes the form: $-2\pi^2[h^2 a^{*2}U^{11} + ... + 2 h k a^* b^* U^{12}]$.

	U^{11}	U^{22}	U^{33}	U^{23}	U^{13}	U^{12}
Pt1	71(10)	66(10)	116(13)	0	17(7)	0
Cl1	130(70)	90(50)	130(70)	10(50)	-10(50)	10(50)
Zn1	51(10)	66(12)	96(14)	11(9)	0	0
P1	60(30)	60(20)	120(40)	0	30(20)	0
O1	90(60)	100(70)	130(80)	20(60)	30(60)	-30(50)

O2	80(60)	90(60)	140(80)	10(60)	30(50)	-20(50)
O3W	150(130)	120(110)	120(100)	-10(90)	0	0
C1	70(70)	70(70)	110(80)	0(60)	30(60)	0(60)
C2	70(80)	70(70)	130(100)	10(70)	30(70)	-10(60)
C3	80(80)	80(80)	110(90)	10(70)	30(70)	-10(70)
C4	70(70)	80(70)	110(90)	20(70)	10(70)	0(60)
C5	80(80)	80(80)	130(100)	0(70)	20(80)	-10(70)
C6	90(80)	70(70)	120(90)	-10(70)	40(70)	-10(60)
C7	70(70)	80(80)	110(100)	30(70)	10(70)	0(60)

Table A1.25: Hydrogen coordinates (x 10^4) and isotropic displacement parameters ($Å^2$ x 10^3) for Pt-PCM-18.

	x	y	z	U(eq)
H3W	5219	4320	-2232	194
H2	3100	3059	832	108
H3	3776	3561	173	112
H5	3714	4541	2232	116
H6	3038	4044	2921	112
H9	3157	3389	4001	155
H10	3641	2946	5096	155

Table A1.26: Crystal data and structure refinement for Pd-PCM-24.

Identification code	sh13001	
Empirical formula	C56 H32 Cl4 Co5 O20.67 P4 Pd2	
Formula weight	1808.61	
Temperature	153(2) K	
Wavelength	0.71073 Å	
Crystal system	hexagonal	
Space group	P -6 2 m	
Unit cell dimensions	a = 23.837(3) Å	α= 90°.
	b = 23.837(3) Å	β= 90°.
	c = 25.446(5) Å	γ = 120°.
Volume	12522(4) $Å^3$	
Z	3	
Density (calculated)	0.720 Mg/m^3	
Absorption coefficient	0.826 mm^{-1}	
F(000)	2665	
Crystal size	0.200 x 0.200 x 0.120 mm^3	
Theta range for data collection	3.548 to 27.562°.	
Index ranges	-29<=h<=30, -30<=k<=26, -33<=l<=31	
Reflections collected	113112	
Independent reflections	10195 [R(int) = 0.1155]	
Completeness to theta = 25.242°	99.4 %	
Refinement method	Full-matrix least-squares on F^2	
Data / restraints / parameters	10195 / 0 / 144	
Goodness-of-fit on F^2	2.270	
Final R indices [I>2sigma(I)]	R1 = 0.2717, wR2 = 0.5779	
R indices (all data)	R1 = 0.2757, wR2 = 0.5801	
Absolute structure parameter	0.488(9)	
Extinction coefficient	n/a	
Largest diff. peak and hole	3.430 and -1.398 e.$Å^{-3}$	

Table A1.27: Atomic coordinates (x 10^4) and equivalent isotropic displacement parameters ($Å^2$ x 10^3) for Pd-PCM-24. U(eq) is defined as one third of the trace of the orthogonalized U^{ij} tensor.

	x	y	z	U(eq)
Pd1	0	2548(2)	7160(2)	80(2)
Cl1	795(11)	2370(12)	6894(11)	144(8)
Pd1'	0	3748(3)	7812(2)	96(2)
Cl1'	798(13)	4687(14)	8161(10)	153(9)
Co1	3937(7)	3937(7)	9309(6)	206(5)
Co2	2604(3)	2604(3)	10000	61(2)
Co3	3492(2)	5907(2)	5000	43(1)
P1	733(3)	3530(4)	7468(3)	86(2)
O3	2114(8)	5780(8)	5574(7)	74(4)
C10	1388(12)	4981(13)	6401(10)	78(6)
C8	1264(13)	4127(13)	7006(11)	84(7)
O2	2240(11)	2915(12)	9426(9)	102(6)
C7	2457(18)	3380(19)	9137(15)	108(10)
C1	1274(14)	3505(13)	7973(11)	85(7)
C11	1932(12)	4972(12)	6169(9)	70(5)
C12	2114(18)	4571(19)	6375(15)	114(11)
C9	1025(14)	4561(13)	6773(11)	86(7)
C6	1059(18)	2948(18)	8220(14)	111(10)
C5	1471(19)	2879(18)	8650(14)	115(10)
C4	2056(15)	3454(15)	8767(13)	95(8)
C2	1823(17)	4050(18)	8087(15)	110(10)
C14	2290(6)	5435(6)	5730(5)	30(3)
O1	3010(20)	3870(20)	9152(15)	178(12)
C3	2280(20)	3990(20)	8470(17)	124(12)
O6	3333	6667	5000	20(4)
O4	2771(9)	5426(9)	5591(8)	90(5)
O5	3541(13)	3541(13)	10000	68(7)

C13	1784(16)	4107(16)	6750(14)	105(9)
O2W	3626(15)	5106(15)	5000	101(8)
O1W	1701(18)	1701(18)	10000	96(11)
O5W	4221(18)	4824(18)	9570(14)	204(11)
O4W	4210(20)	4210(20)	8410(20)	216(18)

Table A1.28: Bond lengths [Å] and angles [°] for Pd-PCM-24.

Pd1-P1#1	2.248(9)	Co2-O1W	2.15(4)
Pd1-P1	2.248(9)	Co2-O5	2.23(3)
Pd1-Cl1	2.24(2)	Co3-O6	2.026(3)
Pd1-Cl1#1	2.24(2)	Co3-O2W	2.09(3)
Pd1'-Cl1'#1	2.27(3)	Co3-O3#5	2.102(16)
Pd1'-Cl1'	2.27(3)	Co3-O3#6	2.102(16)
Pd1'-P1	2.236(10)	Co3-O4#7	2.13(2)
Pd1'-P1#1	2.236(10)	Co3-O4	2.13(2)
Co1-O5W	1.99(4)	P1-C8	1.79(3)
Co1-O5W#2	1.98(4)	P1-C1	1.84(3)
Co1-O5	2.00(2)	O3-C14	1.164(19)
Co1-O4W	2.38(6)	O3-Co3#8	2.102(16)
Co1-O1#2	2.17(4)	C10-C9	1.33(4)
Co1-O1	2.17(4)	C10-C11	1.43(3)
Co2-O2#2	2.02(2)	C10-H10A	0.9500
Co2-O2#3	2.02(2)	C8-C13	1.42(4)
Co2-O2#4	2.02(2)	C8-C9	1.53(4)
Co2-O2	2.02(2)	O2-C7	1.21(4)

C7-O1	1.25(5)	P1-Pd1'-P1#1	85.2(5)
C7-C4	1.42(4)	O5W-Co1-O5W#2	78(2)
C1-C6	1.32(4)	O5W-Co1-O5	92.1(13)
C1-C2	1.34(4)	O5W#2-Co1-O5	92.2(13)
C11-C12	1.34(4)	O5W-Co1-O4W	96.6(15)
C11-C14	1.50(3)	O5W#2-Co1-O4W	97.5(15)
C12-C13	1.37(5)	O5-Co1-O4W	168.2(18)
C12-H12A	0.9500	O5W-Co1-O1#2	163.4(17)
C9-H9A	0.9500	O5W#2-Co1-O1#2	86.1(15)
C6-C5	1.53(5)	O5-Co1-O1#2	84.5(13)
C6-H6A	0.9500	O4W-Co1-O1#2	89.3(14)
C5-C4	1.41(5)	O5W-Co1-O1	86.1(15)
C5-H5A	0.9500	O5W#2-Co1-O1	163.3(17)
C4-C3	1.34(5)	O5-Co1-O1	84.5(13)
C2-C3	1.52(5)	O4W-Co1-O1	88.2(14)
C2-H2A	0.9500	O1#2-Co1-O1	110(2)
C14-O4	1.21(2)	O2#2-Co2-O2#3	92.6(13)
C3-H3A	0.9500	O2#2-Co2-O2#4	176.4(14)
O6-Co3#8	2.026(3)	O2#3-Co2-O2#4	87.3(13)
O6-Co3#5	2.026(3)	O2#2-Co2-O2	87.3(13)
O5-Co1#4	2.00(2)	O2#3-Co2-O2	176.4(14)
C13-H13A	0.9500	O2#4-Co2-O2	92.6(13)
P1#1-Pd1-P1	84.6(5)	O2#2-Co2-O1W	88.3(7)
P1#1-Pd1-Cl1	175.1(8)	O2#3-Co2-O1W	88.3(7)
P1-Pd1-Cl1	90.7(8)	O2#4-Co2-O1W	88.2(7)
P1#1-Pd1-Cl1#1	90.7(8)	O2-Co2-O1W	88.2(7)
P1-Pd1-Cl1#1	175.1(8)	O2#2-Co2-O5	91.8(7)
Cl1-Pd1-Cl1#1	94.0(14)	O2#3-Co2-O5	91.8(7)
Cl1'#1-Pd1'-Cl1'	93.1(15)	O2#4-Co2-O5	91.8(7)
Cl1'#1-Pd1'-P1	175.6(8)	O2-Co2-O5	91.8(7)
Cl1'-Pd1'-P1	90.8(8)	O1W-Co2-O5	179.969(4)
Cl1'#1-Pd1'-P1#1	90.8(8)	O6-Co3-O2W	178.4(9)
Cl1'-Pd1'-P1#1	175.6(8)	O6-Co3-O3#5	92.6(5)

O2W-Co3-O3#5	88.5(8)	C12-C11-C10	118(3)
O6-Co3-O3#6	92.6(5)	C12-C11-C14	123(2)
O2W-Co3-O3#6	88.5(8)	C10-C11-C14	118.7(19)
O3#5-Co3-O3#6	88.1(9)	C11-C12-C13	126(3)
O6-Co3-O4#7	91.2(5)	C11-C12-H12A	117.1
O2W-Co3-O4#7	87.7(8)	C13-C12-H12A	116.9
O3#5-Co3-O4#7	176.2(7)	C10-C9-C8	118(3)
O3#6-Co3-O4#7	91.1(7)	C10-C9-H9A	121.4
O6-Co3-O4	91.2(5)	C8-C9-H9A	121.1
O2W-Co3-O4	87.7(8)	C1-C6-C5	120(3)
O3#5-Co3-O4	91.1(7)	C1-C6-H6A	120.0
O3#6-Co3-O4	176.2(7)	C5-C6-H6A	120.0
O4#7-Co3-O4	89.5(11)	C4-C5-C6	115(3)
C8-P1-C1	104.8(13)	C4-C5-H5A	122.8
C8-P1-Pd1'	113.3(9)	C6-C5-H5A	122.4
C1-P1-Pd1'	112.1(10)	C3-C4-C5	122(3)
C8-P1-Pd1	118.2(10)	C3-C4-C7	122(3)
C1-P1-Pd1	113.6(9)	C5-C4-C7	115(3)
Pd1'-P1-Pd1	95.0(3)	C1-C2-C3	116(3)
C14-O3-Co3#8	136.4(13)	C1-C2-H2A	122.0
C9-C10-C11	122(2)	C3-C2-H2A	121.9
C9-C10-H10A	118.8	O3-C14-O4	126.3(16)
C11-C10-H10A	119.1	O3-C14-C11	120.0(16)
C13-C8-C9	118(3)	O4-C14-C11	113.6(16)
C13-C8-P1	124(2)	C7-O1-Co1	129(3)
C9-C8-P1	116(2)	C4-C3-C2	120(4)
C7-O2-Co2	135(2)	C4-C3-H3A	119.8
O1-C7-O2	127(4)	C2-C3-H3A	120.3
O1-C7-C4	112(4)	Co3#8-O6-Co3#5	120.0
O2-C7-C4	121(3)	Co3#8-O6-Co3	120.001(1)
C6-C1-C2	125(3)	Co3#5-O6-Co3	119.999(1)
C6-C1-P1	116(2)	C14-O4-Co3	135.4(14)
C2-C1-P1	119(2)	Co1-O5-Co1#4	123.5(18)

Co1-O5-Co2	118.2(9)	C12-C13-H13A	121.7
Co1#4-O5-Co2	118.2(9)	C8-C13-H13A	121.5
C12-C13-C8	117(3)		

Symmetry transformations used to generate equivalent atoms:

#1 -x,-x+y,z #2 y,x,z #3 y,x,-z+2 #4 x,y,-z+2
#5 -y+1,x-y+1,z #6 -y+1,x-y+1,-z+1 #7 x,y,-z+1
#8 -x+y,-x+1,z

Table A1.29: Anisotropic displacement parameters ($Å^2 x\ 10^3$) for Pd-PCM-24. The anisotropic displacement factor exponent takes the form: $-2\pi^2[h^2\ a^{*2}U^{11} + ... + 2\ h\ k\ a^*\ b^*\ U^{12}]$.

	U^{11}	U^{22}	U^{33}	U^{23}	U^{13}	U^{12}
Pd1	109(4)	85(2)	55(3)	30(2)	0	54(2)
Cl1	126(15)	154(17)	170(20)	52(16)	48(15)	82(14)
Pd1'	106(4)	114(4)	64(3)	36(3)	0	53(2)
Cl1'	156(19)	180(20)	121(16)	13(16)	-9(14)	81(17)
Co1	218(9)	218(9)	163(10)	-3(8)	-3(8)	95(11)
Co2	75(3)	75(3)	36(2)	0	0	39(3)
Co3	56(2)	40(2)	42(2)	0	0	30(2)
P1	60(3)	104(5)	78(4)	55(4)	3(3)	30(3)

Table A1.30: Hydrogen coordinates (x 10^4) and isotropic displacement parameters ($Å^2$ x 10^3) for Pd-PCM-24.

	x	y	z	U(eq)
H10A	1283	5297	6286	93
H12A	2508	4610	6249	136
H9A	633	4533	6889	103
H6A	649	2589	8131	134
H5A	1342	2481	8825	138
H2A	1924	4455	7937	132
H3A	2714	4321	8498	149
H13A	1898	3789	6835	126

Table A1.31: Crystal data and structure refinement for Pt-PCM-27.

Identification code	sh14019	
Empirical formula	C38.50 H30.50 Cl2 Co2 N1.50 O12.75 P2 Pt	
Formula weight	1163.93	
Temperature	143(2) K	
Wavelength	0.71073 Å	
Crystal system	monoclinic	
Space group	C 2/c	
Unit cell dimensions	a = 36.833(3) Å	α= 90°.
	b = 12.1094(9) Å	β= 98.635(8)°.
	c = 35.282(2) Å	γ = 90°.
Volume	15558(2) $Å^3$	
Z	8	
Density (calculated)	0.994 Mg/m^3	
Absorption coefficient	2.360 mm^{-1}	

F(000)	4560
Crystal size	0.360 x 0.130 x 0.030 mm^3
Theta range for data collection	3.515 to 24.997°.
Index ranges	-43<=h<=43, -14<=k<=14, -41<=l<=41
Reflections collected	98317
Independent reflections	13599 [R(int) = 0.1627]
Completeness to theta = 25.242°	96.5 %
Refinement method	Full-matrix least-squares on F^2
Data / restraints / parameters	13599 / 64 / 560
Goodness-of-fit on F^2	0.980
Final R indices [I>2sigma(I)]	R1 = 0.0789, wR2 = 0.1896
R indices (all data)	R1 = 0.1877, wR2 = 0.2137
Extinction coefficient	n/a
Largest diff. peak and hole	1.400 and -0.419 e.$Å^{-3}$

Table A1.32: Atomic coordinates (x 10^4) and equivalent isotropic displacement parameters ($Å^2$x 10^3) for Pt-PCM-27. U(eq) is defined as one third of the trace of the orthogonalized U^{ij} tensor.

	x	y	z	U(eq)
Pt1	1297(1)	1363(1)	3635(1)	73(1)
Cl1	1774(1)	2425(3)	3460(1)	90(1)
Cl2	1169(1)	2758(3)	4051(1)	94(1)
C1	1030(2)	-957(6)	3202(2)	79(5)
C2	768(2)	-819(6)	3444(2)	78(5)
C3	466(2)	-1521(8)	3413(2)	82(5)
C4	427(2)	-2361(8)	3142(3)	89(4)
C5	689(3)	-2499(7)	2900(2)	91(4)
C6	991(2)	-1796(7)	2930(2)	79(5)

Pt1'	915(1)	-819(2)	3334(1)	81(1)
Cl1'	361(4)	-1680(16)	3418(5)	135(6)
Cl2'	1004(5)	-2089(13)	2848(5)	123(6)
C1'	1177(3)	1482(10)	3773(3)	186(18)
C2'	1439(3)	1345(10)	3531(3)	195(18)
C3'	1693(5)	2176(14)	3500(6)	198(18)
C4'	1685(7)	3144(15)	3710(8)	184(17)
C5'	1424(7)	3281(15)	3952(8)	175(17)
C6'	1169(5)	2450(13)	3983(5)	182(18)
Co1	1831(1)	346(1)	872(1)	72(1)
Co2	1355(1)	2771(1)	993(1)	64(1)
P2	853(1)	331(2)	3793(1)	69(1)
P1	1420(1)	20(2)	3266(1)	66(1)
O1	1480(2)	2111(7)	1518(2)	99(3)
O2	1698(2)	463(7)	1417(2)	95(3)
O3	3103(2)	-1795(6)	4008(2)	74(2)
O4	2801(2)	-3396(7)	4030(2)	77(2)
O5	1231(2)	-2914(7)	5377(2)	74(2)
O6	1379(2)	-1297(5)	5649(2)	62(2)
O7	-803(2)	2376(7)	4009(2)	101(3)
O8	-666(3)	3574(9)	3571(3)	168(5)
O9	2273(2)	-712(7)	1077(2)	115(3)
O10	1252(2)	4382(7)	1207(2)	107(2)
O11	1496(2)	-1051(6)	806(2)	117(3)
C7	1490(3)	356(10)	2789(3)	74(3)
C8	1328(3)	1336(10)	2617(3)	89(4)
C9	1347(3)	1525(10)	2226(3)	95(4)
C10	1553(3)	855(10)	2028(3)	67(3)
C11	1713(3)	-79(10)	2199(3)	83(3)
C12	1695(3)	-338(10)	2572(3)	91(4)
C13	1581(3)	1177(13)	1626(3)	79(4)
C14	1828(3)	-765(11)	3473(3)	73(3)
C15	2164(3)	-206(10)	3487(3)	88(4)

C16	2477(3)	-738(10)	3654(3)	81(3)
C17	2470(3)	-1785(10)	3803(2)	65(3)
C18	2130(3)	-2301(9)	3784(3)	73(3)
C19	1820(3)	-1795(9)	3622(3)	70(3)
C20	2831(3)	-2385(11)	3967(3)	60(3)
C21	964(2)	-361(11)	4260(3)	66(3)
C22	1025(3)	-1445(11)	4284(3)	75(3)
C23	1122(3)	-1968(8)	4632(3)	67(3)
C24	1169(3)	-1327(11)	4957(3)	72(3)
C25	1122(3)	-209(10)	4940(3)	74(3)
C26	1013(3)	291(10)	4578(3)	79(3)
C27	1272(3)	-1878(11)	5354(3)	67(3)
C28	408(3)	999(10)	3784(3)	77(3)
C29	177(3)	652(10)	4028(3)	106(4)
C30	-153(3)	1250(12)	4029(4)	132(6)
C31	-241(3)	2120(14)	3799(4)	133(6)
C32	-11(3)	2471(12)	3532(4)	124(5)
C33	323(3)	1852(10)	3534(3)	88(4)
C34	-604(3)	2778(14)	3798(5)	126(5)
O50	1957(2)	205(7)	311(2)	84(2)
N50	2046(2)	-750(9)	-212(3)	100(3)
C50	2023(3)	-689(12)	167(4)	96(4)
C51	2103(4)	-1899(11)	-375(4)	128(5)
C52	2011(3)	174(12)	-458(3)	121(5)
O51	0	1132(19)	2500	124(8)
O100	1919(7)	4140(20)	5241(6)	189(9)
N100	2049(5)	5617(17)	4886(6)	102(6)
C100	1975(7)	5190(20)	5191(8)	114(8)
C101	2107(9)	6720(30)	4982(8)	165(12)
C102	2072(7)	5144(19)	4523(6)	109(8)

Table A1.33: Bond lengths [Å] and angles [°] for Pt-PCM-27.

Pt1-P1	2.173(3)	C6'-H6'A	0.9500
Pt1-P2	2.197(3)	Co1-O4#1	2.035(7)
Pt1-Cl2	2.331(4)	Co1-O2	2.060(8)
Pt1-Cl1	2.334(4)	Co1-O6#2	2.080(7)
C1-C2	1.3900	Co1-O11	2.086(7)
C1-C6	1.3900	Co1-O50	2.108(7)
C1-P1	1.848(8)	Co1-O9	2.112(8)
C2-C3	1.3900	Co2-O1	2.006(7)
C2-P2	1.856(8)	Co2-O3#1	2.063(6)
C3-C4	1.3900	Co2-O7#3	2.088(7)
C3-H3A	0.9500	Co2-O10	2.146(8)
C4-C5	1.3900	Co2-O5#2	2.161(6)
C4-H4A	0.9500	Co2-O6#2	2.169(6)
C5-C6	1.3900	Co2-C27#2	2.478(10)
C5-H5A	0.9500	P2-C28	1.823(10)
C6-H6A	0.9500	P2-C21	1.839(10)
Pt1'-P1	2.163(3)	P1-C7	1.786(9)
Pt1'-P2	2.176(3)	P1-C14	1.835(10)
Pt1'-Cl1'	2.351(16)	O1-C13	1.232(13)
Pt1'-Cl2'	2.362(16)	O2-C13	1.254(13)
C1'-C2'	1.3900	O3-C20	1.222(11)
C1'-C6'	1.3900	O3-Co2#4	2.063(6)
C1'-P2	1.843(11)	O4-C20	1.252(11)
C2'-C3'	1.3900	O4-Co1#4	2.036(7)
C2'-P1	1.853(11)	O5-C27	1.268(11)
C3'-C4'	1.3900	O5-Co2#5	2.161(6)
C3'-H3'A	0.9500	O6-C27	1.267(12)
C4'-C5'	1.3900	O6-Co1#5	2.080(7)
C4'-H4'A	0.9500	O6-Co2#5	2.169(6)
C5'-C6'	1.3900	O7-C34	1.221(14)
C5'-H5'A	0.9500	O7-Co2#3	2.088(7)

O8-C34	1.252(14)	C26-H26A	0.9500
C7-C8	1.423(13)	C27-Co2#5	2.478(10)
C7-C12	1.429(13)	C28-C29	1.363(12)
C8-C9	1.408(12)	C28-C33	1.365(12)
C8-H8A	0.9500	C29-C30	1.414(13)
C9-C10	1.373(13)	C29-H29A	0.9500
C9-H9A	0.9500	C30-C31	1.339(15)
C10-C11	1.373(13)	C30-H30A	0.9500
C10-C13	1.490(13)	C31-C32	1.424(14)
C11-C12	1.365(12)	C31-C34	1.558(16)
C11-H11A	0.9500	C32-C33	1.440(14)
C12-H12A	0.9500	C32-H32A	0.9500
C14-C19	1.356(13)	C33-H33A	0.9500
C14-C15	1.405(14)	O50-C50	1.235(12)
C15-C16	1.374(13)	N50-C50	1.353(13)
C15-H15A	0.9500	N50-C52	1.410(13)
C16-C17	1.374(13)	N50-C51	1.533(14)
C16-H16A	0.9500	C50-H50A	0.9500
C17-C18	1.392(12)	C51-H51A	0.9800
C17-C20	1.549(13)	C51-H51B	0.9800
C18-C19	1.345(12)	C51-H51C	0.9800
C18-H18A	0.9500	C52-H52A	0.9800
C19-H19A	0.9500	C52-H52B	0.9800
C21-C22	1.333(13)	C52-H52C	0.9800
C21-C26	1.363(13)	O100-C100	1.31(3)
C22-C23	1.380(12)	N100-C100	1.26(3)
C22-H22A	0.9500	N100-C101	1.39(3)
C23-C24	1.377(12)	N100-C102	1.42(2)
C23-H23A	0.9500	C100-H10B	0.9500
C24-C25	1.364(12)	C101-H10C	0.9800
C24-C27	1.547(13)	C101-H10D	0.9800
C25-C26	1.416(12)	C101-H10E	0.9800
C25-H25A	0.9500	C102-H10F	0.9800

C102-H10G	0.9800	C2'-C1'-P2	116.5(5)
C102-H10H	0.9800	C6'-C1'-P2	123.5(5)
P1-Pt1-P2	87.51(10)	C1'-C2'-C3'	120.0
P1-Pt1-Cl2	177.80(12)	C1'-C2'-P1	115.9(5)
P2-Pt1-Cl2	91.34(13)	C3'-C2'-P1	124.1(5)
P1-Pt1-Cl1	91.20(12)	C4'-C3'-C2'	120.0
P2-Pt1-Cl1	178.69(12)	C4'-C3'-H3'A	120.0
Cl2-Pt1-Cl1	89.94(15)	C2'-C3'-H3'A	120.0
C2-C1-C6	120.0	C3'-C4'-C5'	120.0
C2-C1-P1	116.6(4)	C3'-C4'-H4'A	120.0
C6-C1-P1	123.4(4)	C5'-C4'-H4'A	120.0
C1-C2-C3	120.0	C6'-C5'-C4'	120.0
C1-C2-P2	115.7(4)	C6'-C5'-H5'A	120.0
C3-C2-P2	124.3(4)	C4'-C5'-H5'A	120.0
C4-C3-C2	120.0	C5'-C6'-C1'	120.0
C4-C3-H3A	120.0	C5'-C6'-H6'A	120.0
C2-C3-H3A	120.0	C1'-C6'-H6'A	120.0
C3-C4-C5	120.0	O4#1-Co1-O2	92.0(3)
C3-C4-H4A	120.0	O4#1-Co1-O6#2	97.2(3)
C5-C4-H4A	120.0	O2-Co1-O6#2	91.5(3)
C6-C5-C4	120.0	O4#1-Co1-O11	173.8(3)
C6-C5-H5A	120.0	O2-Co1-O11	86.6(3)
C4-C5-H5A	120.0	O6#2-Co1-O11	88.8(3)
C5-C6-C1	120.0	O4#1-Co1-O50	89.2(3)
C5-C6-H6A	120.0	O2-Co1-O50	178.8(3)
C1-C6-H6A	120.0	O6#2-Co1-O50	88.1(3)
P1-Pt1'-P2	88.29(13)	O11-Co1-O50	92.3(3)
P1-Pt1'-Cl1'	178.1(5)	O4#1-Co1-O9	86.3(3)
P2-Pt1'-Cl1'	89.9(5)	O2-Co1-O9	90.0(3)
P1-Pt1'-Cl2'	90.6(4)	O6#2-Co1-O9	176.1(3)
P2-Pt1'-Cl2'	177.9(5)	O11-Co1-O9	87.7(3)
Cl1'-Pt1'-Cl2'	91.2(6)	O50-Co1-O9	90.3(3)
C2'-C1'-C6'	120.0	O1-Co2-O3#1	90.9(3)

O1-Co2-O7#3	90.0(3)	C14-P1-C1	106.9(5)
O3#1-Co2-O7#3	178.5(3)	C7-P1-C2'	106.2(5)
O1-Co2-O10	93.9(3)	C14-P1-C2'	106.4(6)
O3#1-Co2-O10	89.6(3)	C7-P1-Pt1'	117.3(3)
O7#3-Co2-O10	89.1(3)	C14-P1-Pt1'	112.2(4)
O1-Co2-O5#2	161.0(3)	C2'-P1-Pt1'	108.6(3)
O3#1-Co2-O5#2	92.1(2)	C7-P1-Pt1	117.8(4)
O7#3-Co2-O5#2	87.5(3)	C14-P1-Pt1	112.4(3)
O10-Co2-O5#2	104.9(3)	C1-P1-Pt1	108.9(2)
O1-Co2-O6#2	99.6(3)	C13-O1-Co2	131.9(8)
O3#1-Co2-O6#2	95.1(3)	C13-O2-Co1	138.3(8)
O7#3-Co2-O6#2	86.0(3)	C20-O3-Co2#4	128.9(7)
O10-Co2-O6#2	165.7(3)	C20-O4-Co1#4	133.4(7)
O5#2-Co2-O6#2	61.5(2)	C27-O5-Co2#5	88.5(6)
O1-Co2-C27#2	130.2(4)	C27-O6-Co1#5	138.5(6)
O3#1-Co2-C27#2	95.5(3)	C27-O6-Co2#5	88.2(6)
O7#3-Co2-C27#2	84.8(3)	Co1#5-O6-Co2#5	109.9(3)
O10-Co2-C27#2	135.4(4)	C34-O7-Co2#3	125.4(7)
O5#2-Co2-C27#2	30.8(3)	C8-C7-C12	118.8(8)
O6#2-Co2-C27#2	30.7(3)	C8-C7-P1	118.9(8)
C28-P2-C21	107.3(5)	C12-C7-P1	122.2(8)
C28-P2-C1'	104.5(5)	C9-C8-C7	118.4(10)
C21-P2-C1'	108.8(6)	C9-C8-H8A	120.8
C28-P2-C2	105.1(4)	C7-C8-H8A	120.8
C21-P2-C2	104.2(5)	C10-C9-C8	121.0(10)
C28-P2-Pt1'	117.8(3)	C10-C9-H9A	119.5
C21-P2-Pt1'	109.9(4)	C8-C9-H9A	119.5
C1'-P2-Pt1'	108.3(3)	C11-C10-C9	119.8(9)
C28-P2-Pt1	116.4(4)	C11-C10-C13	123.3(11)
C21-P2-Pt1	114.4(3)	C9-C10-C13	116.9(11)
C2-P2-Pt1	108.4(2)	C12-C11-C10	122.3(10)
C7-P1-C14	105.6(5)	C12-C11-H11A	118.8
C7-P1-C1	104.4(4)	C10-C11-H11A	118.8

C11-C12-C7	119.2(10)	C24-C23-C22	117.9(10)
C11-C12-H12A	120.4	C24-C23-H23A	121.1
C7-C12-H12A	120.4	C22-C23-H23A	121.1
O1-C13-O2	124.5(10)	C25-C24-C23	121.6(10)
O1-C13-C10	118.3(13)	C25-C24-C27	118.7(11)
O2-C13-C10	117.2(13)	C23-C24-C27	119.7(11)
C19-C14-C15	120.1(10)	C24-C25-C26	118.7(10)
C19-C14-P1	124.5(9)	C24-C25-H25A	120.6
C15-C14-P1	115.3(10)	C26-C25-H25A	120.6
C16-C15-C14	117.8(11)	C21-C26-C25	118.7(11)
C16-C15-H15A	121.1	C21-C26-H26A	120.7
C14-C15-H15A	121.1	C25-C26-H26A	120.7
C15-C16-C17	122.4(10)	O6-C27-O5	121.6(9)
C15-C16-H16A	118.8	O6-C27-C24	120.4(11)
C17-C16-H16A	118.8	O5-C27-C24	117.9(11)
C16-C17-C18	117.6(9)	O6-C27-Co2#5	61.0(5)
C16-C17-C20	120.8(10)	O5-C27-Co2#5	60.7(5)
C18-C17-C20	121.6(11)	C24-C27-Co2#5	172.9(7)
C19-C18-C17	121.2(10)	C29-C28-C33	122.4(9)
C19-C18-H18A	119.4	C29-C28-P2	119.8(8)
C17-C18-H18A	119.4	C33-C28-P2	117.7(8)
C18-C19-C14	121.1(11)	C28-C29-C30	117.5(10)
C18-C19-H19A	119.5	C28-C29-H29A	121.2
C14-C19-H19A	119.5	C30-C29-H29A	121.2
O3-C20-O4	130.1(10)	C31-C30-C29	122.0(10)
O3-C20-C17	114.4(11)	C31-C30-H30A	119.0
O4-C20-C17	115.5(10)	C29-C30-H30A	119.0
C22-C21-C26	121.3(10)	C30-C31-C32	121.5(12)
C22-C21-P2	121.2(9)	C30-C31-C34	122.3(11)
C26-C21-P2	117.3(10)	C32-C31-C34	116.2(12)
C21-C22-C23	121.7(10)	C31-C32-C33	115.7(11)
C21-C22-H22A	119.1	C31-C32-H32A	122.2
C23-C22-H22A	119.1	C33-C32-H32A	122.2

C28-C33-C32	120.7(10)	H10C-C101-H10D	109.5
C28-C33-H33A	119.6	N100-C101-H10E	109.5
C32-C33-H33A	119.6	H10C-C101-H10E	109.5
O7-C34-O8	129.0(11)	H10D-C101-H10E	109.5
O7-C34-C31	112.9(13)	N100-C102-H10F	109.5
O8-C34-C31	118.0(12)	N100-C102-H10G	109.5
C50-O50-Co1	122.8(8)	H10F-C102-H10G	109.5
C50-N50-C52	123.4(11)	N100-C102-H10H	109.5
C50-N50-C51	117.0(12)	H10F-C102-H10H	109.5
C52-N50-C51	119.6(10)	H10G-C102-H10H	109.5
O50-C50-N50	119.9(13)		
O50-C50-H50A	120.0		
N50-C50-H50A	120.0		
N50-C51-H51A	109.5		
N50-C51-H51B	109.5		
H51A-C51-H51B	109.5		
N50-C51-H51C	109.5		
H51A-C51-H51C	109.5		
H51B-C51-H51C	109.5		
N50-C52-H52A	109.5		
N50-C52-H52B	109.5		
H52A-C52-H52B	109.5		
N50-C52-H52C	109.5		
H52A-C52-H52C	109.5		
H52B-C52-H52C	109.5		
C100-N100-C101	103(2)		
C100-N100-C102	131(2)		
C101-N100-C102	126(2)		
N100-C100-O100	125(3)		
N100-C100-H10B	117.6		
O100-C100-H10B	117.6		
N100-C101-H10C	109.5		
N100-C101-H10D	109.5		

Symmetry transformations used to generate equivalent atoms:

#1 -x+1/2,y+1/2,-z+1/2 #2 x,-y,z-1/2 #3 -x,y,-z+1/2
#4 -x+1/2,y-1/2,-z+1/2 #5 x,-y,z+1/2

Table A1.34: Anisotropic displacement parameters ($Å^2 x\ 10^3$) for Pt-PCM-27. The anisotropic displacement factor exponent takes the form: $-2\pi^2[h^2 a^{*2} U^{11} + ... + 2\ h\ k\ a^*\ b^*\ U^{12}]$.

	U^{11}	U^{22}	U^{33}	U^{23}	U^{13}	U^{12}
Pt1	52(1)	99(1)	70(1)	14(1)	13(1)	16(1)
Cl1	73(3)	85(3)	114(3)	5(2)	19(2)	-1(2)
Cl2	94(3)	107(3)	84(3)	4(2)	19(2)	30(3)
C1	63(8)	102(10)	73(8)	11(7)	10(7)	-8(7)
C2	61(9)	100(9)	72(8)	13(7)	13(7)	-8(7)
C3	58(9)	112(9)	75(8)	17(7)	7(7)	-12(7)
C4	67(8)	114(8)	82(7)	8(7)	0(6)	-22(7)
C5	69(7)	113(8)	86(7)	-8(7)	-7(6)	-10(7)
C6	60(8)	104(10)	71(8)	-2(7)	6(7)	-6(8)
Pt1'	49(1)	121(2)	70(1)	7(1)	2(1)	2(1)
Cl1'	39(7)	183(16)	178(15)	13(14)	-1(9)	-15(9)
Cl2'	143(15)	98(10)	120(11)	-44(9)	-4(10)	-43(10)
Co1	65(1)	90(1)	62(1)	-5(1)	15(1)	-8(1)
Co2	43(1)	89(1)	61(1)	-6(1)	7(1)	-19(1)
P2	44(2)	96(2)	68(2)	18(2)	13(1)	18(2)

P1	39(2)	94(2)	64(2)	14(2)	8(1)	15(2)
O1	146(8)	96(7)	54(5)	20(4)	15(5)	-9(6)
O2	65(5)	158(8)	62(5)	18(5)	7(4)	17(5)
O3	36(4)	94(6)	88(5)	-4(4)	-10(4)	14(4)
O4	49(4)	97(6)	88(5)	17(5)	17(4)	24(5)
O5	66(5)	97(6)	55(4)	21(4)	0(3)	17(5)
O6	45(4)	85(5)	53(4)	8(4)	-5(3)	12(4)
O7	42(4)	148(7)	121(6)	58(5)	40(4)	36(5)
O8	93(7)	205(11)	226(11)	123(9)	86(7)	69(7)
O9	102(7)	122(7)	121(6)	-6(5)	18(5)	32(5)
O10	55(5)	131(7)	139(6)	-12(5)	27(5)	4(5)
O11	124(7)	102(6)	121(6)	10(5)	8(5)	-32(5)
C7	55(7)	105(9)	65(7)	31(6)	24(6)	7(6)
C8	72(8)	125(10)	78(8)	20(7)	33(6)	45(7)
C9	82(9)	148(11)	55(7)	36(7)	10(6)	42(8)
C10	57(7)	91(9)	54(7)	-2(6)	13(6)	-3(6)
C11	68(8)	124(10)	61(7)	14(7)	19(6)	38(7)
C12	72(8)	130(11)	73(8)	21(7)	20(7)	37(7)
C13	58(8)	134(13)	47(7)	21(8)	8(6)	-24(8)
C14	53(8)	119(10)	51(6)	8(6)	16(5)	25(7)
C15	62(8)	103(10)	103(9)	31(7)	26(7)	20(8)
C16	43(7)	92(9)	108(9)	30(7)	11(6)	-6(7)
C17	36(6)	107(9)	51(6)	4(6)	9(5)	0(6)
C18	50(7)	96(9)	77(7)	32(6)	24(6)	-4(7)
C19	56(7)	87(9)	65(7)	18(6)	1(6)	15(6)
C20	38(7)	83(9)	56(6)	-20(6)	-3(5)	17(7)
C21	37(6)	105(10)	53(7)	16(7)	1(5)	21(6)
C22	67(7)	98(10)	58(7)	11(7)	-1(5)	19(7)
C23	69(7)	63(7)	63(7)	-7(6)	-6(6)	-1(6)
C24	50(7)	86(9)	80(8)	8(8)	16(6)	20(7)
C25	60(7)	87(9)	77(8)	-13(7)	17(6)	20(7)
C26	65(8)	113(10)	59(7)	22(8)	13(6)	15(7)
C27	55(7)	72(9)	75(8)	33(7)	15(6)	8(6)

C28	46(7)	132(10)	56(6)	21(6)	14(5)	16(6)
C29	50(7)	142(11)	137(10)	89(9)	49(7)	47(7)
C30	74(9)	199(15)	135(11)	120(11)	58(8)	68(10)
C31	64(9)	222(17)	124(10)	80(11)	48(8)	19(10)
C32	79(10)	173(13)	123(10)	70(9)	26(8)	38(9)
C33	46(7)	136(10)	85(8)	52(8)	17(6)	28(7)
C34	41(8)	171(15)	174(14)	72(12)	38(9)	46(9)
O50	75(5)	118(7)	62(4)	-9(4)	19(4)	1(5)
N50	75(7)	117(9)	105(8)	-22(7)	2(6)	13(6)
C50	90(10)	128(12)	70(9)	-19(8)	11(7)	-2(9)
C52	116(11)	163(13)	90(9)	52(9)	31(8)	23(10)

Table A1.35: Hydrogen coordinates (x 10^4) and isotropic displacement parameters ($Å^2$ x 10^3) for Pt-PCM-27.

	x	y	z	U(eq)
H3A	287	-1427	3578	98
H4A	221	-2841	3121	107
H5A	662	-3072	2715	109
H6A	1170	-1890	2766	94
H3'A	1872	2083	3334	237
H4'A	1859	3712	3689	220
H5'A	1418	3942	4096	210
H6'A	991	2543	4149	219
H8A	1211	1851	2762	107
H9A	1214	2124	2098	114
H11A	1841	-561	2053	100
H12A	1818	-973	2686	109
H15A	2174	516	3384	106
H16A	2706	-369	3667	97

H18A	2117	-3022	3887	87
H19A	1591	-2166	3612	84
H22A	1002	-1870	4055	91
H23A	1156	-2746	4646	80
H25A	1161	225	5167	89
H26A	975	1066	4558	95
H29A	235	32	4191	127
H30A	-317	1027	4198	158
H32A	-75	3075	3363	149
H33A	485	2039	3359	106
H50A	2058	-1332	322	115
H51A	2113	-2451	-171	191
H51B	2334	-1912	-482	191
H51C	1898	-2069	-578	191
H52A	1995	847	-307	182
H52B	1788	99	-646	182
H52C	2226	219	-591	182
H10B	1958	5677	5400	137
H10C	2076	6830	5251	248
H10D	1930	7176	4817	248
H10E	2357	6929	4948	248
H10F	2023	4349	4531	163
H10G	2318	5264	4458	163
H10H	1890	5491	4328	163

Appendix II: NMR Spectra

SYNTHESIS OF TCTPOH_3 AND TCTP$^+H_3$ LIGANDS

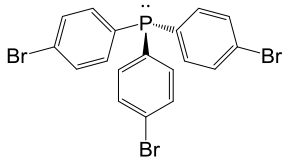

ttpBr$_3$

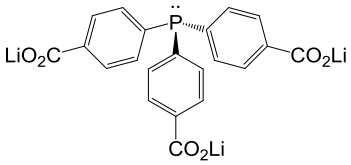

tctpLi$_3$

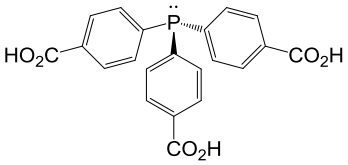

tctpH$_3$

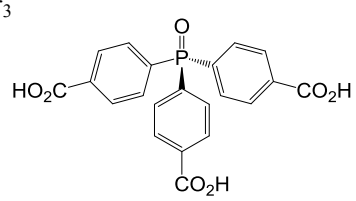

tctpoH$_3$

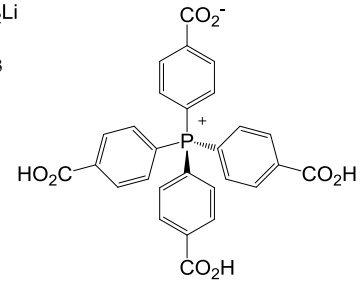

tctp$^+H_3$

^{1}H NMR spectra

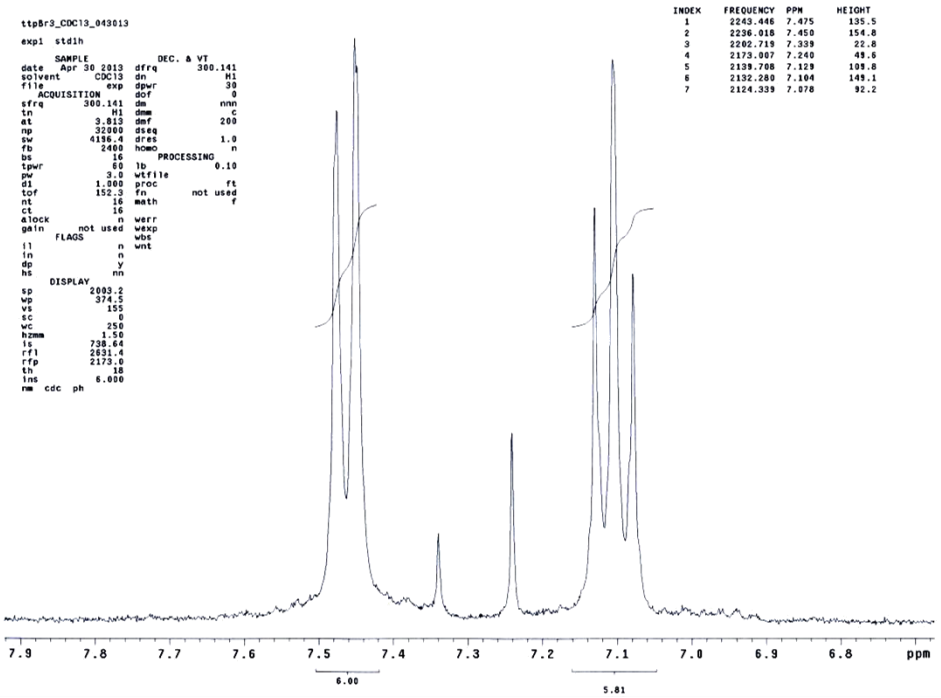

Figure A2.1: ^{1}H NMR spectrum of the ttpBr$_3$ ligand.

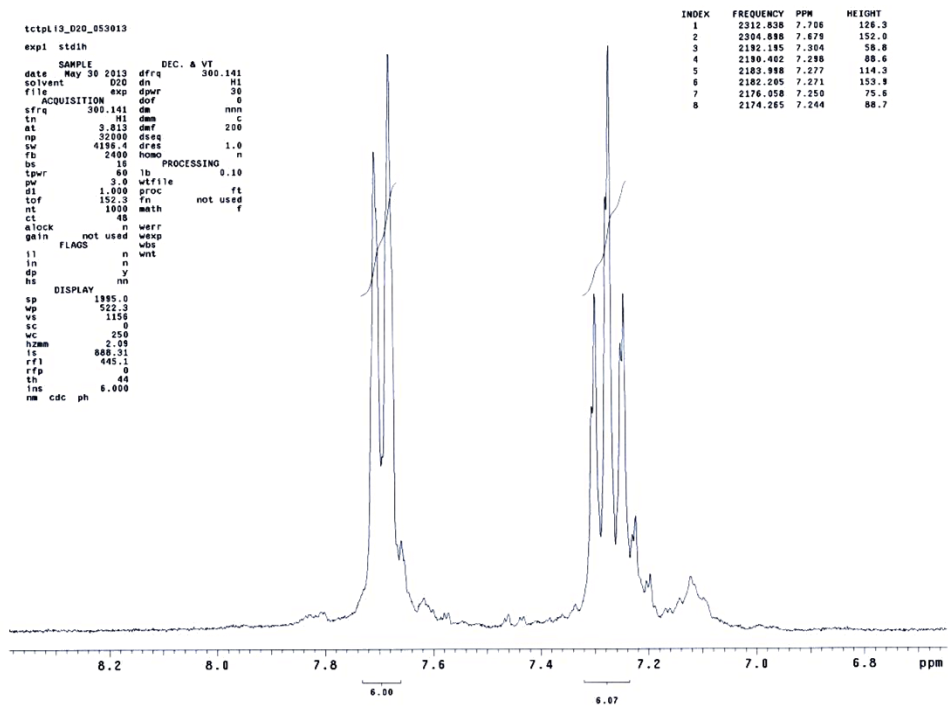

Figure A2.2: ^{1}H NMR spectrum of the tctpLi_3 ligand.

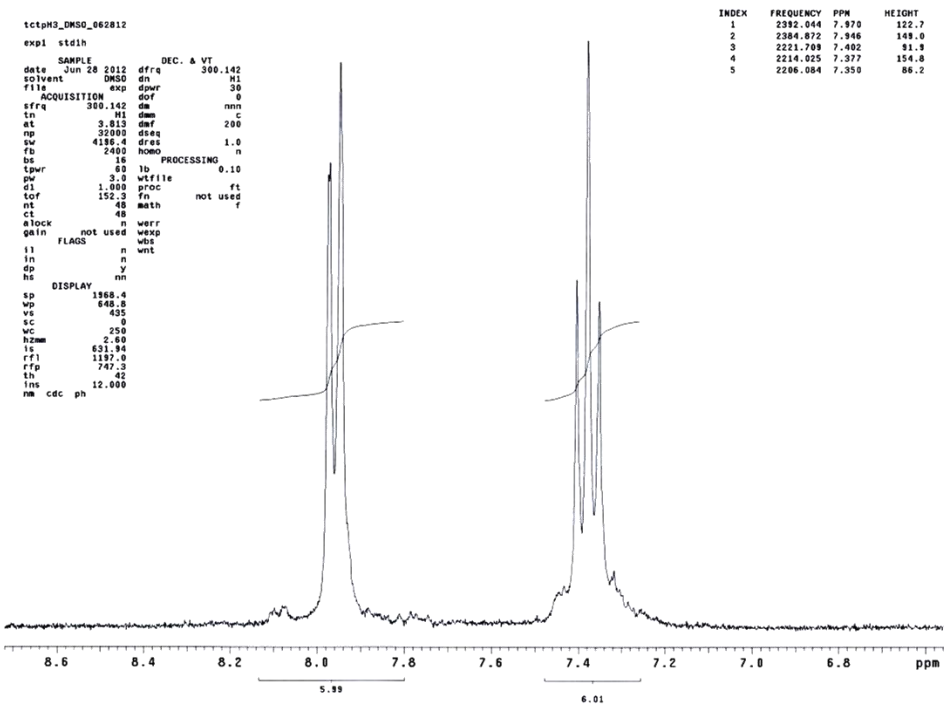

Figure A2.3: ^{1}H NMR spectrum of the tctpH_3 ligand.

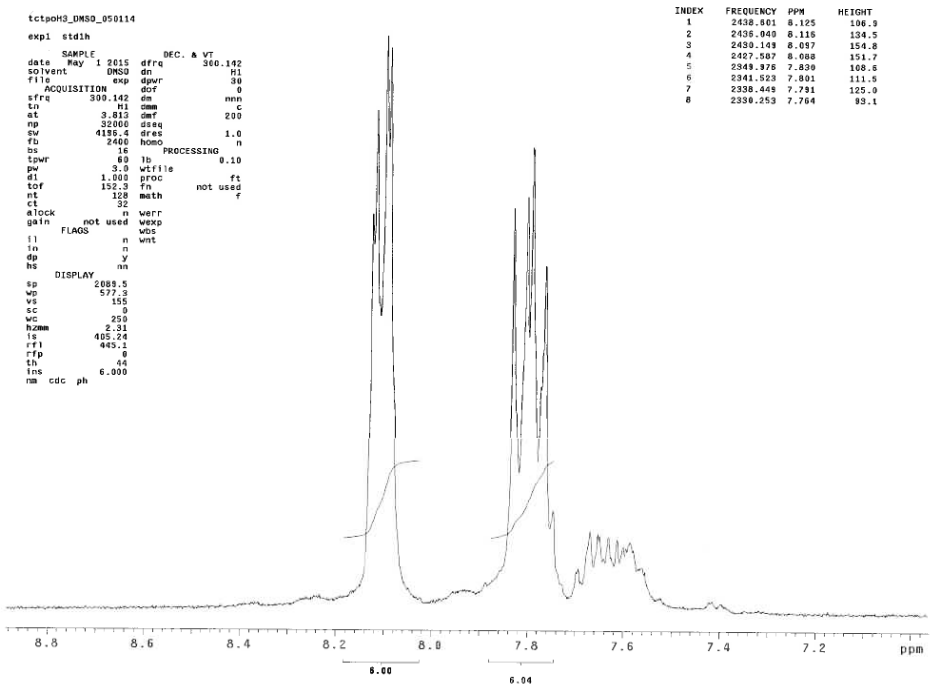

Figure A2.4: ^{1}H NMR spectrum of the tctpoH_3 ligand.

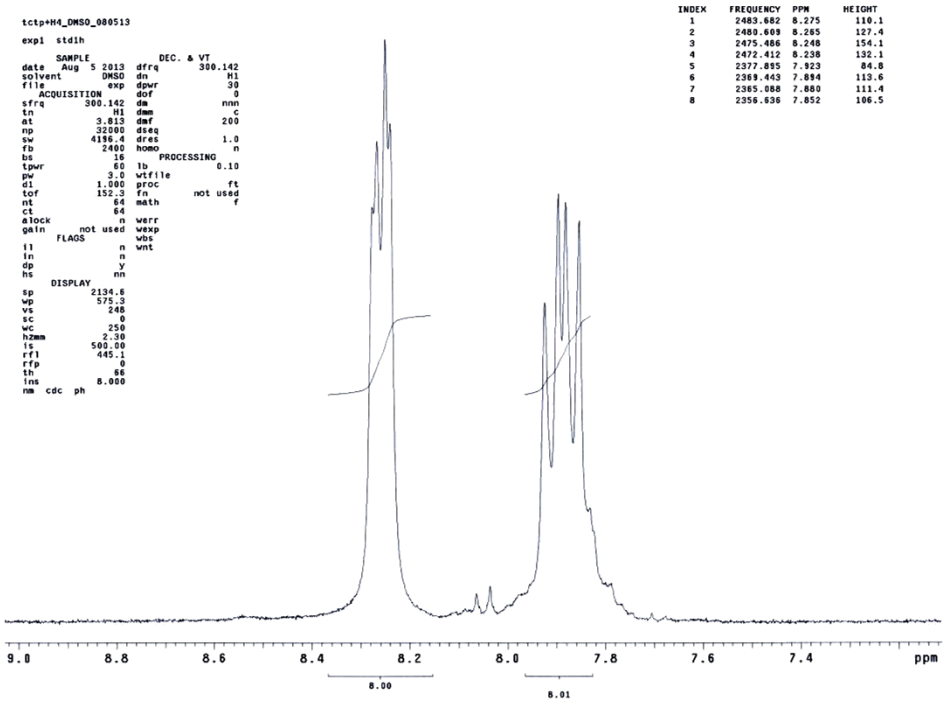

Figure A2.5: ^{1}H NMR spectrum of the tctp$^{+}H_3$ ligand.

$^{13}C\{^{1}H\}$ NMR spectra

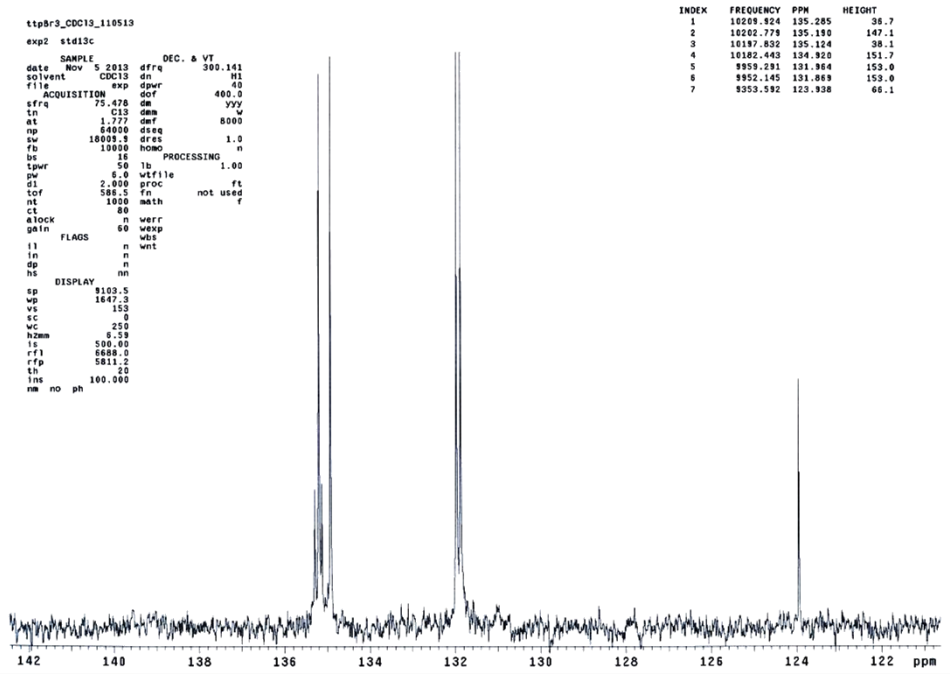

Figure A2.6: $^{13}C\{^{1}H\}$ NMR spectrum of $ttpBr_3$ ligand.

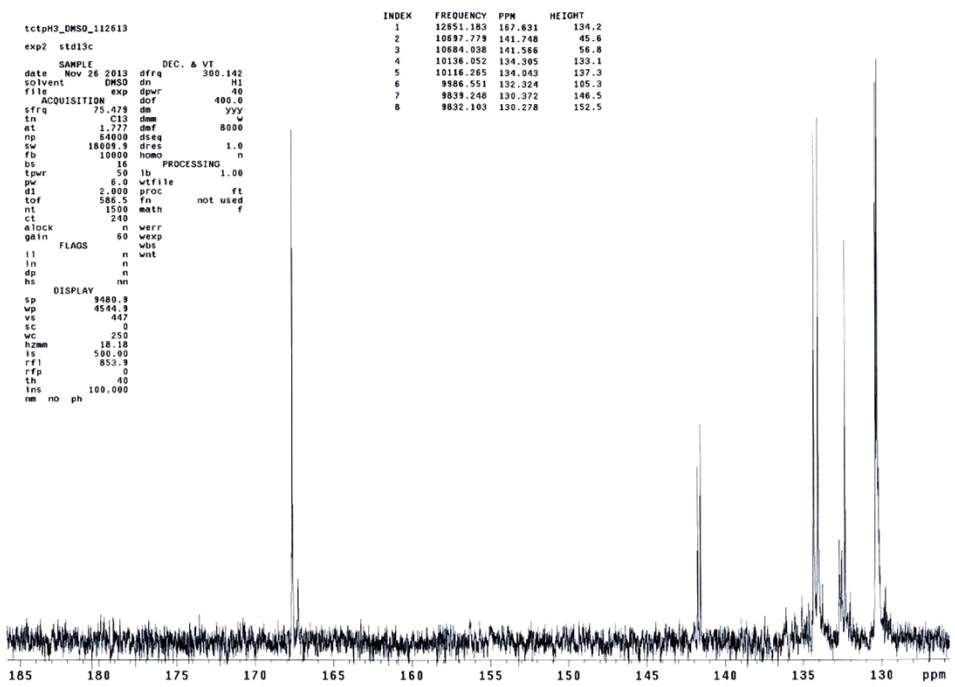

Figure A2.7: $^{13}C\{^{1}H\}$ NMR spectrum of the $tctpH_3$ ligand.

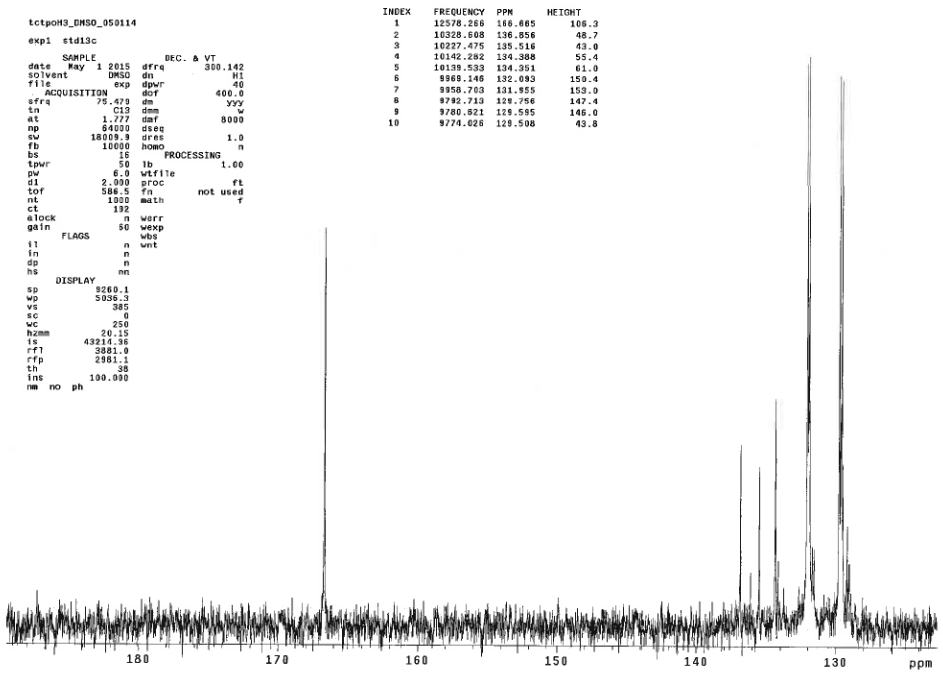

Figure A2.8: $^{13}C\{^{1}H\}$ NMR spectrum of the tctpoH_3 ligand.

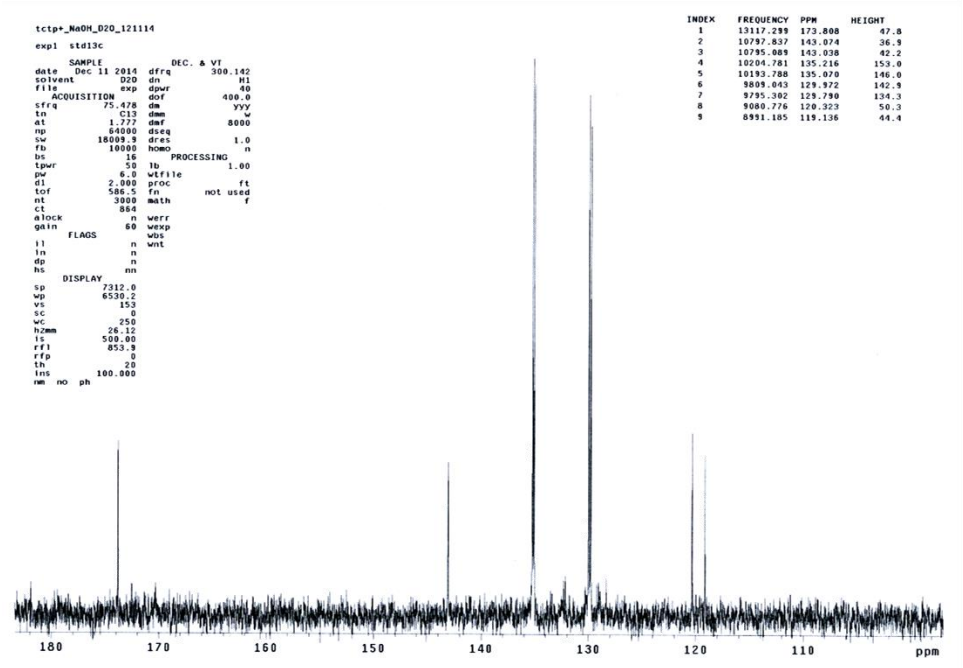

Figure A2.9: $^{13}C\{^{1}H\}$ NMR spectrum of the $[tctp^{+}]^{3-}$ ligand.

$^{31}P\{^{1}H\}$ NMR spectra

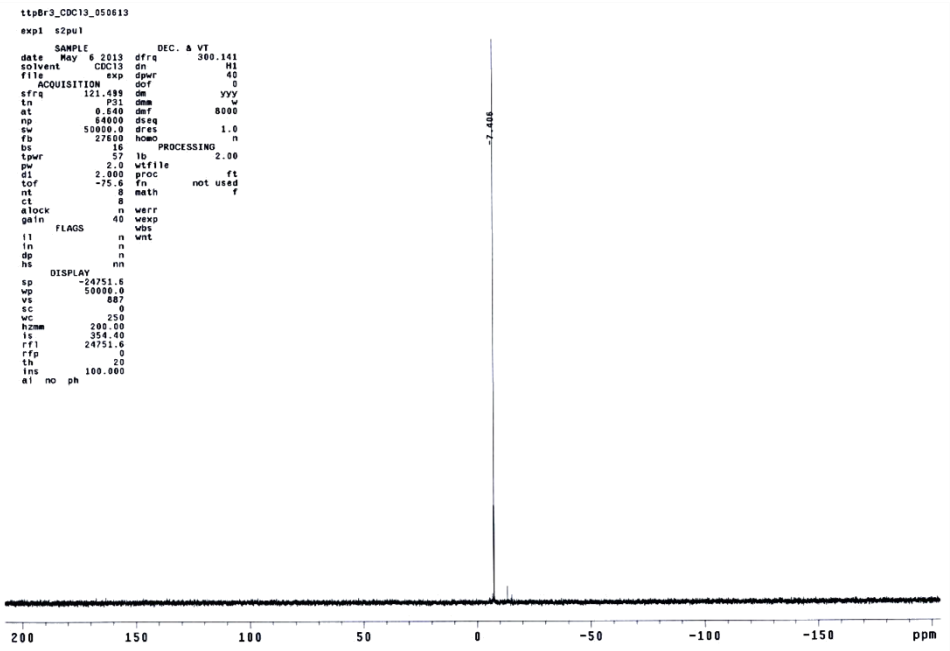

Figure A2.10: $^{31}P\{^{1}H\}$ NMR spectrum of the $ttpBr_3$ ligand.

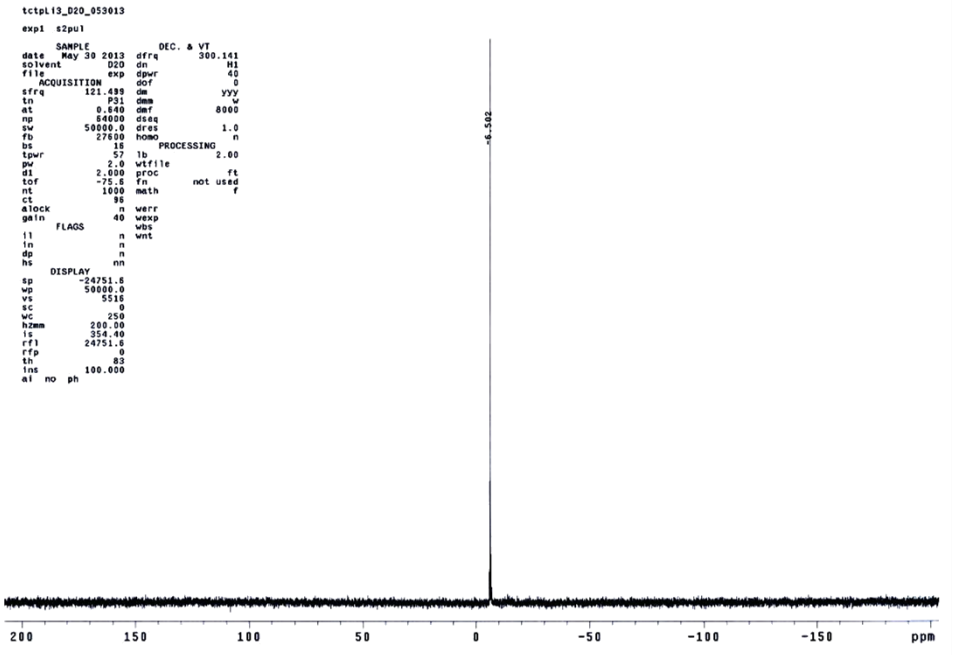

Figure A2.11: $^{31}P\{^{1}H\}$ NMR spectrum of the $tctpLi_3$ ligand.

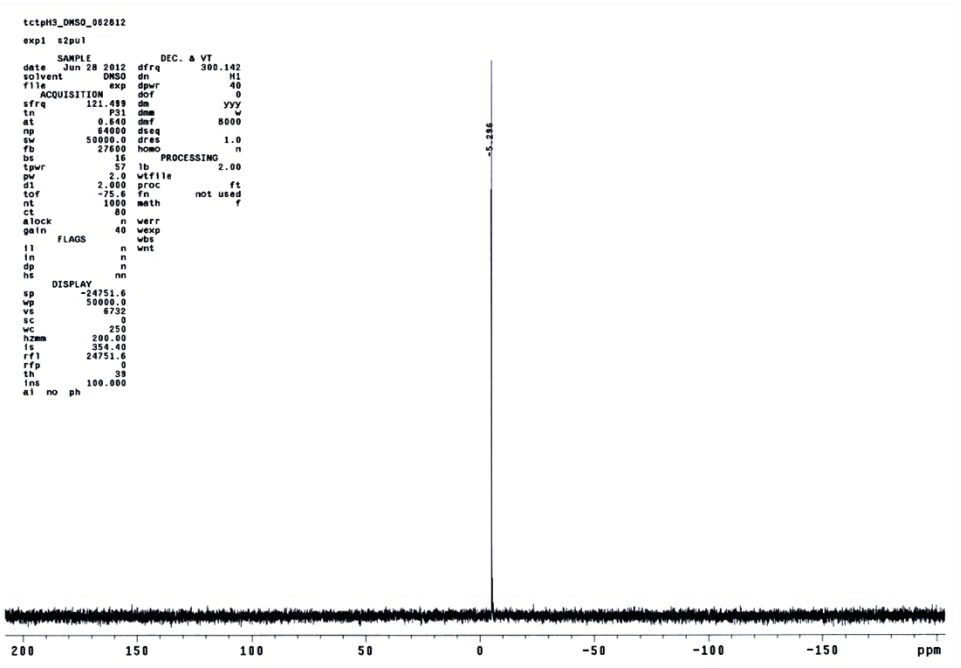

Figure A2.12: $^{31}P\{^{1}H\}$ NMR spectrum of the $tctpH_3$ ligand.

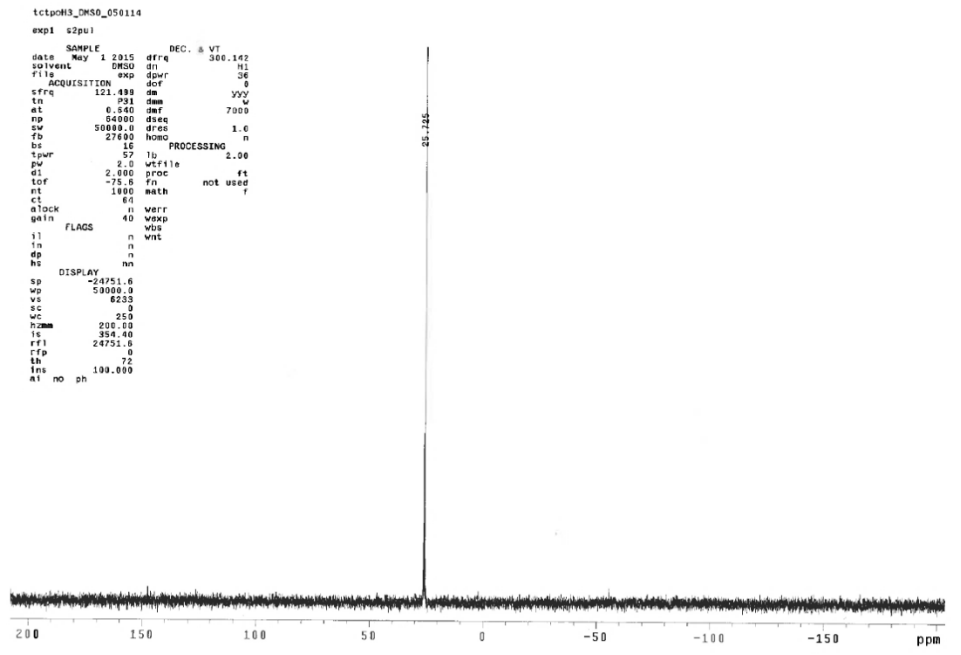

Figure A2.13: $^{31}P\{^{1}H\}$ NMR spectrum of the $tctpoH_3$ ligand.

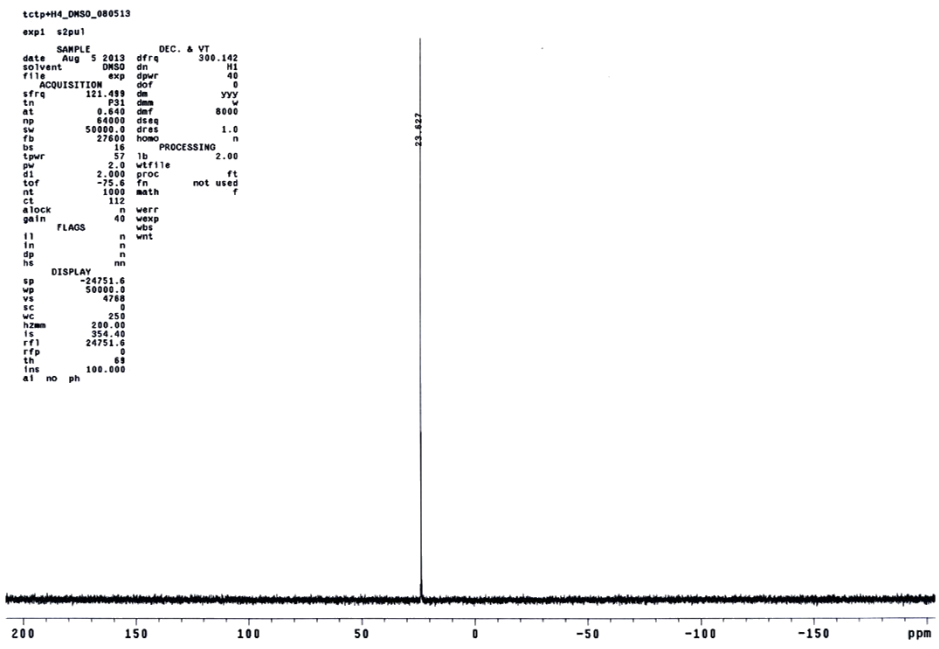

Figure A2.14: $^{31}P\{^{1}H\}$ NMR spectrum of the $tctp^{+}H_3$ ligand.

SYNTHESIS OF BBCB-MCL$_2$ (M = PD, PT) COMPLEXES

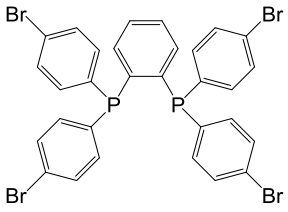

BBCB-Br$_4$

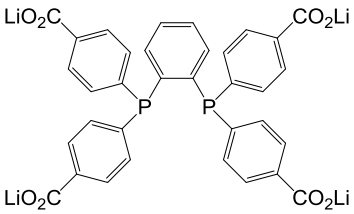

BBCB-Li$_4$

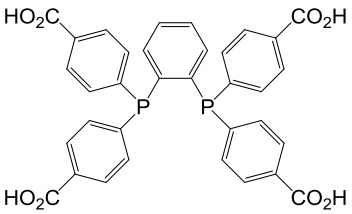

BBCB

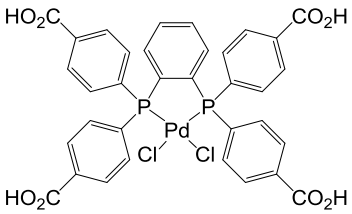

BBCB-PdCl$_2$

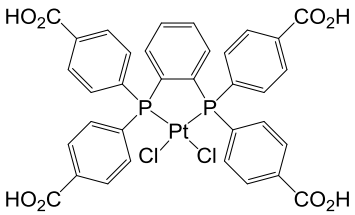

BBCB-PtCl$_2$

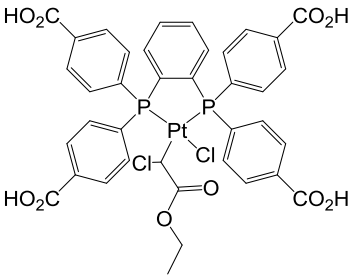

BBCB-PtCl(CHClCO$_2$C$_2$H$_5$)

^{1}H NMR spectra

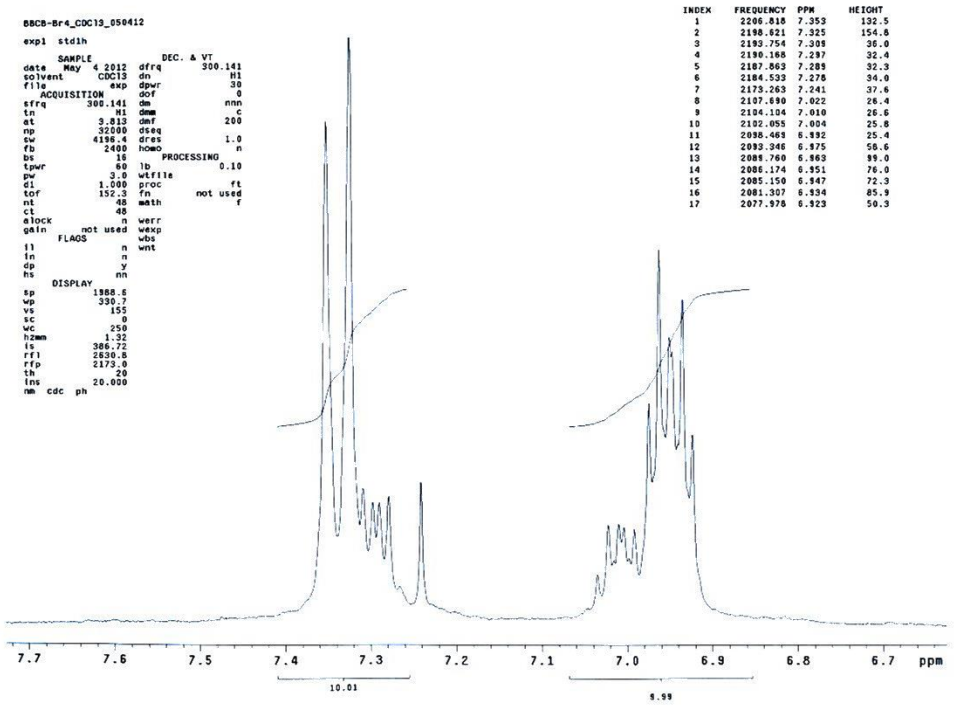

Figure A2.15: ^{1}H NMR spectrum of the BBCB-Br$_4$ ligand.

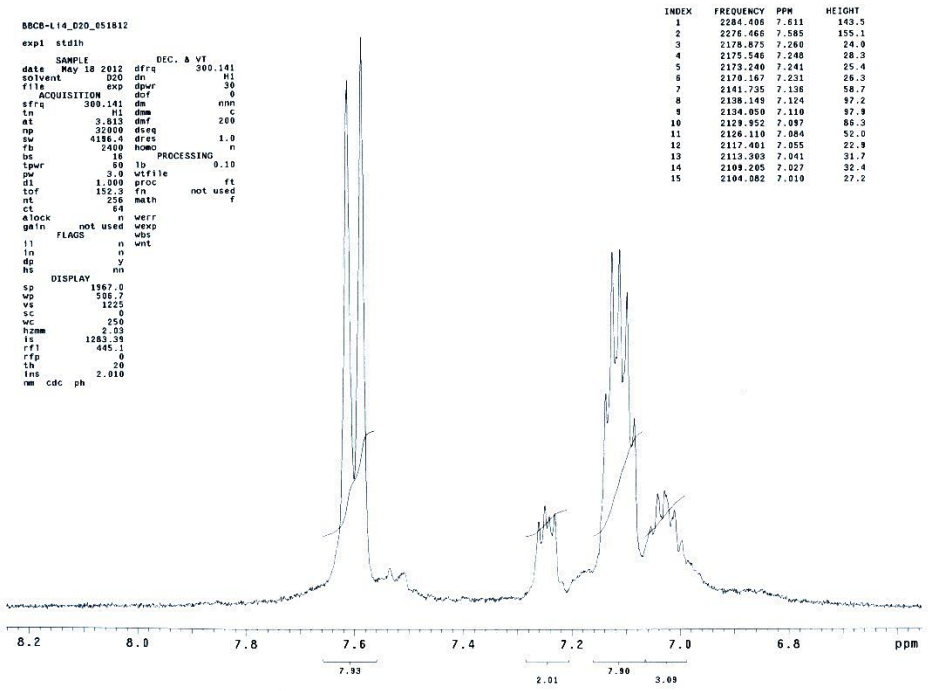

Figure A2.16: ^{1}H NMR spectrum of BBCB-Li_4 ligand.

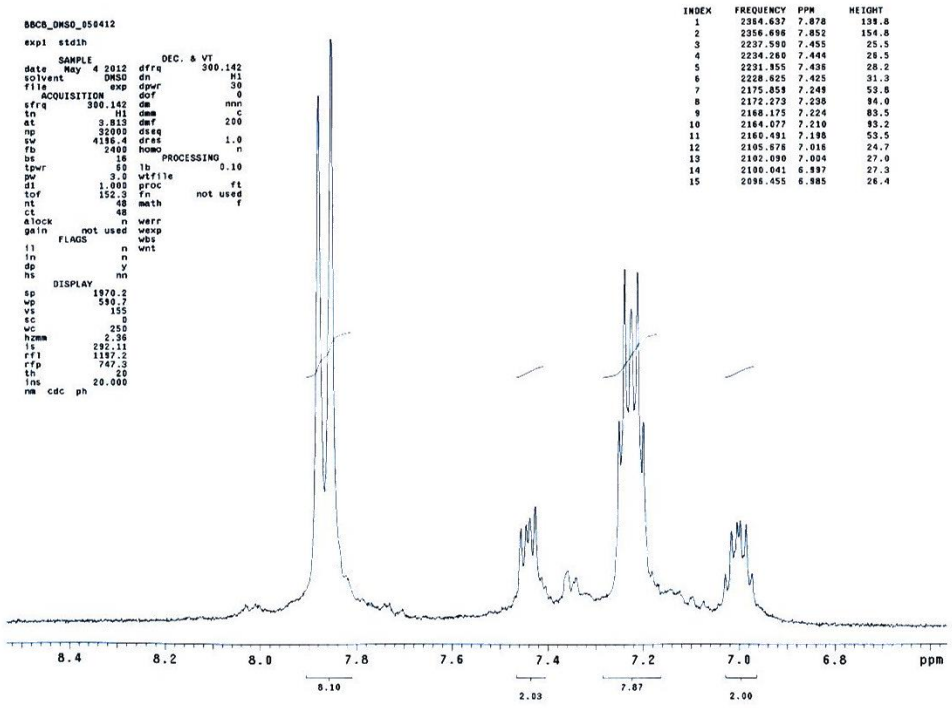

Figure A2.17: ^{1}H NMR spectrum of BBCB ligand.

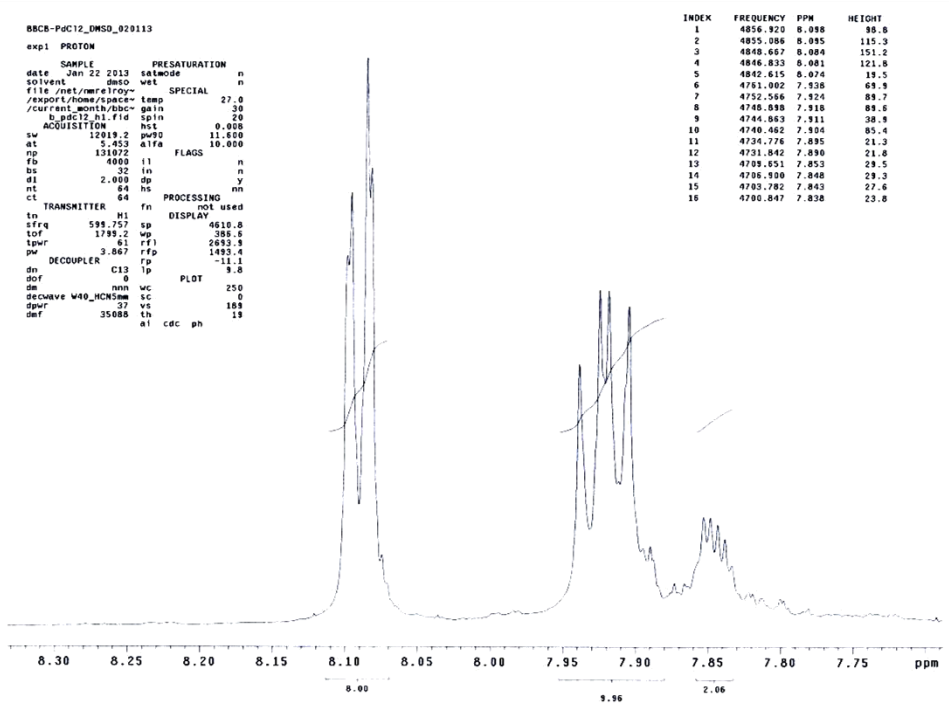

Figure A2.18: ^{1}H NMR spectrum of the BBCB-$PdCl_2$ complex.

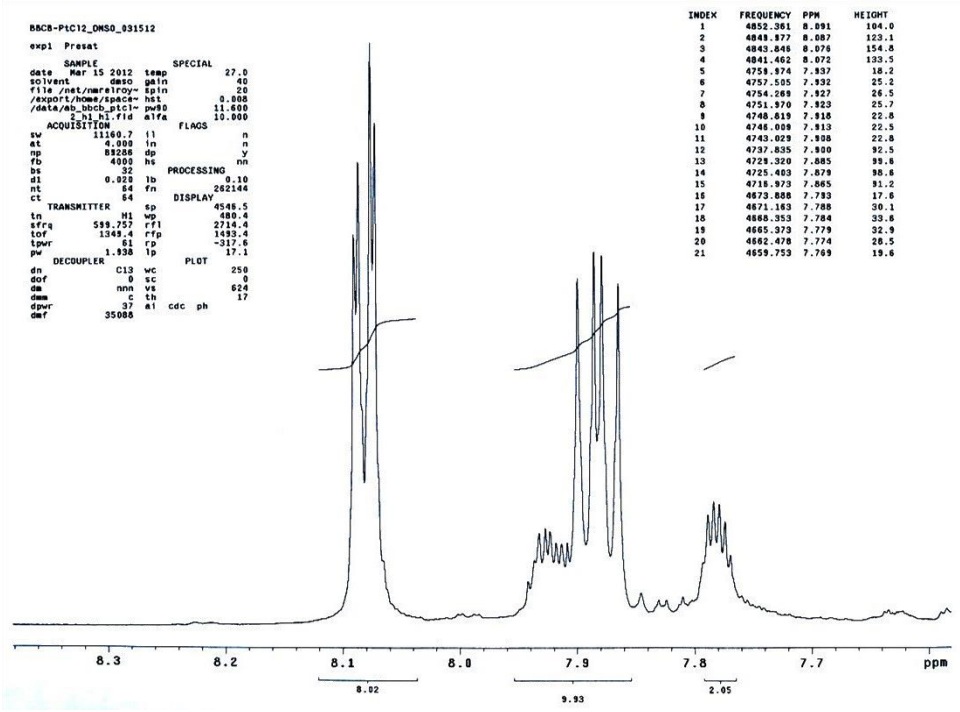

Figure A2.19: ^{1}H NMR spectrum of the BBCB-$PtCl_2$ complex.

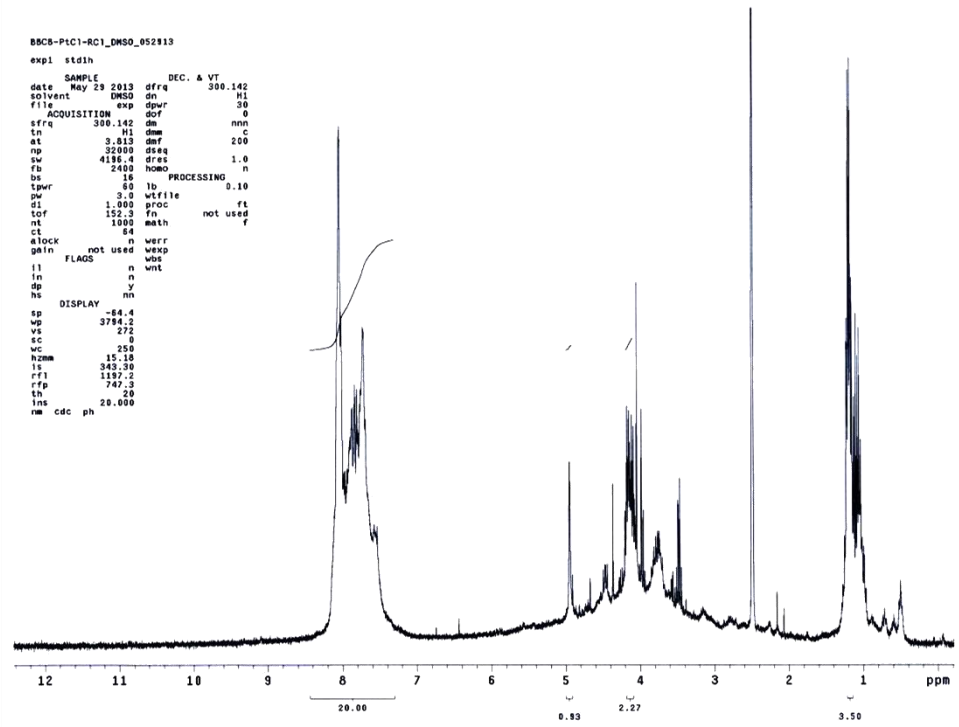

Figure A2.20: ^{1}H NMR spectrum of the BBCB-PtCl($CHClCO_2C_2H_5$) complex.

$^{13}C\{^{1}H\}$ NMR spectra

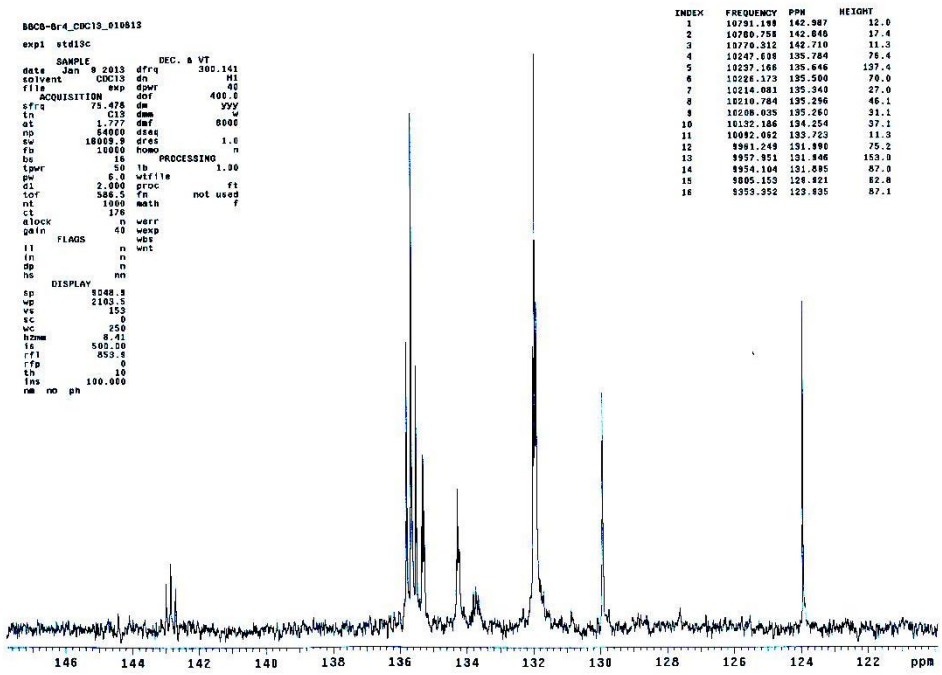

Figure A2.21: $^{13}C\{^{1}H\}$ NMR spectrum of the BBCB-Br_4 ligand.

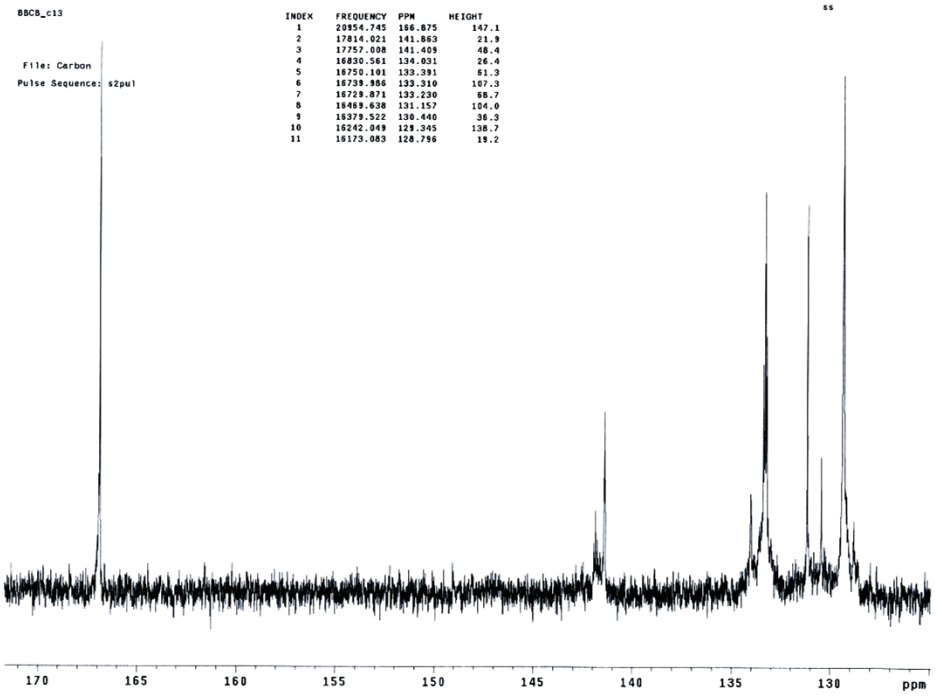

Figure A2.22: $^{13}C\{^{1}H\}$ NMR spectrum of the BBCB-Li_4 ligand.

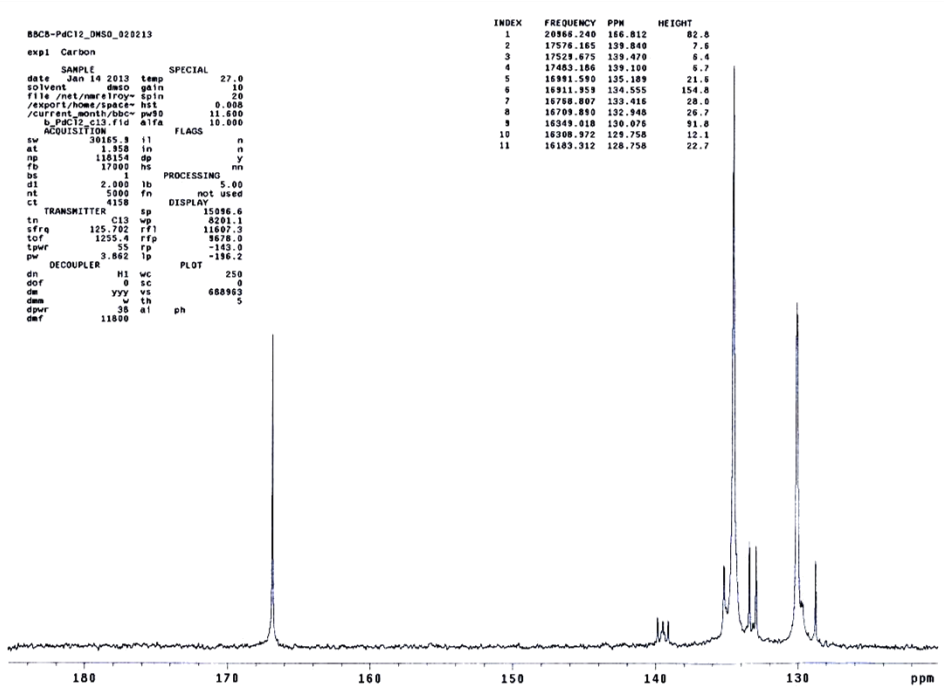

Figure A2.23: $^{13}C\{^{1}H\}$ NMR spectrum of the BBCB-$PdCl_2$ complex.

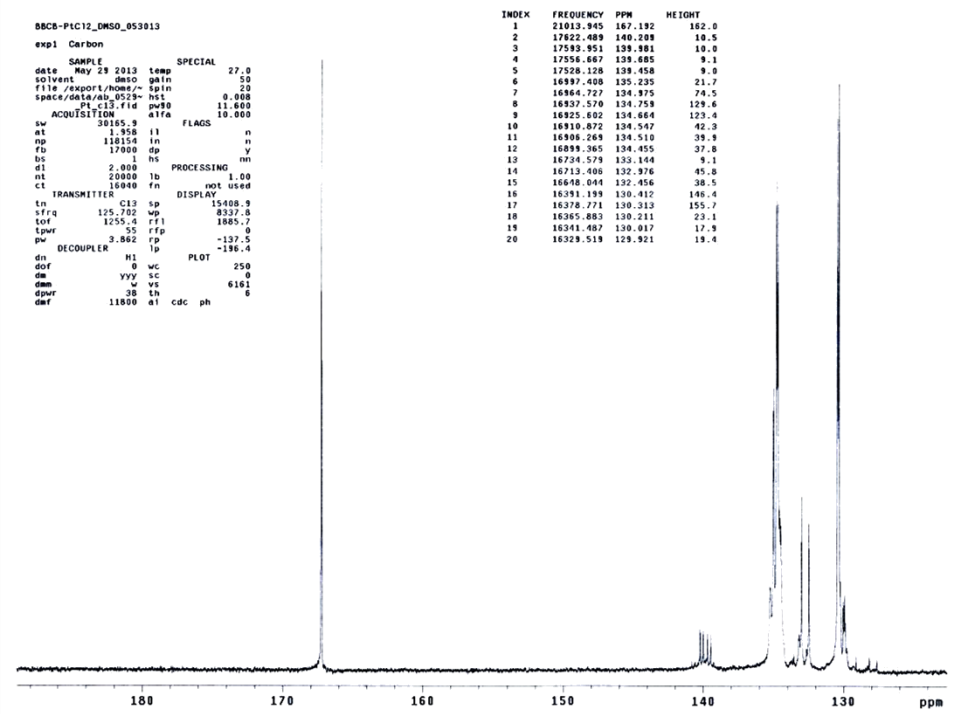

Figure A2.24: $^{13}C\{^{1}H\}$ NMR spectrum of the BBCB-$PtCl_2$ complex.

$^{31}P\{^{1}H\}$ NMR spectra

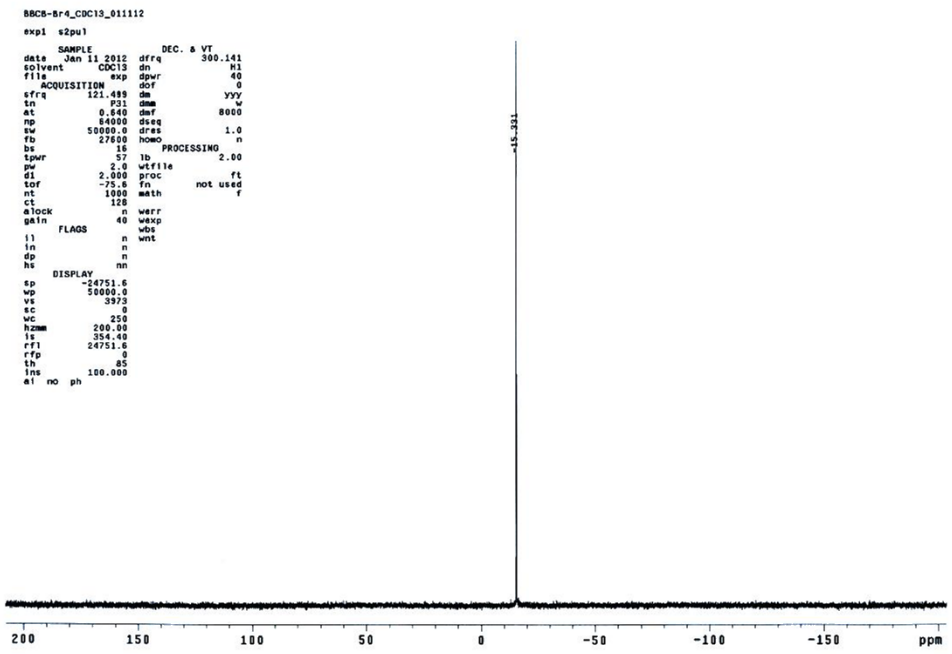

Figure A2.25: $^{31}P\{^{1}H\}$ NMR spectrum of the BBCB-Br_4 ligand.

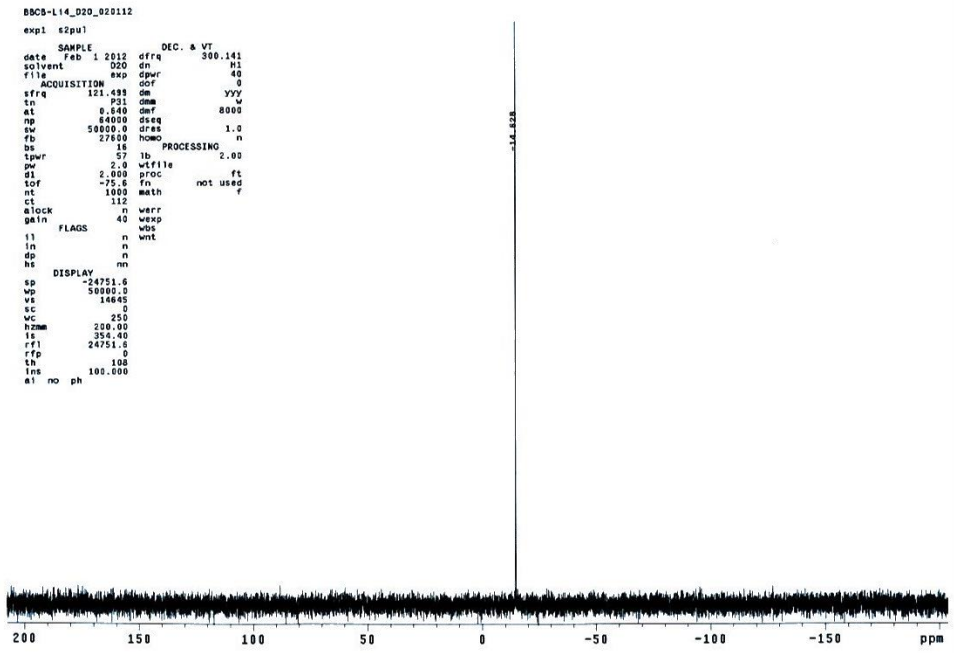

Figure A2.26: $^{31}P\{^{1}H\}$ NMR spectrum of the BBCB-Li_4 ligand.

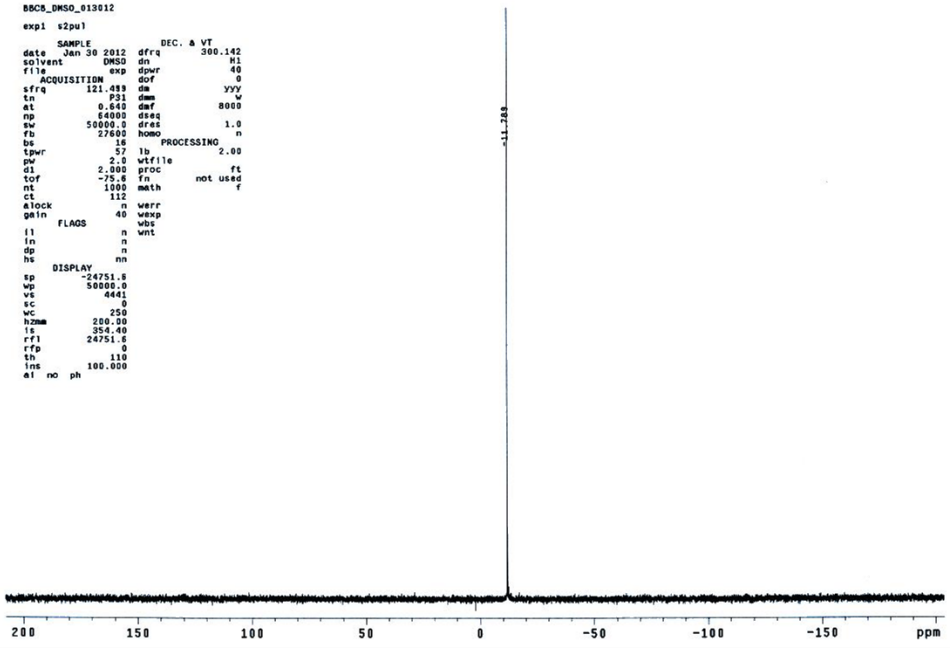

Figure A2.27: $^{31}P\{^{1}H\}$ NMR spectrum of the BBCB ligand.

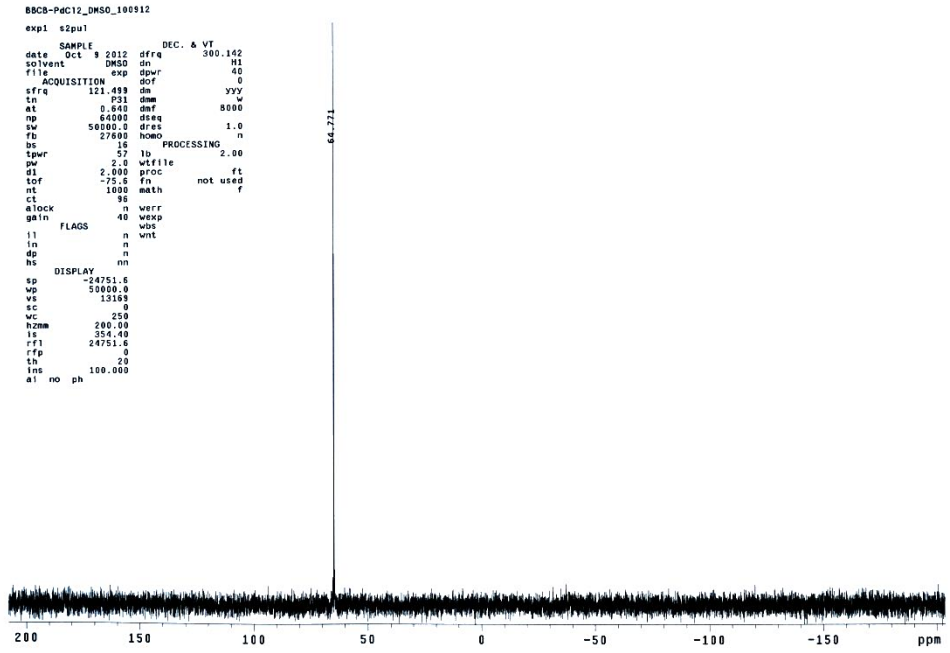

Figure A2.28: $^{31}P\{^{1}H\}$ NMR spectrum of the BBCB-$PdCl_2$ complex.

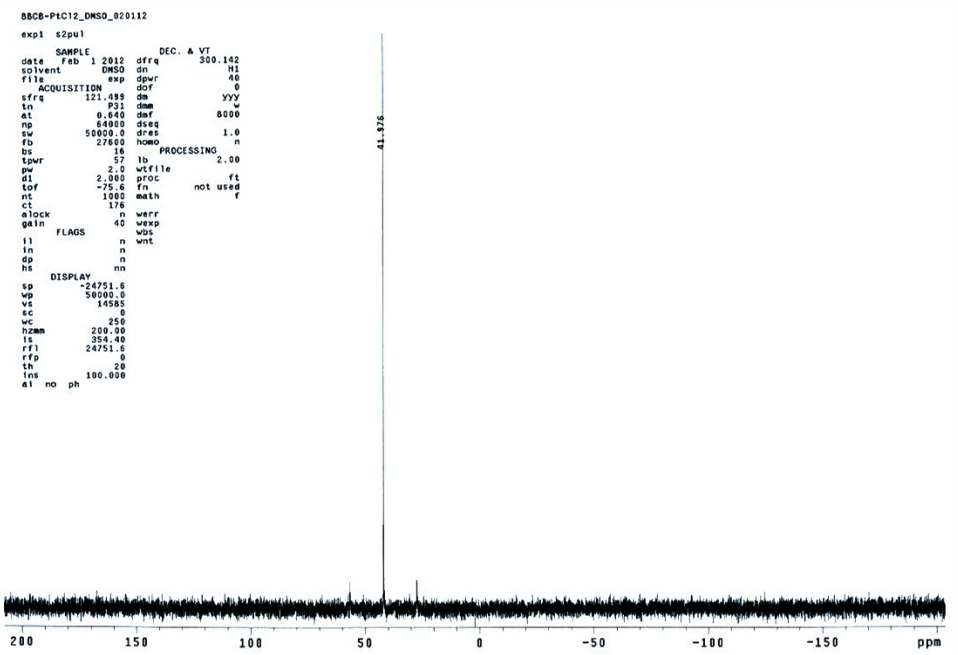

Figure A2.29: $^{31}P\{^{1}H\}$ NMR spectrum of the BBCB-$PtCl_2$ complex.

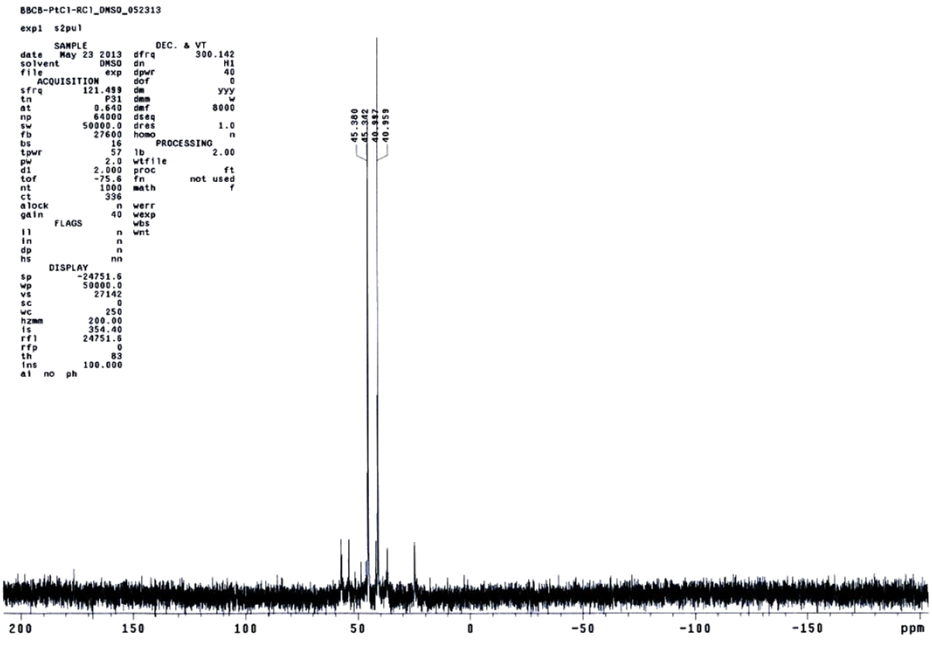

Figure A2.30: $^{31}P\{^{1}H\}$ NMR spectrum of the BBCB-PtCl($CHClCO_2C_2H_5$) complex.

Appendix III: FTIR Spectra

PHOSPHINE PRECURSORS

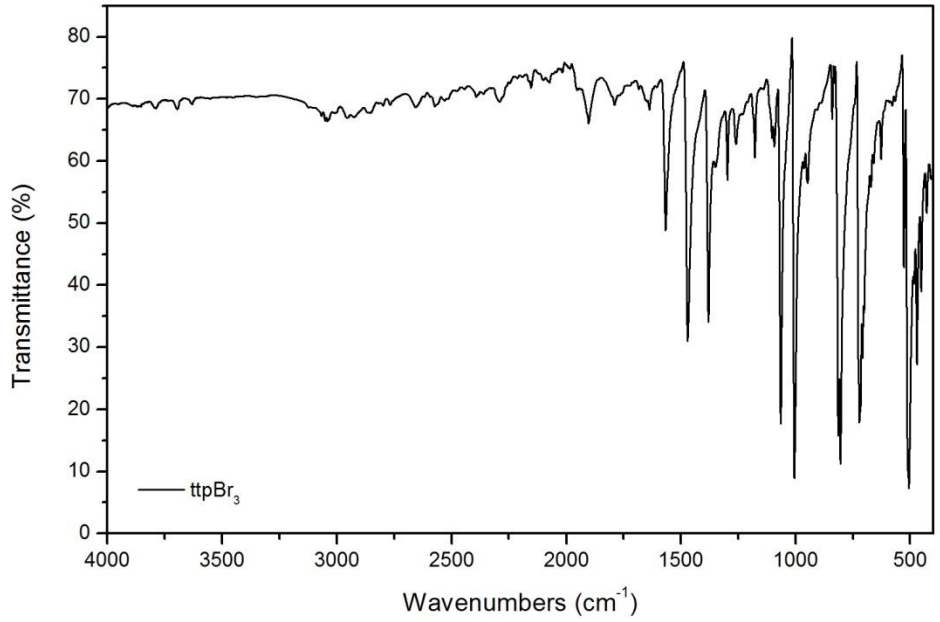

Figure A3.1: FTIR of the $ttpBr_3$ ligand.

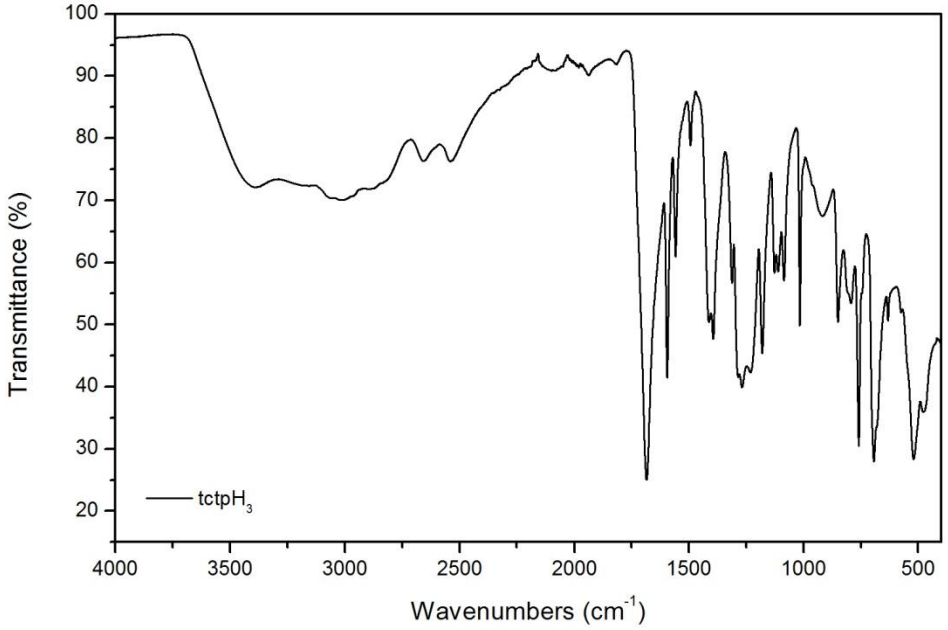

Figure A3.2: FTIR of the $tctpH_3$ ligand.

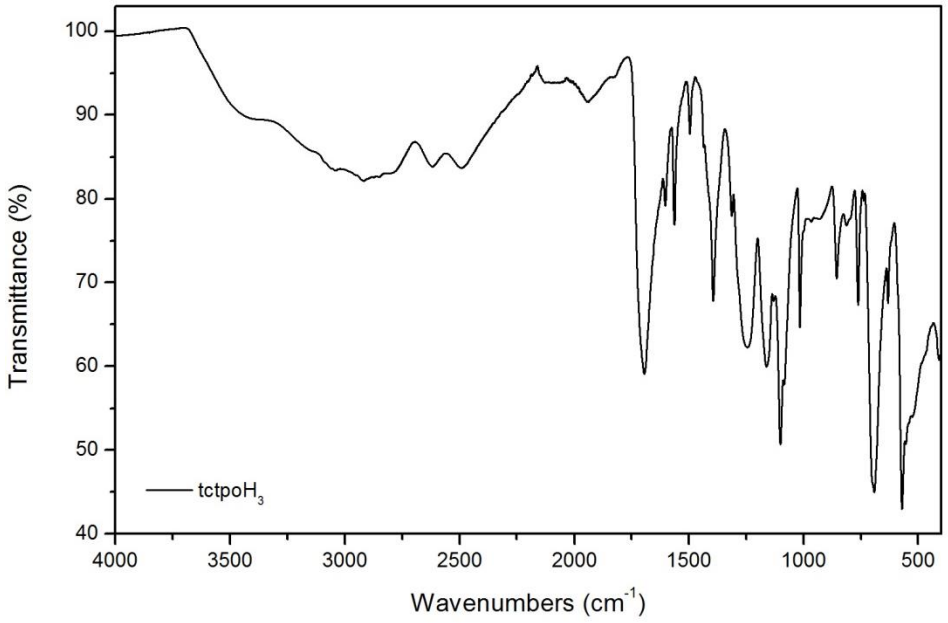

Figure A3.3: FTIR of the tctpoH_3 ligand.

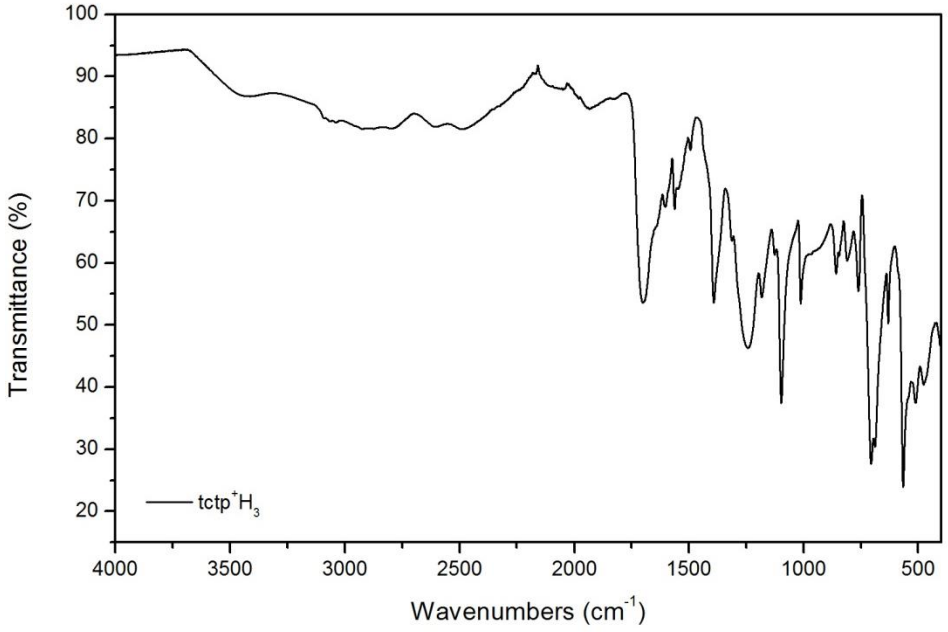

Figure A3.4: FTIR of the tctp$^{+}H_3$ ligand.

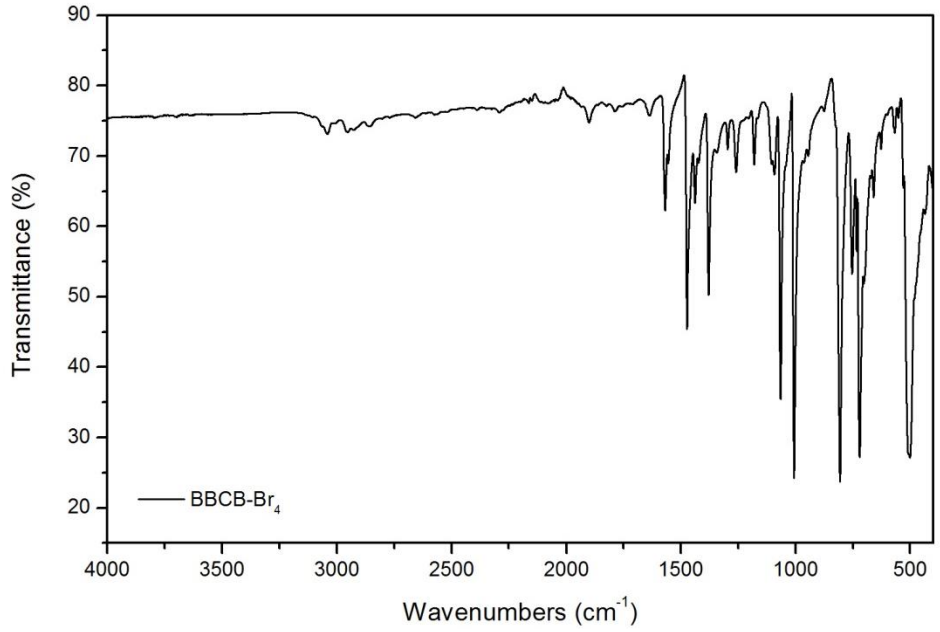

Figure A3.5: FTIR of the BBCB-Br_4 ligand.

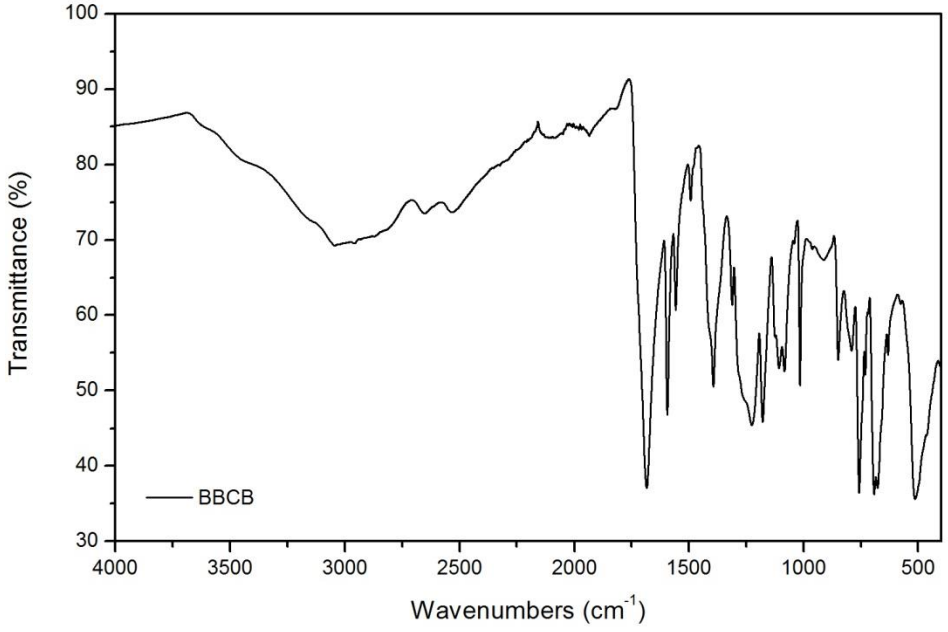

Figure A3.6: FTIR of the BBCB ligand.

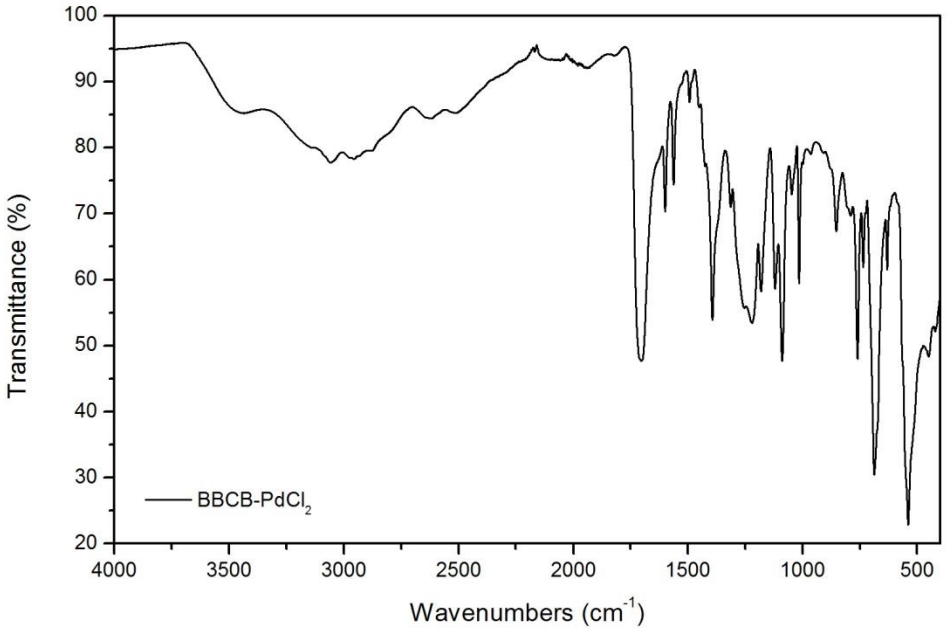

Figure A3.7: FTIR of the BBCB-$PdCl_2$ complex.

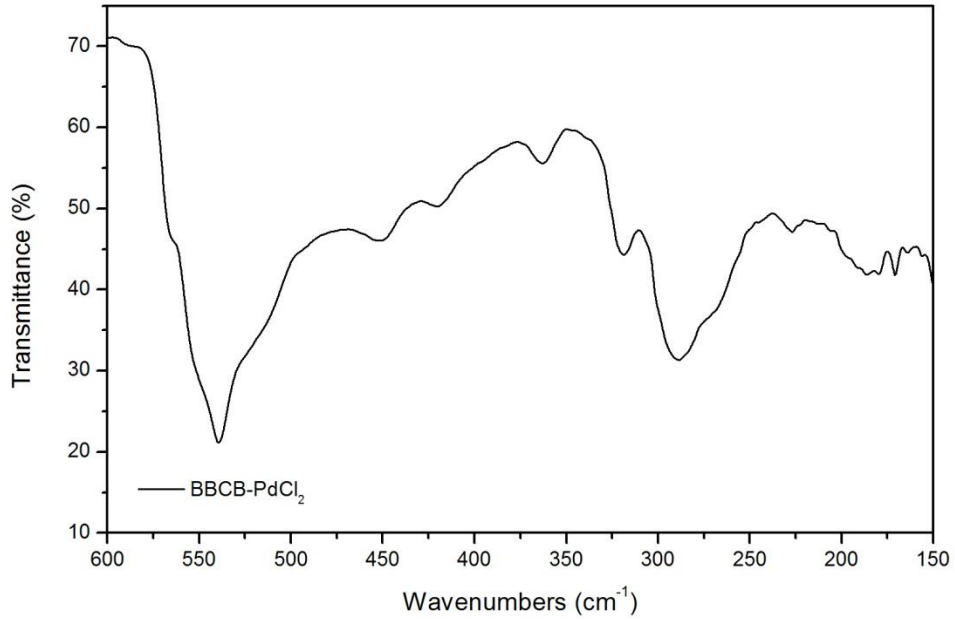

Figure A3.8: Far-IR of the BBCB-$PdCl_2$ complex.

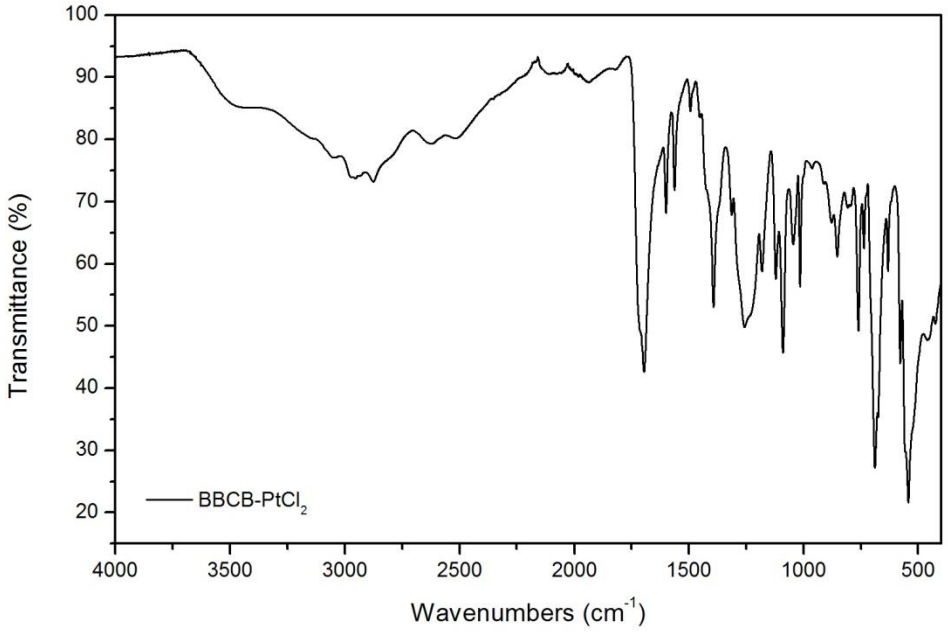

Figure A3.9: FTIR of the BBCB-$PtCl_2$ complex.

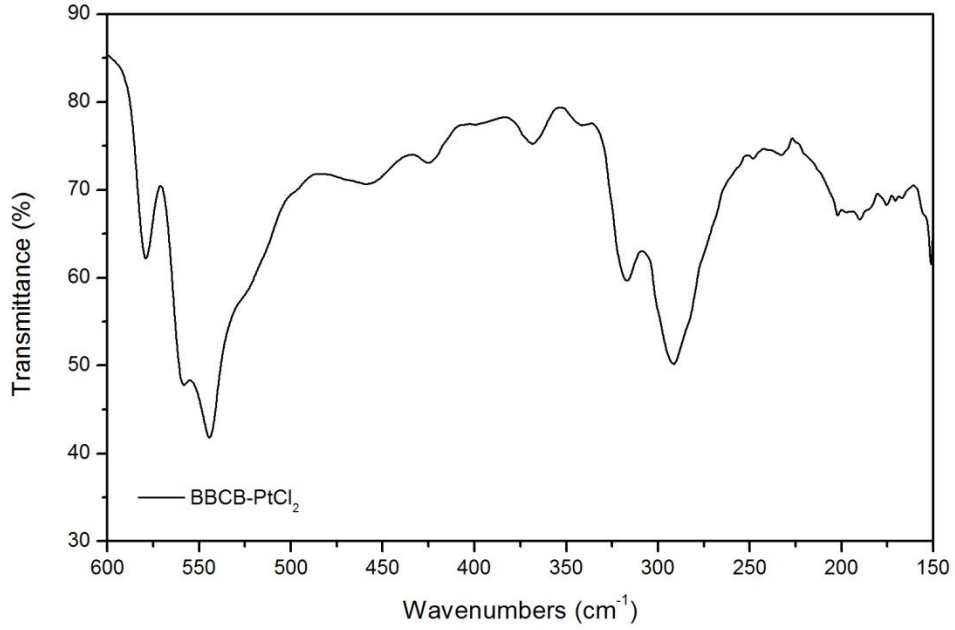

Figure A3.10: Far-IR of the BBCB-$PtCl_2$ complex.

PCMs

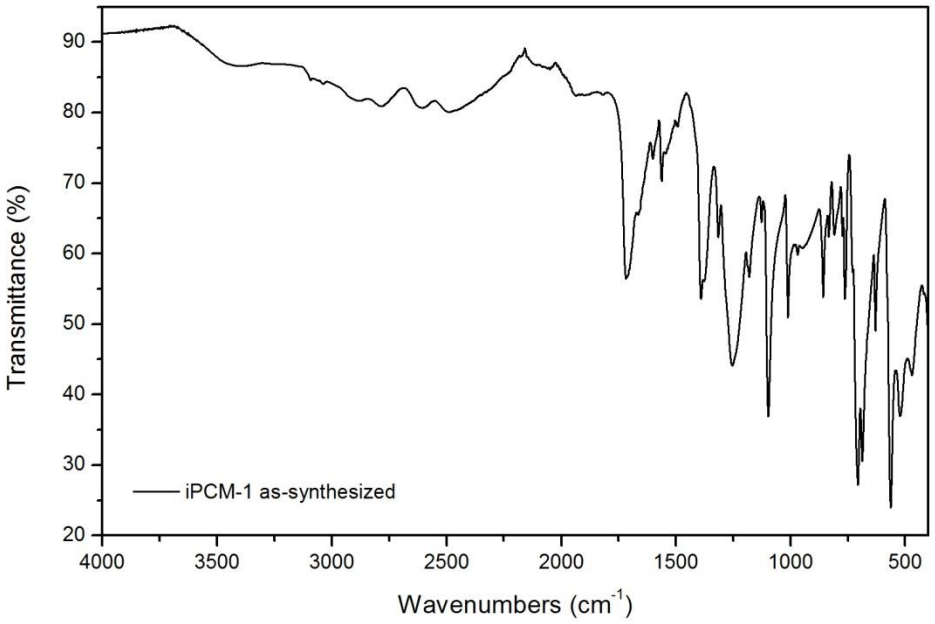

Figure A3.11: FTIR of as-synthesized iPCM-1.

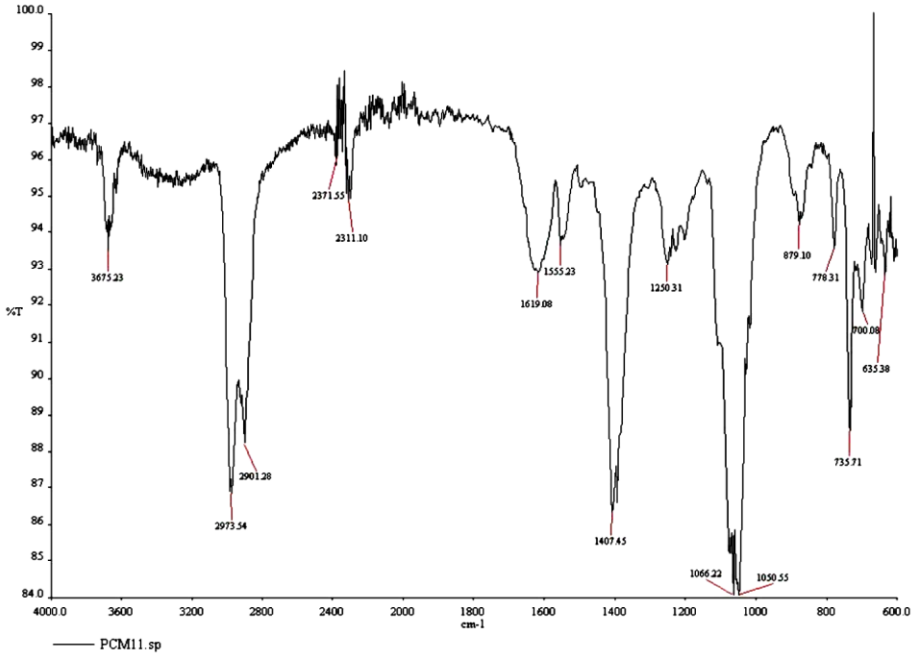

Figure A3.12: FTIR of as-synthesized PCM-11.

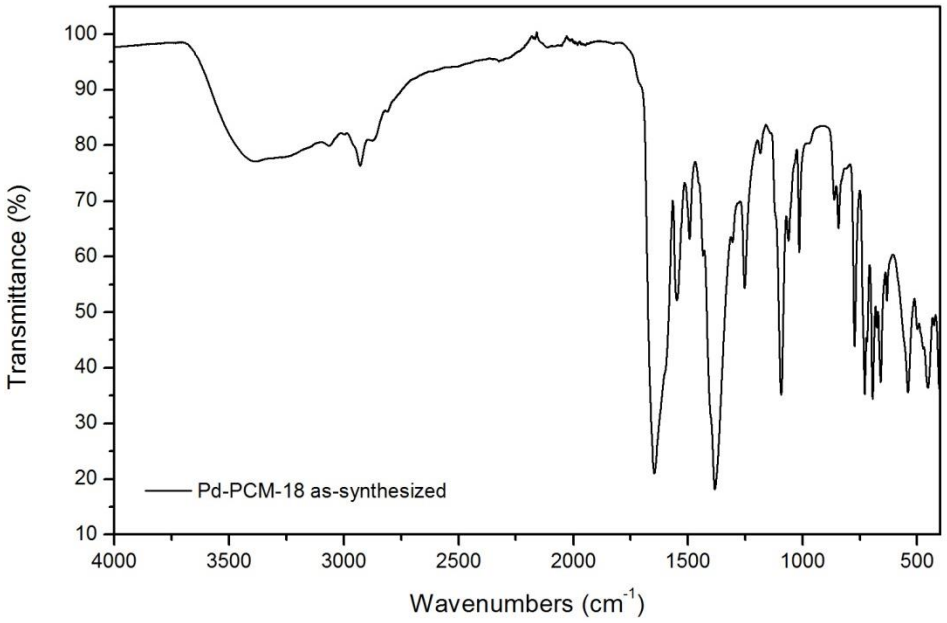

Figure A3.13: FTIR of as-synthesized Pd-PCM-18.

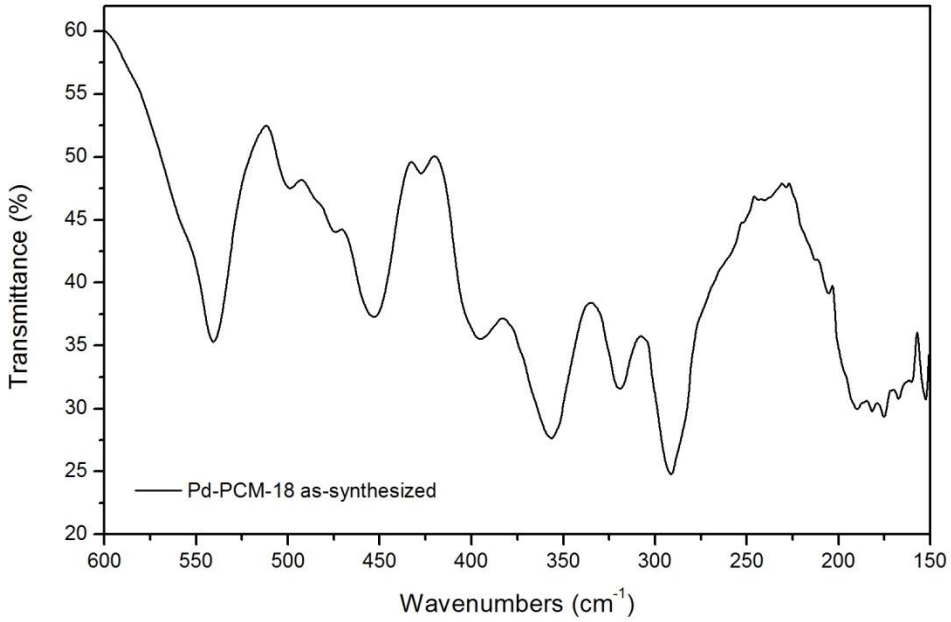

Figure A3.14: Far-IR of as-synthesized Pd-PCM-18.

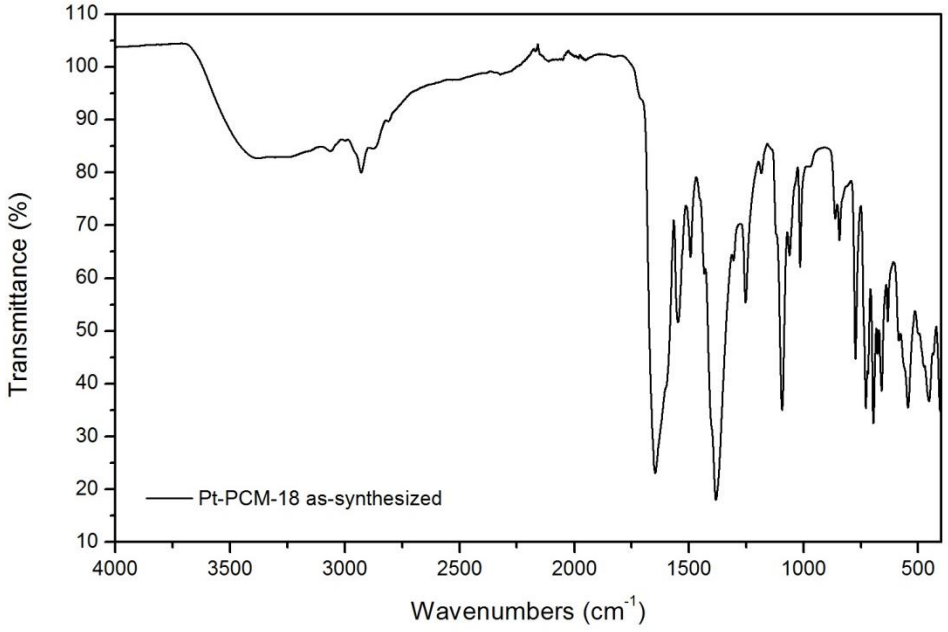

Figure A3.15: FTIR of as-synthesized Pt-PCM-18.

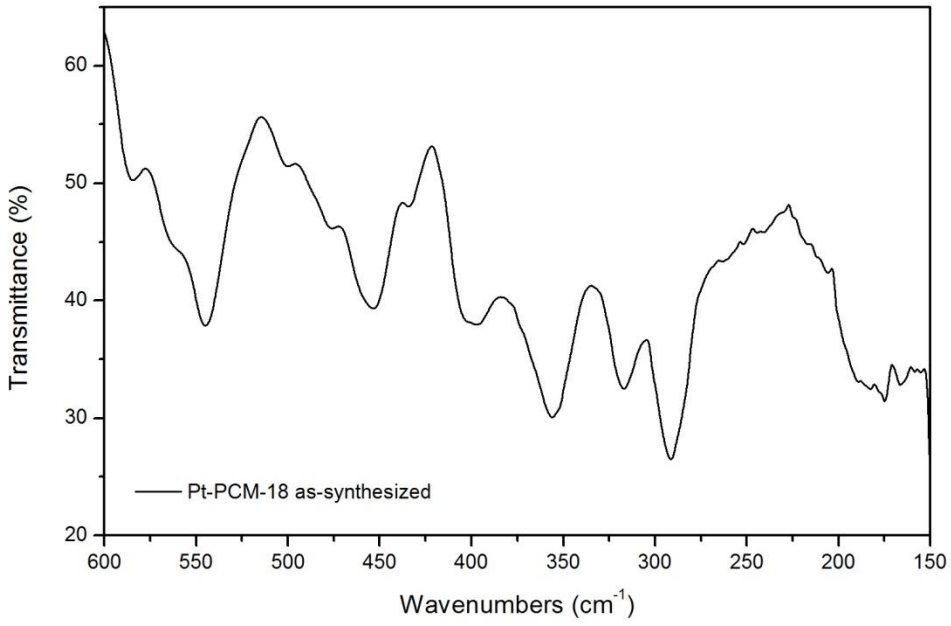

Figure A3.16: Far-IR of as-synthesized Pt-PCM-18.

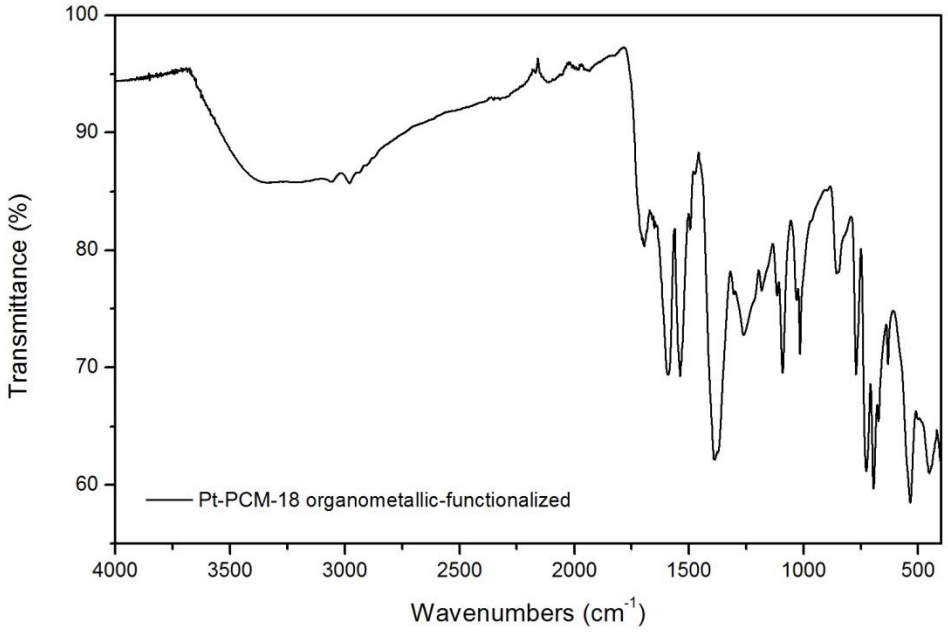

Figure A3.17: FTIR of organometallic-functionalized Pt-PCM-18.

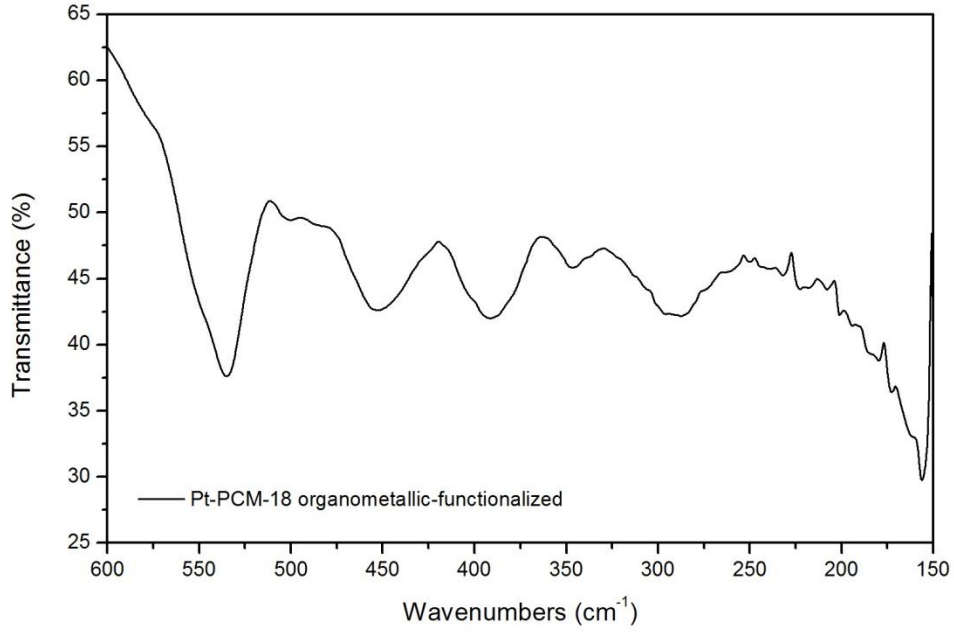

Figure A3.18: Far-IR of organometallic-functionalized Pt-PCM-18.

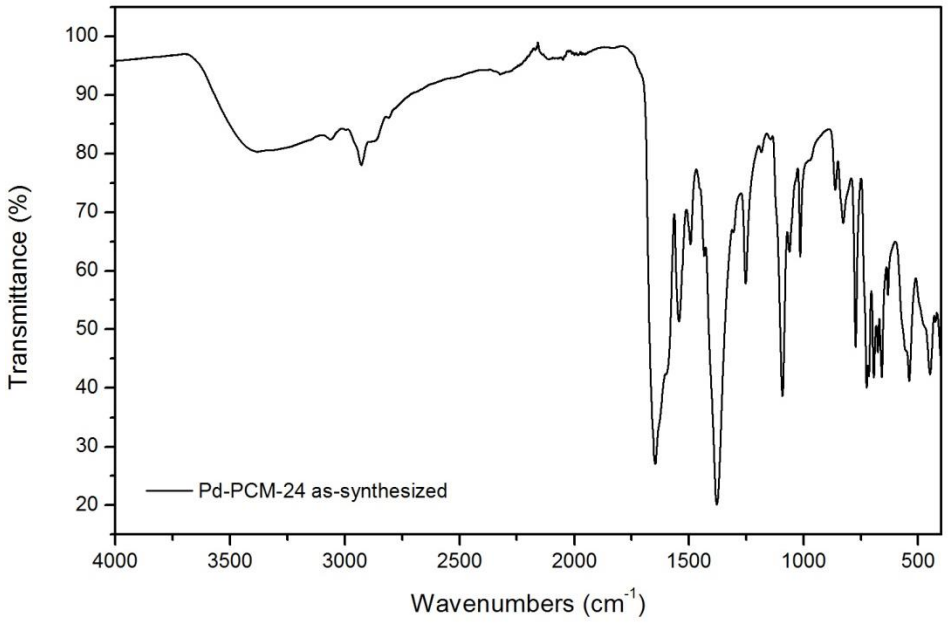

Figure A3.19: FTIR of as-synthesized Pd-PCM-24.

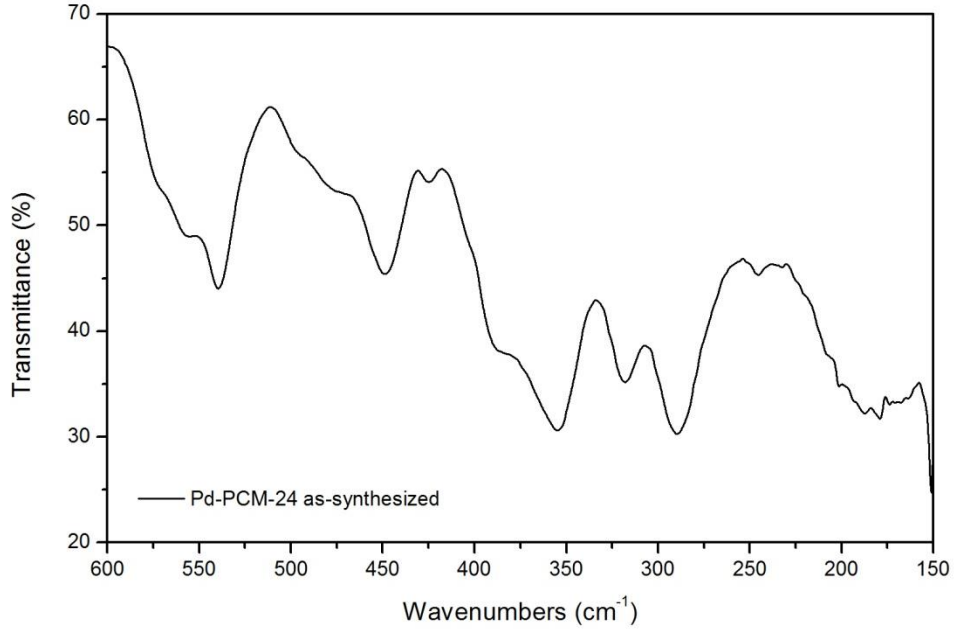

Figure A3.20: Far-IR of as-synthesized Pd-PCM-24.

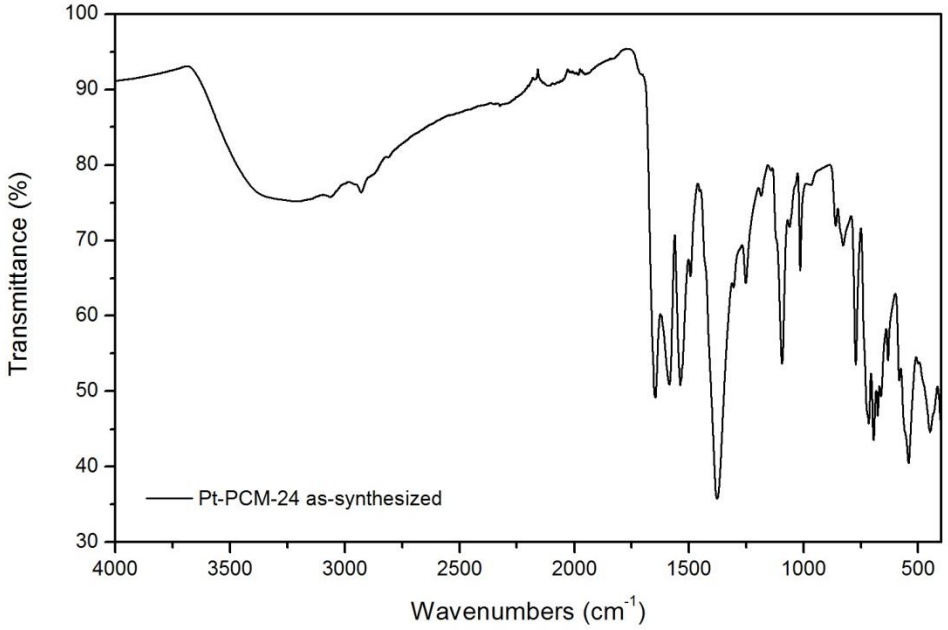

Figure A3.21: FTIR of as-synthesized Pt-PCM-24.

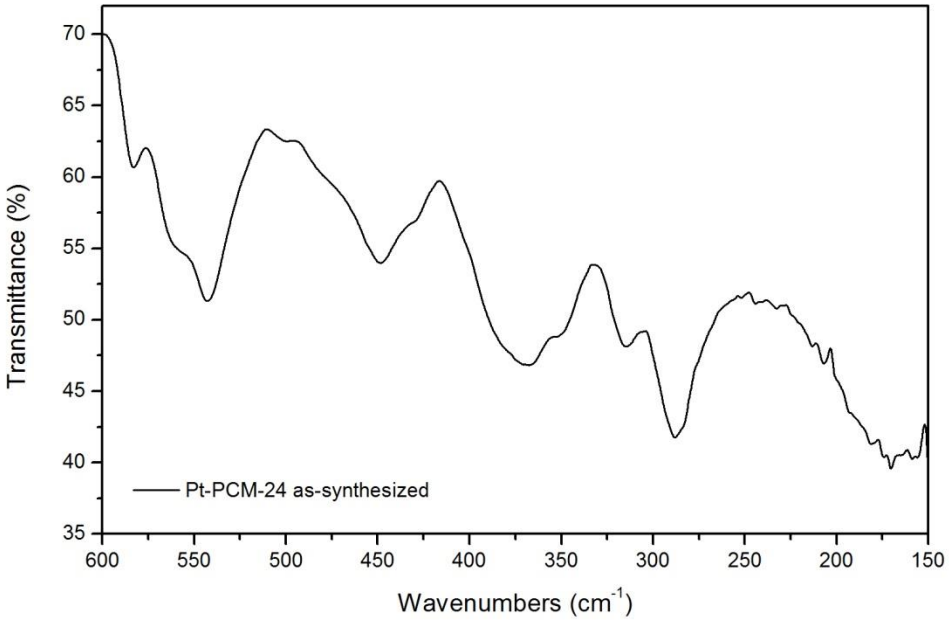

Figure A3.22: Far-IR of as-synthesized Pt-PCM-24.

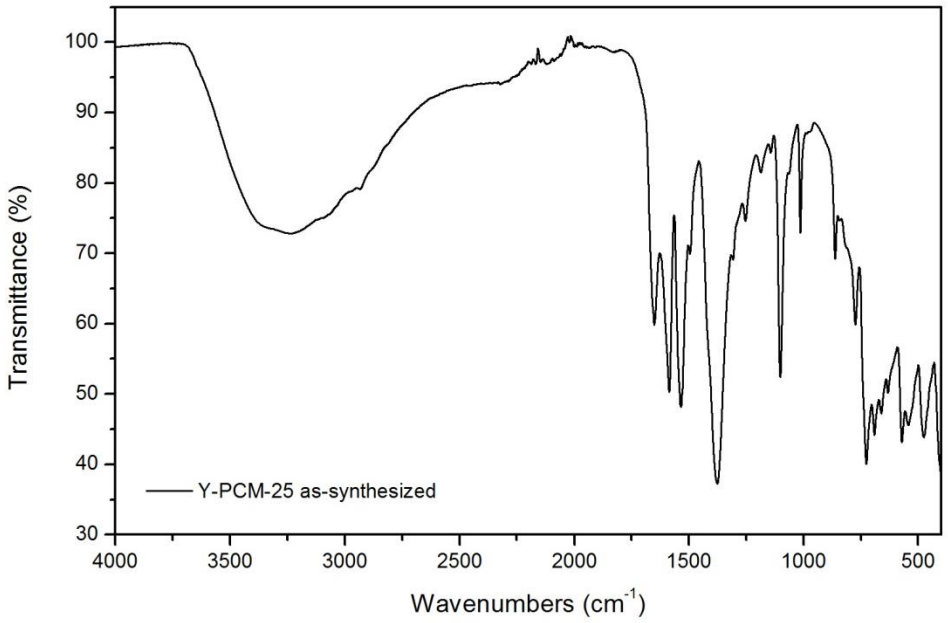

Figure A3.23: FTIR of as-synthesized Y-PCM-25.

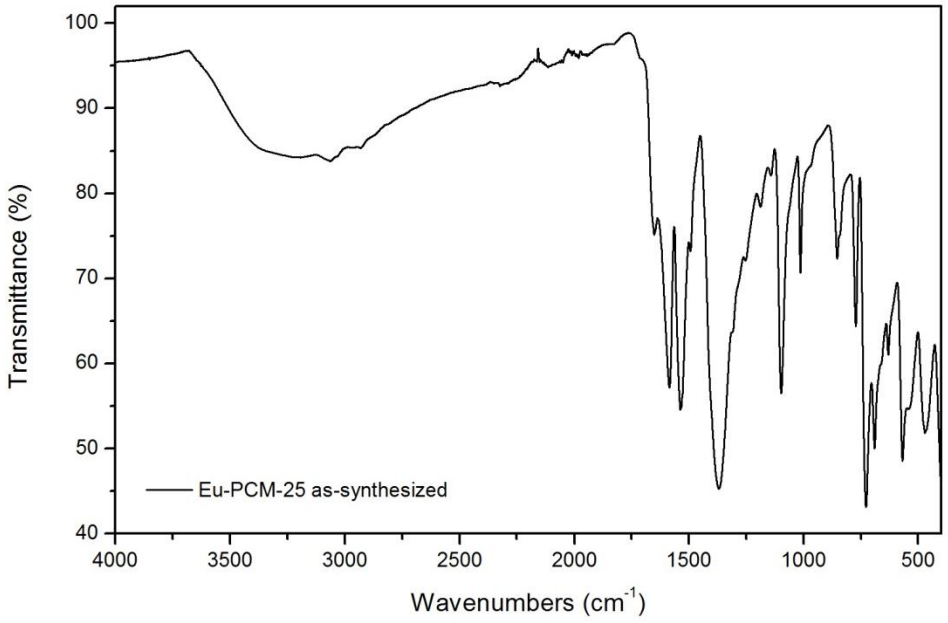

Figure A3.24: FTIR of as-synthesized Eu-PCM-25.

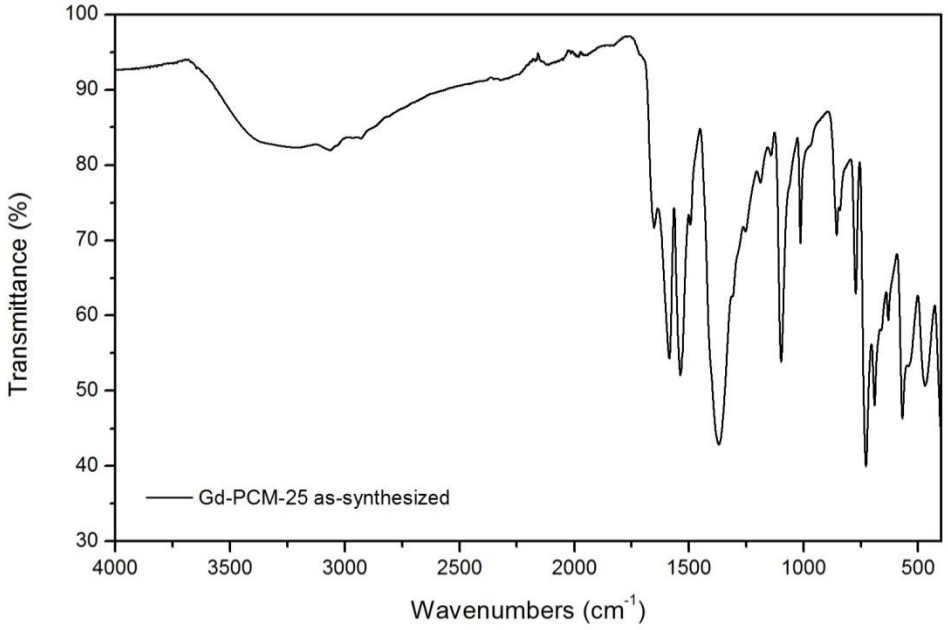

Figure A3.25: FTIR of as-synthesized Gd-PCM-25.

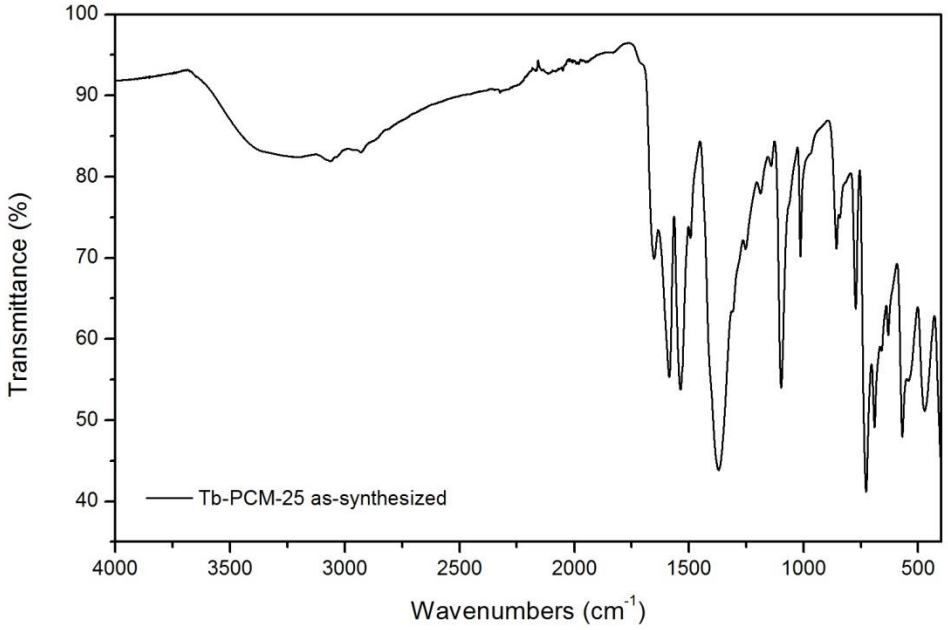

Figure A3.26: FTIR of as-synthesized Tb-PCM-25.

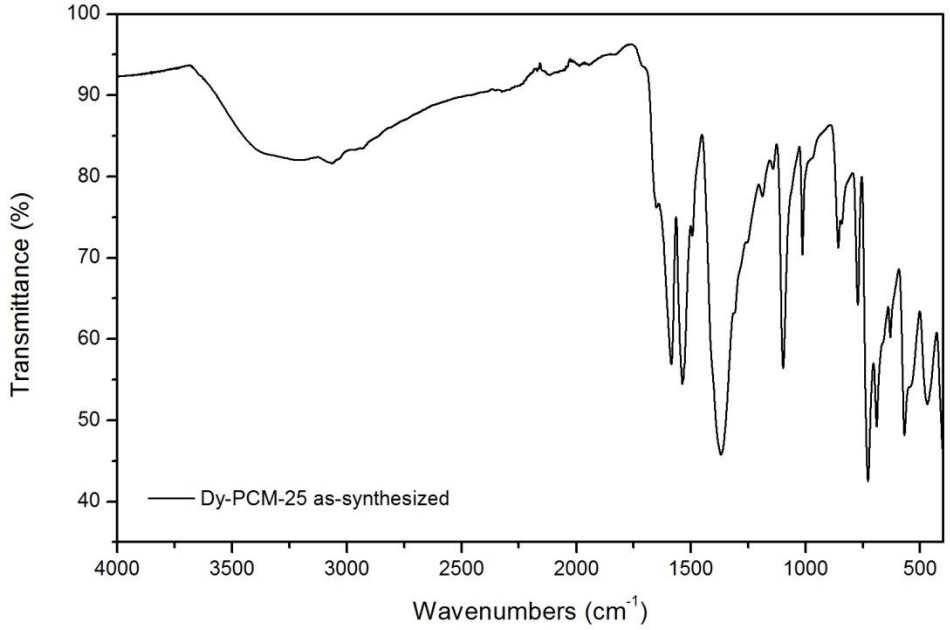

Figure A3.27: FTIR of as-synthesized Dy-PCM-25.

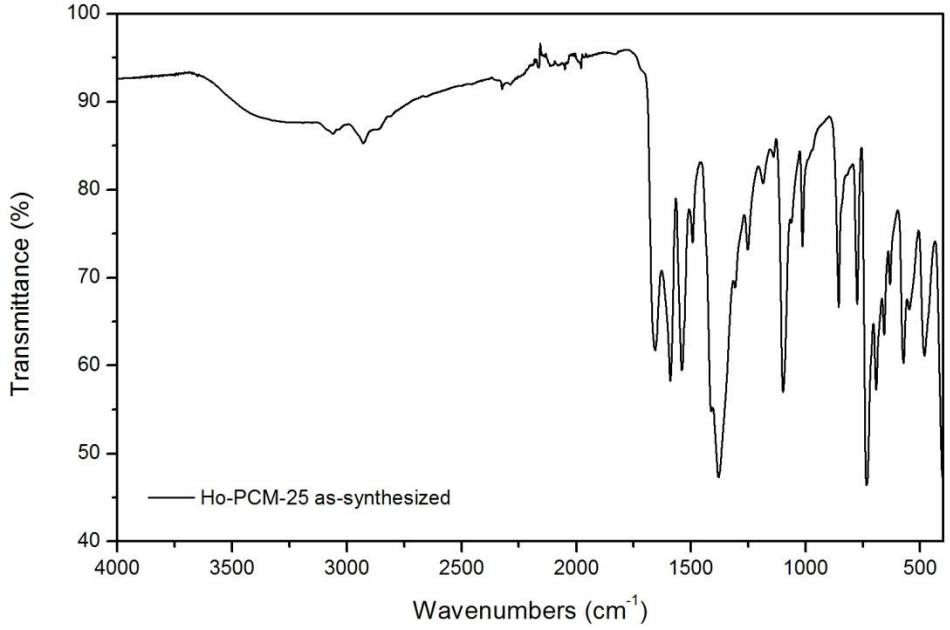

Figure A3.28: FTIR of as-synthesized Ho-PCM-25.

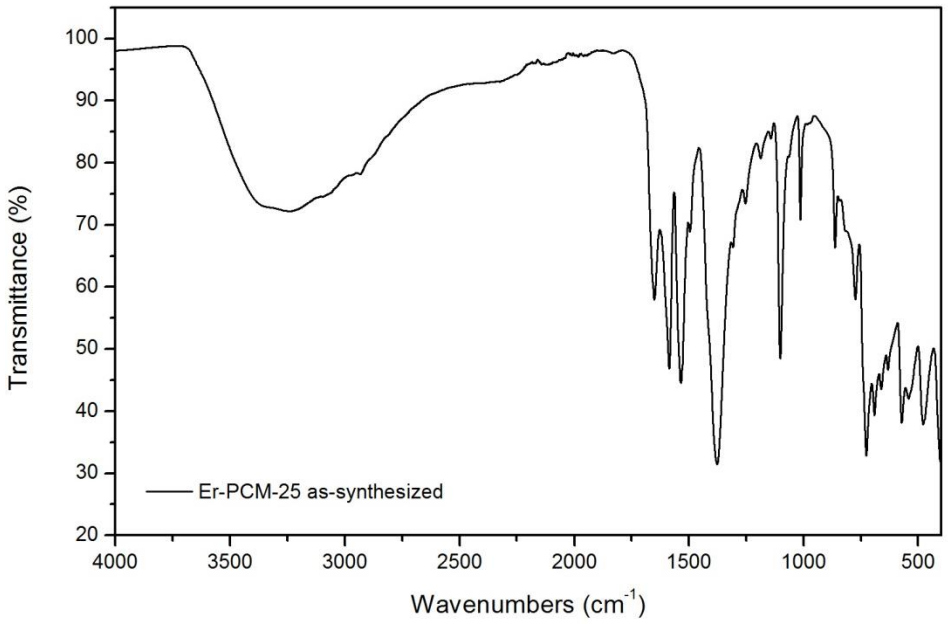

Figure A3.29: FTIR of as-synthesized Er-PCM-25.

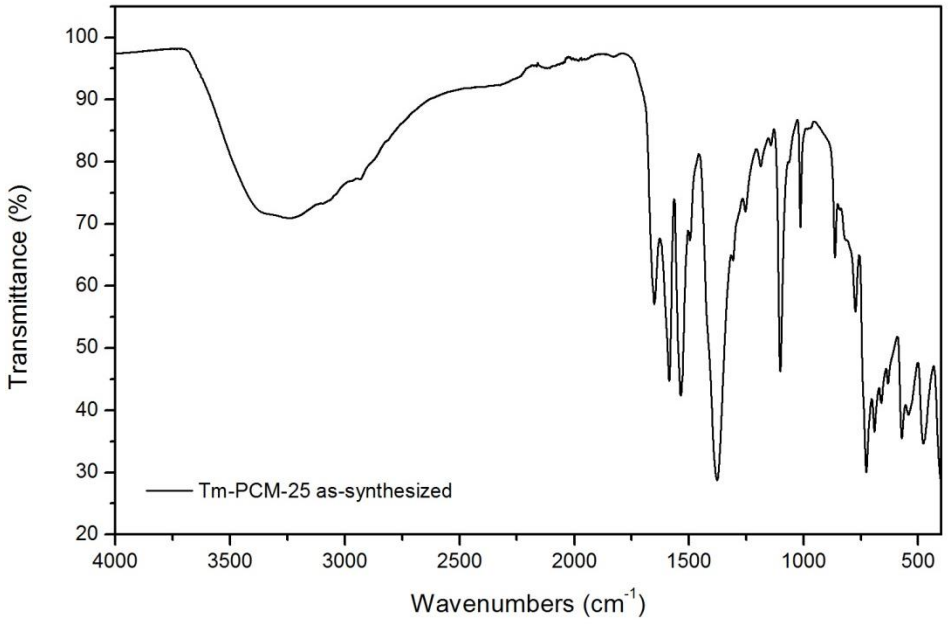

Figure A3.30: FTIR of as-synthesized Tm-PCM-25.

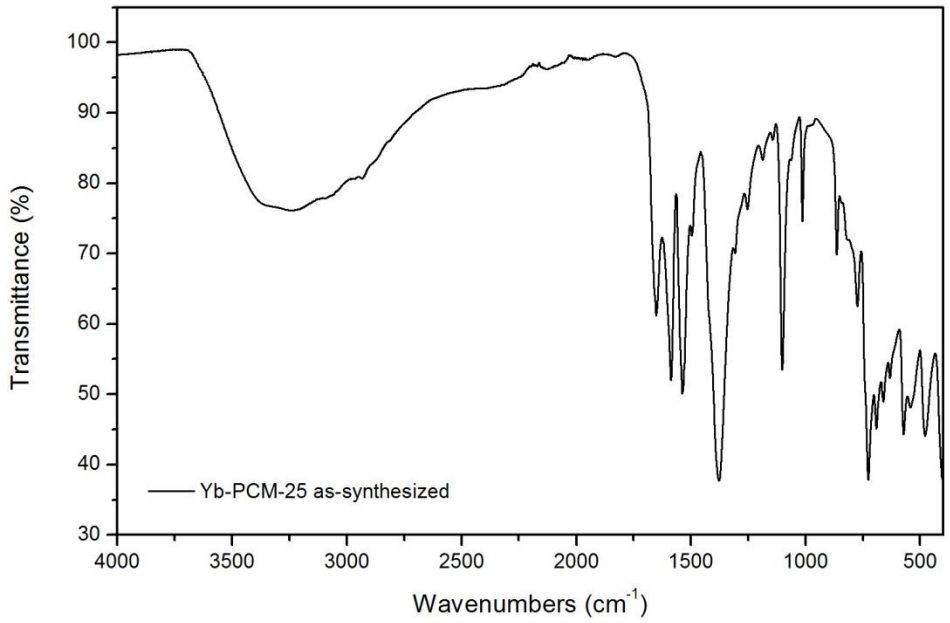

Figure A3.31: FTIR of as-synthesized Yb-PCM-25.

References

[1] H. Furukawa, K. E. Cordova, M. O'Keeffe, O. M. Yaghi, *Science* **2013**, *341*, 974.

[2] S. Kitagawa, R. Kitaura, S. Noro, *Angew. Chem. Int. Ed.* **2004**, *43*, 2334.

[3] P. Venuto, *Microporous Mater.* **1994**, *2*, 297.

[4] D. W. Breck, *Zeolite Molecular Sieves: Structure, Chemistry, and Use*, Wiley, New York, **1974**.

[5] J. Smith, *Chem. Rev.* **1988**, *88*, 149.

[6] P. Bénard, R. Chahine, *Langmuir* **2001**, *17*, 1950.

[7] N. Texier-Mandoki, J. Dentzer, T. Piquero, S. Saadallah, P. David, C. Vix-Guterl, *Carbon* **2004**, *42*, 2744.

[8] B. Hoskins, R. Robson, *J. Am. Chem. Soc.* **1990**, *112*, 1546.

[9] O. Yaghi, H. Li, *J. Am. Chem. Soc.* **1995**, *117*, 10401.

[10] H. Li, M. Eddaoudi, T. L. Groy, O. M. Yaghi, *J. Am. Chem. Soc.* **1998**, *120*, 8571.

[11] M. Kondo, T. Yoshitomi, K. Seki, H. Matsuzaka, S. Kitagawa, *Angew. Chem. Int. Ed.* **1997**, *36*, 1725.

[12] O. M. Yaghi, M. O'Keeffe, N. W. Ockwig, H. K. Chae, M. Eddaoudi, J. Kim, *Nature* **2003**, *423*, 705.

[13] H. Furukawa, J. Kim, N. W. Ockwig, M. O'Keeffe, O. M. Yaghi, *J. Am. Chem. Soc.* **2008**, *130*, 11650.

[14] D. J. Tranchemontagne, J. L. Mendoza-Cortés, M. O'Keeffe, O. M. Yaghi, *Chem. Soc. Rev.* **2009**, *38*, 1257.

[15] M. O'Keeffe, O. M. Yaghi, *Chem. Rev.* **2012**, *112*, 675.

[16] J. J. P. Iv, J. A. Perman, M. J. Zaworotko, *Chem. Soc. Rev.* **2009**, *38*, 1400.

[17] A. Rabenau, *Angew. Chem. Int. Ed. Engl.* **1985**, *24*, 1026.

[18] N. Stock, S. Biswas, *Chem. Rev.* **2012**, *112*, 933.

[19] H. Deng, S. Grunder, K. E. Cordova, C. Valente, H. Furukawa, M. Hmadeh, F. Gandara, A. C. Whalley, Z. Liu, S. Asahina, H. Kazumori, M. O'Keeffe, O. Terasaki, J. F. Stoddart, O. M. Yaghi, *Science* **2012**, *336*, 1018.

[20] O. K. Farha, I. Eryazici, N. C. Jeong, B. G. Hauser, C. E. Wilmer, A. A. Sarjeant, R. Q. Snurr, S. T. Nguyen, A. O. Yazaydin, J. T. Hupp, *J. Am. Chem. Soc.* **2012**, *134*, 15016.

[21] G. Ferey, C. Mellot-Draznieks, C. Serre, F. Millange, J. Dutour, S. Surble, I. Margiolaki, *Science* **2005**, *309*, 2040.

[22] K. Koh, A. G. Wong-Foy, A. J. Matzger, *J. Am. Chem. Soc.* **2009**, *131*, 4184.

[23] H. Furukawa, N. Ko, Y. B. Go, N. Aratani, S. B. Choi, E. Choi, A. O. Yazaydin, R. Q. Snurr, M. O'Keeffe, J. Kim, O. M. Yaghi, *Science* **2010**, *329*, 424.

[24] O. K. Farha, A. O. Yazaydin, I. Eryazici, C. D. Malliakas, B. G. Hauser, M. G. Kanatzidis, S. T. Nguyen, R. Q. Snurr, J. T. Hupp, *Nat. Chem.* **2010**, *2*, 944.

[25] H. Furukawa, Y. B. Go, N. Ko, Y. K. Park, F. J. Uribe-Romo, J. Kim, M. O'Keeffe, O. M. Yaghi, *Inorg. Chem.* **2011**, *50*, 9147.

[26] K. S. Park, Z. Ni, A. P. Cote, J. Y. Choi, R. Huang, F. J. Uribe-Romo, H. K. Chae, M. O'Keeffe, O. M. Yaghi, *Proc. Natl. Acad. Sci. U. S. A.* **2006**, *103*, 10186.

[27] J. H. Cavka, S. Jakobsen, U. Olsbye, N. Guillou, C. Lamberti, S. Bordiga, K. P. Lillerud, *J. Am. Chem. Soc.* **2008**, *130*, 13850.

[28] O. K. Farha, J. T. Hupp, *Acc. Chem. Res.* **2010**, *43*, 1166.

[29] A. Y. Robin, K. M. Fromm, *Coord. Chem. Rev.* **2006**, *250*, 2127.

[30] Z. Wang, S. M. Cohen, *Chem. Soc. Rev.* **2009**, *38*, 1315.

[31] A. D. Burrows, C. G. Frost, M. F. Mahon, C. Richardson, *Angew. Chem. Int. Ed.* **2008**, *47*, 8482.

[32] Z. Wang, K. K. Tanabe, S. M. Cohen, *Chem. Eur. J.* **2010**, *16*, 212.

[33] V. Valtchev, G. Majano, S. Mintova, J. Perez-Ramirez, *Chem. Soc. Rev.* **2013**, *42*, 263.

[34] A. M. Bohnsack, I. A. Ibarra, V. I. Bakhmutov, V. M. Lynch, S. M. Humphrey, *J. Am. Chem. Soc.* **2013**, *135*, 16038.

[35] B. L. Chen, C. D. Liang, J. Yang, D. S. Contreras, Y. L. Clancy, E. B. Lobkovsky, O. M. Yaghi, S. Dai, *Angew. Chem. Int. Ed.* **2006**, *45*, 1390.

[36] B. Chen, S. Ma, F. Zapata, F. R. Fronczek, E. B. Lobkovsky, H. -C. Zhou, *Inorg. Chem.* **2007**, *46*, 1233.

[37] J. -R. Li, R. J. Kuppler, H. -C. Zhou, *Chem. Soc. Rev.* **2009**, *38*, 1477.

[38] H. Furukawa, O. M. Yaghi, *J. Am. Chem. Soc.* **2009**, *131*, 8875.

[39] J. -R. Li, J. Sculley, H. -C. Zhou, *Chem. Rev.* **2012**, *112*, 869.

[40] M. D. Allendorf, C. A. Bauer, R. K. Bhakta, R. J. T. Houk, *Chem. Soc. Rev.* **2009**, *38*, 1330.

[41] B. Chen, S. Xiang, G. Qian, *Accounts Chem. Res.* **2010**, *43*, 1115.

[42] Y. Cui, Y. Yue, G. Qian, B. Chen, *Chem. Rev.* **2012**, *112*, 1126.

[43] Z. Hu, B. J. Deibert, J. Li, *Chem. Soc. Rev.* **2014**, *43*, 5815.

[44] L. E. Kreno, K. Leong, O. K. Farha, M. Allendorf, R. P. Van Duyne, J. T. Hupp, *Chem. Rev.* **2012**, *112*, 1105.

[45] E. Coronado, G. Minguez Espallargas, *Chem. Soc. Rev.* **2013**, *42*, 1525.

[46] M. -C. Dul, E. Pardo, R. Lescouëzec, Y. Journaux, J. Ferrando-Soria, R. Ruiz-García, J. Cano, M. Julve, F. Lloret, D. Cangussu, C. L. M. Pereira, H. O. Stumpf, J. Pasán, C. Ruiz-Pérez, *Coord. Chem. Rev.* **2010**, *254*, 2281.

[47] H. A. Habib, J. Sanchiz, C. Janiak, *Inorg. Chim. Act.* **2009**, *362*, 2452.

[48] M. Kurmoo, *Chem. Soc. Rev.* **2009**, *38*, 1353.

[49] J. Della Rocca, D. Liu, W. Lin, *Accounts Chem. Res.* **2011**, *44*, 957.

[50] P. Horcajada, T. Chalati, C. Serre, B. Gillet, C. Sebrie, T. Baati, J. F. Eubank, D. Heurtaux, P. Clayette, C. Kreuz, J. -S. Chang, Y. K. Hwang, V. Marsaud, P. -N. Bories, L. Cynober, S. Gil, G. Ferey, P. Couvreur, R. Gref, *Nat. Mater.* **2010**, *9*, 172.

[51] P. Horcajada, R. Gref, T. Baati, P. K. Allan, G. Maurin, P. Couvreur, G. Ferey, R. E. Morris, C. Serre, *Chem. Rev.* **2012**, *112*, 1232.

[52] W. J. Rieter, K. M. Pott, K. M. L. Taylor, W. Lin, *J. Am. Chem. Soc.* **2008**, *130*, 11584.

[53] K. M. L. Taylor-Pashow, J. Della Rocca, Z. Xie, S. Tran, W. Lin, *J. Am. Chem. Soc.* **2009**, *131*, 14261.

[54] N. C. Jeong, B. Samanta, C. Y. Lee, O. K. Farha, J. T. Hupp, *J. Am. Chem. Soc.* **2012**, *134*, 51.

[55] X. Liang, F. Zhang, W. Feng, X. Zou, C. Zhao, H. Na, C. Liu, F. Sun, G. Zhu, *Chem. Sci.* **2013**, *4*, 983.

[56] A. Shigematsu, T. Yamada, H. Kitagawa, *J. Am. Chem. Soc.* **2011**, *133*, 2034.

[57] G. K. H. Shimizu, J. M. Taylor, S. Kim, *Science* **2013**, *341*, 354.

[58] A. Corma, H. Garcia, F. X. L. I. Llabres i Xamena, *Chem. Rev.* **2010**, *110*, 4606.

[59] D. Farrusseng, S. Aguado, C. Pinel, *Angew. Chem. Int. Ed.* **2009**, *48*, 7502.

[60] J. Lee, O. K. Farha, J. Roberts, K. A. Scheidt, S. T. Nguyen, J. T. Hupp, *Chem. Soc. Rev.* **2009**, *38*, 1450.

[61] M. Yoon, R. Srirambalaji, K. Kim, *Chem. Rev.* **2012**, *112*, 1196.

[62] W. Lu, Z. Wei, Z. -Y. Gu, T. -F. Liu, J. Park, J. Park, J. Tian, M. Zhang, Q. Zhang, T. Gentle, M. Bosch, H. -C. Zhou, *Chem. Soc. Rev.* **2014**, *43*, 5561.

[63] Matsuda, R. Kitaura, S. Kitagawa, Y. Kubota, R. V. Belosludov, T. C. Kobayashi, H. Sakamoto, T. Chiba, M. Takata, Y. Kawazoe, Y. Mita, *Nature* **2005**, *436*, 238.

[64] D. Zhao, D. Yuan, R. Krishna, J. M. van Baten, H. -C. Zhou, *Chem. Commun.* **2010**, *46*, 7352.

[65] K. Sumida, D. L. Rogow, J. A. Mason, T. M. McDonald, E. D. Bloch, Z. R. Herm, T. -H. Bae, J. R. Long, *Chem. Rev.* **2012**, *112*, 724.

[66] P. D. C. Dietzel, V. Besikiotis, R. Blom, *J. Mater. Chem.* **2009**, *19*, 7362.

[67] A. Mallick, S. Saha, P. Pachfule, S. Roy, R. Banerjee, *J. Mater. Chem.* **2010**, *20*, 9073.

[68] S. R. Caskey, A. G. Wong-Foy, A. J. Matzger, *J. Am. Chem. Soc.* **2008**, *130*, 10870.

[69] I. P. O'koye, M. Benham, K. M. Thomas, *Langmuir* **1997**, *13*, 4054.

[70] D. Leaf, H. J. H. Verolme, W. F. Hunt, *Environ. Int.* **2003**, *29*, 303.

[71] M. Tucker, *Ecol. Econ.* **1995**, *15*, 215.

[72] U.S. Environmental Protection Agency: http://www.epa.gov/climatechange/emissions/co2_human.html

[73] R. K. Pachauri, A. Reisinger, Eds., *Climate Change 2007: Synthesis Report*, IPCC, Geneva, Switzerland, **2008**.

[74] D. M. D'Alessandro, B. Smit, J. R. Long, *Angew. Chem. Int. Ed.* **2010**, *49*, 6058.

[75] J. -R. Li, Y. Ma, M. C. McCarthy, J. Sculley, J. Yu, H. -K. Jeong, P. B. Balbuena, H. -C. Zhou, *Coord. Chem. Rev.* **2011**, *255*, 1791.

[76] M. Nandi, H. Uyama, *Chem. Rec.* **2014**, *14*, 1134.

[77] A. Phan, C. J. Doonan, F. J. Uribe-Romo, C. B. Knobler, M. O'Keeffe, O. M. Yaghi, *Accounts Chem. Res.* **2010**, *43*, 58.

[78] L. J. Murray, M. Dinca, J. R. Long, *Chem. Soc. Rev.* **2009**, *38*, 1294.

[79] M. P. Suh, H. J. Park, T. K. Prasad, D. -W. Lim, *Chem. Rev.* **2012**, *112*, 782.

[80] B. Kesanli, Y. Cui, M. R. Smith, E. W. Bittner, B. C. Bockrath, W. B. Lin, *Angew. Chem. Int. Ed.* **2005**, *44*, 72.

[81] D. J. Collins, H. -C. Zhou, *J. Mater. Chem.* **2007**, *17*, 3154.

[82] M. Dinca, J. R. Long, *Angew. Chem. Int. Ed.* **2008**, *47*, 6766.

[83] http://www1.eere.energy.gov/hydrogenandfuelcells/storage/current_technology.html

[84] J. -M. Zhou, W. Shi, N. Xu, P. Cheng, *Inorg. Chem.* **2013**, *52*, 8082.

[85] J. J. Perry IV, C. A. Bauer, M. D. Allendorf, *Metal-Organic Frameworks*, Wiley-VCH, Weinheim, **2011**, Chapter 12, pp. 267-308.

[86] G. Korotcenkov, *Chemical Sensors*, Momentum Press, New York, vol. 6, **2011**.

[87] P.-I. Gouma, *Nanomaterials for Chemical Sensors and Biotechnology*, Pan Stanford Publishing, Singapore, **2009**.

[88] P. Gründler, *Chemical Sensors*, Springer, Berlin, **2010**.

[89] L. Prodi, M. Montalti ,N. Zaccheroni, Eds., *Luminescence Applied in Sensor Science*, Springer, **2013**.

[90] R. C. Ropp, *Luminescence and the Solid State*, Elsevier Science, Amsterdam, 2 edition, **2004**.

[91] K. Binnemans, *Chem. Rev.* **2009**, *109*, 4283.

[92] V. Balzani, *Supramolecular Photochemistry*, D. Reidel Publishing Company, Anacapri, **1987**.

[93] N. J. Turro, J. C. Scaiano, V. Ramamurthy, *Modern Molecular Photochemistry of Organic Molecules*, University Science Books, Sausalito, **2010**.

[94] V. Ramamurthy, Y. Inoue, Eds., *Supramolecular Photochemistry: Controlling Photochemical Processes*, Wiley, Hoboken, **2011**.

[95] V. Ramamurthy, K. S. Schanze, *Solid State and Surface Photochemistry*, CRC Press, New York, **2000**.

[96] T. J. Penfold, S. Karlsson, G. Capano, F. A. Lima, J. Rittmann, M. Reinhard, M. H. Rittmann-Frank, O. Braem, E. Baranoff, R. Abela, I. Tavernelli, U. Rothlisberger, C. J. Milne, M. Chergui, *J. Phys. Chem. A*, **2013**, *117*, 4591.

[97] A. P. Demchenko, *Introduction to Fluorescence Sensing*, Springer, Netherlands, **2008**.

[98] E. G. Moore, A. P. S. Samuel, K. N. Raymond, *Acc. Chem. Res.*, **2009**, *42*, 542.

[99] S. V. Eliseeva, J. -C. G. Bünzli, *Chem. Soc. Rev.* **2009**, *39*, 189.

[100] Z. Liu, W. He, Z. Guo, *Chem. Soc. Rev.* **2013**, *42*, 1568.

[101] J. Rocha, L. D. Carlos, F. A. Almeida Paz, D. Ananias, *Chem. Soc. Rev.* **2011**, *40*, 926.

[102] S. M. Humphrey, P. K. Allan, S. E. Oungoulian, M. S. Ironside, E. R. Wise, *Dalton Trans.* **2009**, 2298.

[103] S. M. Humphrey, S. E. Oungoulian, J. W. Yoon, Y. K. Hwang, E. R. Wise, J. -S. Chang, *Chem. Commun.* **2008**, 2891.

[104] N. W. Waggoner, P. K. Allan, T. Kornfuehrer, S. M. Humphrey, *manuscript in prep.*

[105] A. J. Nunez, L. N. Shear, N. Dahal, I. A. Ibarra, J. Yoon, Y. K. Hwang, J. -S. Chang, S. M. Humphrey, *Chem. Commun.* **2011**, *47*, 11855.

[106] A. J. Nunez, M. S. Chang, I. A. Ibarra, S. M. Humphrey, *Inorg. Chem.* **2014**, *53*, 282.

[107] A. M. Bohnsack, I. A. Ibarra, P. W. Hatfield, J. W. Yoon, Y. K. Hwang, J. -S. Chang, S. M. Humphrey, *Chem. Commun.* **2011**, *47*, 4899.

[108] I. A. Ibarra, K. E. Tan, V. M. Lynch, S. M. Humphrey, *Dalton Trans.* **2012**, *41*, 3920.

[109] I. A. Ibarra, T. W. Hesterberg, B. J. Holliday, V. M. Lynch, S. M. Humphrey, *Dalton Trans.* **2012**, *41*, 8003.

[110] I. A. Ibarra, T. W. Hesterberg, J. -S. Chang, J. W. Yoon, B. J. Holliday, S. M. Humphrey, *Chem. Commun.* **2013**, *49*, 7156.

[111] I. A. Ibarra, J. W. Yoon, J. -S. Chang, S. K. Lee, V. M. Lynch, S. M. Humphrey, *Inorg. Chem.* **2012**, *51*, 12242.

[112] N. W. Waggoner, B. Saccoccia, I. A. Ibarra, V. M. Lynch, P. T. Wood, S. M. Humphrey, *Inorg. Chem.* **2014**, *53*, 12674.

[113] H. H. Willard, L. R. Perkins, *Anal. Chem.* **1953**, *25*, 1634.

[114] G. W. Kaatz, S. M. Seo, *J. Antimicrob. Chemother.* **2004**, *54*, 364.

[115] D. Marcoux, A. B. Charette, *J. Org. Chem.* **2008**, *73*, 590.

[116] H.-D. Guo, D.-F. Qiu, X.-M. Guo, G.-L. Zheng, X. Wang, S. Dang, H.-J. Zhang, *CrystEngComm* **2009**, *11*, 2425.

[117] L.-J. Li, G. Yuan, L. Chen, D.-Y. Du, X.-L. Wang, G.-J. Xu, H.-N. Wang, K.-Z. Shao, Z.-M. Su, *J. Coord. Chem.* **2011**, *64*, 1578.

[118] L. Carlucci, G. Ciani, D. M. Proserpio, *Coord. Chem. Rev.* **2003**, *246*, 247.

[119] J. -R. Li, Y. Tao, Q. Yu, X. -H. Bu, H. Sakamoto, S. Kitagawa, *Chem. Eur. J.* **2008**, *14*, 2771.

[120] C. Ritchie, F. Li, C. P. Pradeep, D. -L. Long, L. Xu, L. Cronin, *Dalton Trans.* **2009**, 6483.

[121] A. J. Blake, N. R. Champness, T. L. Easun, D. R. Allan, H. Nowell, M. W. George, J. Jia, X. -Z. Sun, *Nat. Chem.* **2010**, *2*, 688.

[122] I. A. Riddell, M. M. J. Smulders, J. K. Clegg, J. R. Nitschke, *Chem. Commun.* **2011**, *47*, 457.

[123] L. Ma, C. -D. Wu, M. M. Wanderley, W. Lin, *Angew. Chem. Int. Ed.* **2010**, *49*, 8244.

[124] X. Lin, N. R. Champness, M. Schröder, "Functional Metal-Organic Frameworks: Gas Storage, Separation and Catalysis," *Top. Curr. Chem.* Springer Berlin Heidelberg: Berlin, Heidelberg, **2009**, *293*, pp. 35–76.

[125] J. Seo, N. Jin, H. Chun, *Inorg. Chem.* **2010**, *49*, 10833.

[126] S. Shimomura, M. Higuchi, R. Matsuda, K. Yoneda, Y. Hijikata, Y. Kubota, Y. Mita, J. Kim, M. Takata, S. Kitagawa, *Nat. Chem.* **2010**, *2*, 633.

[127] A. Demessence, J. R. Long, *Chem. Eur. J.* **2010**, *16*, 5902.

[128] M. J. Ingleson, J. P. Barrio, J. Bacsa, C. Dickinson, H. Park, M. J. Rosseinsky, *Chem. Commun.* **2008**, 1287.

[129] X. Zhang, F. X. Llabrés i Xamena, A. Corma, *J. Catal.* **2009**, *265*, 155.

[130] D. Dang, P. Wu, C. He, Z. Xie, C. Duan, *J. Am. Chem. Soc.* **2010**, *132*, 14321.

[131] K. K. Tanabe, S. M. Cohen, *Angew. Chem. Int. Ed.* **2009**, *48*, 7424.

[132] L. H. Wee, S. R. Bajpe, N. Janssens, I. Hermans, K. Houthoofd, C. E. A. Kirschhock, J. A. Martens, *Chem. Commun.* **2010**, *46*, 8186.

[133] W. E. McEwen, L. Maier, B. Miller, *Topics in Phosphorus Chemistry*, M. Grayson and E. J. Griffith, eds., Wiley, **1965**, *1–2*.

[134] Y. -Y. Liu, J. Zhang, F. Xu, L. -X. Sun, T. Zhang, W. -S. You, Y. Zhao, J. Zeng, Z. Cao, D. Yang, *Cryst. Growth Des.* **2008**, *8*, 3127.

[135] A. E. Platero-Prats, V. A. de la Peña-O'Shea, N. Snejko, Á. Monge, E. Gutiérrez-Puebla, *Chem. Eur. J.* **2010**, *16*, 11632.

[136] R. Amengual, E. Genin, V. Michelet, M. Savignac, J.-P. Genêt, *Adv. Synth. Catal.* **2002**, *344*, 393.

[137] Z. Zhang, S. Xiang, Y. -S. Chen, S. Ma, Y. Lee, T. Phely-Bobin, B. Chen, *Inorg. Chem.* **2010**, *49*, 8444.

[138] C. Volkringer, T. Loiseau, G. Férey, C. M. Morais, F. Taulelle, V. Montouillout, D. Massiot, *Micropor. Mesopor. Mater.* **2007**, *105*, 111.

[139] S. M. Humphrey, J. -S. Chang, S. H. Jhung, J. W. Yoon, P. T. Wood, *Angew. Chem. Int. Ed.* **2007**, *46*, 272.

[140] A. Galarneau, H. Cambon, F. Di Renzo, F. Fajula, *Langmuir* **2001**, *17*, 8328.

[141] Y. J. Choi, J. H. Choi, K. M. Choi, J. K. Kang, *J. Mater. Chem.* **2011**, *21*, 1073.

[142] L. Valenzano, B. Civalleri, S. Chavan, G. T. Palomino, C. O. Areán, S. Bordiga, *J. Phys. Chem. C* **2010**, *114*, 11185.

[143] Z. Bao, L. Yu, Q. Ren, X. Lu, S. Deng, *J. Colloid Interf. Sci.* **2011**, *353*, 549.

[144] R. Vaidhyanathan, S. S. Iremonger, K. W. Dawson, G. K. H. Shimizu, *Chem. Commun.* **2009**, 5230.

[145] M. Dincă, J. R. Long, *Journal of the American Chemical Society* **2005**, *127*, 9376.

[146] H. -K. Liu, T. -H. Tsao, Y. -T. Zhang, C. -H. Lin, *CrystEngComm* **2009**, *11*, 1462.

[147] B. R. Srinivasan, S. C. Sawant, *Thermochim. Acta* **2003**, *402*, 45.

[148] O. K. Farha, I. Eryazici, N. C. Jeong, B. G. Hauser, C. E. Wilmer, A. A. Sarjeant, R. Q. Snurr, S. T. Nguyen, A. O. Yazaydin, J. T. Hupp, *J. Am. Chem. Soc.* **2012**, *134*, 15016.

[149] Y. -Q. Chen, G. -R. Li, Z. Chang, Y. -K. Qu, Y. -H. Zhang, X. -H. Bu, *Chem. Sci.* **2013**, *4*, 3678.

[150] Z. -F. Wu, B. Tan, M. -L. Feng, A. -J. Lan, X. -Y. Huang, *J. Mater. Chem. A* **2014**, *2*, 6426.

[151] B. V. Harbuzaru, A. Corma, F. Rey, J. L. Jorda, D. Ananias, L. D. Carlos, J. Rocha, *Angew. Chem. Int. Ed.* **2009**, *48*, 6476.

[152] R. -B. Lin, F. Li, S. -Y. Liu, X. -L. Qi, J. -P. Zhang, X. -M. Chen, *Angew. Chem. Int. Ed.* **2013**, *52*, 13429.

[153] X. Wei, L. Zheng, F. Luo, Z. Lin, L. Guo, B. Qiu, G. Chen, *J. Mater. Chem. B* **2013**, *1*, 1812.

[154] J. C. G. Bunzli, C. Piguet, *Chem. Soc. Rev.* **2005**, *34*, 1048.

[155] A. de Bettencourt-Dias, *Dalton Trans.* **2007**, 2229.

[156] Q. Dai, M. E. Foley, C. J. Breshike, A. Lita, G. F. Strouse, *J. Am. Chem. Soc.* **2011**, *133*, 15475.

[157] J. Kido, Y. Okamoto, *Chem. Rev.* **2002**, *102*, 2357.

[158] A. -L. Penard, T. Gacoin, J. -P. Boilot, *Accounts Chem. Res.* **2007**, *40*, 895.

[159] L. D. Carlos, R. A. S. Ferreira, V. de Z. Bermudez, S. J. L. Ribeiro, *Adv. Mater.* **2009**, *21*, 509.

[160] K. Kuriki, Y. Koike, Y. Okamoto, *Chem. Rev.* **2002**, *102*, 2347.

[161] L. Wang, Y. Li, *Chem. Mater.* **2007**, *19*, 727.

[162] Y. Fan, P. Yang, S. Huang, J. Jiang, H. Lian, J. Lin, *J. Phys. Chem. C* **2009**, *113*, 7826.

[163] B. Andes Hess, A. Kędziorski, L. Smentek, D. J. Bornhop, *J. Phys. Chem. A* **2008**, *112*, 2397.

[164] C. P. Montgomery, B. S. Murray, E. J. New, R. Pal, D. Parker, *Acc. Chem. Res.* **2009**, *42*, 925.

[165] B. Song, V. Sivagnanam, C. D. B. Vandevyver, I. Hemmilä, H. -A. Lehr, M. A. M. Gijs, J. -C. G. Bünzli, *Analyst* **2009**, *134*, 1991.

[166] T. Gunnlaugsson, J. P. Leonard, *Chem. Commun.* **2005**, 3114.

[167] H. Tsukube, S. Shinoda, *Chem. Rev.* **2002**, *102*, 2389.

[168] O. S. Wolfbeis, A. Durkop, M. Wu, Z. H. Lin, *Angew. Chem. Int. Ed.* **2002**, *41*, 4495.

[169] B. D. Chandler, D. T. Cramb, G. K. H. Shimizu, *J. Am. Chem. Soc.* **2006**, *128*, 10403.

[170] J. -C. G. Bunzli, *J. Coord. Chem.* **2014**, *67*, 3706.

[171] W. Horrocks, D. Sudnick, *Accounts Chem. Res.* **1981**, *14*, 384.

[172] Y. Yu, J.-P. Ma, Y. -B. Dong, *Crystengcomm* **2012**, *14*, 7157.

[173] C. -Y. Sun, X. -L. Wang, C. Qin, J. -L. Jin, Z. -M. Su, P. Huang, K. -Z. Shao, *Chem. Eur. J.* **2013**, *19*, 3639.

[174] Y. Xiao, Y. Cui, Q. Zheng, S. Xiang, G. Qian, B. Chen, *Chem. Commun.* **2010**, *46*, 5503.

[175] B. Chen, L. Wang, Y. Xiao, F. R. Fronczek, M. Xue, Y. Cui, G. Qian, *Angew. Chem. Int. Ed.* **2009**, *48*, 500.

[176] X. -H. Zhou, L. Li, H. -H. Li, A. Li, T. Yang, W. Huang, *Dalton Trans.* **2013**, *42*, 12403.

[177] K. Jayaramulu, R. P. Narayanan, S. J. George, T. K. Maji, *Inorg. Chem.* **2012**, *51*, 10089.

[178] B. Liu, C. Sun, Y. Chen, *J. Mater. Chem. B* **2014**, *2*, 1661.

[179] Q. -B. Bo, H. -T. Zhang, H. -Y. Wang, J. -L. Miao, Z. -W. Zhang, *Chem. Eur. J.* **2014**, *20*, 3712.

[180] S. Mohapatra, B. Rajeswaran, A. Chakraborty, A. Sundaresan, T. K. Maji, *Chem. Mater.* **2013**, *25*, 1673.

[181] T. -F. Liu, W. Zhang, W. -H. Sun, R. Cao, *Inorg. Chem.* **2011**, *50*, 5242.

[182] W. -H. Zhu, Z. -M. Wang, S. Gao, *Inorg. Chem.* **2007**, *46*, 1337.

[183] Z. Dou, J. Yu, Y. Cui, Y. Yang, Z. Wang, D. Yang, G. Qian, *J. Am. Chem. Soc.* **2014**, *136*, 5527.

[184] J. Demel, P. Kubat, F. Millange, J. Marrot, I. Cisarova, K. Lang, *Inorg. Chem.* **2013**, *52*, 2779.

[185] Z. Hao, G. Yang, X. Song, M. Zhu, X. Meng, S. Zhao, S. Song, H. Zhang, *J. Mater. Chem. A* **2014**, *2*, 237.

[186] C. Zhan, S. Ou, C. Zou, M. Zhao, C.-D. Wu, *Anal. Chem.* **2014**, *86*, 6648.

[187] Z. Guo, H. Xu, S. Su, J. Cai, S. Dang, S. Xiang, G. Qian, H. Zhang, M. O'Keeffe, B. Chen, *Chem. Commun.* **2011**, *47*, 5551.

[188] K. A. White, D. A. Chengelis, K. A. Gogick, J. Stehman, N. L. Rosi, S. Petoud, *J. Am. Chem. Soc.* **2009**, *131*, 18069.

[189] J. -J. Wu, Y. -X. Ye, Y. -Y. Qiu, Z. -P. Qiao, M. -L. Cao, B. -H. Ye, *Inorg. Chem.* **2013**, *52*, 6450.

[190] Y. -N. Gong, L. Jiang, T. -B. Lu, *Chem. Commun.* **2013**, *49*, 11113.

[191] H. Xu, F. Liu, Y. Cui, B. Chen, G. Qian, *Chem. Commun.* **2011**, *47*, 3153.

[192] X. Zhou, H. Li, H. Xiao, L. Li, Q. Zhao, T. Yang, J. Zuo, W. Huang, *Dalton Trans.* **2013**, *42*, 5718.

[193] J. -D. Xiao, L. -G. Qiu, F. Ke, Y. -P. Yuan, G. -S. Xu, Y. -M. Wang, X. Jiang, *J. Mater. Chem. A* **2013**, *1*, 8745.

[194] S. -B. Ding, W. Wang, L. -G. Qiu, Y. -P. Yuan, F. -M. Peng, X. Jiang, A. -J. Xie, Y. -H. Shen, J. -F. Zhu, *Mater. Lett.* **2011**, *65*, 1385.

[195] X. Rao, T. Song, J. Gao, Y. Cui, Y. Yang, C. Wu, B. Chen, G. Qian, *J. Am. Chem. Soc.* **2013**, *135*, 15559.

[196] Y. Cui, H. Xu, Y. Yue, Z. Guo, J. Yu, Z. Chen, J. Gao, Y. Yang, G. Qian, B. Chen, *J. Am. Chem. Soc.* **2012**, *134*, 3979.

[197] K. Miyata, Y. Konno, T. Nakanishi, A. Kobayashi, M. Kato, K. Fushimi, Y. Hasegawa, *Angew. Chem. Int. Ed.* **2013**, *52*, 6413.

[198] R. F. D'Vries, S. Alvarez-Garcia, N. Snejko, L. E. Bausa, E. Gutierrez-Puebla, A. de Andres, M. Angeles Monge, *J. Mater. Chem. C* **2013**, *1*, 6316.

[199] A. Cadiau, C. D. S. Brites, P. M. F. J. Costa, R. A. S. Ferreira, J. Rocha, L. D. Carlos, *ACS Nano* **2013**, *7*, 7213.

[200] M. D. Ward, *Chem. Soc. Rev.* **1997**, *26*, 365.

[201] A. P. Nelson, O. K. Farha, K. L. Mulfort, J. T. Hupp, *J. Am. Chem. Soc.* **2009**, *131*, 458.

[201] P. D. C. Dietzel, P. A. Georgiev, J. Eckert, R. Blom, T. Strässle, T. Unruh, *Chem. Commun.* **2010**, *46*, 4962.

[203] S. Barman, H. Furukawa, O. Blacque, K. Venkatesan, O. M. Yaghi, H. Berke, *Chem. Commun.* **2010**, *46*, 7981.

[204] D. -C. Zhong, J.-B. Lin, W. -G. Lu, L. Jiang, T.-B. Lu, *Inorg. Chem.* **2009**, *48*, 8656.

[205] R. Sanz, F. Martínez, G. Orcajo, L. Wojtas, D. Briones, *Dalton Trans.* **2013**, *42*, 2392.

[206] H. Fei, J. F. Cahill, K. A. Prather, S. M. Cohen, *Inorg. Chem.* **2013**, *52*, 4011.

[207] S. Kim, K. W. Dawson, B. S. Gelfand, J. M. Taylor, G. K. H. Shimizu, *J. Am. Chem. Soc.* **2013**, *135*, 963.

[208] M. Kim, J. F. Cahill, H. Fei, K. A. Prather, S. M. Cohen, *J. Am. Chem. Soc.* **2012**, *134*, 18082.

[209] X. -S. Wang, S. Ma, P. M. Forster, D. Yuan, J. Eckert, J. J. López, B. J. Murphy, J. B. Parise, H. -C. Zhou, *Angew. Chem. Int. Ed.* **2008**, *47*, 7263.

[210] H. Wu, W. Zhou, T. Yildirim, *J. Am. Chem. Soc.* **2009**, *131*, 4995.

[211] S. S. Kaye, J. R. Long, *J. Am. Chem. Soc.* **2008**, *130*, 806.

[212] K. Oisaki, Q. Li, H. Furukawa, A. U. Czaja, O. M. Yaghi, *J. Am. Chem. Soc.* **2010**, *132*, 9262.

[213] T. Jacobs, R. Clowes, A. I. Cooper, M. J. Hardie, *Angew. Chem. Int. Ed.* **2012**, *51*, 5192.

[214] C. J. Doonan, W. Morris, H. Furukawa, O. M. Yaghi, *J. Am. Chem. Soc.* **2009**, *131*, 9492.

[215] K. C. Szeto, K. O. Kongshaug, S. Jakobsen, M. Tilset, K. P. Lillerud, *Dalton Trans.* **2008**, 2054.

[216] J. L. Crossland, D. M. Young, L. N. Zakharov, D. R. Tyler, *Dalton Trans.* **2009**, 9253.

[217] K. K. Majumdar, H. V. Nanishankar, B. R. Jagirdar, *Eur. J. Inorg. Chem.* **2001**, *2001*, 1847.

[218] G. Minghetti, A. Albinati, A. L. Bandini, G. Banditelli, *Angew. Chem. Int. Ed.* **1985**, *24*, 120.

[219] A. L. Bandini, G. Banditelli, M. Manassero, A. Albinati, D. Colognesi, J. Eckert, *Eur. J. Inorg. Chem.* **2003**, *2003*, 3958.

[220] X. Lin, I. Telepeni, A. J. Blake, A. Dailly, C. M. Brown, J. M. Simmons, M. Zoppi, G. S. Walker, K. M. Thomas, T. J. Mays, P. Hubberstey, N. R. Champness, M. Schröder, *J. Am. Chem. Soc.* **2009**, *131*, 2159.

[221] A. M. Shultz, O. K. Farha, J. T. Hupp, S. T. Nguyen, *J. Am. Chem. Soc.* **2009**, *131*, 4204.

[222] G. J. Kubas, *J. Organomet. Chem.* **2001**, *635*, 37.

[223] G. J. Kubas, *J. Organomet. Chem.* **2009**, *694*, 2648.

[224] N. K. Szymczak, D. A. Braden, J. L. Crossland, Y. Turov, L. N. Zakharov, D. R. Tyler, *Inorg. Chem.* **2009**, *48*, 2976.

[225] D. M. Heinekey, J. K. Law, S. M. Schultz, *J. Am. Chem. Soc.* **2001**, *123*, 12728.

[226] M. Findlater, K. M. Schultz, W. H. Bernskoetter, A. Cartwright-Sykes, D. M. Heinekey, M. Brookhart, *Inorg. Chem.* **2012**, *51*, 4672.

[227] J. L. Mendoza-Cortes, W. A. Goddard, H. Furukawa, O. M. Yaghi, *J. Phys. Chem. Lett.* **2012**, *3*, 2671.

[228] M. Kosa, M. Krack, A. K. Cheetham, M. Parrinello, *J. Phys. Chem. C* **2008**, *112*, 16171.

[229] T. K. A. Hoang, A. Hamaed, G. Moula, R. Aroca, M. Trudeau, D. M. Antonelli, *J. Am. Chem. Soc.* **2011**, *133*, 4955.

[230] K. Q. Almeida Leñero, Y. Guari, P. C. J. Kamer, P. W. N. M. van Leeuwen, B. Donnadieu, S. Sabo-Etienne, B. Chaudret, M. Lutz, A. L. Spek, *Dalton Trans.* **2013**, *42*, 6495.

[231] P.-Z. Li, Y. Maeda, Q. Xu, *Chem. Comm.* **2011**, *47*, 8436.

[232] P. Bergamini, E. Costa, S. Sostero, A. G. Orpen, P. G. Pringle, *Organometallics* **1991**, *10*, 2989.

[233] G. L. Casty, J. M. Stryker, *Organometallics* **1997**, *16*, 3083.

[234] E. Tsivion, J. R. Long, M. Head-Gordon, *J. Am. Chem. Soc.* **2014**, *136*, 17827.

[235] Q. Chen, Z. Chang, W. -C. Song, H. Song, H.-B. Song, T. -L. Hu, X. -H. Bu, *Angew. Chem. Int. Ed.* **2013**, *52*, 11550.

[236] X. -N. Cheng, W. -X. Zhang, Y. -Y. Lin, Y. -Z. Zheng, X. -M. Chen, *Adv. Mater.* **2007**, *19*, 1494.

[237] L. Wang, S. Lu, Y. Zhou, X. Guo, Y. Lu, J. He, D. G. Evans, *Chem. Commun.* **2011**, *47*, 11002.